

©2017

Yike Jiang

ALL RIGHTS RESERVED

NOVEL POLYSACCHARIDE-POLYPEPTIDES NANOCOMPLEXES: ASSEMBLY,
CHARACTERIZATION, AND APPLICATIONS IN DELIVERY OF BLACK TEA
POLYPHENOLS

by

YIKE JIANG

A dissertation submitted to the

School of Graduate Studies

Rutgers, The State University of New Jersey

In partial fulfillment of the requirements

For the degree of

Doctor of Philosophy

Graduate Program in Food Science

Written under the direction of

Qingrong Huang

And approved by

New Brunswick, New Jersey

October, 2017

ABSTRACT OF THE DISSERTATION

Novel Polysaccharide-Polypeptides Nanocomplexes: Assembly, Characterization, and
Applications in Delivery of Black Tea Polyphenols

By YIKE JIANG

Dissertation Director:

Qingrong Huang

In this dissertation, a novel polysaccharide-polypeptides nanocomplex was assembled from chitosan (CS) and caseinophosphopeptides (CPPs). CS is a biodegradable, biocompatible, and non-toxic cationic polysaccharide. CPPs are a group of anionic bioactive polypeptides hydrolyzed from caseins, which are the most abundant proteins in milk. CS and CPPs can self-assemble into complexes through predominantly electrostatic attraction when they are oppositely charged. In the first part of this dissertation, the black tea polyphenol theaflavin-3,3'-digallate (TF-3) was encapsulated in the CS-CPPs nanocomplex, aiming to improve its intestinal permeability. The interactions and microstructural changes involved in each step of the encapsulation process were characterized by multiple techniques including turbidimetric titration, fluorescence quenching, circular dichroism, quartz crystal microbalance with dissipation monitoring, small angle X-ray scattering, and ultra-small angle X-ray scattering. The results indicated that TF-3 firstly associated with CPPs through mainly hydrogen bond. The TF-3/CPPs mixture further interacted with CS via

predominantly electrostatic interactions. TF-3 was then encapsulated in the CS-CPPs nanocomplex with high encapsulation efficiency. The CS-CPPs nanocomplex can effectively enhance the intestinal permeability of TF-3.

As the CS-CPPs nanocomplexes were associated predominantly by electrostatic attraction, which is susceptible to pH change. To prevent the low pH-induced disassemble of the nanocomplexes and burst release of the encapsulated TF-3, the nanocomplexes encapsulated with TF-3 were chemically crosslinked by genipin. The Caco-2 monolayer transport results demonstrated that the cumulative amount of transported TF-3 during 2h experiment increased at least 7.8 folds after being encapsulated in the crosslinked nanocomplexes.

In the second part of this dissertation, the CS-CPPs nanocomplexes composed of different CS:CPPs weight ratios were applied to stabilize Pickering emulsions. These gel-like oil-in-water type Pickering emulsions, however, were not stable at low pH due to disassembly of the nanocomplexes. To solve this problem, the CS-CPPs nanocomplexes were crosslinked with genipin at different conditions. These genipin crosslinked CS-CPPs nanocomplexes (GCNs) were further applied to stabilize Pickering emulsions, which showed outstanding stability in a wide pH range. After incorporation of TF-3 in the GCNs, the stability of Pickering emulsions against lipid oxidation has been improved significantly.

ACKNOWLEDGEMENTS

My past six years at the Department of Food Science, Rutgers University is wonderful and memorable. It is a precious experience which will benefit for life. I would take this opportunity to thank all the people who helped me during my study at Rutgers University.

I sincerely acknowledge my Ph. D. advisor Dr. Qingrong Huang who brought me to the fascinating research area of food nanotechnology. Starting from scratch, this dissertation would not be completed without his patient guidance and support. He dedicated his effort to assist me and constantly encouraged me to overcome the obstacles. He helped me sharpen as a critical thinker. His profound knowledge, rigorous attitude towards research, and optimistic, enthusiastic, and charming personality are the characters I need to learn. Dr. Huang is not only a respectable advisor but also an amiable friend who always care about our needs, emotion, life, and career development. Dr. Huang is always offering good opportunities for me to show myself. It was my fortune and honor to work with and learn from Dr. Huang.

I would like to thank my committee members Dr. Chi-Tang Ho, Dr. Qing-Li Wu, and Dr. Shiming Li not only for their invaluable suggestions and comments for my Ph. D. research, but also for writing recommendation letters and providing the black tea extract. I also want to thank all the faculties at Rutgers University and Jiangnan University who gave me instruction and help, which inspired my interest and illuminated my way in food science research.

Definitely, I would express my deepest gratitude to my parents for their love, education, encouragement, and unconditional support to cheer me through all the difficult times, especially when I just came to the United States.

I also want to thank all my labmates and friends who made my life at Rutgers University so colorful and enjoyable. I would appreciate Dr. Wen Wang from Zhejiang Academy of Agricultural Sciences (Hangzhou, China) for fitting the size distribution of Pickering emulsions (chapter VIII,

IX, and X in this dissertation); Margaret Wang, Jessica Li, Yuxin Shi, and Wesly L. Pan for their voluntary helps in my research and the grammatical correction of my research papers; the staffs in the Department of Food Science, Rutgers University for their support.

Last but not least, I would like to express my special thanks to China Scholarship Council for the continuous financial support, which enabled me to concentrate on my research.

CONTENTS

ABSTRACT OF THE DISSERTATION	ii
ACKNOWLEDGEMENTS	iv
CONTENTS.....	vi
LIST OF TABLES	xi
LIST OF ILLUSTRATIONS	xiii
CHAPTER I. INTRODUCTION	1
1.1. Introduction of Polysaccharide-Protein/Polypeptide Complexes	1
1.1.1. Interactions in the Polysaccharide-Protein/Polypeptide Complexation	5
1.1.2. Factors that Affect the Interactions between Polysaccharides and Proteins/Polypeptides.....	8
1.1.3. Thermodynamics of Polysaccharide-Protein/Polypeptide Complexation.....	10
1.1.4. Application of the Polysaccharide-Protein/Polypeptide Complexes	12
1.2. Introduction of Pickering Emulsion	15
1.3. Introduction of Chitosan	18
1.4. Introduction of Caseinophosphopeptides	20
1.5. Introduction of Tea and Tea Polyphenols	22
1.5.1. Teas	22
1.5.2. Theaflavins and Their Bio-efficacies	24
1.5.3. Bioavailability of Theaflavins.....	30
CHAPTER II. CHARACTERIZATION OF CHITOSAN, CASEINOPHOSPHOPEPTIDES, AND THEAFLAVINS	33
2.1. Introduction.....	33
2.2. Materials and Methods.....	33
2.2.1. Materials	33
2.2.2. NMR Measurement.....	34
2.2.3. GPC-MALLS Measurement	34
2.2.4. Viscosity Measurement.....	34
2.2.5. LC-MS/MS of CPPs	35
2.2.6. ζ -potential Measurement.....	35
2.2.7. SAXS Measurements	35
2.2.8. Purification of TFs	36
2.2.9. HPLC Analysis of TFs.....	36
2.3. Results and Discussion	37

2.3.1.	DD and Mw of CS	37
2.3.2.	Viscosity Measurement.....	38
2.3.3.	SAXS of CS	39
2.3.4.	LC-MS/MS of CPPs	40
2.3.5.	ζ-Potential Measurement.....	44
2.3.6.	SAXS of CPPs	44
2.3.7.	Purification of Theaflavins.....	47
2.4.	Conclusions.....	49
CHAPTER III. ASSEMBLY AND CHARACTERIZATION OF THE CHITOSAN-CASEINOPHOSPHOPEPTIDES NANOCOMPLEXES.....		50
3.1.	Abstract.....	50
3.2.	Introduction.....	50
3.3.	Materials and Methods.....	51
3.3.1.	Materials	51
3.3.2.	Turbidimetric Titration	51
3.3.3.	Preparation and Characterization of the CS-CPPs Nanocomplexes	52
3.3.4.	SAXS and USAXS Measurements	52
3.4.	Results and Discussion	53
3.4.1.	Turbidimetric Titration	53
3.4.2.	Characterization of the CS-CPPs Nanocomplexes	60
3.4.3.	SAXS and USAXS Measurements	62
3.5.	Conclusions.....	65
CHAPTER IV. INVESTIGATION OF THE INTERACTIONS BETWEEN CASEINOPHOSPHOPEPTIDES AND THEAFLAVIN-3,3'-DIGALLATE		66
4.1.	Abstract.....	66
4.2.	Introduction.....	66
4.3.	Materials and Methods.....	67
4.3.1.	Materials	67
4.3.2.	Fluorescence Quenching.....	67
4.3.3.	CD Spectra.....	68
4.3.4.	SAXS Measurement.....	68
4.3.5.	QCM-D Measurement.....	69
4.4.	Results and Discussion	70
4.4.1.	Fluorescence Quenching.....	70

4.4.2.	CD Spectra.....	75
4.4.3.	SAXS Measurement.....	76
4.4.4.	QCM-D Study.....	78
4.5.	Conclusions.....	83
CHAPTER V. ENCAPSULATION OF THEAFLAVIN-3,3'-DIGALLATE IN THE CHITOSAN-CASEINOPHOSHOPEPTIDES NANOCOMPLEX		85
5.1.	Abstract.....	85
5.2.	Introduction.....	85
5.3.	Materials and Methods.....	86
5.3.1.	Materials	86
5.3.2.	Encapsulate TF-3 in the CS-CPPs Nanocomplex	87
5.3.3.	Evaluation of Cytotoxicity.....	88
5.3.4.	Caco-2 Transport Experiment.....	88
5.4.	Results and Discussion	90
5.4.1.	Characterization of the CS-CPPs Nanocomplexes Encapsulated with TF-3	90
5.4.2.	Evaluation of Cytotoxicity.....	93
5.4.3.	Caco-2 Transport Experiment.....	96
5.5.	Conclusions.....	97
CHAPTER VI. ENHANCING INTESTINAL PERMEABILITY OF THEAFLAVIN-3,3'-DIGALLATE BY GENIPIN CROSSLINKED CHITOSAN-CASEINOPHOSHOPEPTIDES NANOCOMPLEXES		98
6.1.	Abstract.....	98
6.2.	Introduction.....	98
6.3.	Materials and Methods.....	99
6.3.1.	Materials	99
6.3.2.	Preparation and Characterization of the GCNs Encapsulated with TF-3.....	99
6.3.3.	Evaluation of Cytotoxicity.....	101
6.3.4.	Caco-2 Transport Experiment.....	101
6.4.	Results and Discussion	103
6.4.1.	UV-Vis Spectrum.....	103
6.4.2.	Characterization of the GCNs Encapsulated with TF-3.....	105
6.4.3.	Evaluation of the Cytotoxicity	114
6.4.4.	Evaluation of the Intestinal Permeability.....	115
6.5.	Conclusions.....	117

CHAPTER VII. FABRICATION AND CHARACTERIZATION OF PICKERING EMULSIONS STABILIZED BY THE CHITOSAN-CASEINOPHOSPHOPEPTIDES NANOCOMPLEXES	118
7.1. Abstract.....	118
7.2. Introduction.....	118
7.3. Materials and Methods.....	119
7.3.1. Materials	119
7.3.2. Preparation and Characterization of the CS-CPPs Nanocomplexes	119
7.3.3. Contact Angle Measurement.....	121
7.3.4. Surface Tension Measurement.....	122
7.3.5. Preparation and Characterization of the Pickering Emulsions.....	122
7.3.6. Visualization of the Pickering Emulsions.....	123
7.3.7. Rheological Measurement.....	123
7.4. Results and Discussion	123
7.4.1. Preparation and Characterization of the CS-CPPs Nanocomplexes	123
7.4.2. Characterization of the Pickering Emulsions.....	125
7.4.3. Rheological Properties	131
7.5. Conclusions.....	132
CHAPTER VIII. STABILIZATION OF PICKERING EMULSIONS BY THE GENIPIN CROSSLINKED CHITOSAN-CASEINOPHOSPHOPEPTIDES NANOCOMPLEXES: IMPACTS OF CROSSLINKING DURATION	134
8.1. Abstract.....	134
8.2. Introduction.....	135
8.3. Materials and Methods.....	136
8.3.1. Materials	136
8.3.2. Preparation and Characterization of the GCNs.....	137
8.3.3. Preparation and Characterization of the GCNs Stabilized Pickering Emulsions .	138
8.4. Results and Discussion	140
8.4.1. UV-Vis Measurements.....	140
8.4.2. Characterization of the GCNs.....	141
8.4.3. Characterization of the GCNs Stabilized Pickering Emulsions.....	147
8.5. Conclusions.....	155
CHAPTER IX. STABILIZATION OF PICKERING EMULSIONS BY THE GENIPIN CROSSLINKED CHITOSAN-CASEINOPHOSPHOPEPTIDES NANOCOMPLEXES:	

IMPACTS OF CROSSLINKER CONCENTRATION AND CROSSLINKING TEMPERATURE	157
9.1. Abstract.....	157
9.2. Introduction.....	158
9.3. Materials and Methods.....	158
9.3.1. Materials	158
9.3.2. Preparation and Characterization of the GCNs.....	158
9.3.3. Preparation and Characterization of the GCNs Stabilized Pickering Emulsions .	160
9.4. Results and Discussion	161
9.4.1. Characterization of the GCNs	161
9.4.2. Characterization of the Pickering Emulsions.....	165
9.5. Conclusions.....	177
CHAPTER X. ENHANCING ANTIOXIDANT CAPACITY OF PICKERING EMULSIONS BY INCORPORATING THEAFLAVIN-3,3'-DIGALLATE	179
10.1. Abstract.....	179
10.2. Introduction.....	179
10.3. Materials and Methods.....	181
10.3.1. Materials	181
10.3.2. Preparation and Characterization of the GTs.....	181
10.3.3. Preparation and Characterization of the Pickering Emulsions.....	183
10.3.4. Determination of the Oxidation Products	184
10.4. Results and Discussion	185
10.4.1. Characterization of the GTs	185
10.4.2. Characterization of the Pickering Emulsions.....	187
10.4.3. Determination of the Oxidation Products	190
10.5. Conclusions.....	194
SUMMARY AND FUTURE WORK	196
REFERENCES	198
APPENDIX: LIST OF ABBREVIATIONS	213

LIST OF TABLES

Table 1-1. Selected polysaccharide-protein/polypeptide complexes	4
Table 1-2. Interactions involved in polysaccharide-protein/polypeptide complexation	7
Table 2-1. Radius of gyration of CS at 0.25-1.25 mg/mL (0.01M NaCl)	40
Table 2-2. Sequence coverage of CPPs sample from LC-MS/MS.....	42
Table 2-3. Radius of gyration of CPPs.....	46
Table 3-1. Particle size, PDI, and ζ – potential of the complexes composed of different CS:CPPs at pH 6.....	61
Table 3-2. Radius of gyration of the CS-CPPs nanocomplexes composed of different CS:CPPs weight ratios.....	64
Table 4-1. Quenching constant (K_{SV}), binding constant (K_A), lifetime and thermodynamic parameters of TF-3 binding to CPPs.....	74
Table 5-1. Particle size, PDI, ζ – potential and encapsulation efficiency of the CS-CPPs nanocomplexes encapsulated with different concentrations of TF-3.....	91
Table 5-2. Radius of gyration of the CS-CPPs nanocomplexes (CS:CPPs=2:1) encapsulated with different amount of TF-3	93
Table 6-1. Radius of gyration of the CS-CPPs nanocomplexes crosslinked by different concentrations of genipin for different crosslinking durations	111
Table 6-2. Radius of gyration of the GCNs encapsulated with different concentrations of TF-3	113
Table 8-1. Radius of gyration of the GCNs with different crosslinking durations	146
Table 8-2. Creaming indexes of Pickering emulsions ($\Phi=0.5$) stabilized by different concentrations of GCNs with different crosslinking durations.....	150
Table 8-3. Creaming indexes of Pickering emulsions containing different fractions of oil (Φ) stabilized by 0.2 wt% GCNs with different crosslinking durations.....	151

Table 9-1. Creaming indexes (%) of the Pickering emulsions ($\Phi=0.5$, w/w) stabilized by 0.05 wt%-0.25 wt% of GCNs.....	167
Table 9-2. Droplet sizes (μm) of the Pickering emulsions ($\Phi=0.5$, w/w) stabilized by 0.05 wt%-0.25 wt% of GCNs.....	169
Table 9-3. Creaming indexes (%) of the Pickering emulsions containing different oil fractions	173
Table 9-4. Droplet size (μm) of the Pickering emulsions containing different oil fractions.....	174

LIST OF ILLUSTRATIONS

Figure 1-1. Typical phase diagram of complex coacervation between protein/polypeptide with anionic polysaccharide.....	9
Figure 1-2. Schematic representation of spherical particle localized at the oil-water interface of the O/W Pickering emulsion with the oil-water-particle three phase contact angle θ	16
Figure 1-3. Schematic illustration of O/W emulsions stabilized by protein-polysaccharide complexes using layer by layer method (left), electrostatically bonded complexes (middle), and chemically bonded complexes (conjugates, right).....	18
Figure 1-4. Chemical structures of the repeat units of (A) chitin (N-acetyl- β -D-glucosamine) and (B) chitosan (β -D-glucosamine).	19
Figure 1-5. Structures of catechins.....	24
Figure 1-6. Structures of theaflavins.....	25
Figure 2-1. CS ^1H NMR spectrum at 70°C	37
Figure 2-2. Specific viscosities of CS solutions (0.1–10 mg/mL) at pH 6 in the presence of 10 mM NaCl.	38
Figure 2-3. (A) Scattering curves and (B) fitting with eq. 2-4 and eq. 2-5 of 0.25-1.25 mg/mL CS (0.01M NaCl). The intensities were vertically shifted for clear visualization.	39
Figure 2-4. LC-MS/MS result of CPPs. The identified major sequences were marked. The lowercase letter P in red color represents phosphorylation and the number after peptide sequence indicates the amount of phosphorylation modifications.	43
Figure 2-5. ζ -potentials of 2 mg/mL CPPs solution at different pH.....	44
Figure 2-6. (A) Scattering profiles and (B) Kratky plot of 0.25–50 mg/mL CPPs solutions (containing 10 mM NaCl) at pH 6 (inset is the Guinier fitting of 30 mg/mL CPPs). (C) Scattering profiles and (D) Kratky plot of 1 mg/mL CPPs at pH 2-10 (containing 10 mM NaCl). The scattering intensities were vertically shifted for clear visualization.	47

Figure 2-7. HPLC results of (A) TF-1, (B) TF-2s, and (C) TF-3 after purification, and (D) mixture of TF-1 and TF-3 analyzed using simplified HPLC program.....	48
Figure 3-1. Turbidity change as a function of pH at CS:CPPs weight ratios of ● 0, ○ 0.125, ▼ 0.25, △ 0.5, ■ 1, □ 2, ◆ 3, ◇ 4, ▲ 5.....	54
Figure 3-2. Turbidity change as a function of pH at CS:CPPs = 0.25 in the presence of ● 0.01 M, ○ 0.05 M, ▼ 0.10 M, △ 0.15 M, ■ 0.3 M, □ 0.5 M, ◆ 1 M NaCl.....	56
Figure 3-3. Turbidity change as a function of pH at CS:CPPs = 0.25 in the presence of ● 0 M, ○ 1 M, ▼ 2 M urea.....	57
Figure 3-4. Turbidity change as a function of pH at CS:CPPs = 0.25 in the presence of ● 0%, ○ 10%, ▼ 30%, and △ 50% ethanol.....	58
Figure 3-5. Turbidity change as a function of pH at CS:CPPs = 0.25 at ● 20 °C, ○ 30 °C, ▼ 40 °C.....	59
Figure 3-6. Morphologies of the CS-CPPs complexes composed of (A) CS:CPPs = 0.5, (B) CS:CPPs = 2, and (C) CS:CPPs = 4.....	61
Figure 3-7. (A) Scattering profiles of the CS-CPPs nanocomplexes composed of 0.25 mg/mL CPPs and 0.25-1.25 mg/mL CS (CS:CPPs=1-5). The scattering curves were vertically shifted for clear visualization. Inset is the fitting (red solid line) of the scattering of the nanocomplex composed of CS:CPPs=1:1. (B) Kratky plot of the nanocomplexes composed of CS:CPPs=1-5.....	63
Figure 3-8. Schematic representation of the CS-CPPs nanocomplexes composed of different CS:CPPs weight ratios.....	64
Figure 4-1. Fluorescence emission spectra of CPPs excited at 295 nm in the presence of increasing concentrations of TF-3 at (A) 20°C, (B) 30°C, and (C) 40°C. The insets are the representative lifetime decay.....	71

Figure 4-2. (A) Far (190 – 260 nm)- and (B) near (260 – 320 nm)-UV CD spectra of 0.25 mg/mL CPPs associating with various concentrations of TF-3: (a) 0 mg/mL; (b) 0.125 mg/mL; (c) 0.0625 mg/mL; (d) 0.03125 mg/mL; (e) 0.015625 mg/mL. 76

Figure 4-3. (A) Small angle X-ray scattering profiles, (B) Kratky plot, (C) Guinier fitting at the region $qR_g < 1.3$, and (D) Debye-Bueche fitting of 2 mg/mL CPPs associated with 0-0.5 mg/mL TF-3. The curves in (A) (C) and (D) were vertically shifted for better visualization of the results. 78

Figure 4-4. Time-dependent (A) frequency shift and (B) energy dissipation at the third overtone upon adsorption of TF-3 onto the CPPs connected quartz crystal surface at different concentrations of TF-3: (a) 0.1 mg/mL; (b) 0.3 mg/mL; (c) 0.5 mg/mL; (d) 0.7 mg/mL; (e) 0.9 mg/mL. TF-3 solution was injected at t1 and the TF-3 adsorbed surface was rinsed with 0.15 M NaCl at t2. (C) Ratios of frequency shift to the corresponding overtone number ($\Delta F_n/n$) at different overtones (n = 3, 5, 7) upon 0.9 mg/mL TF-3 adsorbing on CPPs surface..... 81

Figure 4-5. (A) Mass per unit area and (B) thickness of adsorbed TF-3 on CPPs surface at different TF-3 concentration. Adsorption isotherm of TF-3 onto CPPs surface fitted by (C) Langmuir model and (D) Frundlich model..... 83

Figure 5-1. Morphologies of the CS-CPPs nanocomplexes encapsulated with TF-3 at TF-3:CPPs ratios of (A) 0, (B) 0.1 and (C) 1. 91

Figure 5-2. (A) Scattering profiles of the nanocomplexes encapsulated with different concentrations of TF-3. The scattering curves were vertically shifted for clear visualization. (B) Kratky plot of the nanocomplexes encapsulated with different concentrations of TF-3. 92

Figure 5-3. Caco-2 cell viability after treating with (A) the CS-CPPs nanocomplexes composed of different CS:CPPs weight ratios; (B) 0–50 μ M TF-3; and (C) the CS-CPPs nanocomplex encapsulated with 0–50 μ M TF-3. 95

Figure 5-4. Cumulative amount of transported TF-3 in pure form and encapsulated by the CS-CPPs nanocomplex 96

Figure 6-1. UV-Vis spectra of the CS-CPPs nanocomplexes crosslinked by (A) 0 mg/mL, (B) 0.5 mg/mL, and (C) 1mg/mL genipin for different crosslinking durations	104
Figure 6-2. Particle sizes of (A) the CS-CPPs nanocomplexes crosslinked by different concentrations of genipin (0-1 mg/mL) and different crosslinking durations (0-48h), and (B) GCNs encapsulated with different concentrations of TF-3 (TF-3:CPPs = 0-0.8, concentration of genipin was 0.5 mg/mL).	106
Figure 6-3. ζ -potentials of (A) CS-CPPs nanocomplexes crosslinked by different concentrations of genipin (0, 0.5, 1 mg/mL) for different crosslinking durations (0-48h), and (B) GCNs encapsulated with different concentrations of TF-3 (TF-3:CPPs=0-0.8, concentration of genipin was 0.5 mg/mL).	107
Figure 6-4. AFM images of the CS-CPPs nanocomplexes crosslinked by 0.5 mg/mL genipin for (A) 0h, (B) 8h, and (C) 24h, and crosslinked by 0.5 mg/mL genipin for 4 h and encapsulated with TF-3 with the TF-3:CPPs weight ratio of (D) 0.1, (E) 0.4, and (F) 0.8.	108
Figure 6-5. USAXS and SAXS of the CS-CPPs nanocomplexes crosslinked by different concentrations of genipin for (A) 4h, (B) 8h, (C) 16h, and (D) 24h (inset is the fitting of nanocomplex crosslinked by 0.1 mg/mL genipin for 24h). The scattering curves were vertically shifted for better visualization.	110
Figure 6-6. USAXS and SAXS of the nanocomplexes encapsulated with different amount of TF-3 and crosslinked by 0.5 mg/mL genipin for (A) 4h (inset is the fitting of TF-3:CPPs=0.1), (B) 8h, (C) 16h, and (D) 24h. The scattering curves are vertically shifted for better visualization.	112
Figure 6-7. Comparison of the particle sizes of the nanocomplexes crosslinked with 0 - 1 mg/mL genipin for (A) 4h, (B) 8h, (C) 16h, and (D) 24h at pH 6 and after exposing at pH 2 for 2h.	114
Figure 6-8. Viabilities of Caco-2 cell treated with GCNs crosslinked with 0.1-1 mg/mL genipin for (A) 4h, (B) 8h, (C) 16h, and (D) 24h at 25°C	115
Figure 6-9. Cumulative fraction of transported TF-3.....	116

Figure 7-1. AFM height images of 0.3 wt% (A) C1P1, (B) C2P1, and (C) C4P1. Correlation function fitting for mean size of 0.3 wt% (D) C1P1, (E) C2P1, and (F) C4P1.....	124
Figure 7-2. Representative contact angles of 8 mg/mL (A) C1P1, (B) C2P1, and (C) C4P1 at the air-water interface.....	125
Figure 7-3. Pickering emulsions stabilized by different concentrations of the CS-CPPs nanocomplexes, $\Phi = 0.5$ w/w. The scale bar is 100 μm	127
Figure 7-4. Fluorescence microscopy (overlay) images of Pickering emulsion formed by Nile red (1 μM)-stained MCT and FITC-labeled 0.25 wt% C1P1. The scale bar is 100 μm	127
Figure 7-5. Pickering emulsions of different oil fractions ($\Phi = 0.2-0.8$ w/w) stabilized by (A) 0.15 wt% C1P1, (B) 0.15 wt% C2P1, (C) 0.15 wt% C4P1, and (D) 0.25 wt% C1P1. The scale bar is 100 μm	128
Figure 7-6. pH stability of Pickering emulsions stabilized by the CS-CPPs nanocomplexes, $\Phi = 0.5$ w/w. The scale bar is 100 μm	130
Figure 7-7. Stability of CS-CPPs nanocomplexes stabilized Pickering emulsions against ionic strength change, $\Phi = 0.5$ w/w. The scale bar is 100 μm	131
Figure 7-8. Frequency sweep of Pickering emulsions stabilized by (A) 0.15 wt% C1P1, (B) 0.15 wt% C2P1, (C) 0.15 wt% C4P1, (D) 0.25 wt% C1P1, and (E) 0.5 wt% C1P1.	132
Figure 8-1. UV-Vis spectra of GCNs with different crosslinking durations.....	141
Figure 8-2. (A) Particle sizes (inset is an example of auto correlation function fitting of GCN crosslinked for 8h) and (B) ζ -potentials of GCNs with different crosslinking durations.	143
Figure 8-3. (A) Contact angles and (B) surface tensions of GCNs with different crosslinking durations.....	144
Figure 8-4. AFM height images of GCNs with (A) 0h, (B) 2h, (C) 4h, (D) 8h, (E) 16h, and (F) 24h reaction.....	145
Figure 8-5. (A) Scattering profiles and (B) fitting (black solid line) of the GCNs with different crosslinking durations. The scattering intensities were vertically shifted for clear visualization.	147

Figure 8-6. Macroscopic and microscopic images of Pickering emulsions ($\Phi=0.5$ w/w) stabilized by GCNs (4h reaction) and emulsion droplet size distribution fitting	148
Figure 8-7. Droplet sizes of Pickering emulsions ($\Phi=0.5$ w/w) stabilized by GCNs with different crosslinking durations at different concentrations	149
Figure 8-8. Microscopic images of Pickering emulsions containing different fractions of oil ($\Phi=0.2-0.6$ w/w) stabilized by 0.2 wt% GCNs with different crosslinking durations.....	151
Figure 8-9. Fluorescence image of GCNs stabilized Pickering emulsion. Inset is the fluorescence emission spectrum of GCNs excited at 550 nm. Emission wavelength was recorded from 610-800 nm	152
Figure 8-10. Droplet sizes of Pickering emulsions ($\Phi=0.5$ w/w) stabilized by 0.25 wt% GCNs with different crosslinking durations (4, 8, 16, 24h) after 24h storage at different (A) pH and (B) ionic strength.....	154
Figure 8-11. (A) Storage modulus G' , loss modulus G'' and (B) complex viscosity η^* of Pickering emulsions ($\Phi=0.5$ w/w) stabilized by 0.25 wt% GCNs with different crosslinking durations	155
Figure 9-1. Particle sizes of the CS-CPPs nanocomplexes crosslinked by 0.1 mg/mL, 0.5 mg/mL, and 1 mg/mL genipin at 30°C, 40°C, and 50°C for 4h. Inset is the fitting (red line) of the auto-correlation function of the CS-CPPs nanocomplexes crosslinked by 0.1 mg/mL genipin at 40°C.	162
Figure 9-2. ζ -potentials of the CS-CPPs nanocomplexes crosslinked by 0.1 mg/mL, 0.5 mg/mL, and 1 mg/mL genipin at 30°C, 40°C, and 50°C for 4h.....	163
Figure 9-3. Contact angles of Milli-Q water on GCNs film.	164
Figure 9-4. AFM images of (A) GCNs1, (B) GCNs5, and (C) GCNs10 crosslinked at 40°C for 4h, and GCNs5 crosslinked at (D) 30°C, (E) 40°C, and (F) 50°C for 4h.....	165
Figure 9-5. Macro- and micro-scopic images of Pickering emulsions ($\Phi=0.5$, w/w) stabilized by 0.05 wt%- 0.25 wt% of GCNs. The scale is 100 μm	166

Figure 9-6. Size distribution fitting of the Pickering emulsions stabilized by (A) 0.05 wt%, (B) 0.15 wt%, and (C) 0.25 wt% of GCNs1 crosslinked at 40°C; 0.25 wt% (D) GCNs 1, (E) GCNs5, and (F) GCNs10 crosslinked at 40°C; and 0.25 wt% GCNs5 crosslinked at (G) 30°C, (H) 40°C, and (I) 50°C.	170
Figure 9-7. Droplet sizes of Pickering emulsions ($\Phi = 0.5$, w/w) stabilized by 0.25 wt% GCNs crosslinked at different conditions. The diameter of the balls represents their relative size distribution.	171
Figure 9-8. Macro- and micro-scopic images of Pickering emulsions ($\Phi = 0.3-0.7$ w/w) stabilized by 0.15 wt% GCNs. The scale is 100 μm	172
Figure 9-9. Size distribution fitting of the Pickering emulsions containing different oil fractions ($\Phi = 0.3-0.7$ w/w) stabilized by 0.15 wt% GCNs1.	173
Figure 9-10. Microscopic images of the fluorescence labeled Pickering emulsions ($\Phi=0.3$, w/w) stabilized by 0.15 wt% GCNs. The green fluorescence is the coumarin 6 labeled MCT. The red fluorescence is the GCNs. The scale is 100 μm	175
Figure 9-11. Storage modulus G' and loss modulus G'' of the Pickering emulsions ($\Phi = 0.7$, w/w) stabilized by 0.15 wt% GCNs crosslinked at (A) 30°C, (B) 40°C, and (C) 50°C. Complex viscosity η^* of the Pickering emulsions ($\Phi = 0.7$, w/w) stabilized by 0.15 wt% GCNs crosslinked at (D) 30°C, (E) 40°C, and (F) 50°C.	177
Figure 10-1. Particle sizes of GT0, GT1, GT2, and GT4.	185
Figure 10-2. ζ -potentials of GT0, GT1, GT2, and GT4.	186
Figure 10-3. AFM height images of (A) GT0, (B) GT1, (C) GT2, and (D) GT4.	187
Figure 10-4. Macroscopic and microscopic images and size distribution of the Pickering emulsions ($\Phi=0.7$, w/w) stabilized by 0.15 wt% (A) GT0, (B) GT1, (C) GT2, and (D) GT4. The scale bar is 100 μm	188
Figure 10-5. Microscopic images of fluorescence labeled Pickering emulsions ($\Phi=0.7$, w/w) stabilized by 0.15 wt% (A) GT0, (B) GT1, (C) GT2, and (D) GT4. The scale bar is 100 μm	189

Figure 10-6. (A) Storage moduli G' and loss moduli G'' and (B) complex viscosities η^* of the Pickering emulsions ($\Phi=0.7$, w/w) stabilized by 0.15 wt% GT0, GT1, GT2, and GT4..... 190

Figure 10-7. Hydroperoxide production in (A) oil-water mixture, conventional emulsion emulsified by tween 80, and Pickering emulsions stabilized by GT0; (B) Pickering emulsions stabilized by 0.15 wt% GT0, GT1, GT2, and GT4; (C) Pickering emulsions with TF-3 located in the oil phase, oil-water interface, and water phase. The oil to water weight ratio of all samples was 7:3. 193

CHAPTER I. INTRODUCTION

As of submission of this dissertation, part of the contents in this chapter has been written as two review papers in the titles of “Molecular Association Between Proteins/Polypeptides, Polysaccharides, and Polyphenols: Mechanisms, Biological Relevance, and Applications” and “Engineering Pickering Emulsions Using Protein/Polysaccharide Complexes” which are ready for submission.

1.1. Introduction of Polysaccharide-Protein/Polypeptide Complexes

Polysaccharides and proteins/polypeptides are important biomolecules in foods. Polysaccharides are the polymeric carbohydrates composed of glycosyl units (commonly much larger than 20 units¹), which are connected by glycosidic linkages. Based on the conformation and charge, food polysaccharides can be generally classified into four groups, which are linear neutral polysaccharides (cellulose, amylose, chitin, guar gum, and locust bean gum, *etc*), linear charged polysaccharides (pectin, carrageenan, chitosan, and xanthan gum, *etc*), branched neutral polysaccharides (amylopectin, and glycogen, *etc*), and branched charged polysaccharides (gum Arabic, *etc*). Polysaccharides are commonly used in food industry as thickening or gelling agents. In addition to the traditional applications, polysaccharides are also applied in drug delivery², tissue engineering^{3, 4}, and biofuel⁵, *etc*. The non-digestible oligo- and polysaccharides, also known as dietary fibers attracted people’s attention in the past decades because epidemiological studies revealed that consumption of dietary fibers were inversely associated with human chronic diseases such as cardiovascular diseases^{6, 7}. Moreover, as important prebiotics, dietary fibers can modulate the profiles of human gut microbiota^{8, 9}. The metabolites of dietary fibers produced by gut microbiota fermentation also exhibited health promotion effects⁹.

Proteins are made up of amino acid residues linked by the peptide bonds. They are vital compositions of organisms and are essential for diverse biological functions such as transportation,

enzymatic catalysis, cell signaling, immune response, and support of structures, *etc.* The food proteins can be classified based on their source (animal proteins *e.g.* β -lactoglobulin, and plant proteins *e.g.* zein), shape (globular proteins *e.g.* lysozyme, and fibrous proteins *e.g.* collagen), solubility (water soluble proteins *e.g.* β -lactoglobulin, and water insoluble proteins *e.g.* zein), and composition (homoproteins or simple proteins *e.g.* albumins, and heteroproteins or conjugated proteins *e.g.* glycoproteins). Proteins exist in foods as important nutrients and building blocks of the food matrix. They attribute to the sensory properties of foods such as texture, viscosity, color, flavor, and emulsification¹. Polypeptides are the hydrolytes of proteins. They occur in different types of foods¹⁰. Some polypeptides possess bioactive functionalities such as antioxidative, antimicrobial, antihypertensive, and mineral binding properties^{10, 11}.

Proteins/polypeptides and charged polysaccharides are polyelectrolytes. When polysaccharides and proteins/polypeptides are oppositely charged, they can associate with each other, giving rise to two phases with one phase concentrated in these biomolecules, and the other one phase depleted in these molecules. This phenomenon of phase separation that occurs when proteins/polypeptides associate with oppositely charged polysaccharides, which is referred to as the polysaccharide-protein/polypeptide complex coacervation was initiatively investigated by Bungenberg de Jong and Kruyt using the system of gum Arabic-gelatin in the early 20th century¹². Since then the polysaccharide-protein/polypeptide complex coacervates have been extensively studied using diverse binary polysaccharide-protein/polypeptide systems (Table 1-1)^{13, 14} with multiple techniques such as turbidimetric titration¹⁵⁻¹⁷, isothermal titration calorimetry (ITC)¹⁸⁻²⁰, differential scanning calorimetry (DSC)²¹⁻²³, light scattering^{17, 24, 25}, small angle X-ray Scattering (SAXS)/small angle neutron scattering (SANS)²⁶⁻³⁰, rheology^{23, 27, 31}, Raman spectroscopy^{32, 33}, Fourier transform infrared spectroscopy (FTIR)³⁴, capillary electrophoresis³⁵, and computer simulation^{36, 37}, *etc.* A series of theories have been developed to describe the complex coacervation^{13, 14, 38}.

The polysaccharide-protein/polypeptide complex coacervates will eventually settle/precipitate in a few days, while sometimes the complex coacervates can remain suspended (turbid liquid) for more than three weeks (incomplete or pseudo-coacervates) at some specific conditions (*e.g.* polymer stoichiometry, pH, and ionic strength)³⁹. These incomplete coacervates are usually in the form of particles with diameter of hundreds of nanometers, which are often used as encapsulation systems. In this dissertation, the general term “polysaccharide-protein/polypeptide complexes” will be used to describe both complete and incomplete coacervates.

Table 1-1. Selected polysaccharide-protein/polypeptide complexes

Polysaccharide	Protein/Polypeptide	Reference
Alginate	β -Lactoglobulin	Harnsilawat <i>et al.</i> ⁴⁰
Alginate	Bovine serum albumin	Zhao <i>et al.</i> ⁴¹
Alginate	Gelatin	Saravanan <i>et al.</i> ⁴²
κ -Carrageenan	β -Lactoglobulin	Croguennoc <i>et al.</i> ⁴³
κ -Carrageenan	Gelatin	Voron'ko <i>et al.</i> ⁴⁴
Carrageenan (mainly κ -)	Soy protein isolate	Molina Ortiz <i>et al.</i> ²²
ι -Carrageenan	Poly(L-lysine)	Girod <i>et al.</i> ⁴⁵
λ -Carrageenan	Whey protein	Weinbreck <i>et al.</i> ¹⁶
κ -, ι -, λ -Carrageenan and furcelleran	Gelatin-A	Jiang ⁴⁶
ι -, κ -Carrageenan	Bovine β -casein	Burova <i>et al.</i> ⁴⁷
Carboxymethyl cellulose	Whey proteins	Hill <i>et al.</i> ⁴⁸
Chitosan	α -Lactalbumin and β -lactoglobulin	Lee <i>et al.</i> ⁴⁹
Chitosan	Bovine serum albumin and human serum albumin	Bekale <i>et al.</i> ⁵⁰
Chitosan	Soybean protein isolate	Huang <i>et al.</i> ⁵¹
Chitosan	Whey protein isolate	Bastos <i>et al.</i> ⁵²
Dextran sulfate	Bovine serum albumin	Galazka <i>et al.</i> ⁵³
Gum Arabic	β -Lactoglobulin	Aberkane <i>et al.</i> ²⁰ Schmitt <i>et al.</i> ^{54, 55} Mekhloufi <i>et al.</i> ⁵⁶
Gum Arabic	Caseinate	Ye <i>et al.</i> ⁵⁷
Gum Arabic	Gelatin	Bungenberg de Jong <i>et al.</i> ⁵⁸
Gum Arabic	Pea globulin and α -gliadin	Chourpa <i>et al.</i> ³²
Gum Arabic	Pea protein isolate	Liu <i>et al.</i> ^{59, 60}
Gum Arabic	Whey Protein	Weinbreck <i>et al.</i> ¹⁷
Pectin	β -Lactoglobulin	Wang <i>et al.</i> ^{15, 26, 31} Girard <i>et al.</i> ^{19, 35, 61}
Pectin	Caseinate	Redigueri <i>et al.</i> ⁶²
Sugar beet pectin	Bovine serum albumin	Li <i>et al.</i> ¹⁸
Xanthan gum	Gelatin	Lii <i>et al.</i> ³⁴

1.1.1. Interactions in the Polysaccharide-Protein/Polypeptide Complexation

The interactions involved in formation of the polysaccharide-protein/polypeptide complexes are predominantly non-covalent and non-specific interactions such as electrostatic interactions, hydrogen bond, and hydrophobic interactions. Examples of these non-covalent interactions are listed in Table 1-2. Although not as common as the non-covalent interactions, covalent bonds sometimes occur through chemical reaction such as Maillard reaction. The polysaccharide-protein/polypeptide complexes connected through covalent bonds are usually referred to as the polysaccharide-protein/polypeptide conjugates, which will not be discussed in this part.

1.1.1.1. Electrostatic Interactions

Electrostatic interactions are the most common and important forces occurring in polysaccharide-protein/polypeptide complexation. Proteins/polypeptides and charged polysaccharides are polyelectrolytes. The charges on these biomolecules are determined by the environmental pH. The charges of proteins/polypeptides reverse at their isoelectric point (pI), which is the pH where the net charge of proteins/polypeptides is 0. Below pI, proteins/polypeptides are positively charged and above pI they are negatively charged. Most of the charged polysaccharides, such as pectin, alginate, carrageenan and gum Arabic are anionic because they carry anionic groups such as carboxyl group and/or sulfate group. Chitosan is a distinct polysaccharide that is naturally cationic due to protonation of the primary amine groups in acidic environment (pH < 6.3-6.4). Therefore, at a certain pH range where proteins/polypeptides and polysaccharides carry opposite net charges, these two types of biomolecules can interact through electrostatic attraction. The electrostatic interactions between charged polysaccharides and proteins/polypeptides can be expressed as eq. 1-1³¹

$$U = -\frac{Q_p}{2\epsilon} \left(\frac{Q_+}{R_+} e^{-R_+/R_d} - \frac{Q_-}{R_-} e^{-R_-/R_d} \right) \quad \text{eq. 1-1}$$

where U is the potential energy for the electrostatic interaction; Q_p is the number of charges of the polysaccharide segments that are associated with the protein/polypeptide molecules that contain Q_+ positive charges and Q_- negative charges; ϵ is the dielectric constant; R_+ is the average distance between the oppositely charged sites on proteins/polypeptides and polysaccharides; R_- is average distance between the like charged sites on proteins/polypeptides and polysaccharides; R_d is the Debye length.

1.1.1.2. Hydrogen Bond

Another important force existing in the polysaccharide-protein/polypeptide complexes is hydrogen bond. Hydrogen bonds occur between molecules carrying hydrogen donors (H) and hydrogen acceptors (*i.e.* N, O, F). Proteins/polypeptides contain large amount of hydrogen donors and acceptors, which can form intramolecular hydrogen bonds to maintain their secondary structures. Polysaccharides contain hydroxyl groups, carbonyl groups, which can form hydrogen bonds with proteins/polypeptides.

1.1.1.3. Hydrophobic Interactions

Hydrophobic interactions are entropy-driven¹³. Formation of hydrophobic interactions within the polysaccharide-protein/polypeptide complex is usually associated with conformational change of the biomacromolecules to facilitate association between the hydrophobic groups.

Owing to these multiple types of interactions, the proteins/polypeptides and polysaccharides start to bind together and expand not only through electrostatic attraction but also through protein aggregation and polysaccharide entanglement³⁷. With the help of SANS, the conformation and composition of each component inside of the complexes can be obtained, which would be beneficial to understand the process of complexation³⁰.

Table 1-2. Interactions involved in polysaccharide-protein/polypeptide complexation

Polysaccharide	Protein/Polypeptide	Interactions	Methods	Reference
Alginate	β -lactoglobulin	Electrostatic interaction	ITC, turbidity measurement	Harnsilawat <i>et al.</i> ⁴⁰
Carrageenan (mainly κ -)	Soy protein isolate	Electrostatic interaction, hydrophobic interaction	Solubility, surface hydrophobicity measurements	Molina Ortiz <i>et al.</i> ²²
λ -carrageenan	Whey proteins	Electrostatic interaction	Turbidimetric titration	Weinbreck <i>et al.</i> ¹⁶
Chitosan	β -lactoglobulin	Electrostatic interaction	ITC, electrophoretic mobility, turbidity, solubility measurements	Guzey <i>et al.</i> ⁶³
Chitosan	Bovine serum albumin and human serum albumin	Hydrophobic interaction, electrostatic interaction	Fluorescence quenching,	Bekale <i>et al.</i> ⁵⁰
Gum Arabic	β -lactoglobulin	Electrostatic interaction, hydrophobic interaction	ITC	Aberkane <i>et al.</i> ²⁰
Gum Arabic	Caseinate	Electrostatic interaction	Turbidimetric titration	Ye <i>et al.</i> ⁵⁷
Gum Arabic	Pea globulin and α -gliadin	Electrostatic interaction, hydrogen bond	Raman microspectroscopy	Chourpa <i>et al.</i> ³²
Gum Arabic	Whey proteins	Electrostatic interaction	Turbidimetric titration	Weinbreck <i>et al.</i> ¹⁷
Pectin	β -lactoglobulin	Electrostatic interaction, hydrogen bond	Potentiometric titration, ultrafiltration	Girard <i>et al.</i> ⁶¹
Pectin (low methoxy)	Gelatin	Electrostatic interaction, hydrogen bond, van der Waals, dipolar	DSC, rheology	Gilsenan <i>et al.</i> ²³
Pectin	Whey protein isolate	Electrostatic interaction, hydrogen bond	Raman spectroscopy	Zhang <i>et al.</i> ³³
Xanthan gum	Gelatin	Electrostatic interaction, hydrogen bond, hydrophobic interaction	Solubility test, thermogravimetric and differential thermogravimetric analyses, FTIR	Lii <i>et al.</i> ³⁴

1.1.2. Factors that Affect the Interactions between Polysaccharides and Proteins/Polypeptides

Multiple environmental factors (pH, ionic strength, temperature, shear, and pressure, *etc.*) and structural characteristics (polymer weight ratio, concentration, chain length, chain flexibility, and chain charge density and distribution, *etc.*) can regulate the magnitude of the non-covalent interactions involved in complexation between polysaccharides and proteins/polypeptides.

1.1.2.1. pH

pH is probably the most important factor for complexation between polysaccharides and proteins/polypeptides because the charges on both proteins/polypeptides and polysaccharides are determined by the environment pH. As discussed in section 1.1.1.1, most of the charged polysaccharides carry negative charges when pH is higher than their pK_A except for chitosan which is positively charged when the pH is below its pK_A . Proteins/polypeptides carry positive and negative net charges when pH is below and above their pI, respectively. The charge density is not evenly distributed on the proteins/polypeptides due to heterogeneity of the amino acids, which even create some local patches carrying charges opposite to the net charge. These features give rise to three critical pH values that characterize the process of polysaccharide-protein/polypeptide complexation (Figure 1-1). Polysaccharides and proteins/polypeptides carrying same sign of net charges start to form soluble complexes at pH_c where oppositely charged patches on proteins/polypeptides electrostatically connect to polysaccharides. Therefore, pH_c is higher and lower than the pI of the proteins/polypeptides when associating with anionic and cationic polysaccharides, respectively. Insoluble complexes start to form at $pH_{\phi 1}$ where polysaccharides and proteins/polypeptides start to carry opposite sign of net charges. It is also the start point of phase separation. The complexes dissociate at $pH_{\phi 2}$ due to neutralization of polysaccharides. The maximum yield of complexes is obtained at the pH where proteins/polypeptides and

polysaccharides carry equal amount of opposite charges, *i.e.* the net charge of the complexes is zero.

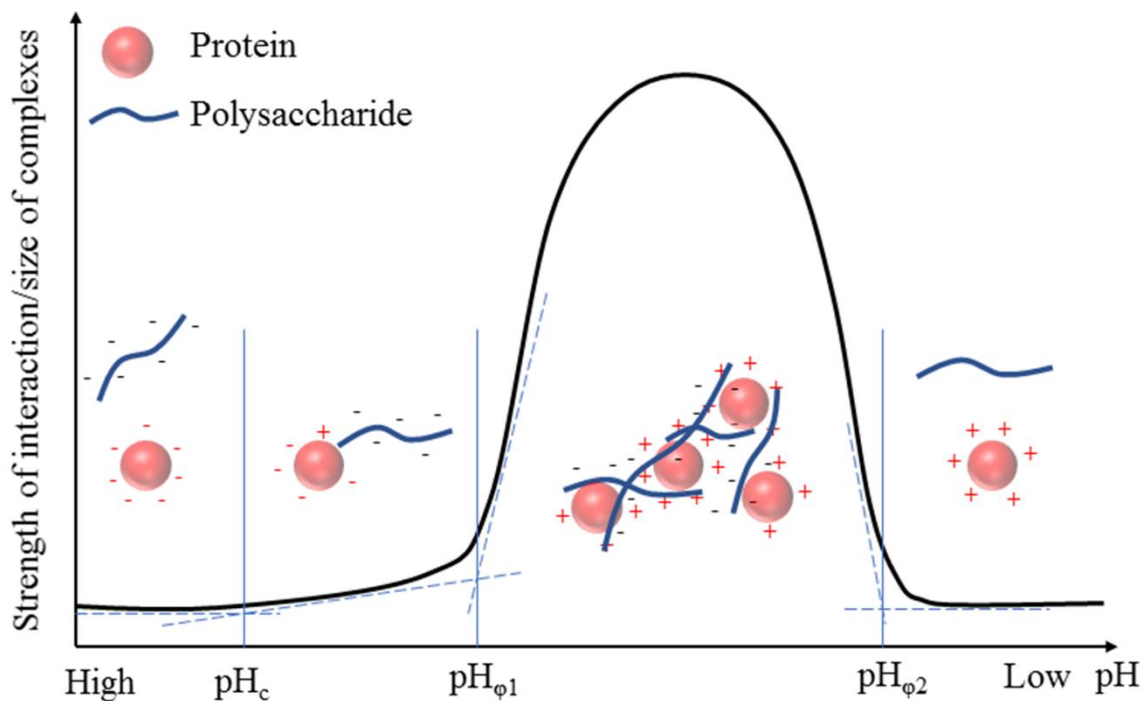


Figure 1-1. Typical phase diagram of complex coacervation between protein/polypeptide with anionic polysaccharide

It is necessary to keep in mind that even at the pH region where polysaccharides are neutral, complexation between proteins/polypeptides and polysaccharides still occurs through hydrogen bonding and hydrophobic interactions between molecules close by³⁶.

1.1.2.2. Ionic Strength

Ionic strength also regulates the affinity between polysaccharides and proteins/polypeptides since it influences the charge densities of proteins/polypeptides and polysaccharides. It is well known that at high concentration, NaCl can screen the charges on both proteins/polypeptides and polysaccharides, and therefore decrease the strength of their electrostatic interaction. Conversely,

at low concentration the screening effect is not notable. Low concentration of NaCl can even enhance formation of the polysaccharide-protein complex coacervates^{16, 17}. Divalent ions such as Ca^{2+} may bridge the proteins/polypeptides and polysaccharides even when they are all negatively charged¹⁶. Ionic strength also alters pH_c , pH_{ϕ_1} , and pH_{ϕ_2} as these critical pH values are directly related to charge density^{15, 64}.

1.1.2.3. Temperature

Temperature is another important factor that determines the strength of interactions between polysaccharides and proteins/polypeptides. Usually low temperature promotes formation of hydrogen bond, while high temperature facilitates hydrophobic interactions and covalent bonding¹³.

Controlled thermal treatment can be used to generate polysaccharide-protein/polypeptide nano- and micro-particles. The first way is to heat the proteins/polypeptides to the temperature above their thermal denaturation temperature followed by complexing with charged polysaccharides. The dimension of this type of complexes is strongly dependent on the proteins/polypeptides after thermal denaturation. The second way is to heat the already formed polysaccharide-protein/polypeptide complexes to the temperature above the thermal denaturation temperature of the protein/polypeptide. The dimension of the second type of particle is majorly determined by the characters of the complexes before heat treatment⁶⁵. Jones *et al.* proposed that the proteins in the complexes formed at the pH close to their pI can be detached due to disruption of the electrostatic interaction by heat. The detached proteins then aggregate followed by complexing with polysaccharides, forming a core-shell structure with the proteins as the core and the polysaccharides as the shell⁶⁵.

1.1.3. Thermodynamics of Polysaccharide-Protein/Polypeptide Complexation

The phase separation phenomenon of mixing two polymers in solution stems from either thermodynamic incompatibility (segregative phase separation) or associative phase separation,

depending on the affinity between two polymers and solvent⁶⁶. Obviously, complexation between oppositely charged polysaccharides and proteins/polypeptides belongs to the secondary scenario. The free energy of mixing of two polymers is determined by the thermodynamic equation

$$\Delta G = \Delta H - T\Delta S \quad \text{eq. 1-2}$$

where ΔG is the Gibbs free energy; ΔH and ΔS are the enthalpy and entropy changes, respectively. T is the absolute temperature (K). The thermodynamics of mixing two oppositely charged polymers is more complicated. The free energy change is given by⁶⁷

$$\Delta G = \Delta G_{\text{Flory-Huggins}}(\text{Entropy}) + \Delta G_{\chi}(\text{VannLaar Chain Segment Interactions}) + \Delta G_{\text{elect}}(\text{Electrostatic Interactions}) + \Delta G_{\gamma}(\text{Other factors}) \quad \text{eq. 1-3}$$

Complexation between oppositely charged polysaccharides and proteins/polypeptides is a spontaneous process because of decrease of Gibbs free energy, *i.e.* $\Delta G < 0$. Decrease of free energy is a balance of favorable enthalpic contribution (electrostatic and non-coulombic interactions) and entropic contribution (release of counterions and water molecules) and unfavorable enthalpic (desolvation of polar groups) and entropic (ordering of macromolecules and water molecules) contributions^{20, 30, 68-70}.

Experiments using ITC revealed that complexation between oppositely charged polysaccharides and proteins/polypeptides may involve more than one thermodynamic stage. Complexation between gum Arabic and β -lactoglobulin at pH 4.2 was an enthalpy driven followed by an entropy driven process at 25-35°C. At 45-50°C, however, this binding process displayed an entropy driven and then enthalpy driven manner²⁰. Girard *et al.* reported that at 22°C and pH 4, formation of soluble complexes between pectin (low- and high-methoxyl) and β -lactoglobulin was enthalpy driven, while both enthalpy and entropy contributed to formation of low- and high-methoxyl pectin- β -lactoglobulin insoluble complexes¹⁹. Since complexation between oppositely charged polysaccharides and proteins/polypeptides is a pH-dependent process, the thermodynamics

involved could also be affected by pH. Harnsilawat and co-workers found complexation between sodium alginate and β -lactoglobulin showed transition from exothermic to endothermic to negligible enthalpies due to changes of charges on both sodium alginate and β -lactoglobulin as the environmental pH increased from pH 3 to pH 7⁴⁰.

1.1.4. Application of the Polysaccharide-Protein/Polypeptide Complexes

Owing to the advantages such as non-involvement of chemical reactions during preparation as well as the adjustable size, morphology and rheological properties, the polysaccharide-protein/polypeptide complexes have been widely applied in the food science, nutraceutical, pharmaceutical, and cosmetic areas.

One application of the polysaccharide-protein/polypeptide complexes is to use polysaccharides to delivery proteins. Multiple polysaccharides for example chitosan and its derivatives were applied to encapsulate and delivery insulin^{2, 71-77}, which showed pronounced hypoglycemic effect.

In food industry, the polysaccharide-protein complexes are widely applied in encapsulating flavors⁷⁸. More applications such as separation and purification of proteins, immobilization of enzymes⁷⁹, inhibition of protein aggregation and denaturation³⁹ through complexation with polysaccharides were also reported. The polysaccharide-protein/polypeptide complexes are also potential fat replacers to reduce the fat intake, which would be beneficial for preventing obesity-related disorders¹³. Nowadays, the coacervate-based materials are used in tissue engineering^{80, 81}, which is a promising application of these biocompatible materials.

Herein two applications of the polysaccharide-protein/polypeptide complexes are reviewed. One is to directly encapsulate nutraceuticals. The other one is using the complexes to stabilize Pickering emulsions, which may be further used to encapsulate nutraceuticals.

1.1.4.1. Using Polysaccharide-Protein/Polypeptide Complexes to Directly Encapsulate Nutraceuticals

An important application of the polysaccharide-protein/polypeptide complexes is to encapsulate nutraceuticals.

Zimet *et al.* reported that DHA encapsulated in the low methoxyl pectin- β -lactoglobulin complex had better stability against degradation during accelerated shelf life stress test⁸². Similarly, the oxidative stability of tuna oil which is rich in ω -3 fatty acids was significantly improved when co-encapsulated with probiotic bacteria in the gum Arabic-whey protein isolate complex⁸³. Various vitamins including water-soluble and water-insoluble vitamins (*e.g.* D2, D3, and α -tocopherol) were encapsulated in multiple polysaccharide-protein complexes. These systems showed higher encapsulation efficiency than using a single biopolymer. They also improved stability and controlled release profile of the vitamins in the simulated gastrointestinal tract (GIT) conditions⁸⁴⁻⁸⁸.

As important nutraceuticals, polyphenols are encapsulated in the polysaccharide-protein/polypeptide complexes to overcome their defects such as low stability and low bioavailability. Xiao *et al.* encapsulated curcumin in kafirin particle and carboxymethyl chitosan-kafirin complex. Compared to using kafirin alone as the encapsulation vehicle, they found the carboxymethyl chitosan-kafirin complex provided better protection for curcumin against UV degradation. Moreover, both encapsulation vehicles facilitated cellular uptake of curcumin by Caco-2 cells with carboxymethyl chitosan-kafirin complex being more efficient for internalization of curcumin into the Caco-2 cells⁸⁹. In another study, Robert *et al.* used maltodextrin-soybean protein isolate complex and inulin-soybean protein isolate complex to encapsulate the polyphenols from cactus pear pulp. These two complexes systems had similar encapsulation efficiency for the polyphenols, meanwhile both of them had higher encapsulation efficiency than using soybean protein isolate alone⁹⁰.

1.1.4.2. Using Polysaccharide-Protein/Polypeptide Complexes to Stabilize Pickering Emulsions and Encapsulate Nutraceuticals

Utilizing polysaccharide-protein/polypeptide complexes to stabilize Pickering emulsions is an emerging research area. Most of the already published work on Pickering emulsion was investigated using the inorganic and non-food grade organic particles such as clay, silica, and latex, *etc.* (details described in section 1.2). Up to now, there are only limited amount of literatures on this area that were carried out using the polysaccharide-protein/polypeptide complexes.

Pickering emulsions stabilized by polysaccharide-protein/polypeptide complexes can be further used to encapsulate nutraceuticals. This application can achieve the goal of encapsulating lipophilic and hydrophilic nutraceuticals simultaneously. The lipophilic nutraceuticals can be encapsulated in the oil phase. Both hydrophilic and hydrophobic nutraceuticals can be encapsulated in the polysaccharide-protein/polypeptide complexes, which are anchored at the oil-water interface. However, Study on this area is still at the initial stage and the number of publications is scarce. Herein, the work of encapsulation of nutraceuticals in the Pickering emulsions stabilized not only by the polysaccharide-protein/polypeptide complexes but also inorganic and organic particles are reviewed since they share the same principles.

Tikekar and co-workers encapsulated curcumin in silica nanoparticle stabilized Pickering emulsion. They reported that the stability of encapsulated curcumin was significantly higher than the unencapsulated curcumin. The encapsulated curcumin showed limited release in simulated gastric environment while in simulated intestinal environment, most of curcumin was released⁹¹. The gelatin stabilized oil-in-water Pickering emulsion was investigated as the carrier of β -carotene. It was found that the release of β -carotene depended on the concentration of gelatin that was used to stabilize the emulsion. Higher concentration of gelatin hindered release of β -carotene⁹². In a recently published paper, curcumin was incorporated in the chitosan-zein complex, which was

further utilized to stabilize the Pickering emulsion. The authors found the antioxidant capacity was enhanced after curcumin was encapsulated. Compared to being encapsulated in the oil phase, curcumin encapsulated in the chitosan-zein complex had better antioxidative capacity⁹³. Curcumin was also encapsulated in the oil phase of Pickering emulsion stabilized by chitosan-tripolyphosphate nanoparticles. The stability of curcumin was improved after encapsulation and the control release profile of curcumin was better than in other delivery system⁹⁴.

In this dissertation, chitosan (section 1.3) was used as the cationic polysaccharide and caseinophosphopeptides (section 1.4) was used as the anionic polypeptides to fabricate a novel polysaccharide-polypeptides complex. The chitosan-caseinophosphopeptides nanocomplexes were used to encapsulate theaflavin-3,3'-digallate and stabilize Pickering emulsions.

1.2. Introduction of Pickering Emulsion

Emulsions are referred to as the dispersion of two immiscible liquids, *e.g.* water and oil that are emulsified by emulsifiers, which can reduce the surface tension. The conventional emulsifiers include amphiphilic small molecules, proteins, and phospholipids. Emulsions are widely used in food, pharmaceutical, and cosmetic areas. Recently, the Pickering emulsion which is stabilized by solid particles received extensive attention due to its excellent stability against coalescence and Ostwald ripening^{95, 96}. In addition, the feature of emulsifiers-free during preparation makes it possible to avoid the adverse effects that are associated with the emulsifiers^{97, 98}. Unlike the conventionally used emulsifiers which are necessarily amphiphilic, the particles for stabilizing Pickering emulsions are only required to be partially wetted by both phases⁹⁷.

The free energy E of detachment of a spherical particle from the interface can be expressed as:

$$E = \gamma\pi R^2(1 - |\cos \theta|)^2 \quad \text{eq. 1-4}$$

where γ is the oil-water interfacial tension; R is the radius of particle; θ is the oil-water-particle three phase contact angle. The desorption energy of a single particle (>10 nm) is thousand times of the kinetic energy of Brownian motion ($K_B T$, where K_B is the Boltzmann constant and T is the absolute temperature) as long as θ is not close to 0° or 180° . The adsorption of particles on the interface is therefore regarded as irreversibly⁹⁵.

The type of Pickering emulsion is determined by θ . The hydrophilic particles ($0^\circ \leq \theta < 90^\circ$) which are preferentially wetted by the water phase stabilize the oil-in-water (O/W) type Pickering emulsions (Figure 1-2), while the hydrophobic particles ($90^\circ < \theta \leq 180^\circ$) which are preferentially wetted by the oil phase stabilize the water-in-oil (W/O) type Pickering emulsions. If the particles are equally wetted by oil and water, the contact angle is 90° .

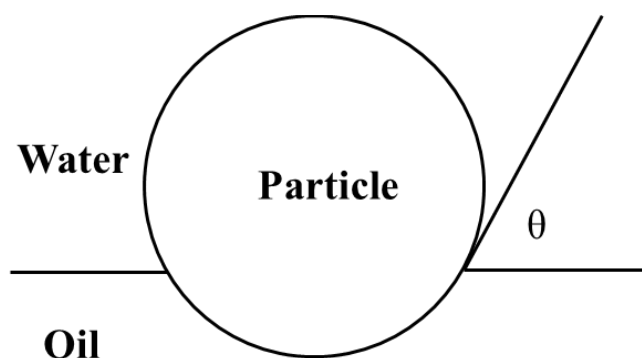


Figure 1-2. Schematic representation of spherical particle localized at the oil-water interface of the O/W Pickering emulsion with the oil-water-particle three phase contact angle θ .

Extensive work has been done on Pickering emulsions stabilized by inorganic and non-food grade organic particles, such as silica, clays, and latexes^{97, 99-101}. Recently, efforts have been made to explore the food-grade particles that can stabilize the Pickering emulsion. Most of these work so far was focused on either proteins¹⁰²⁻¹⁰⁴ or polysaccharides^{105, 106}, while using the polysaccharide-protein/polypeptide complexes as the Pickering stabilizers was relatively less reported.

Generally, there are three approaches to generate the polysaccharide-protein/polypeptide complex stabilized emulsions (Figure 1-3). The first way is to use proteins/polypeptides as the emulsifiers to stabilize the primary emulsions, then polysaccharides are coated on the protein/polypeptide shell as a secondary layer (layer by layer method). With rational design, more than two layers on the oil droplets can be achieved through electrostatic deposition^{107, 108}.

The second way is to prepare the polysaccharide-protein/polypeptide complexes through electrostatic attraction followed by using these already formed complexes to stabilize emulsions. Since the protein/polypeptide-polysaccharide complexes are generally insoluble particles, the yielding emulsions belong to Pickering emulsions.

Instead of using the electrostatically bonded complexes, the polysaccharide-protein/polypeptide complexes can also be chemically bonded through chemical reaction such as Maillard reaction. The chemically connected protein-polysaccharide complexes are referred to as polysaccharide-protein conjugates. These conjugates can also stabilize Pickering emulsions, which is the third method.

Among the limited publications in this area, the majority employed the first approach while the second and third approaches were scarce.

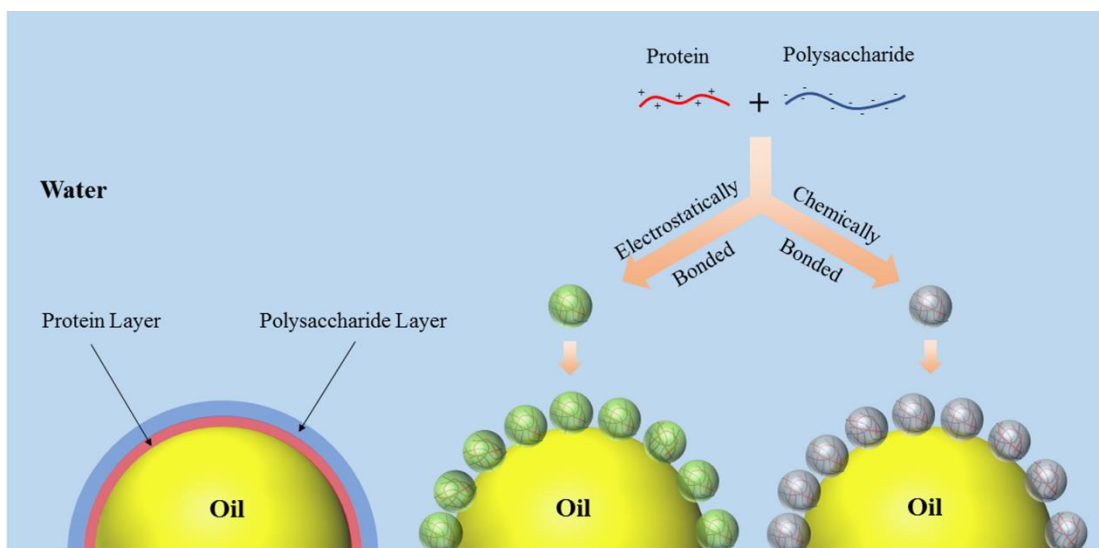


Figure 1-3. Schematic illustration of O/W emulsions stabilized by protein-polysaccharide complexes using layer by layer method (left), electrostatically bonded complexes (middle), and chemically bonded complexes (conjugates, right).

1.3. Introduction of Chitosan

Chitosan (CS, Figure 1-4B) is a biocompatible, biodegradable, and non-toxic polysaccharide deacetylated from chitin [β -(1 \rightarrow 4)-*N*-acetyl-D-glucosamine, Figure 1-4A], which is the second most abundant natural polymer in the world, just after cellulose¹⁰⁹. Molecular weight (Mw) and degree of deacetylation (DD) are two important factors that determine the physical and chemical properties of CS. CS can be dissolved in acidic environments when the primary amine groups (pKa \sim 6.3-6.4) on CS backbone are protonated by the acid. Usually, 1% acetic acid is used to dissolve CS. CS has diverse bioefficacies including antibacterial, antifungal, immunostimulatory activities¹¹⁰. The *in vivo* distribution, degradation, and elimination of CS are closely related to their Mw and DD. Lysozyme is considered as one of the most important enzymes that degrades CS, and gut is regarded as the primary site for CS digestion¹¹¹. The *in vivo* biodistribution of CS is not well demonstrated. It is generally believed that this process is Mw-, DD-, and formulation-dependent. Higher Mw may decrease the absorption of CS into bloodstream after oral administration. Liver is

an important organ of CS accumulation after intravenous administration¹¹¹. The *in vitro* toxicity of CS is also Mw- and DD-dependent. Schipper *et al.* found that CS with high DD showed Mw- and concentration-dependent cytotoxicity in Caco-2 cells, while at low DD, the toxicity was less pronounced. Kean *et al.* proposed that the toxicity of CS is correlated to the charge density¹¹¹. In an *in vivo* study, the LD₅₀ of CS was higher than 16 g/kg when orally administered to mice. This value is greater than sucrose¹¹⁰.

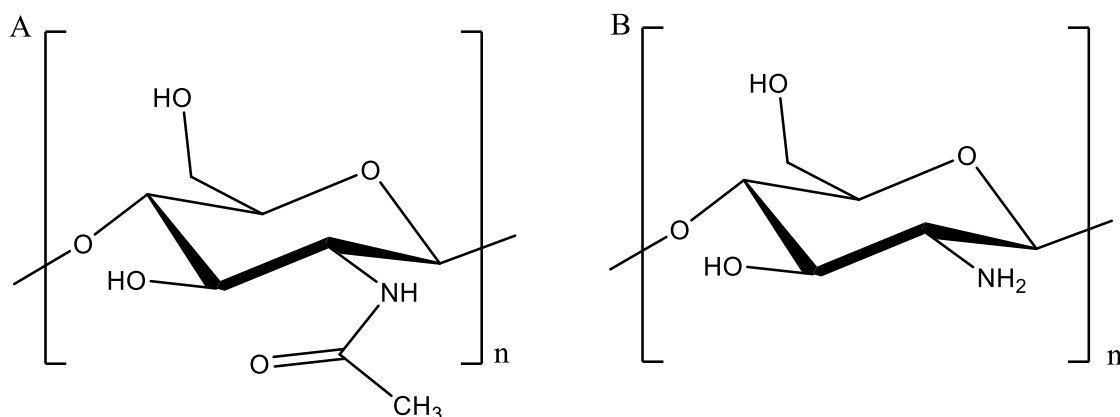


Figure 1-4. Chemical structures of the repeat units of (A) chitin (*N*-acetyl- β -D-glucosamine) and (B) chitosan (β -D-glucosamine).

CS has been widely applied in food, cosmetic, biomedical and pharmaceutical areas in different forms, including nanoparticles, microspheres, hydrogels, films, fibers and tablets¹¹². It has been approved for dietary applications in Japan, Italy, and Finland. The Food and Drug Administration (FDA) has approved the application of CS in wound dressings¹¹¹. CS derived from shrimp (notice number 000443) and *Aspergillus niger* (notice number 000397) received Generally Recognized as Safe (GRAS) status in the United States. The extensive application of CS as an oral route delivery carrier in food science and pharmaceuticals is due to its cationic nature that enables it to interact with the negatively charged sialic acid residues in mucus layer¹¹³. This remarkable mucoadhesive property can prolong the intestinal residence time, which extends absorption process of nutraceuticals and drugs. In addition, *in vitro* and *in vivo* studies demonstrated that CS is able to

transiently and reversibly open the tight junctions between small intestinal epithelial cells¹¹⁴. The tight junctions are composed of trans-membrane proteins (*e.g.* claudins, occludins, and junctional adhesion molecules (JAMs)) and cytoplasmic proteins (*e.g.* ZO-1, ZO-2, ZO-3, and cingulin)¹¹⁴. Tight junctions can selectively limit diffusion through paracellular route based on the molecule size and charge¹¹⁵. Studies revealed that regulating the redistribution and reconstruction of claudin-4, ZO-1, JAM-1, and occludin proteins were involved in the process of CS reversibly opening the tight junctions^{114, 116-119}. Moreover, CS nanoparticles and CS solution showed similar ability to open tight junction¹¹⁷. As an absorption enhancer, CS can facilitate both transcellular and paracellular transports of poorly absorbed nutraceuticals and drugs¹²⁰. Schipper *et al.* studied the permeability enhancing effects of CS with different Mw and DD for the model hydrophilic drugs ¹⁴C-mannitol and atenolol using Caco-2 monolayer model. They found that both Mw and DD can affect the kinetics of permeability enhancement^{121, 122}. These outstanding properties make CS an ideal building block of the polysaccharide-protein/polypeptide complexes to encapsulate nutraceuticals for oral delivery.

1.4. Introduction of Caseinophosphopeptides

Caseins are the most abundant milk proteins, constituting about 80% of the total milk proteins¹²³. Caseins are consisted of α 1-, α 2-, β -, and κ -casein, existing in proportions of 4:1:4:1 by weight in cow milk¹²⁴. The secondary and tertiary structures of caseins have been investigated for decades. However, the results are still under controversy¹²⁵. Caseins are rich in proline, which may interrupt the secondary structures, such as α -helix and β -sheet. Therefore, caseins were traditionally thought as lack of defined structures¹²⁶. However, some studies using instruments such as circular dichroism (CD) and FTIR revealed that the secondary structures actually exist in caseins^{127, 128}. Caseins, especially α s- and β -caseins are naturally occurred with different degree of phosphorylation on the seryl residues¹²⁹, which provides the binding site for calcium. Binding of calcium to these types of caseins can lead to precipitation. κ -casein is singly phosphorylated. Even

high concentrations of calcium do not precipitate this type of casein¹³⁰. A characteristic property of caseins (α s and β) is forming micelles in the presence of calcium phosphate with κ -casein coated on the surface, which helps to stabilize the casein micelles^{123, 130}. The opacity of milk is attributed to the presence of casein micelles¹³¹. Since caseins are natural proteins and have GRAS status, they have been widely used in developing delivery systems for drug/nutraceutical, including film coatings, hydrogels, floating beads, microparticles, micelles, and polysaccharide-casein complexes¹²⁴.

Caseinophosphopeptides (CPPs) are a group of phosphorylated bioactive polypeptides hydrolyzed from caseins. The composition of CPPs may vary with the origin of caseins, enzymes, and pH that are used during hydrolysis¹³²⁻¹³⁴. However, there is a common sequence, *i.e.* three phosphorylated seryl residues followed by two glutamic acid residues (SerP-SerP-SerP-Glu-Glu), appearing in α s1 (66-70)-, α s2 (8-12, 56-60)-, and β (17-21)-casein derived CPPs¹³⁵. CPPs have diverse bio-functionalities. The anionic nature of CPPs resulted from phosphorylation of seryl residues gives CPPs the ability to bind a range of metal ions, such as calcium, magnesium, iron, zinc, barium, chromium, nickel, cobalt, and selenium^{135, 136}. It was thought that CPPs could improve the bioavailability of calcium by preventing precipitation of calcium at alkaline pH, which is the pH of distal ileum¹³⁵. Ferraretto *et al.* found that CPPs increased uptake of calcium in human intestinal HT-29 cells¹³⁷. An early study reported that co-ingestion of CPPs with calcium significantly increased the calcium absorption in post-menopausal women with low basal absorptive performance¹³⁸. Bouhallab *et al.* reported that the Fe-CPPs complex improved absorption of iron, and this enhancement was highly depending on the origin and structure of CPPs¹³⁹. It was reported that Fe binding to phosphopeptides prevented formation of high molecular weight ferric hydroxides, which is poorly absorbed¹⁴⁰. In addition, absorption of Zn can be improved by binding with CPPs¹⁴⁰. The ability of CPPs to solubilize minerals in alkaline environment, and as a result increase their bioavailabilities may help to prevent ion-deficiency

related diseases, such as osteoporosis, anemia, and acrodermatitis enteropathica, *etc.* The antioxidant capacity of CPPs was tested using the oxygen radical absorbance capacity (ORAC) assay against the hydroxyl radicals. The result indicated that the antioxidant activity of CPPs was resulted from scavenging hydroxyl radical and chelating metal¹³². A more recent study using the Trolox equivalent antioxidant capacity (TEAC) and ORAC assays also revealed that CPPs were antioxidant. They also reported the cytoprotective effect of CPPs in Caco-2 cells against the H₂O₂ induced oxidative stress via scavenging free radical, chelating metal, and modulating the intracellular signaling cascades¹³³.

CPPs are generated *in vivo* by digesting caseins with gastrointestinal proteinases¹³⁴, and they were detected in stomach, duodenum¹⁴¹, and ileostomy fluid¹⁴², indicating that they can survive from further proteolysis in human distal ileum¹³⁴, which could be resulted from the negative charges on CPPs¹⁴⁰. The proteolysis-resistant property combined with the anionic nature at physiological pH make them ideal building material for the oral polysaccharide-protein/polypeptide complex delivery systems.

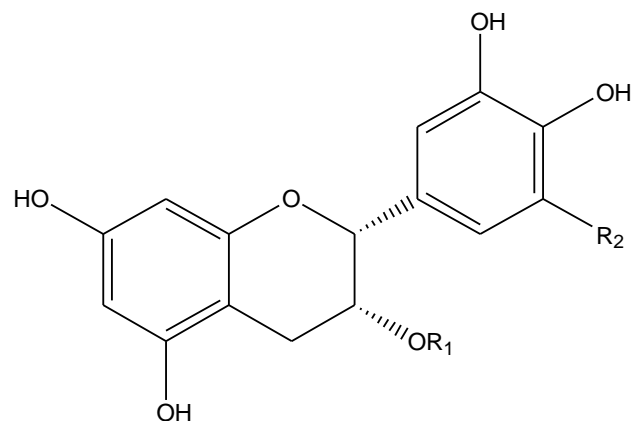
1.5. Introduction of Tea and Tea Polyphenols

1.5.1. Teas

Tea is the second most consumed beverage worldwide, just next to water. According to the degree of enzymatic fermentation, tea can be generally grouped into green tea (non-fermented), Oolong tea (semi-fermented), and black tea (fully fermented). Green tea is popular in some Asian countries, such as China and Japan. Black tea is largely consumed in India, United Kingdom, and United States, *etc.* About 78% of the global tea production is black tea. Green tea constitutes approximately 20% and Oolong tea accounts for the rest 2% of tea production worldwide¹⁴³. According to the Food and Agriculture Organization (FAO) of the United Nations, world black tea consumption keeps an annual growth rate of 1-2% for more than 10 years.

Polyphenols are the secondary metabolites of plants. Polyphenols can be generally classified into flavonoids and non-flavonoids. Flavonoids can be further classified into flavones, flavonols, flavanones, flavan-3-ols, anthocyanidins, isoflavonoids, and neoflavonoids. Polyphenols are ubiquitous in plants and foods such as fruits, vegetables, and wines. *In vitro* and *in vivo* studies revealed that polyphenols have multiple bio-functionalities including anti-oxidative¹⁴⁴, anti-inflammatory¹⁴⁵, anti-carcinogenic^{146, 147}, and cardiovascular protective¹⁴⁸ effects, *etc.*

Tea is a rich source of polyphenols. Catechins, which belong to the monomer flavan-3-ols are the main polyphenols in green tea. The major catechins in teas include (-)-epicatechin (EC), (-)-epigallocatechin (EGC), (-)-epicatechin gallate (ECG), and (-)-epigallocatechin gallate (EGCG). Their structures are shown in Figure 1-5. The major polyphenols in black tea include catechins, theaflavins, and thearubigins, accounting for up to 10%, 6%, and 60% of solids in the black tea infusion^{149, 150}. Theaflavins are the characteristic polyphenols in black tea. Their chemical and biological properties are reviewed in section 1.5.2. Thearubigins are the polymeric forms of flavan-3-ols in black tea. The color of thearubigins is red-brown or dark brown. Their structures and formation mechanisms are still poorly understood until now¹⁴⁹. In addition to these three major groups of polyphenols, flavonols such as quercetin, kaempferol, myricetin, and their glycosides were also identified in black tea¹⁵¹.

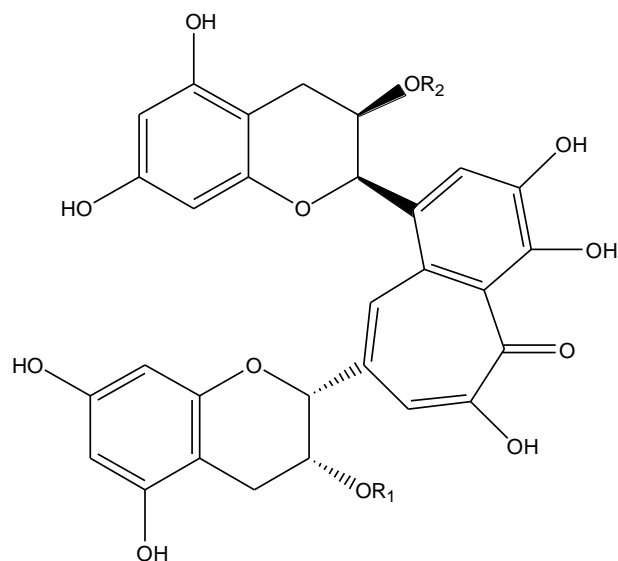


(-)-Epicatechin	$R_1 = H$	$R_2 = H$
(-)-Epicatechin gallate	$R_1 = \text{Galloyl}$	$R_2 = H$
(-)-Epigallocatechin	$R_1 = H$	$R_2 = OH$
(-)-Epigallocatechin gallate	$R_1 = \text{Galloyl}$	$R_2 = OH$

Figure 1-5. Structures of catechins

1.5.2. Theaflavins and Their Bio-efficacies

Theaflavins (TFs) are an important group of polyphenols in black tea, contributing greatly to the characteristic color and mouth feel of black tea¹⁴³. There are four major theaflavins, namely theaflavin (TF-1), theaflavin-3-gallate (TF-2a), theaflavin-3'-gallate (TF-2b), and theaflavin-3,3'-digallate (TF-3). They are differentiated by the number and position of galloyl groups attached on a benzotropolone derived skeleton (Figure 1-6). They have the characteristic orange or orange-red color¹⁴³.



Theaflavin	$R_1 = H$	$R_2 = H$
Theaflavin-3-gallate	$R_1 = \text{Galloyl}$	$R_2 = H$
Theaflavin-3'-gallate	$R_1 = H$	$R_2 = \text{Galloyl}$
Theaflavin-3,3'-digallate	$R_1 = \text{Galloyl}$	$R_2 = \text{Galloyl}$

Figure 1-6. Structures of theaflavins

TFs are synthesized in black tea during fermentation process, which is actually enzymatic oxidation. It is generally accepted that TFs are biosynthesized from the catechins in the presence of polyphenol oxidase (PPO, EC 1.14.18.1 or EC 1.10.3.2) and peroxidase (POD, EC 1.11.1.7). PPO is of vital importance in the oxidation of catechins into TFs. It can catalyze conversion of *o*-dihydroxyphenol to *o*-benzoquinone¹⁵². Studies using purified green tea catechins and enzymes (tea PPO and POD) or enzymes isolated from other sources have revealed that TFs were fermented from one catechol (*ortho*-dihydroxyphenyl)-type catechin (EC, ECG) and one pyrogallol (*vic*-trihydroxyphenyl)-type catechin (EGC, EGCG). The specific formation routes are listed as follows¹⁵³:



Compared to catechins, TFs are much more vulnerable to both pH- and thermo-induced degradations¹⁵⁴. The lower stabilities might be owing to their higher chemical reactivity¹⁵³. Similar to catechins, TFs also have pH-dependent stabilities. In general, TFs remain relatively stable in acidic environments while higher pH promotes their degradation. In pH 7.4 sodium phosphate buffer, their resistance to alkaline varied with time. TF-2b exhibited the highest stability in the first three hours, while afterwards TF-3 turned to the most stable one. TF-1 and TF-2a were consistently less stable than the other two components¹⁵⁴. About 34.8% of TF-1 was degraded after 8h at this pH¹⁵⁵. In pH 7.3 phosphate buffer (0.1 M), TF-1 degraded into theanaphthoquinone and bistheafavin B by auto-oxidation¹⁵⁶. Another study also identified theanaphthoquinone as the auto-oxidation product of TF-1 at pH 7.4 and 8.5¹⁵⁵. In boiling water, more than 40% degradation of TFs occurred in the first hours¹⁵⁴. TF-3 and TF-2b showed relatively higher thermo-stabilities than TF-1 and TF-2a in boiling water¹⁵⁴. TFs in solid form were rather stable. Li *et al.* reported that the contents of individual TFs was almost unchanged during a one-year storage test at different temperatures and humidities (27°C/60% humidity and 37°C/70% humidity)¹⁵³. The TFs mixture in black tea extract can even tolerate higher temperature (75°C) for two weeks without observable loss¹⁵³.

Epidemiological studies revealed inverse relationship between consumption of fruits, vegetables, and teas and the incidence of some degenerative diseases, such as cancer¹⁵⁷, cardiovascular diseases¹⁵⁸, and type II diabetes¹⁵⁹. These health benefits may be attributed to the polyphenols in these foods. TFs as an important group of polyphenols in black tea have diverse

bio-efficacies, including anti-oxidative, anti-inflammatory, anti-carcinogenic, anti-diabetic, anti-bacterial, and neuro-protective effects *etc.*

Oxidative and nitrosative stresses, which are raised from the imbalance between generation of reactive oxygen species (ROS) and reactive nitrogen species (RNS) and the ability to neutralize them, are associated with the development of various diseases. Excess generation of ROS, such as superoxide ($O_2^{\cdot -}$), peroxy (ROO^{\cdot}), alkoxy (RO^{\cdot}), and hydroxyl (HO^{\cdot}) radicals, and RNS, such as nitric oxide, can lead to damage of DNA, proteins, and lipids. There are diverse endogenous antioxidants, such as superoxide dismutase (SOD), polyphenols, ascorbic acid, tocopherol, and glutathione existing in our body, serving as the defense system against the oxidative and nitrosative stresses. Antioxidation is a remarkable property of polyphenols. They can scavenge the free radicals, chelate metal ions, inhibit free radical-generating enzymes, and up-regulate antioxidant enzymes. The potency of these capacities is highly depending on their structures. The antioxidant activities of TFs have been studied by various *in vitro* models. The general trend is that the antioxidant activity increases with the number of galloyl group. The relative antioxidant potency between specific TFs and catechins, however, may vary with the methods that were employed. Yang *et al.* compared the antioxidant capacities of TFs and EGCG and they found that the sequences of the antioxidant activities of these polyphenols was TF-3 > TF-2s > TF-1 > EGCG against hydroxyl radicals and TF-3 > TF-2s > EGCG > TF-1 using 2,2-diphenyl-1-picrylhydrazyl (DPPH) method¹⁶⁰. The A-ring fission compounds were identified as the oxidation products of TF-3 by hydroxyl radicals generated by hydrogen peroxide¹⁶¹, while theanaphthoquinone was identified as the oxidation product of TF-1 by DPPH model¹⁵⁵. Another paper reported similar result of reducing the xanthine oxidase activity by tea polyphenols as Yang's DPPH result¹⁶². Miller *et al.* reported the abilities of TFs to scavenge ABTS⁺ radical as TF-3 > TF-2b \geq TF-2a > TF-1. They also investigated the capacity of TFs against low-density lipoprotein (LDL) oxidation, and the sequence of reactivity was TF-3 > TF-2a \geq TF-2b > TF-1¹⁶³. Leung *et al.* further compared the antioxidant

activities of TFs and catechins against human LDL oxidation model, and they reported that these two groups of polyphenols had equally potent antioxidant capacities with the sequence in decreasing order as TF-3 > ECG > EGCG \geq TF-2b \geq TF-2a > TF-1 \geq EC > EGC¹⁶⁴. TFs can also bind the metal ions^{163, 165}, which are the catalysts of the oxidation reactions.

Chronic inflammation is associated with diverse diseases, such as cancer, cardiovascular disease, obesity, aging, diabetes, neurological disease, and metabolic disorder¹⁶⁶. TFs can exert the anti-inflammatory effects through diverse mechanisms. Antioxidation described above is an important mechanism as ROS and RNS are produced during inflammation^{167, 168}. Increased expression of the pro-inflammatory cytokines, including tumor necrosis factor α (TNF- α), interleukin-1 (IL-1), interleukin-6 (IL-6), and enhanced levels of arachidonic acid (AA) metabolites such as prostaglandins (PGs) generated through cyclooxygenase (COX) pathway and leukotrienes (LTs) through lipoxygenase (LOX) pathway are involved in inflammation. The anti-inflammatory effect of TFs was proved by *in vivo* 12-*O*-tetradecanoylphorbol-13-acetate (TPA)-induced mouse ear inflammatory model¹⁶⁹. Expression of the pro-inflammatory cytokines IL-1 β , IL-6, and levels of AA metabolites PGE₂, and LTB₄ were reduced. The authors also found that the degree of anti-inflammatory effect increased with the number of phenolic group, and the anti-inflammatory effect of TFs was stronger than EGCG¹⁶⁹. Another important anti-inflammation mechanism of TFs is inhibiting expression of pro-inflammatory gene. Nuclear factor- κ B (NF- κ B) is associated with activating expression of cytokines, chemokines, enzymes, and adhesion molecules. Under inflammatory states, NF- κ B is released, which promotes transcription of the pro-inflammatory genes. TFs significantly inhibited the protein level of inducible NO synthase and production of NO, which plays an important role in inflammation, through inactivation of NF- κ B in macrophage RAW 264.7 cells¹⁷⁰.

Cardiovascular diseases are still the leading causes of death in the United States. Epidemiological study revealed that black tea consumption may reduce the risk of cardiovascular

disease¹⁷¹. Atherosclerosis is a chronic inflammatory pathological condition¹⁷². TFs can prevent atherosclerosis via the anti-inflammatory mechanisms described above. Vinson *et al.* reported that black tea inhibited atherosclerosis in hamster model via hypolipemic, antioxidant, and antifibrinolytic effects¹⁷³. LDL oxidation is involved in all stages of atherosclerotic development¹⁷⁴. TF-3 reduced LDL oxidation in macrophages through decreasing superoxide production and iron chelating¹⁷⁵. The ability of preventing LDL from oxidation may prevent development of atherosclerosis. Besides, black tea consumption was associated with reducing platelet activation¹⁷⁶. TFs may reduce production of platelet activating factor by inhibiting acetyl-CoA:lysoPAF acetyltransferase¹⁷⁷. These properties may prevent formation of thrombus.

Cancer is one of the most intractable diseases. Development of cancer can be generally divided into initiation (normal cell to initiated cell), promotion (initiated cell to preneoplastic cell), and progression (preneoplastic cell to neoplastic cell) stages¹⁷⁸. At the initiation stage, TFs can prevent development of cancers by scavenging ROS. On the other hand, TFs can regulate the phase I enzymes, particularly cytochrome P450 (CYP450), which promote the reaction between carcinogens and DNA. Feng *et al.* reported that TFs can protect DNA from damage by inhibiting the CYP450 1A1¹⁷⁹. The promotion stage is a relatively slower process than the initiation stage. At the promotion stage, strategies such as regulating cell-cycle, arrest uncontrolled cell division or induce apoptosis of damaged cells that can lead to the balance of proliferation and apoptosis may inhibit development of cancers. TF-3 can significantly inhibit proliferation of human A431 epidermoid carcinoma cells¹⁸⁰. TF-1 inhibited proliferation of human prostate cancer cell line PC-3, and arrested the G2/M phase through inhibition of cyclin-regulated signaling pathways. TF-1 also increased apoptosis of the PC-3 cells through up-regulating the pro-apoptotic proteins Bax, caspase-3 and caspase-9, and down-regulating the anti-apoptotic protein Bcl-2¹⁸¹. Angiogenesis and metastasis are usually involved in the progression stage. Vascular endothelial growth factor (VEGF) is an important inducer of angiogenesis. Inhibiting VEGF is an effective mechanism of

suppressing angiogenesis. Siddiqui *et al.* reported black tea extract and TFs inhibited the prostate cancer in athymic nude mice via reducing the level of VEGF protein as one mechanism¹⁸². Matrix metalloproteinases (MMPs) are involved in tumor cell invasion and metastasis. TF-1 significantly inhibited invasion of human fibrosarcoma HT1080 cells, and suppressed secretion of MMP-2 and MMP-9 in a dose-dependent manner¹⁸³. TF-1 and TF-3 were also able to inhibit production of MMP-2 and MMP-9 and invasion of mouse Lewis lung carcinoma LL2-Lu3 cells¹⁸⁴.

1.5.3. Bioavailability of Theaflavins

Although TFs have been documented to have diverse bio-efficacies in *in vitro* models as described in section 1.5.2, *in vivo* studies sometimes show contradictory results^{185, 186}. The explanation for the inconsistency of *in vitro* and *in vivo* results could be due to their extremely low bioavailabilities. The pharmacokinetic study on TFs is very limited, while an early study revealed that the maximum concentration of TF-1 in blood plasma and urine of two volunteers (one male and one female) were 1.0 µg/L and 4.2 µg/L, respectively, which were detected 2h after consuming 700 mg TFs. Neither TF-2s nor TF-3 was detected¹⁸⁷.

The definition of bioavailability may vary with discipline¹⁸⁸. According FDA, bioavailability is defined in 21CFR320.1 as “the rate and extent to which the active ingredient or active moiety is absorbed from a drug product and becomes available at the site of action”. Considering that the bioavailability is affected by absorption, metabolism, and excretion of the target compound in human body, the bioavailability (F) can be expressed as the following equation:

$$F = F_B \times F_T \times f_M \quad \text{eq. 1-5}$$

where F_B represents the fraction of bioactive compound that is bioaccessible for intestinal absorption. F_T represents the fraction of bioactive compound that can transport through the mucus layer and epithelial cells and is being absorbed across the intestinal lumen. f_M represents the fraction

of bioactive compound that remain unmetabolized by the enzymes in the lumen, epithelial cells, systemic circulation, or liver¹⁸⁹.

There are many factors that may affect the bioavailability of polyphenols. After ingestion, polyphenols such as catechins can interact with the salivary proline-rich proteins, followed by precipitation of these proteins, which is responsible for the astringency sensory of tea and wine¹⁹⁰. This process was traditionally regarded as a defensive mechanism against the harmful tannins¹⁹⁰, while recent studies indicated that these interactions can affect the bioavailability of polyphenols. pH stability is of key importance when polyphenols go through the upper GIT, where the pH increases dramatically from pH 1-3 in the stomach to pH 5.7-7.4 in the small intestine. Catechins and TFs are stable in acidic environment, while after being exposed in neutral to alkaline conditions, they are degraded very rapidly through auto-oxidation^{154, 156}. Solubility is another limitation for the bioavailability of polyphenols since only the solubilized or dispersed polyphenols are bioaccessible, which is the prerequisite for bioavailability. Permeation through the small intestinal membrane (F_T) also determines the bioavailability of polyphenols. The polyphenols can come across the small intestinal membrane by transcellular (active or passive) and paracellular routes. The multidrug resistance proteins (MRPs) located in the small intestine could pump out a fraction of absorbed catechins and TFs back to the intestinal lumen, and therefore decreases their bioavailabilities^{191, 192}. Presence of the mucus layer on the small intestinal epithelial cells can further associate with polyphenols and impede entrance of polyphenols into the circulatory system. Besides, the pH gradient across the mucus layer from the weak acidic in upper intestinal lumen to neutral to weak alkaline also increase the possibility of pH-induced degradation. Once absorbed, catechins undergo metabolisms, such as methylation, glucuronidation, sulfation, and ring-fission. These processes are catalyzed by diverse enzymes which are ubiquitously distributed in tissues¹⁴³. These biotransformations can also affect the bioavailability (f_M) of catechins. Compared to catechins, the biotransformation of theaflavins was less studied¹⁴³.

Overall, the major reason for the low bioavailability of TFs which is similar to catechins could be due to their low permeability through the small intestinal membrane. According to Lipinski's "rule of 5", any molecule satisfies 2 of the following 4 parameters would be expected to have poor absorption or permeation: (1) Mw over 500, (2) logP over 5 or MlogP over 4.15, (3) has more than 5 hydrogen bond donors, (4) has more than 10 hydrogen bond acceptors¹⁹³. Obviously, TFs meet at least 2 of these 4 conditions. TFs are polyhydroxylated polyphenols that can bind water molecules to form large hydration shell. This large hydration shell can increase their apparent sizes, which makes them hard to penetrate through the lipophilic cell membrane (transcellular route)¹⁴³. Improving the intestinal permeability of TFs is therefore the key to increase their bioavailabilities. As described in section 1.3, CS is a permeation enhancer. Using the CS-based delivery systems is one of the feasible approaches to solve this problem. In this dissertation, the CS-CPPs nanocomplexes were used to encapsulate TF-3, which is a model of TFs, aiming to improve its intestinal permeability.

CHAPTER II. CHARACTERIZATION OF CHITOSAN, CASEINOPHOSHOPEPTIDES, AND THEAFLAVINS

2.1. Introduction

The aim of this chapter is to characterize the physiochemical properties of the main materials, *i.e.* CS, CPPs, and TF-3 that were used in this whole dissertation. The DD of CS was characterized by the nuclear magnetic resonance (NMR). The Mw of CS was measured by the gel permeation chromatography multi-angle laser light scattering (GPC-MALLS). The overlap concentration (C^*) of CS was determined by measuring its intrinsic viscosity using the Ubbelohde capillary viscometer. The amino acid sequences of the CPPs sample were determined by the liquid chromatography-tandem mass spectrometry (LC-MS/MS) and the pI of CPPs was determined by measuring the ζ -potential. The conformations of CS and CPPs were investigated by the SAXS. Each fraction of TFs, *i.e.* TF-1, TF-2a, TF-2b, and TF-3 was purified by the column liquid chromatography. Their purities were analyzed by the high performance liquid chromatography (HPLC).

2.2. Materials and Methods

2.2.1. Materials

CS (labeled as 130 kDa and DD of 98%) was purchased from Kunpoong Bio. Co., Ltd. (South Korea) and used as received without further treatment. CPPs was purchased from Greencream Biotechnology Co., Ltd. (Guangzhou, China). Black tea extract was provided by Dr. Shiming Li in Department of Food Science, Rutgers University. 95% ethyl alcohol, ACS/USP/NF grade acetone, HPLC grade acetonitrile, and water were purchased from Pharmco-AAPER (CT, USA). HPLC grade acetic acid was purchased from EMD Chemicals Inc. Deuterium oxide (D_2O) and deuterium chloride (DCI) were purchased from Sigma-Aldrich (MO, USA).

2.2.2. NMR Measurement

The DD of the CS sample was measured by a Varian VNMRs 500 MHz spectrometer (Agilent Technologies, CA, USA) according to Lavertu *et al.* method¹⁹⁴. Briefly, 10 mg CS was dissolved in 1.96 mL D₂O and 0.04 mL DCI (20% w/v). ¹H NMR spectrum was obtained at 70°C after 10 min equilibration of sample. The chemical shifts were reported in ppm. The DD was calculated by

$$DD(\%) = \left(\frac{H1D}{H1D+HAc/3} \right) \times 100 \quad \text{eq. 2-1}$$

where H1D is the integral of the peak of proton H1 of the deacetylated monomer; HAc is the integral of the peak of the three protons of the acetyl group.

2.2.3. GPC-MALLS Measurement

The Mw of the CS sample was measured by the GPC-MALLS equipped with a multi-angle light scattering detector (DAWN HELEOS-II, Wyatt Technology, USA) and a refractometer (Optilab T-rEX, Wyatt Technology, USA). Acetate buffer containing 0.2 M acetic acid and 0.1 M sodium acetate (pH 4.8) was prepared and filtered by 0.22 μm filter as the eluent. 2 mg/mL CS was prepared by dissolving CS in the acetate buffer and filtered through 0.22 μm filter before injection into the OHPak SB-804HQ column. The experiment was performed at 25°C with the eluent flow rate of 0.4 mL/min.

2.2.4. Viscosity Measurement

CS was dissolved in 1% acetic acid (10 mM NaCl) and the pH of the CS solution was adjusted to 6, which is condition for preparation of the CS-CPPs nanocomplexes in the following experiments. The intrinsic viscosity of CS (0.1 - 10 mg/mL) at this condition was measured using an Ubbelohde capillary viscometer. At least 10 measurements were repeated for each concentration. All measurements were conducted at 25°C. The specific viscosity η_{sp} was then calculated by

$$\eta_{sp} = \frac{\eta - \eta_0}{\eta_0} \quad \text{eq. 2-2}$$

where η is the viscosity of solution and η_0 is the viscosity of solvent.

2.2.5. LC-MS/MS of CPPs

The primary structures of CPPs were analyzed by the nanospray LC-MS/MS using an LTQ-Orbitrap mass spectrometer. The LC-MS/MS gradient was 4-15% 80% acetonitrile/0.16% formic acid (B) in 10 min, then 15-50% B in 45 min, then 50-90% B in 5 min. The mass spectrometry conditions were set that MS was acquired in orbitrap with 60000 resolutions, top 10 HCD with 7500 resolutions. The data were searched against Uniprot bovine database using Mascot Search Engine with following parameters: enzyme non-specific; variable modification: oxidation (Met), phosphorylation (STY); Mass error tolerances of ± 10 ppm for MS and ± 0.1 Da for MS/MS.

2.2.6. ζ -potential Measurement

The pI of CPPs was determined by measuring the ζ -potentials of CPPs on a Zetasizer Nano (Malvern Instruments Ltd., UK). CPPs were dissolved in Milli-Q water (2 mg/mL) and the pH was adjusted to around 4 before measurement. The ζ -potentials were measured during gradually acidification of the CPPs solution by hydrochloric acid until it turned to positive. The measurements were conducted at 25°C.

2.2.7. SAXS Measurements

The SAXS experiments were conducted at the BioCAT 18-ID beamline at the Advanced Photon Source (APS) at Argonne National Laboratory (Chicago, IL). CS was dissolved in 1% acetic acid (10 mM NaCl) to prepare a 5 mg/mL CS stock solution. The stock solution was diluted with 1% acetic acid (10 mM NaCl) to the required concentrations and the pH of the CS solutions was adjusted to pH 6. CPPs was dissolved in Milli-Q water (10 mM NaCl) with the concentration ranging from 0.25 mg/mL to 50 mg/mL, and they were adjusted to the designated pH. A short exposure of 1 s followed by 2 s cooling was used to acquire the scattering data. The final SAXS profiles were obtained by subtracting the solvent from the average of 5 measurements.

2.2.8. Purification of TFs

TFs were isolated from black tea extract by using column liquid chromatography with Sephadex LH-20 as the stationary phase. Black tea extract was first dissolved in 95% (v/v) ethanol and filtered through 0.45 μm filter before being applied on the top of the column. The column was equilibrated with 95% (v/v) ethanol for at least 2 bed volumes before the experiment. After subjecting the black tea extract solution to the top of the column, the sample was eluted successively by 95% (v/v) ethanol and 40% (v/v) acetone. The purity of TFs was then monitored by HPLC. The eluates were rotary evaporated and freeze-dried immediately for further experiments.

2.2.9. HPLC Analysis of TFs

The purity of TFs was monitored by HPLC on a Dionex UltiMate 3000 LC Modules equipped with a pump (Model: LPG-3400A), autosampler (Model: WPS-3000 SL), and an ultraviolet-visible (UV-Vis) detector (Model: VWD-3400). A Luna C₁₈ (Phenomenex, Torrance, CA) column (150 \times 4.6 mm i.d., 3 μm particle size) was used. The TFs were detected at 280 nm and the flow rate was kept at 0.8 mL/min. 0.2% (v/v) acetic acid (solvent A) and acetonitrile (solvent B) were chosen as the mobile phases. The elution gradient was as follows: solvent B increased from 8% to 12% in 10 min, then linearly increased to 18% in 30 min, then increased to 21% in 1 min, then increased to 28% in 29 min, then kept for 4 min, then linearly increased to 80% in 1 min, and kept for 5 min, and then decreased to 8% in additional 1 min and kept for 5 min for equilibrium.

A simplified HPLC program was used to quantify the concentrations of TF-1 and TF-3 in the Caco-2 monolayer transport experiments. The elution gradient was as follows: solvent B increased from 21% to 28% in 15 min and kept for 5 min, from 28% to 21% in 5 min and kept for 3 min for equilibrium.

2.3. Results and Discussion

2.3.1. DD and Mw of CS

The DD of the CS used in this dissertation was measured by ^1H NMR. The ^1H NMR spectrum at 70°C is shown in Figure 2-1. The chemical shifts of the proton H1 of deacetylated monomer (H1D) and the proton of the acetyl group (HAc) are 5.25 ppm and 2.36 ppm, respectively. The DD of the CS was 92.6% calculated by eq. 2-1.

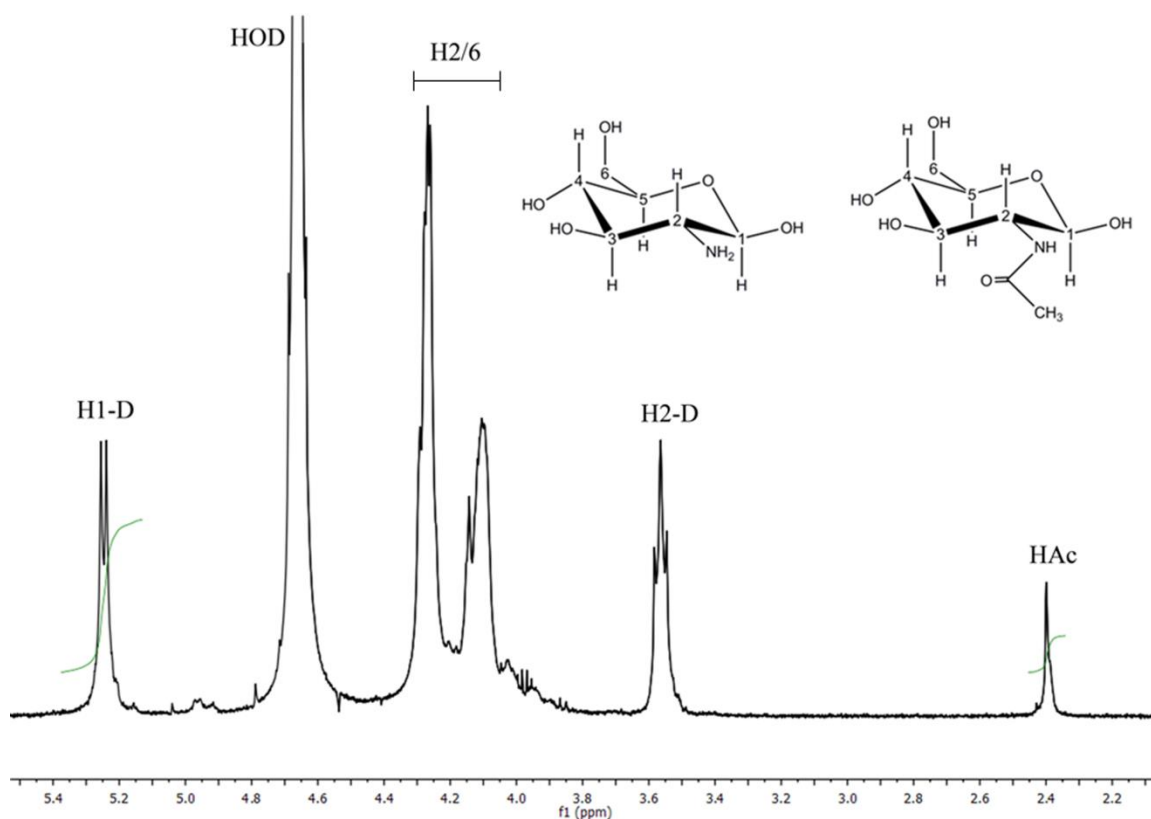


Figure 2-1. CS ^1H NMR spectrum at 70°C

The GPC-MALLS result shows that the Mw of the CS sample was 57 kDa, which is smaller than the labeled Mw. The polydispersity of the CS sample was 1.015, indicating the molecular weight distribution of the CS sample was narrow.

2.3.2. Viscosity Measurement

The intrinsic viscosity of CS was measured at pH 6 (10 mM NaCl), which is the condition for preparation of the CS-CPPs nanocomplexes in the following experiments. The intrinsic viscosity was converted to η_{sp} by eq. 2-2. The specific viscosity was plotted versus CS concentration as shown in Figure 2-2. The C^* of CS at this condition was 3.47 mg/mL, from where the CS solution changed from dilute to semidilute solution. In the dilute region ($C < C^*$), CS molecules remain single chains, and they interact primarily with the solvent. In the semidilute region ($C^* < C < C^{**}$, C^{**} is the critical concentration between semidilute and concentrated solution, which was not determined in this study), CS molecules are no longer isolated from each other. They start to overlap and entangle.

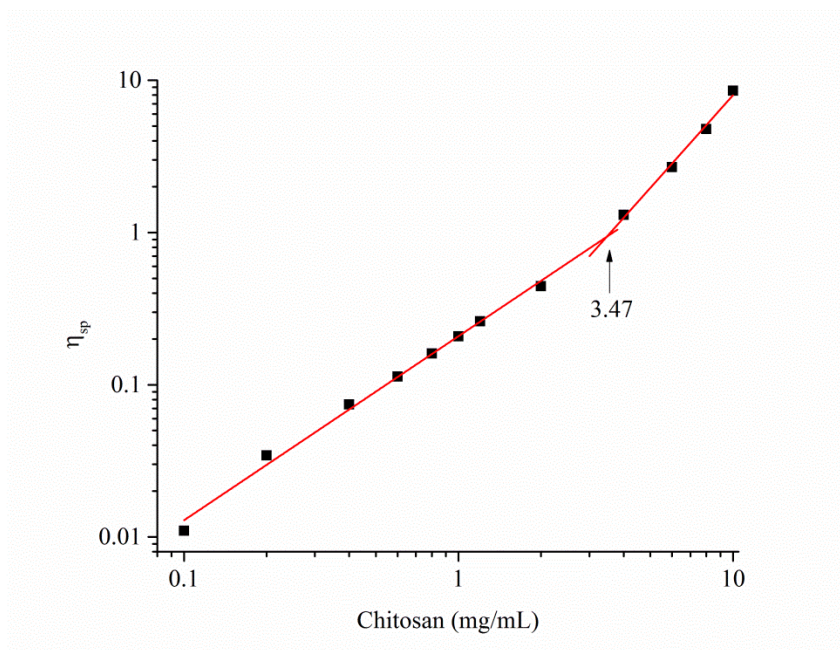


Figure 2-2. Specific viscosities of CS solutions (0.1–10 mg/mL) at pH 6 in the presence of 10 mM NaCl.

2.3.3. SAXS of CS

The versatility of SAXS provides us a wealth of structural information of biomolecules such as molecular mass, radius of gyration (R_g), maximum diameter, overall shape, aggregation number, surface roughness, *etc.* The scattering vector q is described as

$$q = \frac{4\pi}{\lambda} \sin\left(\frac{\theta}{2}\right) \quad \text{eq. 2-3}$$

where λ is the wavelength of the incident beam and θ is the scattering angle.

The conformation of polymers in solution is usually described by the term fractal dimension α . The scattering intensity $I(q)$ of the molecule with fractal dimension α follows the power law $I(q) \sim q^{-\alpha}$. The scattering curves of 0.25–1.25 mg/mL CS generally follows $I(q) \sim q^{-2}$ (Figure 2-3A), suggesting that the CS molecules exist in solution as Gaussian chain at these concentrations¹⁹⁵.

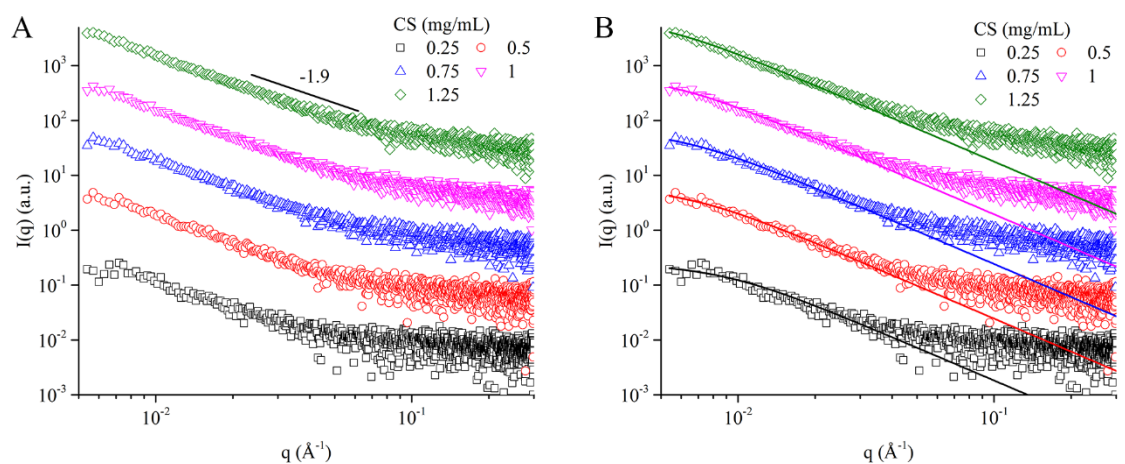


Figure 2-3. (A) Scattering curves and (B) fitting with eq. 2-4 and eq. 2-5 of 0.25-1.25 mg/mL CS (0.01M NaCl). The intensities were vertically shifted for clear visualization.

The scattering intensity $I(q)$ is expressed as

$$I(q) = \phi V_p (\Delta\rho)^2 P(q) S(q) \quad \text{eq. 2-4}$$

where q is the scattering vector; Φ is volume fraction of CS; V_p is the molecular volume of CS; $\Delta\rho$ is the X-ray electron density contrast between CS and buffer; $P(q)$ is the form factor, and $S(q)$ is the structure factor. The concentrations of the CS samples were within the dilute solution region ($C < C^*$, section 2.3.2). At these concentrations, $S(q)=1$, and the form factor $P(q)$ is fitted by the Debye function expressed as

$$P(q) = \frac{2}{(qR_g)^4} [\exp(-q^2R_g^2) + q^2R_g^2 - 1] \quad \text{eq. 2-5}$$

The R_g of CS at different concentrations listed in Table 2-1 was obtained by fitting the scattering curves with eq. 2-4 and eq. 2-5 (Figure 2-3B), which displayed an increased R_g as the concentration increased.

Table 2-1. Radius of gyration of CS at 0.25-1.25 mg/mL (0.01M NaCl)

Concentration (mg/mL)	R_g (Å)
0.25	169.6
0.5	233.2
0.75	246.6
1	277.5
1.25	309.0

2.3.4. LC-MS/MS of CPPs

Caseins can be grouped into four types, *i.e.* α_{s1} -, α_{s2} -, β - and κ -caseins. α_{s1} -, α_{s2} -, and β -caseins are rich in phosphate groups while κ -casein only contains one¹²⁹. CPPs are the phosphoserine-containing polypeptides hydrolyzed from caseins.

The amino acid sequences of CPPs sample were detected by the LC-MS/MS. The identified sequences are listed in Table 2-2 with underlines and the major sequences with different amount of phosphorylation are shown in Figure 2-4. As shown in Table 2-2, polypeptides derived from α_{s1} -,

α_{s2} -, and β -caseins were detected with high sequence coverage while peptides derived from κ -casein were not detected. The typical regions which contain three phosphorylated serines followed by two glutamic acid residues, *i.e.* SerP-SerP-SerP-Glu-Glu were present in the detected sequences.

Table 2-2. Sequence coverage of CPPs sample from LC-MS/MS

CAS α 1_BOVIN	
1	MKLLILTCLV AVALARPKHP <u>IKHQGLPQEV</u> <u>LNENLLRFFV</u> <u>APFPEVFGKE</u>
51	<u>KVNELSKDIG</u> <u>SESTEDQAME</u> <u>DIKQMEAESI</u> <u>SSSEEIVPNS</u> <u>VEQKHIQKED</u>
101	<u>VPSERYLGYL</u> <u>EQLLRLLKKYK</u> <u>VPQLEIVPNS</u> <u>AEERLHSMKE</u> <u>GIHAQQKEPM</u>
151	<u>IGVNOELAYF</u> <u>YPELFRQFYQ</u> <u>LDAYPSGAWY</u> <u>YVPLGTQYTD</u> <u>APSFSDIPNP</u>
201	<u>IGSENSEKTT</u> MPLW
CAS α 2_BOVIN	
1	MKFFIFTCLL AVALAKNTME <u>HVSSSEESII</u> <u>SQETYKQEK</u> <u>MAINPSKENL</u>
51	CSTFCKEVVR <u>NANEEEEYSIG</u> <u>SSSEESAeva</u> <u>TEEVKITVDD</u> <u>KHYQKALNEI</u>
101	<u>NOFYQKFPQY</u> <u>LOYLYOGPIV</u> <u>LNPWDQVKN</u> <u>AVPITPTLNR</u> <u>EQLSTSEENS</u>
151	<u>KKTVDMESTE</u> <u>VFTKKTCLTE</u> <u>EEKNRLNFLK</u> <u>KISQRYQKFA</u> <u>LPOYLKTVYQ</u>
201	HQKAMKPWIQ <u>PKTKVIPYVR</u> YL
CAS β _BOVIN	
1	MKVLILACLV ALALARELEE <u>LNVPGEIVES</u> <u>LSSSEESITR</u> <u>INKKIEKFQS</u>
51	<u>EEQQQTEDEL</u> <u>QDKIHPFAQT</u> <u>QSLVYFPFPGP</u> <u>IPNSLPQNI</u> <u>PLTQTPVVVP</u>
101	<u>PFLQPEVMGV</u> <u>SKVKEAMAPK</u> <u>HKEMPFPKYP</u> <u>VEPFTESQSL</u> <u>TLTDVENLHL</u>
151	<u>PLPLLQSWMH</u> <u>OPHQPLPPTV</u> <u>MFPQSVLSL</u> <u>SQSKVLPVPQ</u> <u>KAVPYPQRDM</u>
201	<u>PIQAFLLYQE</u> <u>PVLGPVRGPF</u> <u>PIIV</u>

The sequences with underlines were detected in our CPPs sample

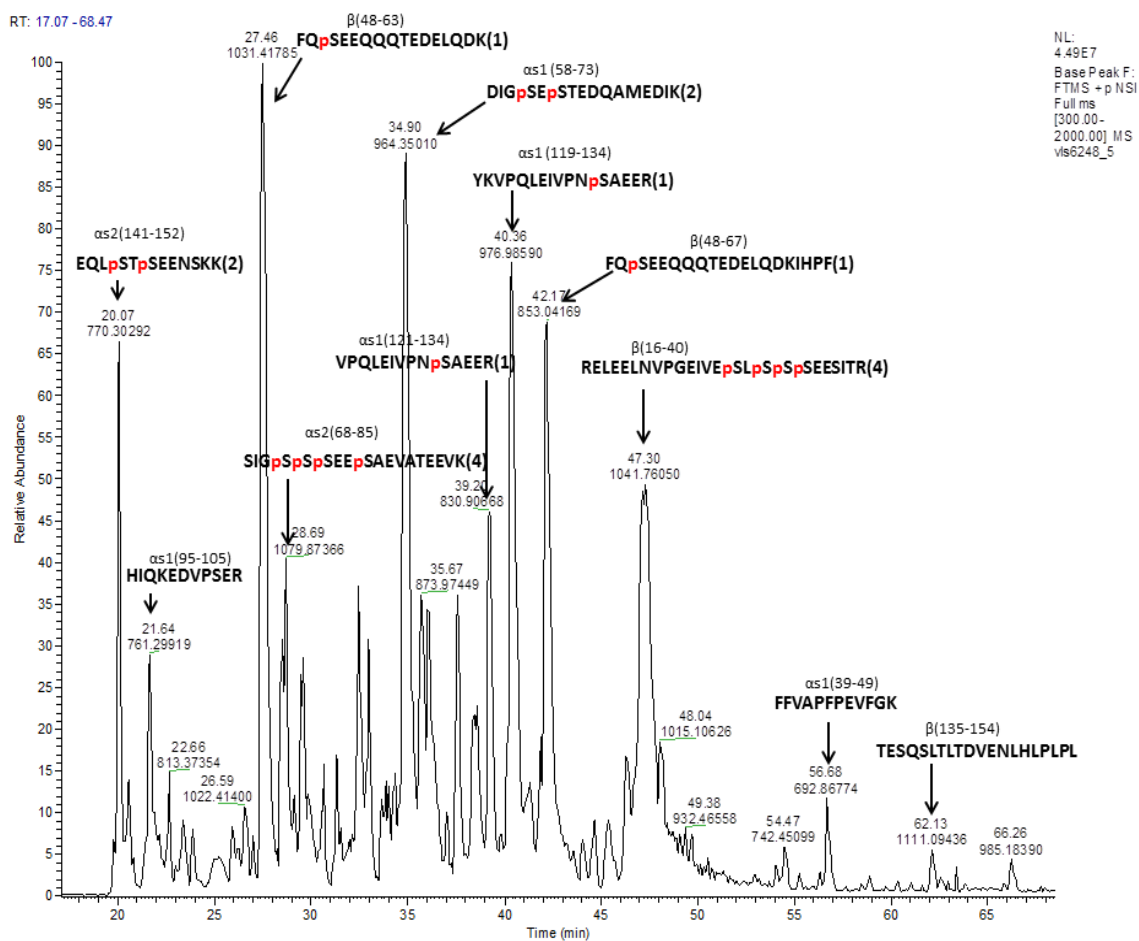


Figure 2-4. LC-MS/MS result of CPPs. The identified major sequences were marked. The lowercase letter P in red color represents phosphorylation and the number after peptide sequence indicates the amount of phosphorylation modifications.

2.3.5. ζ -Potential Measurement

The surface charge (ζ -potential) of CPPs was investigated as a function of pH to determine its pI. As shown in Figure 2-5, in the studied pH range, the ζ -potential increased linearly during the acidification process, and the ζ -potential reached 0 at $\text{pH} \approx 3.3$, which was determined as the pI of CPPs.

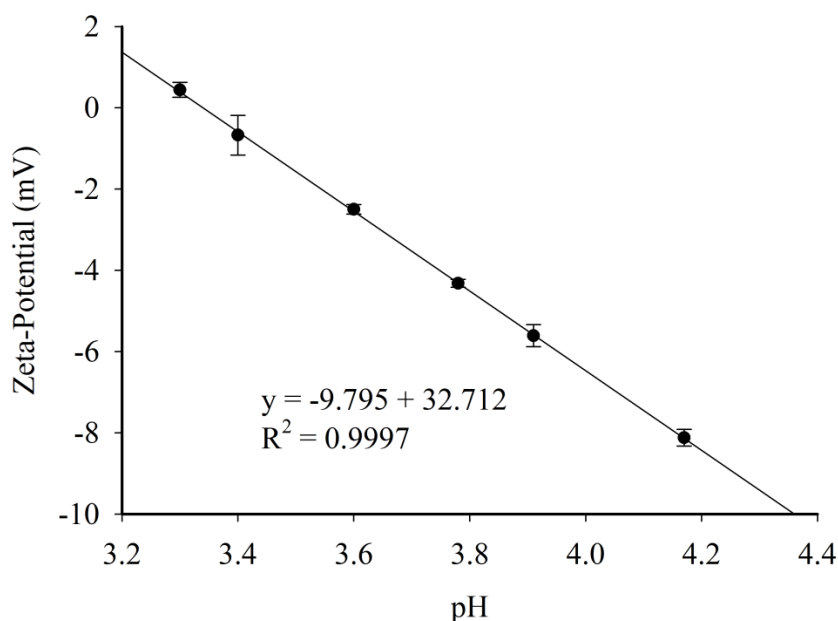


Figure 2-5. ζ -potentials of 2 mg/mL CPPs solution at different pH

2.3.6. SAXS of CPPs

The conformations of CPPs at different concentrations and pH were investigated by the SAXS.

The scattering profiles of 0.25–50 mg/mL CPPs solutions (10 mM NaCl) at pH 6 are shown in Figure 2-6A. In the large q range, the slope of the scattering curves changed from -1.06 (0.25 mg/mL) to -1.98 (50 mg/mL), indicating that the shape of CPPs molecules in the solution changed from rod-like to disk-like as the concentration increased¹⁹⁶. In the small q range, the scattering curves show upturn when CPPs concentration was higher than 5 mg/mL, suggesting that CPPs aggregated at these concentrations. The aggregates existed in the fractal dimension from 1.40 (5

mg/mL) to 1.79 (50 mg/mL). In the Kratky plot (Figure 2-6B), no peak was observed, which means that CPPs remained unfolded at these concentrations.

The R_g of CPPs was calculated by the classic Guinier equation expressed as

$$I(q) = I(0)e^{-\frac{(qR_g)^2}{3}} \quad \text{eq. 2-6}$$

where $I(0)$ is the scattering intensity at zero-vector. This equation can be further converted into

$$\ln(I(q)) = \ln(I(0)) - \frac{(qR_g)^2}{3} \quad \text{eq. 2-7}$$

Therefore, R_g can be determined by linearly fitting the Guinier plot [$\ln(I(q))$ vs. q^2] (Figure 2-6A inset). The fitting region satisfy $qR_g < 1.3$. The R_g of CPPs at these concentrations are listed in Table 2-3. The R_g increased from 13.1 Å to 15.4 Å when the concentration increased from 0.25 mg/mL to 0.5 mg/mL. The R_g remained at 15.5 Å at 1 mg/mL. Further increase the concentration to 30 mg/mL, the R_g slightly decreased to 13-14 Å. At 50 mg/mL, the R_g returned to 14.9 Å.

The conformation of proteins/polypeptides is determined by the environmental pH. Figure 2-6C shows the scattering profiles of 1 mg/mL CPPs in 10 mM NaCl solutions at pH 2-10. In the large q range, the scattering intensity decayed in $I(q) \sim q^{-1.04}$ to $I(q) \sim q^{-1.54}$. In the small q range, it was noticed that the slopes of pH 2-4 increased, suggesting that large structures formed. This pH range was close to the pI (section 2.3.5). The net charge of CPPs was low and therefore CPPs aggregated due to loss of electrostatic repulsion. There was no peak showing in the Kratky plot (Figure 2-6D), which means pH change did not induce folding of CPPs. The R_g of 1 mg/mL CPPs at these pH values are also listed in Table 2-3. At pH 2 where CPPs were positively charged, the R_g was 15.3 Å. The R_g decreased to 13.3 Å when pH was increased to the pI (pH 3.3), which means CPPs are more compact at pI. When pH was increased away from the pI (pH 4-8), R_g returned to around 15 Å. When pH was further increased to pH 10, the R_g increased considerably to 17.9 Å, which may result from fully unfolding of CPPs molecules.

Table 2-3. Radius of gyration of CPPs

Concentration (mg/mL)	pH	R _g (Å)
0.25	6.0	13.1
0.5	6.0	15.4
1	6.0	15.5
5	6.0	13.9
10	6.0	13.4
30	6.0	13.9
50	6.0	14.9
1	2.0	15.3
1	3.3	13.3
1	4.0	16.0
1	8.0	15.3
1	10.0	17.9

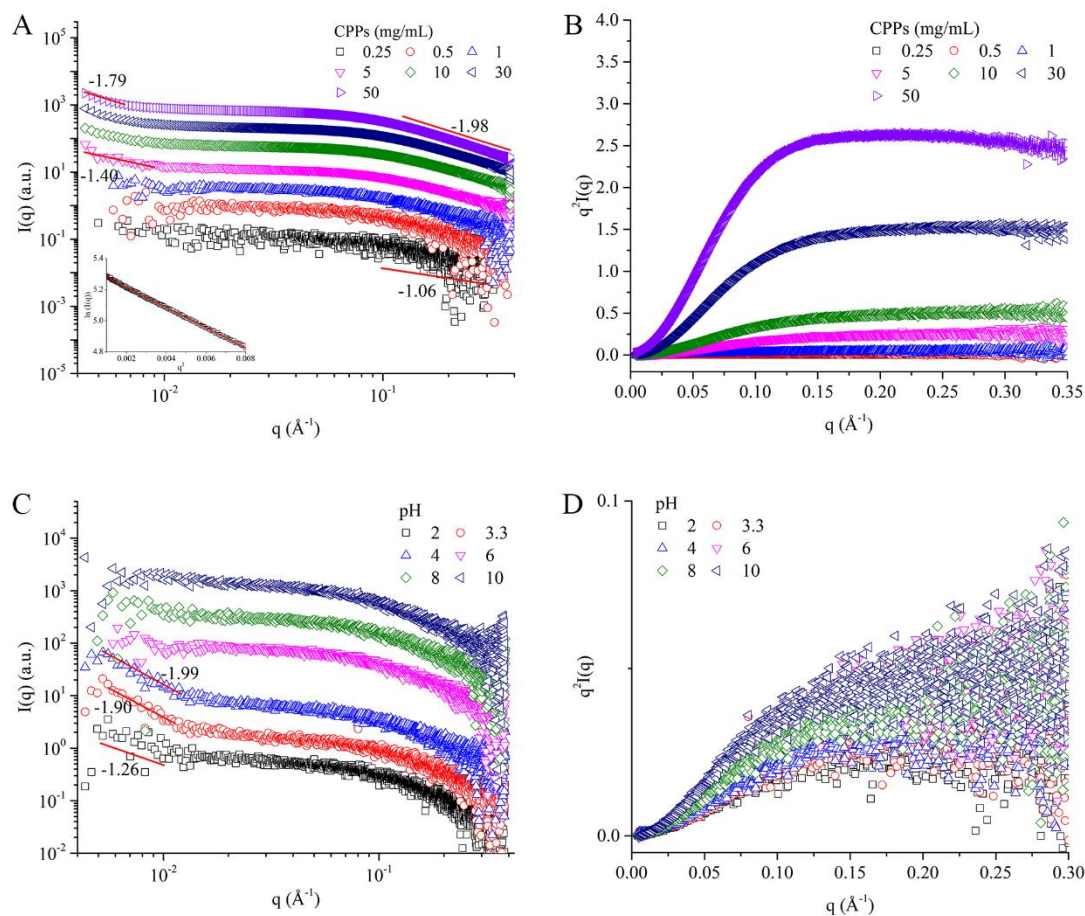


Figure 2-6. (A) Scattering profiles and (B) Kratky plot of 0.25–50 mg/mL CPPs solutions (containing 10 mM NaCl) at pH 6 (inset is the Guinier fitting of 30 mg/mL CPPs). (C) Scattering profiles and (D) Kratky plot of 1 mg/mL CPPs at pH 2–10 (containing 10 mM NaCl). The scattering intensities were vertically shifted for clear visualization.

2.3.7. Purification of Theaflavins

The purities of theaflavins after column liquid chromatography purification were analyzed by HPLC. As shown in Figure 2-7, the purities of TF-1 (Figure 2-7A) and TF-3 (Figure 2-7C) were almost 100%. TF-2a and TF-2b still remained as a mixture (Figure 2-7B). However, their relative ratio (TF-2a:TF-2b) varied with elution time. Longer elution time lead to higher TF-2a:TF-2b ratio. TF-2a could reach higher than 98% of the mixture. Other purification approaches such as

preparative HPLC may be applied to obtain pure TF-2a and TF-2b. As TF-2a and TF-2b were not used in this dissertation, they were not further purified. The purified TF-1 and TF-3 were lyophilized and was used in subsequent experiments.

The simplified HPLC program was used to quantify the concentrations of TF-1 and TF-3 in the Caco-2 monolayer transport experiment. As presented in Figure 2-7D, this simplified HPLC program can effectively separate the peaks of TF-1 and TF-3.

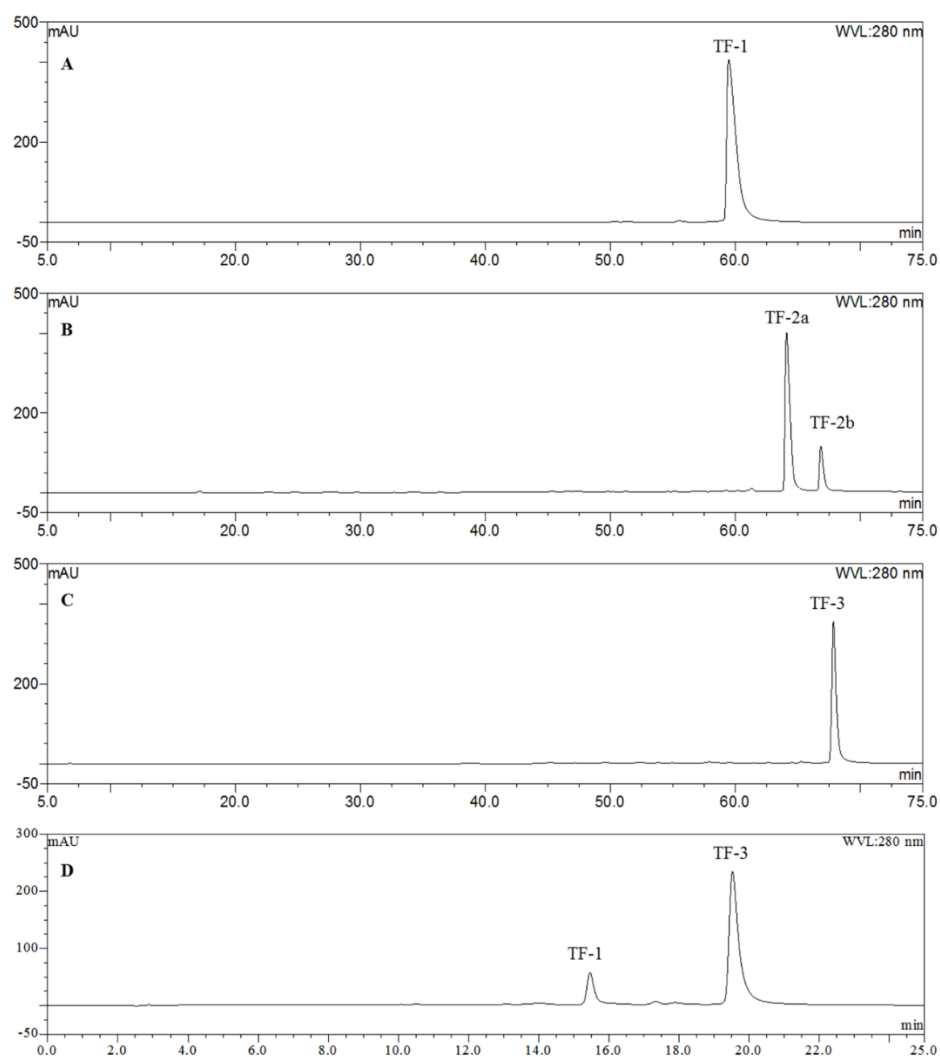


Figure 2-7. HPLC results of (A) TF-1, (B) TF-2s, and (C) TF-3 after purification, and (D) mixture of TF-1 and TF-3 analyzed using simplified HPLC program.

2.4. Conclusions

In this chapter, the basic physicochemical properties of the major material used in this Ph.D. research *i.e.* DD, Mw, viscosity, and R_g of CS, amino acid sequence, pI, and R_g of CPPs, and purity of TF-1 and TF-3 were characterized. Understanding these physicochemical characteristics would be beneficial for the following experiments.

CHAPTER III. ASSEMBLY AND CHARACTERIZATION OF THE CHITOSAN-CASEINOPHOSHOPEPTIDES NANOCOMPLEXES

As of submission of this dissertation, the work in this chapter has been written as two research papers in the titles of “Assembly of Chitosan-Caseinophosphopeptides Nanocomplexes to Encapsulate and Enhance Intestinal Permeation of Theaflavin-3,3'-digallate” and “Microstructures of Chitosan-Caseinophosphopeptides Nanocomplexes Encapsulated with Theaflavin-3,3'-digallate: A Small Angle X-Ray Scattering and Ultra-Small Angle X-Ray Scattering Study” which are ready for submission.

3.1. Abstract

The associations between CS and CPPs were investigated by turbidimetric titration by varying the CS:CPPs weight ratio, ionic strength, temperature, contents of urea, and ethanol. The results indicate that electrostatic interaction was the major force between CS and CPPs. Hydrogen bond and hydrophobic interactions may also be involved in the complexation process. The complexes assembled from CS and CPPs at different CS:CPPs weight ratios were characterized in terms of their particle sizes, polydispersity indexes (PDI), and ζ – potentials. Their morphologies were monitored by the atomic force microscopy (AFM). The microstructures of these nanocomplexes were characterized by the ultra-small angle X-ray scattering (USAXS) combined with SAXS.

3.2. Introduction

It is necessary to build the phase diagram of the CS-CPPs complexation process before encapsulation of TF-3 in the CS-CPPs nanocomplexes. In this chapter, the phase diagram and associations of CS-CPPs complexation were characterized by turbidimetric titration. The CS-CPPs complexes were assembled at pH 6, which is in the pH range of human small intestine. The CS-

CPPs nanocomplexes composed of CS:CPPs = 1-5 were further investigated by the SAXS and USAXS to gain insight of their microstructures..

3.3. Materials and Methods

3.3.1. Materials

CS was purchased from Kunpoong Bio. Co., Ltd. (South Korea) and used as received without further treatment. CPPs was purchased from Greencream Biotechnology Co., Ltd. (Guangzhou, China). Milli-Q water was used in all experiments.

3.3.2. Turbidimetric Titration

The pH-dependent turbidity was monitored by a Brinkmann PC910 colorimeter equipped with a 1 cm-path-length optical probe at light wavelength of 420 nm. The colorimeter was calibrated with Milli-Q water as 100% transmittance. CS was dissolved in 1% acetic acid. CPPs was dissolved Milli-Q water. Both CS and CPPs solutions were filtrated through 0.45 μm filter and adjusted to pH 2 before use. For studying the turbidity changes at different CS:CPPs weight ratios, 0.5 mg/mL CPPs solution (containing 0.01 M NaCl) and equal volumes of CS solution (containing 0.01 M NaCl) at various concentrations were mixed at ambient temperature with magnetic stirring, and pH was increased from 2.0 to 10.0 gradually. Turbidity and pH of the mixed system were monitored simultaneously. For investigating the effect of ionic strength on the associations between CS and CPPs, 0.5 mg/mL CPPs and same volume of 0.125 mg/mL CS were mixed in the presence of 0.01 M, 0.05 M, 0.1 M, 0.15 M, 0.3 M, 0.5 M, and 1.0 M NaCl. Turbidity was monitored from pH 2.0 to 10.0. To study the effects of temperature and urea on complexation between CS and CPPs, equal volumes of 0.5 mg/mL CPPs (0.01 M NaCl) and 0.125 mg/mL CS (0.01 M NaCl) were mixed with different concentrations of urea (0 M, 1 M and 2 M), or at different temperatures (20°C, 30°C, and 40°C). Turbidity was also recorded from pH 2.0 to 10.0. For studying the effect of ethanol on turbidity change, CS (final concentration 0.0625 mg/mL) and CPPs (final concentration 0.25

mg/mL) solutions were mixed with ethanol to reach the final concentrations of 0%, 10%, 30%, and 50% ethanol. Turbidity was also recorded from pH 2.0 to 10.0. The experiments were conducted in triplicate. Error bars were omitted for the clearance of the figures.

3.3.3. Preparation and Characterization of the CS-CPPs Nanocomplexes

CS was dissolved in 1% acetic acid (0.01 M NaCl) with moderate stirring, and adjusted to pH 6 after fully dissolved. CPPs was dissolved in 0.01 M NaCl solution and the pH was adjusted to 6. The CS-CPPs complexes were prepared by mixing 0.5 mg/mL CPPs with same volume of CS solution of different concentrations at ambient temperature with magnetic stirring.

Particle size, PDI, and ζ – potential of the complexes composed of various CS:CPPs weight ratios were measured by a Zetasizer Nano ZS90 (Malvern Instruments Ltd, Westborough, MA). The measurements were conducted in triplicate at 25°C.

The morphology of the CS-CPPs complexes was monitored by a Nanoscope IIIa Multi-Mode AFM (Veeco Instruments Inc., Santa Barbara, CA). Fresh made complexes were dripped on the surface of pre-cleaned mica slides for 1 h. The surface of the mica slides was rinsed with Milli-Q water and dried with nitrogen. Tapping mode was utilized.

3.3.4. SAXS and USAXS Measurements

The SAXS experiments were conducted at BioCAT 18-ID beamline of the APS at Argonne National Laboratory (Chicago, USA). A short exposure of 1 s followed by 5 s cooling was used to acquire the scattering data. The final SAXS profiles were obtained by subtracting the solvent from the average of 10 measurements. The USAXS experiments were performed at beamline 9-ID-C of the APS at Argonne National Laboratory. The samples were sealed in the 1 mm-thick silicone isolators (Grace Bio-Labs, Inc., OR, USA) with glass slides. The USAXS and SAXS data were merged and analyzed by the Irena software package¹⁹⁷.

3.4. Results and Discussion

3.4.1. Turbidimetric Titration

It is generally accepted that the primary interaction between proteins/polypeptides and oppositely charged polyelectrolytes is electrostatic interaction, which is pH dependent. Therefore, it is necessary to clarify how they interact at different pH. As an indicator of the strength of electrostatic interaction, turbidity of the CS-CPPs binary-component system was firstly monitored at different CS:CPPs weight ratios in a broad pH range from pH 2 to 10.

As shown in Figure 3-1, CPPs without addition of CS (CS:CPPs = 0) reached its maximum turbidity at approximately pH 4, which was attributed to the loss of electrostatic repulsion close to the pI. Below pH 4, the turbidities were very low for all CS:CPPs weight ratios, reflecting that there were no insoluble complexes formed by CS and CPPs. Starting from pH 4, all the curves increased vigorously at different initial pH ($\text{pH}_{\phi 1}$) until the turbidities reached their maximum values at various pH (pH_{max}), indicating that more insoluble complexes were assembled when pH increased from $\text{pH}_{\phi 1}$ to pH_{max} . Both $\text{pH}_{\phi 1}$ and pH_{max} shifted to higher pH when the CS:CPPs weight ratio increased. Notable, the curves of CS:CPPs from 2 to 5 almost overlapped between $\text{pH}_{\phi 1}$ and pH_{max} , which could be resulted from saturation of CPPs by CS when CS:CPPs was higher than 2. Further increasing pH above pH_{max} resulted in different patterns of turbidity change. For CS:CPPs ≤ 2 , the turbidity decreased and then leveled off, and the final levels of turbidities increased with CS concentrations. For CS:CPPs = 3-5, the turbidities tended to be stable after pH_{max} . No apparent sharp decreases were observed in this weight ratio range.

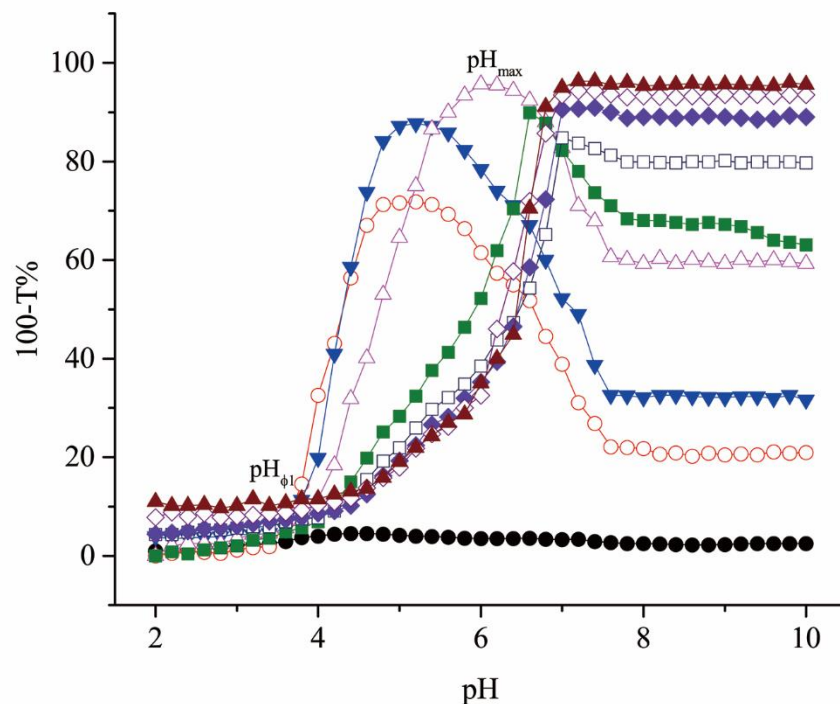


Figure 3-1. Turbidity change as a function of pH at CS:CPPs weight ratios of ● 0, ○ 0.125, ▼ 0.25, △ 0.5, ■ 1, □ 2, ◆ 3, ◇ 4, ▲ 5.

The turbidity change of the CS-CPPs mixtures at different pH indicates their complexation process. In general, two specific pH values *i.e.* pH_c and $pH_{\phi 1}$ are characterized as the onset of formation of soluble and insoluble complexes, respectively. The soluble complexes were formed by electrostatic attraction between positively charged CS and negatively charged patches on CPPs, although the net charge of CPPs was still positive at this pH. This process occurred at the pH (pH_c) lower than the pI of CPPs, prior to formation of the insoluble complexes. When pH was higher than $pH_{\phi 1}$, CS and CPPs were oppositely charged. They were strongly associated by electrostatic attraction, leading to phase separation. As correspond to the increased concentrations of CS, $pH_{\phi 1}$ shifted to higher value where CPPs carried more negative charges to associate with the extra amount of positive charges derived from CS. The pH_{max} at which the charges of the systems inverted shifted to higher pH as well. The maximum turbidity increased when the concentration of CS became higher, indicating the size and/or number of insoluble complexes increased. When pH

increased over the pK_a (6.3-6.4) of CS, the amine cations on CS molecular chains became deprotonated, and as a result CS became insoluble. The insolubility of CS in neutral to alkaline conditions explains the final high turbidities at high CS concentrations (CS:CPPs = 3-5).

The strength of electrostatic interactions is also affected by ionic strength. Therefore, the effect of ionic strength was characterized. As displayed in Figure 3-2, pH_{ϕ_1} and pH_{max} shifted to higher pH and the turbidity at pH_{max} decreased accordingly with increasing concentration of NaCl. The maximum turbidity in the presence of 0.3 M NaCl was only half of the maximum turbidity in the presence of 0.01 M NaCl. Further increasing ionic strength to 0.5 M NaCl and higher almost completely inhibited the interaction between CPPs and CS, which was reflected by the almost flat turbidity curves before CS became insoluble. It is worth noting that at pH 6–7.5, which is the physiological pH range of small intestine, the turbidities did not show significant difference when NaCl concentration was lower than 0.15 M. This phenomenon indicates when using the CS-CPPs complex as a delivery system, the difference of ionic strength between the physiological condition (0.15 M) and nanocomplex preparation condition (0.01 M, method in section 3.3.3) may not significantly affect the interaction between CS and CPPs at the site of intestinal absorption.

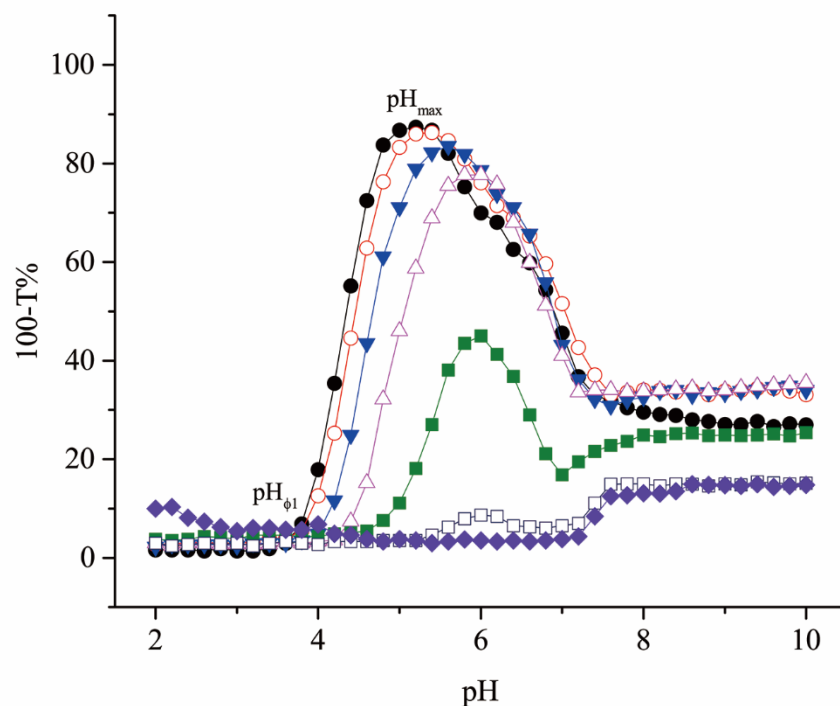


Figure 3-2. Turbidity change as a function of pH at CS:CPPs = 0.25 in the presence of ● 0.01 M, ○ 0.05 M, ▼ 0.10 M, △ 0.15 M, ■ 0.3 M, □ 0.5 M, ◆ 1 M NaCl

It is generally accepted that salt has charge screening effect at high concentration. Weinbreck *et al.* reported that at low concentration (17 mM), NaCl enhanced complexation between whey proteins and gum Arabic by increasing the solubility of polymers¹⁷. They also found the similar effect between whey proteins and carrageenan in the presence of 45 mM NaCl. They attributed this result to neutralization of extra charges by small amount of NaCl and thereby reduced of the electro-repulsion between the complexes¹⁶. This phenomenon was not observed in the CS-CPPs system. In a broad NaCl concentration (0.01–1 M), $\text{pH}_{\phi 1}$ shifted to higher pH where CPPs carried more negative charges. The maximum turbidity decreased as the concentration of NaCl increased. When high concentrations of NaCl (> 0.5 mg/mL) were applied to the system, the electrostatic interactions were almost suppressed, which was reflected by the very low turbidities before CS became

deprotonated. The electrostatic screening effect combined with pH-dependent turbidity proved that electrostatic interaction was the predominant interaction between CS and CPPs.

To further understand the forces that were involved in complexation between CS and CPPs, different concentrations of urea were added into their mixture and the turbidity was monitored upon alkalization. It was reported that urea can effectively suppress hydrogen bond¹⁹⁸. In CS, the deacetylated glucosamine units have both proton donor and acceptor¹⁹⁸, which can form hydrogen bond with certain groups such as the peptide bond in CPPs. Similar to the effects of ionic strengths, addition of urea disrupted formation of the CS-CPPs complexes (Figure 3-3), which was reflected by shifting of $pH_{\phi 1}$ and pH_{max} to higher pH and decreasing of the highest turbidity with increasing concentration of urea. The final levels of turbidity also decreased with increasing amount of urea.

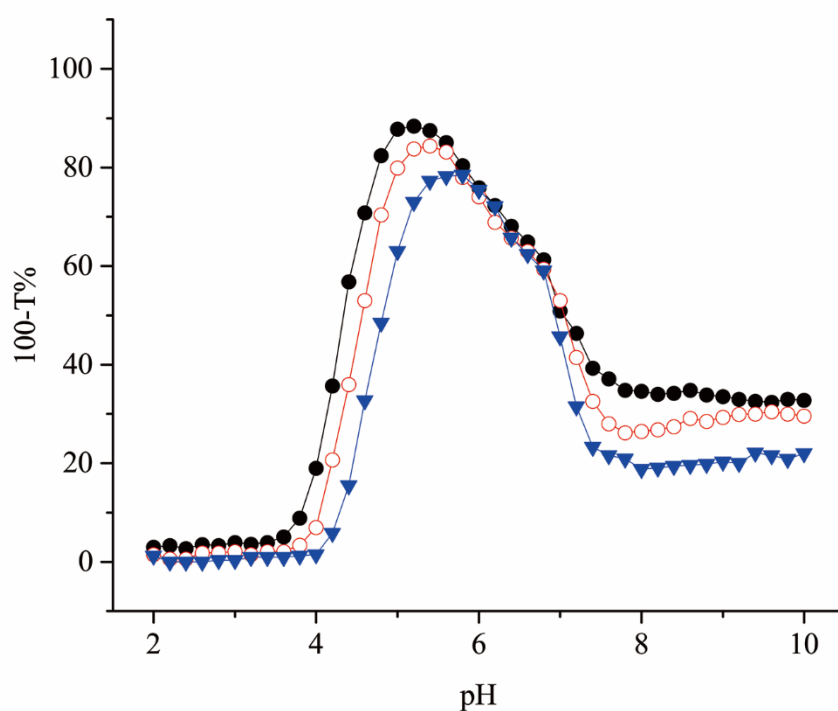


Figure 3-3. Turbidity change as a function of pH at CS:CPPs = 0.25 in the presence of ● 0 M, ○ 1 M, ▼ 2 M urea.

Although urea is an effective hydrogen bond inhibitor, it may also suppress the hydrophobic interaction^{113, 198}. Ethanol was used to clarify whether hydrophobic interaction was involved in complexation between CS and CPPs because ethanol can disrupt the hydrophobic interaction¹⁹⁸. As shown in Figure 3-4, the turbidity decreased with increasing content of ethanol (from 10% to 30%) when pH was between $\text{pH}_{\phi 1}$ to pH_{max} , while above pH_{max} the difference was not obvious. 50% ethanol significantly changed the process of CS-CPPs complexation where $\text{pH}_{\phi 1}$ shifted to lower pH and the maximum turbidity was about 20% smaller than that at lower ethanol contents. This result allows us to suggest that hydrophobic interaction was involved in CS-CPPs complexation.

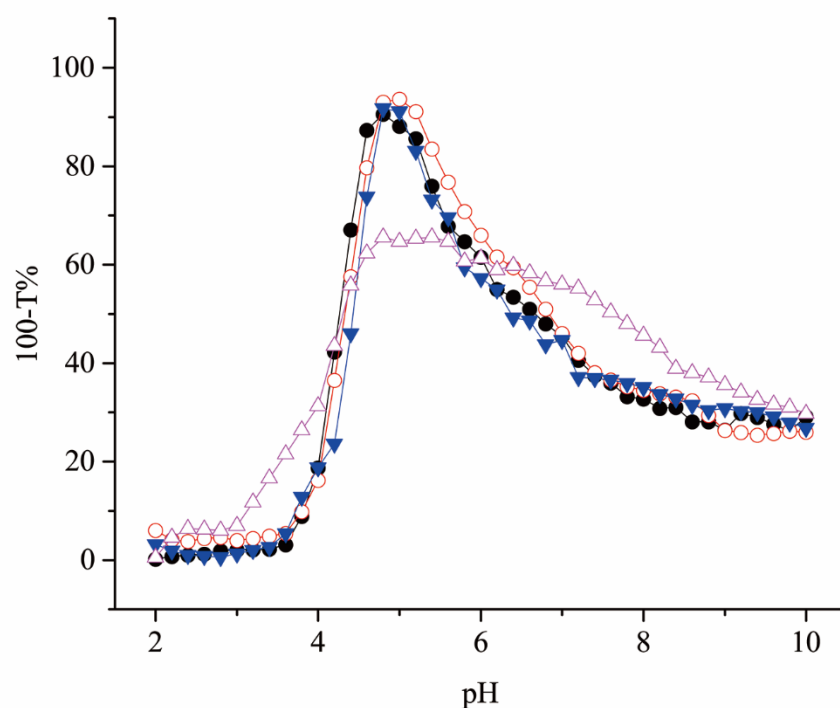


Figure 3-4. Turbidity change as a function of pH at CS:CPPs = 0.25 in the presence of ● 0%, ○ 10%, ▼ 30%, and △ 50% ethanol.

The effect of temperature on CS-CPPs complexation was also investigated. As illustrated in Figure 3-5, the turbidities at the studied three temperatures almost overlapped, indicating that the tested temperature range had negligible effect on formation of the CS-CPPs complexes.

Temperature can affect the interactions between polymers by influencing the Flory-Huggins interaction energy¹⁶. Generally, higher temperature suppresses formation of hydrogen bond, while it promotes the magnitude of hydrophobic interaction¹⁶. In the studied temperature range (20°C-40°C), temperature had little role on complexation between CS and CPPs. $pH_{\phi 1}$, pH_{max} , and maximum turbidities were almost identical at these three different temperatures, which may be resulted from involvement of entropy effect, such as hydrophobic interaction¹⁶. Therefore, the invariability of CS-CPPs complexation upon temperature change (20°C-40°C) could be resulted from a balance between the strength change of hydrogen bond and hydrophobic interaction. The temperatures tested in this study covered the room temperature and body temperature. Overlapping of the turbidities at this temperature range indicates that the difference of temperature between physiological condition (37°C) and nanocomplex preparation condition (25°C) may not disrupt the interactions between CPPs and CS if the CS-CPPs complexes are used as oral delivery system.

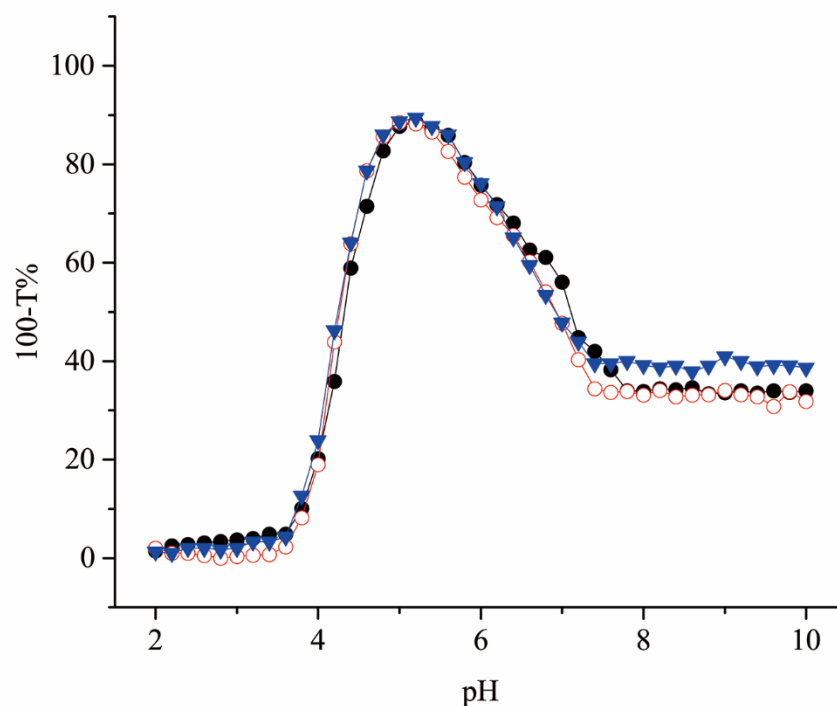


Figure 3-5. Turbidity change as a function of pH at CS:CPPs = 0.25 at ● 20 °C, ○ 30 °C, ▼ 40 °C.

3.4.2. Characterization of the CS-CPPs Nanocomplexes

The CS-CPPs nanocomplexes were assembled at pH 6 where CS molecule was positively charged. In addition, pH 6 is in the pH range of duodenum¹⁹⁹ and is very close to the pH of proximal part of jejunum²⁰⁰.

The physical properties including particle size, ζ – potential, and PDI of the CS-CPPs complexes composed of different CS:CPPs weight ratios at pH 6 are listed in Table 3-1. The particle size of the CS-CPPs complexes increased with the CS:CPPs weight ratio until CS:CPPs = 0.5 then decreased dramatically. This is consistent with the titration result (Figure 3-1). The size of the complex decreased until CS:CPPs=2 then gradually increased as the content of CS increased. The PDI which is a measure of the homogeneity of the system also decreased significantly when the CS:CPPs was higher than 0.5. The PDI value smaller than 0.3 is generally regarded as a narrow size distribution of the particles. The complexes assembled at CS:CPPs=1-3 had PDI smaller than 0.3, indicating that these complexes were more homogenous than the complexes assembled at other CS:CPPs weight ratios. CS was cationic at pH 6. Not surprisingly, as the amount of CS increased in the complexes, the ζ – potential experienced a significant increase from +2.82 mV to + 26.9 mV. It was noticed that the ζ – potential change was highly correlated to the weight ratio change when CS:CPPs was between 0.125 – 1, as reflected by doubling of the ζ – potential when the concentration of CS doubled. While when CS:CPPs = 1 and higher, the ζ – potential change was not proportional to the CS concentration change. This result could be ascribed to gradually saturation of the complexes surface with the CS molecules after CS:CPPs was higher than 1. This result was consistent with the titration result (Figure 3-1), in which the turbidities at CS:CPPs = 2 – 5 almost overlapped at in the pH range between $\text{pH}_{\phi 1}$ and pH_{max} .

Table 3-1. Particle size, PDI, and ζ – potential of the complexes composed of different CS:CPPs at pH 6

CS : CPPs	Particle Size (nm)	PDI	ζ - Potential (mV)
0.125 : 1	661.4±28.4	0.153±0.008	+ 2.8±0.3
0.25 : 1	681.5±36.6	0.519±0.028	+ 4.4±0.2
0.5 : 1	764.9±9.6	0.494±0.087	+ 9.0±0.0
1 : 1	174.3±3.0	0.158±0.037	+ 17.7±0.3
2 : 1	186.0±2.6	0.192±0.016	+ 21.9±0.6
3 : 1	201.8±3.6	0.217±0.005	+ 23.1±1.1
4 : 1	264.7±16.2	0.322±0.048	+ 24.9±0.9
5 : 1	338.8±37.3	0.418±0.070	+ 26.9±0.5

AFM was utilized with tapping mode to study the morphology of the CS-CPPs complexes. As shown in Figure 3-6A, large aggregates were observed at CS:CPPs = 0.5. The complex assembled at CS:CPPs = 2 had sphere shape and smooth surface (Figure 3-6B). When CS:CPPs increased to 4, the sphere complexes still existed, but some larger particles were observed (Figure 3-6C). These observations were consistent with the particle size measurement.

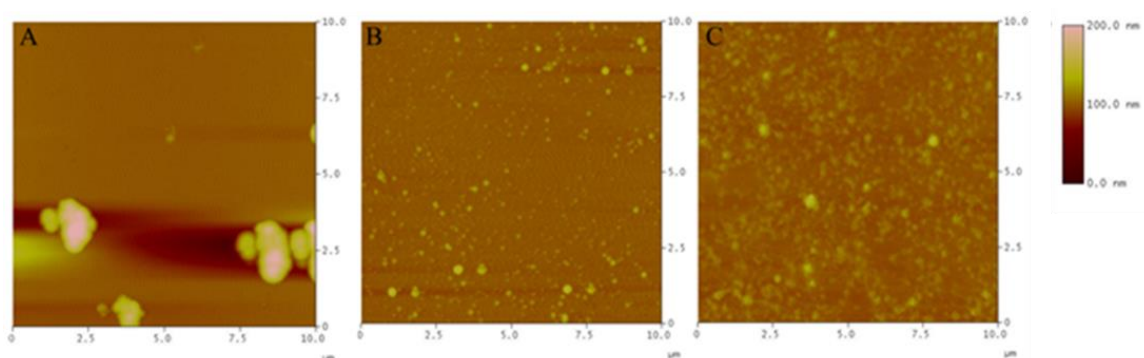


Figure 3-6. Morphologies of the CS-CPPs complexes composed of (A) CS:CPPs = 0.5, (B) CS:CPPs = 2, and (C) CS:CPPs = 4

3.4.3. SAXS and USAXS Measurements

The CS-CPPs nanocomplexes composed of CS:CPPs=1-5 were further subjected to SAXS and USAXS studies. The scattering profiles of these CS-CPPs nanocomplexes are shown in Figure 3-7A.

The scattering profiles of the CS-CPPs nanocomplexes composed of different CS:CPPs weight ratios were firstly qualitatively analyzed. They displayed completely different patterns of single CS and CPPs at same concentrations (section 2.3.3 and 2.3.6). The shape of these nanocomplexes can be manifested in $0.005 \text{ \AA}^{-1} < q < 0.03 \text{ \AA}^{-1}$, where the scattering intensities decayed in $I(q) \sim q^{-3.7}$ to $I(q) \sim q^{-4}$ (Figure 3-7A). This means these CS-CPPs nanocomplexes existed as compact globular structures in solution and the surface of these nanocomplexes was relatively smooth. The scattering curves of CS:CPPs = 4 and 5 in the ultra-small q region ($q < 0.001 \text{ \AA}^{-1}$) upturned in $I(q) \sim q^{-1.3}$ and $I(q) \sim q^{-3.3}$ manners. This increase of intensity was due to formation of larger structures (aggregates) in this length scale. The shape of the aggregates may experience a transition from rod-like ($\alpha=1$) to sphere ($\alpha=3$)¹⁹⁶.

The peaks presented in the Kratky plot (Figure 3-7B) indicate existence of folded structures. The peak shifted to higher q as CS:CPPs increased from 1 to 4, then it shifted back to lower q at CS:CPPs=5. The peak position in the Kratky plot can reflect R_g . The peak position at higher q represents smaller size²⁰¹. Therefore, the R_g of the CS-CPPs nanocomplexes initially decrease and then rise.

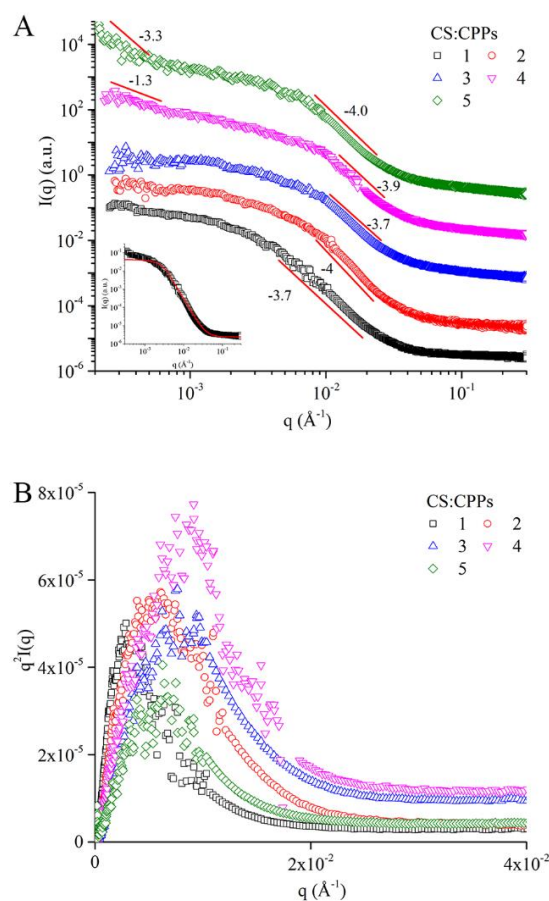


Figure 3-7. (A) Scattering profiles of the CS-CPPs nanocomplexes composed of 0.25 mg/mL CPPs and 0.25-1.25 mg/mL CS (CS:CPPs=1-5). The scattering curves were vertically shifted for clear visualization. Inset is the fitting (red solid line) of the scattering of the nanocomplex composed of CS:CPPs=1:1. (B) Kratky plot of the nanocomplexes composed of CS:CPPs=1-5.

The R_g of these CS-CPPs nanocomplexes was quantitatively analyzed by fitting the scattering curves with the Irena software¹⁹⁷ (Figure 3-7A inset). Table 3-2 shows the R_g of the CS-CPPs nanocomplexes. Same as the result obtained from the Kratky plot, as the CS:CPPs weight ratio increased, the R_g of the CS-CPPs nanocomplexes initially decreased from 698 \AA (CS:CPPs=1) to 289 \AA (CS:CPPs=4), then increased to 331 \AA (CS:CPPs=5) again.

Table 3-2. Radius of gyration of the CS-CPPs nanocomplexes composed of different CS:CPPs weight ratios

CS:CPPs	R_g (Å)
1:1	698±13.36
2:1	417±9.80
3:1	319±9.26
4:1	289±10.08
5:1	331±9.21

Based on these results, complexation between CS and CPPs is proposed in the following ways (Figure 3-8). When CS:CPPs weight ratio was low, the system was relatively rich in CPPs, which can act as the linkers between the CS molecules. The CS-CPPs nanocomplexes were loose CS network connected by CPPs (Figure 3-8A). When the concentration of CS increased, the system was gradually dominated by CS. More CS molecules bind to a single CPPs molecules until the CPPs molecule was almost surrounded by the CS molecules (Figure 3-8B), which inhibited further linking with another CPPs-bonded CS. Thus, the R_g of the nanocomplexes decreased. When CS:CPPs further increased to 5, the CPPs molecules in the system were insufficient to constrain the CS in a compact structure (Figure 3-8C). Therefore, the R_g increased again.

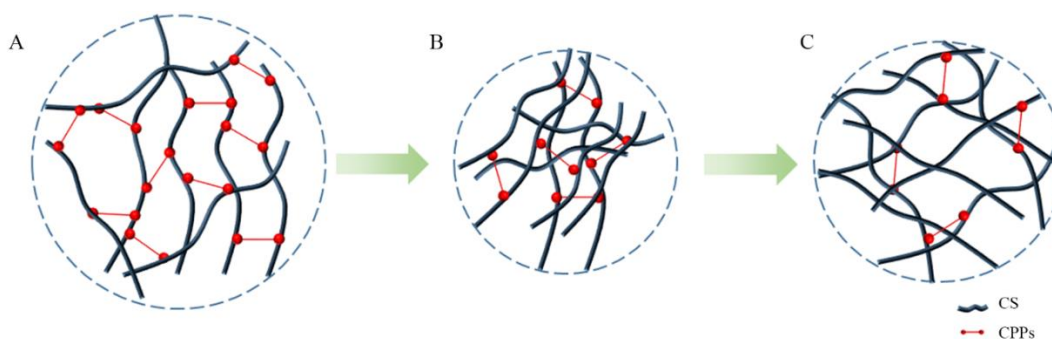


Figure 3-8. Schematic representation of the CS-CPPs nanocomplexes composed of different CS:CPPs weight ratios.

3.5. Conclusions

In this chapter, the phase diagram and interactions involved in complexation of CS and CPPs were systematically studied using turbidimetric titration by varying the weight ratio, ionic strength, temperature, and the contents of urea and ethanol. Electrostatic interaction was the predominant force between these two building materials. Hydrogen bond and hydrophobic interaction may also be involved in formation of the CS-CPPs complexes. The CS-CPPs nanocomplexes composed of CS:CPPs = 1-5 showed increased particle size, PDI and ζ -potential. However, change of R_g of these nanocomplexes did not follow the same pattern, which stem from the microstructural change induced by the relative weight ratio between CS and CPPs.

CHAPTER IV. INVESTIGATION OF THE INTERACTIONS BETWEEN CASEINOPHOSHOPEPTIDES AND THEAFLAVIN- 3,3'-DIGALLATE

As of submission of this dissertation, the work in this chapter has been written as a research paper in the title of “Investigation of the Associations Between Caseinophosphopeptides and Theaflavin-3,3'-digallate” which is ready for submission.

4.1. Abstract

In this chapter, the interactions between CPPs and TF-3 in aqueous environment and on the solid-liquid interface had been systematically studied with fluorescence quenching, CD, SAXS, and quartz crystal microbalance with dissipation monitoring (QCM-D). The binding process in the aqueous environment was enthalpy driven and hydrogen bond was the major force. Addition of TF-3 did not change the secondary structures and R_g of CPPs, but it could induce aggregation of CPPs. The size of aggregates increased with the concentration of TF-3. QCM-D results revealed that hydrogen bond was involved in the adsorption of TF-3 onto the CPPs modified gold-coated quartz crystal surface.

4.2. Introduction

The CS-CPPs nanocomplex was used to encapsulate TF-3 in this dissertation. The procedure of encapsulation was firstly mixing CPPs solution with TF-3 solution. The CPPs/TF-3 mixture was then added into the CS solution. In this chapter, multiple approaches including fluorescence quenching, CD, SAXS, and QCM-D were employed to gain insight into the interactions and conformational changes involved in the first step of encapsulation, which is mixing CPPs with TF-3.

Studying the interactions between CPPs and TF-3 also has its biological significance. Drinking black tea with milk is a tradition in many countries. However, the impact of milk proteins on the functionalities of tea polyphenols and vice versa are still controversial²⁰²⁻²⁰⁹. As TF-3 is a major polyphenol in black tea and CPPs are the polypeptides hydrolyzed from caseins, which are the most abundant proteins in milk, studying their association at the small intestinal physiological condition would be beneficial for clarifying these controversies.

4.3. Materials and Methods

4.3.1. Materials

CPPs was purchased from Greencream Biotechnology Co., Ltd. (Guangzhou, China). TF-3 was purified from black tea extract as described in section 2.2.8. 11-Mercaptoundecanoic acid (11-MUA), 1-ethyl-3-(3-dimethylaminopropyl)carbodiimide hydrochloride (EDC), and N-hydroxysuccinimide (NHS) were purchased from Sigma-Aldrich (MO, USA). Gold-coated quartz crystal was obtained from Q-Sense AB (Sweden). Milli-Q water was used in all experiments.

4.3.2. Fluorescence Quenching

The fluorescence emission spectra and lifetime were recorded with a FluoroMax-3 spectrofluorometer (Horiba Jobin Yvon, Inc., NJ, USA). The excitation wavelength (λ_{ex}) and emission wavelength (λ_{em}) were 295 nm and 320-500 nm, respectively. The excitation and emission slit widths were kept at 5 nm. CPPs and TF-3 were dissolved in Milli-Q water containing 0.15M NaCl at pH 6. A series of TF-3 solutions (1.95×10^{-3} - 0.0625 mg/mL) were prepared from 0.125 mg/mL TF-3 stock solution by successive dilution. 0.5 mg/mL CPPs and equal volume of TF-3 solutions were mixed to obtain the final concentrations of 9.77×10^{-4} - 0.03125 mg/mL TF-3 and 0.25 mg/mL CPPs. The measurements were conducted at 20°C, 30°C, and 40°C. Each measurement was triplicated.

The time-resolved (time-domain) fluorescence lifetime was calculated by fitting the William-Watts (WW) stretched exponential function²¹⁰ expressed as

$$I(t) = I_0 \exp[-(t/\tau)^\beta] \quad \text{eq. 4-1}$$

where I_0 is the pre-exponential factor; τ is the lifetime; β is the stretching coefficient ranging from 0 to 1, which reflects the distribution of local environment of the fluorophore. For a uniform local environment, $\beta = 1$, while for a distribution of local environment, $0 < \beta < 1$. The average lifetime $\langle \tau \rangle$ was calculated by

$$\langle \tau \rangle = \frac{\tau}{\beta} \Gamma\left(\frac{1}{\beta}\right) \quad \text{eq. 4-2}$$

where Γ is the gamma function.

4.3.3. CD Spectra

The secondary and tertiary structural changes of CPPs after associating with different concentrations of TF-3 were studied on an Aviv 420SF circular dichroism spectrometer (Biomedical, Inc., Lakewood, NJ, USA) using quartz cell with the path length of 1 mm. CPPs and TF-3 were dissolved in 0.15 M NaCl at pH 6.0 before mixing. 0.5 mg/mL CPPs and same volume of TF-3 (0.0315, 0.625, 0.125, 0.25 mg/mL) were mixed and measured in the far (190-260 nm) - and near (260-320 nm)-UV regions in nitrogen atmosphere at 25 °C. Each sample was scanned with a scan speed of 5 s/nm and data were collected for each nm. The results were expressed in terms of mean residue ellipticity $[\theta]$ in $\text{deg cm}^2 \text{ dmol}^{-1}$. The secondary structures of CPPs before and after binding with TF-3 were analyzed by the CDPro software using CONTIN/LL procedure with the database of Sreerama and Woody.

4.3.4. SAXS Measurement

The SAXS experiments were conducted at BioCAT 18-ID beamline of the APS at Argonne National Laboratory (Chicago, USA). CPPs and TF-3 were dissolved in Milli-Q water containing

0.15 M NaCl at pH 6 and mixed at ambient temperature. The final concentration of CPPs was fixed at 2 mg/mL and the final concentrations of TF-3 varied from 0.03125-0.5 mg/mL. A short exposure of 1 s followed by 5 s cooling was used to acquire the scattering data. The final SAXS profiles were obtained by subtracting the solvent from the average of 10 measurements.

4.3.5. QCM-D Measurement

The CPPs modified gold-coated quartz crystals were prepared according to Wang *et al.* method²¹¹. Briefly, the gold-coated quartz crystals were cleaned in an UV/ozone chamber for 10 min and then immersed in a mixture of 25% NH₄OH, 30% H₂O₂, and Milli-Q water (1:1:5, v/v) for 5 min at 75°C, then the gold-coated quartz crystals were cleaned by UV/ozone again for 10 min. After rinsed with Milli-Q water and dried with N₂, the gold-coated quartz crystals were immersed in 10 mM 11-MUA dissolved in 100% ethanol at 60°C for at least 24 h, and then rinsed with 100% ethanol and dried with N₂. The 11-MUA attached gold-coated quartz crystals were activated by a mixture of 100 mg/mL NHS and 100 mg/mL EDC (1:1, v/v) for 1 h, and they were transferred to 10 mg/mL CPPs solution (0.15 M NaCl, pH 6) for at least 24 h at 4°C. The CPPs modified gold-coated quartz crystal surface was rinsed with Milli-Q water and dried by N₂ before use.

The interaction between CPPs and TF-3 on the solid-liquid interface was studied on a Q-Sense D300 system (Q-Sense AB, Sweden). The loop and sensor were rinsed before the CPPs modified gold-coated quartz crystal was placed in the QCM-D chamber. 0.15 M NaCl solution (pH 6) was pumped into the chamber. After a stable baseline was obtained, different concentrations (0.1, 0.3, 0.5, 0.7, and 0.9 mg/mL) of TF-3 solutions (0.15 M NaCl, pH 6) were injected into the QCM-D chamber to interact with CPPs that were chemically connected to the quartz crystal surface as described above. The shift of frequency (ΔF) and energy dissipation (ΔD) at the fundamental resonant frequency, as well as the third, fifth, and seventh overtones were monitored simultaneously, and the results were analyzed by the QTools software. The experiments were conducted in triplicate at 25°C, and the results were expressed as mean \pm standard deviation.

4.4. Results and Discussion

4.4.1. Fluorescence Quenching

Fluorescence quenching has been widely used in studying the interactions between polyphenols and proteins/polypeptides. Tryptophan (Trp, W), tyrosine (Tyr, Y) and phenylalanine (Phe, F) are fluorescent amino acids which contribute to the fluorescence of proteins and polypeptides. Among these three fluorescent amino acids, tryptophan is very sensitive to polarity and local environment changes. Therefore, tryptophan which has a typical emission peak at 350 nm in water is often used as the indicator in studying the fluorescence properties of proteins and polypeptides. The characteristic emission peak of tyrosine at 303 nm in water may shift to 350 nm at certain conditions that can cause ionization of the phenolic hydroxyl group, *e.g.* in the pH higher than the pK_A of the phenolic hydroxyl group at excited state ($pK_A = 4$) or in buffers that can accept protons²¹². Therefore, when proteins/polypeptides are rich in tyrosine, exciting at 280 nm (which is often applied in studying the fluorescence of proteins) at these conditions could result in the co-excitation of tryptophan (278 nm) and tyrosine (275 nm), and the emission from tyrosine can interfere with the emission spectrum of tryptophan. The LC-MS/MS result of the primary structures of CPPs (section 2.3.4) revealed that the CPPs sample is rich in tyrosine. Therefore, the fluorescence quenching experiments were performed at the excitation wavelength of 295 nm to only excite tryptophan, and the interference from tyrosine was eliminated.

The fluorescence quenching experiments were performed at pH 6, which is within the pH range of human duodenum and is very close to the pH of the proximal part of jejunum^{199, 200}. TF-3 was also relatively stable at this pH. 0.15M NaCl was used since it is the physiological NaCl concentration. The fluorescence quenching of CPPs by TF-3 was studied at 20°C, 30°C, and 40°C. Figure 4-1 shows the fluorescence emission spectra of CPPs with addition of various concentrations of TF-3 as quenchers. As the concentration of TF-3 increased, the fluorescence intensity decreased

accordingly. No apparent red shift or blue shift was observed, indicating that the polarity of environment around tryptophan did not change.

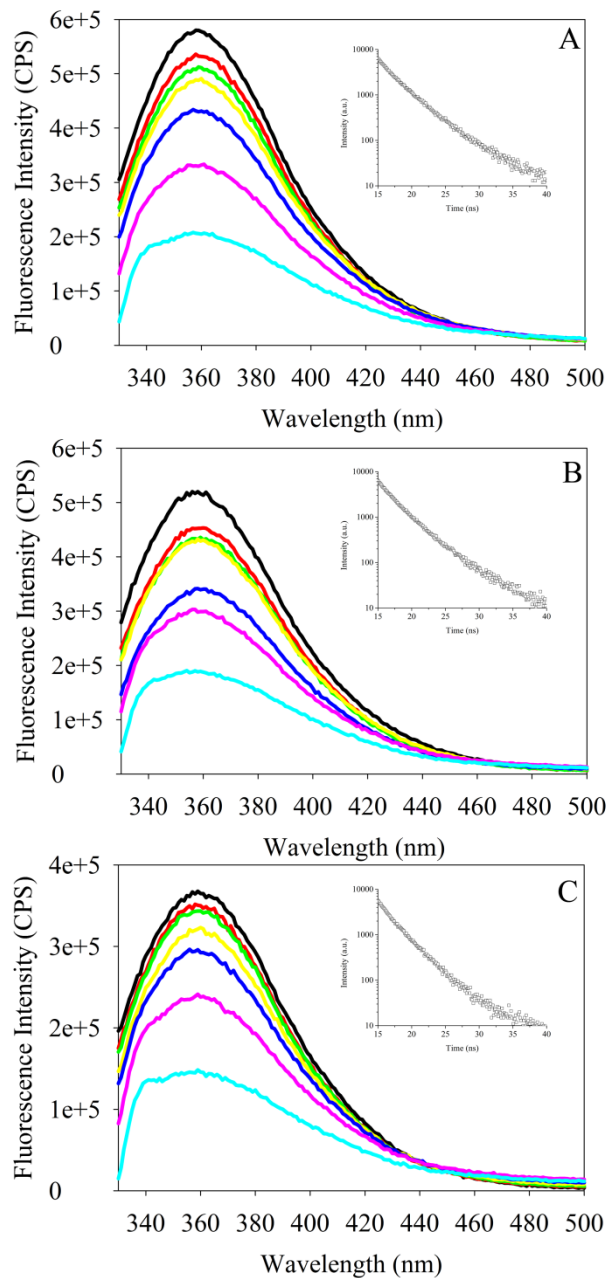


Figure 4-1. Fluorescence emission spectra of CPPs excited at 295 nm in the presence of increasing concentrations of TF-3 at (A) 20°C, (B) 30°C, and (C) 40°C. The insets are the representative lifetime decay.

Fluorescence quenching can be subdivided into static quenching and dynamic (collisional) quenching depending on how fluorophore contacts with the quencher. The most accurate way to determine the type of fluorescence quenching is to measure the fluorescence lifetime²¹². The fluorescence lifetime of CPPs in the absence and presence of TF-3 (Figure 4-1 insets) were calculated with eq. 4-1 and eq. 4-2. It was found that the fluorescence lifetime of CPPs did not change after associating with TF-3 ($\tau_0/\tau = 1$). This result suggests that the type of quenching between CPPs and TF-3 was static quenching²¹². The non-fluorescent complexes at the ground energy state were formed after adding TF-3 to CPPs. The static quenching process can be expressed as



where B is the fluorophore (CPPs); Q represents the quencher (TF-3); n is the number of binding sites; Q_nB is the non-fluorescent complexes formed between CPPs and TF-3. The binding constant K_A between fluorophore and quencher can be expressed as

$$K_A = \frac{[Q_nB]}{[Q]^n[B]} \quad \text{eq. 4-4}$$

where [Q] and [B] are the concentrations of quencher and fluorophore, respectively. $[Q_nB]$ is the concentration of the complexes, which can be expressed as

$$[Q_nB] = [B]_0 - [B] \quad \text{eq. 4-5}$$

where $[B]_0$ is the concentration of total CPPs. By substituting eq. 4-5 into eq. 4-4, the binding constant K_A can be expressed as

$$K_A = \frac{[B]_0 - [B]}{[Q]^n[B]} \quad \text{eq. 4-6}$$

The fluorescence intensity (F) is proportional to the concentration of fluorophore in static quenching

$$\frac{[B]}{[B]_0} \propto \frac{F}{F_0} \quad \text{eq. 4-7}$$

here F_0 is fluorescence intensity of CPPs without TF-3. The binding constant K_A can be obtained from the following equation with logarithmic form derived eq. 4-6²¹³

$$\log \left[\frac{(F_0 - F)}{F} \right] = \log K_A + n \log [Q] \quad \text{eq. 4-8}$$

The fractional accessibility of tryptophan to the quencher and the Stern-Volmer quenching constant (K_{SV}) can be calculated from the modified Stern-Volmer equation²¹²

$$\frac{F_0}{(F_0 - F)} = \frac{1}{fK_{SV}[Q]} + \frac{1}{f} \quad \text{eq. 4-9}$$

where F is the fluorescence intensity of CPPs with TF-3; K_{SV} is the Stern-Volmer quenching constant; f is the fraction of the initial fluorescence that is accessible to quencher.

K_A and K_{SV} were determined graphically by eq. 4-8 and eq. 4-9. A plot of $\log [(F_0 - F)/F]$ versus $\log [Q]$ yields $\log K_A$ as the intercept on the y axis and the number of binding sites n as the slope. The quenching constant K_{SV} can be obtained from a plot of $F_0/(F_0 - F)$ versus $1/[Q]$. The binding constant K_A , Stern-Volmer quenching constant K_{SV} , and fluorescence lifetime τ (calculated by eq. 4-1 and eq. 4-2) at different temperatures are listed in Table 4-1.

Table 4-1. Quenching constant (K_{sv}), binding constant (K_A), lifetime and thermodynamic parameters of TF-3 binding to CPPs

Temperature (K)	K_{sv} ($\times 10^4 M^{-1}$)	K_A ($\times 10^4 M^{-1}$)	Lifetime (ns)	ΔH ($kJ \cdot mol^{-1}$)	ΔS ($J \cdot mol^{-1} \cdot K^{-1}$)	ΔG ($kJ \cdot mol^{-1}$)
293	6.56 \pm 0.063	14.00 \pm 0.064	8.72 \pm 0.11			-29.00
303	3.79 \pm 0.29	9.57 \pm 0.12	8.55 \pm 0.18	-39.32	-35.19	-28.65
313	1.88 \pm 0.11	4.98 \pm 0.12	8.16 \pm 0.36			-28.30

Enthalpy change (ΔH), entropy change (ΔS), and free energy change (ΔG) are important thermodynamic parameters in determining the type of interactions between CPPs and TF-3. In this research, 293 K, 303 K, and 313 K were applied in studying this temperature-dependent binding process. In this temperature range, CPPs and TF-3 were stable and ΔH and ΔS were considered constant, so ΔH and ΔS can be calculated by the van't Hoff equation

$$\ln K = \frac{-\Delta H}{RT} + \frac{\Delta S}{R} \quad \text{eq. 4-10}$$

where K is the binding constant at the corresponding temperature; R is the gas constant; and T is the Kelvin temperature. The free energy change (ΔG) was calculated by the following equation

$$\Delta G = \Delta H - T\Delta S = -RT \ln K \quad \text{eq. 4-11}$$

The negative ΔH and ΔS values listed in Table 4-1 indicate that the binding process was enthalpy driven, and hydrogen bond was the predominant interaction between CPPs and TF-3 in the studied aqueous environment²¹⁴. The negative free energy change (ΔG) suggests that this binding process was spontaneous.

4.4.2. CD Spectra

The bio-functionalities of proteins and polypeptides significantly rely on their conformations. The conformations including secondary and tertiary structures might be changed after binding with polyphenols. In the present study, the conformations of CPPs after associating with different concentrations of TF-3 were studied by measuring the far- and near-UV CD spectra.

Farrell *et al.* reported that β -sheet (34%), turns (28%), and random coil (29%) were the dominant secondary structures of a phosphopeptide derived from β -casein at 25°C²¹⁵. By measuring the far-UV (190-260 nm) CD spectra (Figure 4-2A), it was found that random coil was one of the major secondary structures of CPPs, as reflected by the characteristic negative band near 195 nm. The weak broad negative shoulder at 220-230 nm indicates the presence of β -sheet¹²⁶. Analyzing by CONTIN/LL revealed that the secondary structures of CPPs contained 2.6% α -helix, 40.9% β -Sheet, 19.4% turn and 37.1% random coil. After adding different concentrations of TF-3 (0.015625 – 0.125 mg/mL) into CPPs solutions, no significant changes were observed, demonstrating that in the tested concentrations, association of TF-3 with CPPs did not induce secondary structural alteration of CPPs.

Binding of CPPs with TF-3 was also characterized by the near-UV (260-320 nm) CD spectra (Figure 4-2B). Pure CPPs showed a weak negative band around 270 – 300 nm. After adding TF-3, there was a dose-dependent increase around 270 - 290 nm, which may be attributed to the tryptophan and tyrosine side chains²¹⁶. This result indicates that binding of TF-3 was close to these groups. The fluorescence quenching of the tryptophan in CPPs by TF-3 confirmed that binding of TF-3 in vicinity of tryptophan. The increase of $[\theta]$ also indicates a decrease of mobility of these aromatic residues²¹⁶.

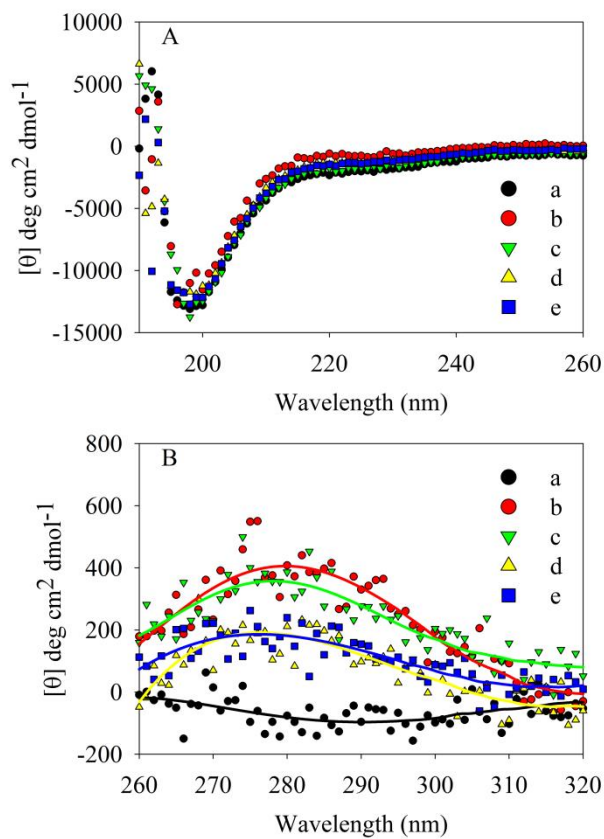


Figure 4-2. (A) Far (190 – 260 nm)- and (B) near (260 – 320 nm)-UV CD spectra of 0.25 mg/mL CPPs associating with various concentrations of TF-3: (a) 0 mg/mL; (b) 0.125 mg/mL; (c) 0.0625 mg/mL; (d) 0.03125 mg/mL; (e) 0.015625 mg/mL.

4.4.3. SAXS Measurement

The conformation of CPPs after associating with TF-3 was further studied by the SAXS. The scattering profiles of CPPs associated with different concentrations of TF-3 are shown in Figure 4-3A. Fitting the power law to the intermediate q range yielded the power about -0.8, which was very close to the power of rod-like structure (power of -1), meaning that the CPPs may exist in a rod-like shape in solution. In the small q range, the power increased significantly from -0.85 to -2.56 upon addition of TF-3, indicating that aggregates were formed, and the aggregates may experience a transformation from the rod-like shape (power of -1) to disk- (power of -2) or sphere-

like (power of -3) shape¹⁹⁶. The Kratky plot (Figure 4-3B) shows the upward curves without peaks, suggesting CPPs remained unfolded upon interacting with TF-3.

The R_g was determined by Guinier fitting (eq. 2-6) at the region of $qR_g < 1.3$ (Figure 4-3C). The R_g of 2 mg/mL CPPs was 1.5 nm. After associating with TF-3, the R_g remained 1.5 - 1.6 nm.

The size of aggregates was obtained by fitting the scattering curves at the small q -ranges with the Debye-Bueche function²¹⁷ (Figure 4-3D), which is expressed as

$$I(q) = \frac{I_{ex}(0)}{(1+\Xi^2 q^2)^2} \quad \text{eq. 4-12}$$

where $I_{ex}(0)$ is the extrapolated scattering intensity at zero wave vector; Ξ is the size of aggregates in the system. The aggregate size after addition of TF-3 increased from 13.1 nm to 19.5 nm.

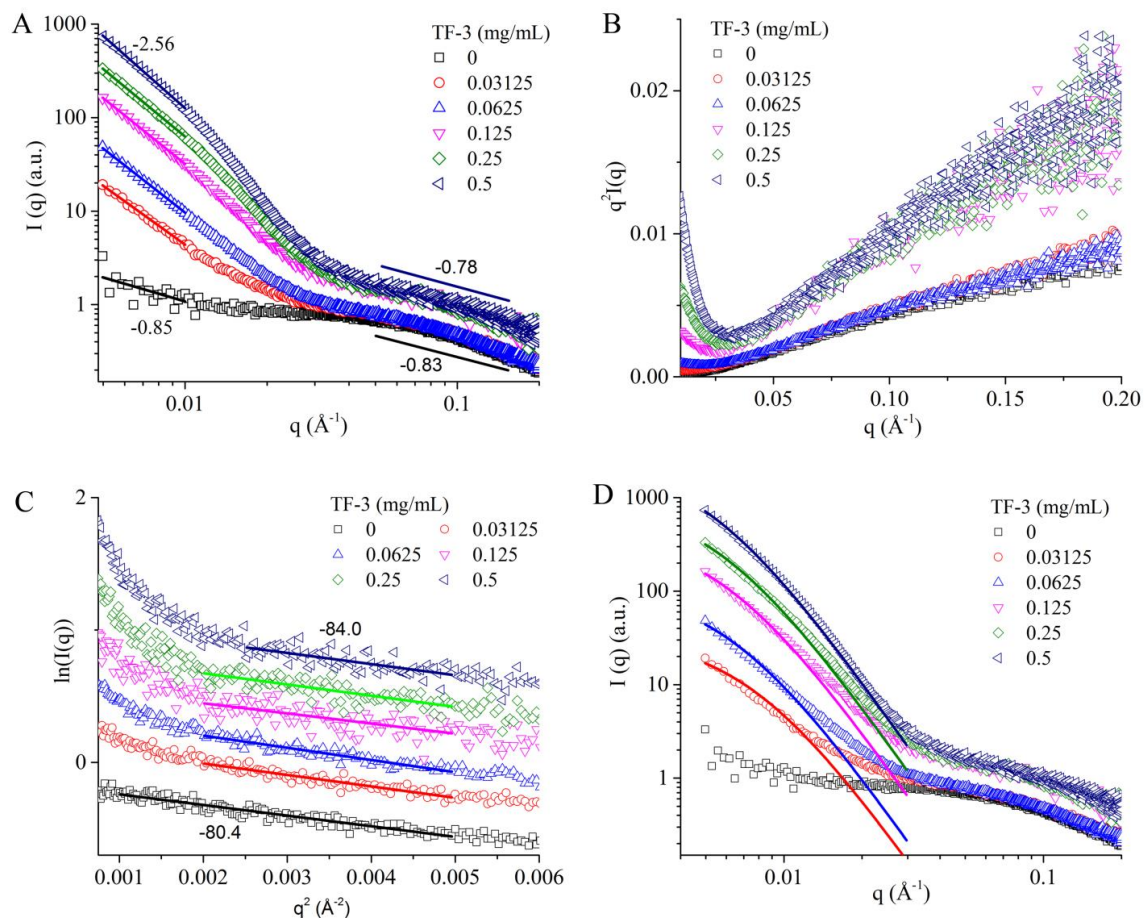


Figure 4-3. (A) Small angle X-ray scattering profiles, (B) Kratky plot, (C) Guinier fitting at the region $qR_g < 1.3$, and (D) Debye-Bueche fitting of 2 mg/mL CPPs associated with 0-0.5 mg/mL TF-3. The curves in (A) (C) and (D) were vertically shifted for better visualization of the results.

4.4.4. QCM-D Study

Most of the studies on the interactions between proteins/polypeptides and polyphenols were carried out in the aqueous environments, while little was known about their associations on the solid-liquid interface, although this situation is often seen *in vivo*. In this study, QCM-D was employed, which recently emerged as a versatile equipment in investigating the *in-situ* association between biomolecules on the solid-liquid interface²¹⁸.

The shift of frequency (ΔF) and energy dissipation (ΔD) were monitored simultaneously. When TF-3 solution was injected into the chamber (at t_1) after a stable baseline was achieved, the shift

of frequency (ΔF) decreased sharply (Figure 4-4A), while the energy dissipation (ΔD) only slightly decreased (Figure 4-4B). Decreasing in ΔF means an increasing amount of TF-3 adsorbed on the CPPs surface. Decreasing in ΔD indicates formation of a more rigid film, while a viscoelastic adlayer can lead to a positive ΔD value. After rinsing with 0.15 M NaCl solution (at t_2), ΔF at each TF-3 concentration increased, suggesting that parts of the adsorbed TF-3 were loosely bound to the CPPs layer and they were washed away with the NaCl solution. As the concentration of injected TF-3 increased from 0.1 mg/mL to 0.9 mg/mL, ΔF became more negative while the corresponding ΔD tended to be less negative, but not very significantly. These results indicate that the amount of TF-3 adsorbed on the CPPs surface increased with concentration, and the rigidity of CPPs film decreased upon contacting with little amount of TF-3. However, further increase the concentration of TF-3 did not significantly influence the rigidity of the TF-3 adsorbed CPPs film.

The ratios of the frequency shift to its corresponding overtone number ($\Delta F_n/n$) at different overtones ($n = 3, 5, 7$) overlapped (Figure 4-4C) at all the studied TF-3 concentrations (0.1 – 0.9 mg/mL), indicating that the TF-3 adsorbed CPPs layer was a rigid film at these TF-3 concentrations, which was in accordance with the negative ΔD values. The adsorbed mass of adsorbate on a thin and rigid layer can be calculated by the Sauerbrey equation

$$M = -\frac{C}{n}\Delta F \quad \text{eq. 4-13}$$

where M is the adsorbed mass of adsorbate per unit area; C is the mass sensitivity constant (17.7 ng/cm² Hz); n is the overtone number; and ΔF is the frequency change. The dissipation factor D can be expressed as

$$D = \frac{1}{\pi f_0 \tau_0} = \frac{2}{\omega \tau_0} \quad \text{eq. 4-14}$$

where f_0 is the resonance frequency and τ_0 is the decay time.

The adsorbed mass of TF-3 per unit area and thickness of TF-3 can be obtained from the QTools software based on the Sauerbrey equation. As shown in Figure 4-5A and B, the adsorbed mass and thickness of TF-3 increased as the TF-3 concentration increased from 0.1 mg/mL to 0.7 mg/mL. Further increasing TF-3 concentration to 0.9 mg/mL did not lead to increase of mass and thickness, suggesting that the CPPs modified surface was saturated with TF-3 at high TF-3 concentration.

The adsorption isotherm of TF-3 on the CPPs modified quartz crystal surface can be determined by the Langmuir model and Freundlich model. The Langmuir model was proposed based on the assumption that the adsorbate on the adsorbent was a monolayer, and there were finite binding sites for the adsorbate. The adsorbate has the ability to occupy these binding sites independently of the occupation of neighboring binding sites. The amount of adsorbed adsorbate can be calculated by

$$M = \frac{M_m K C}{1 + K C} \quad \text{eq. 4-15}$$

It can also be expressed as

$$\frac{C}{M} = \frac{1}{K M_m} + \frac{1}{M_m} C \quad \text{eq. 4-16}$$

where M represents the amount of adsorbate on the adsorbent; C is the concentration of adsorbate; M_m is a constant related to the area of adsorbed adsorbate; and K is a direct measure of the intensity of the adsorption process.

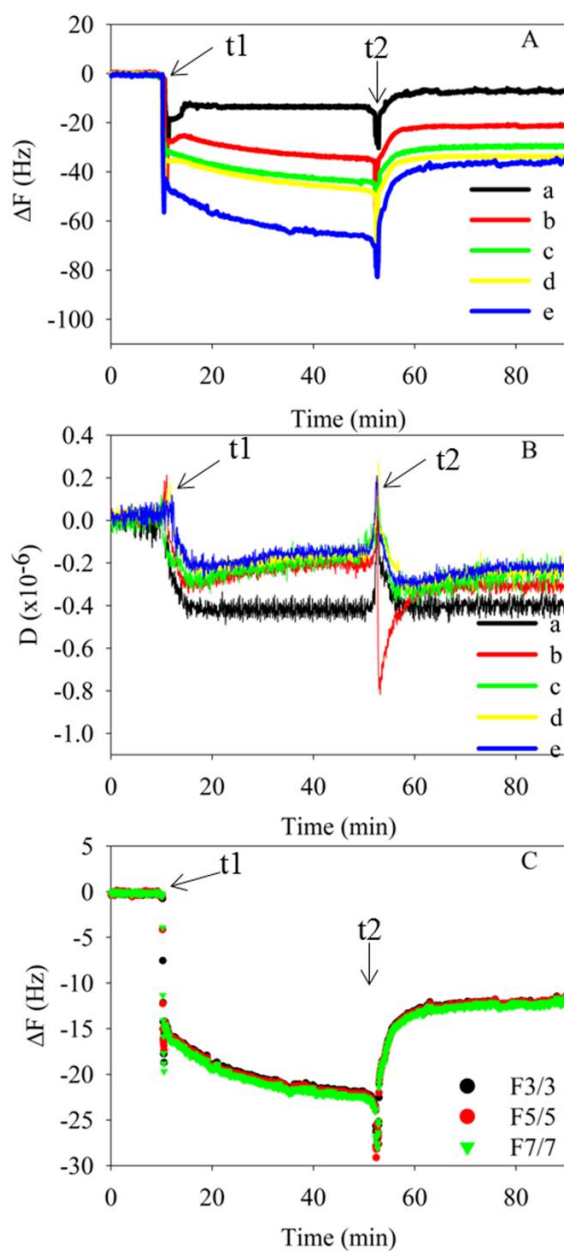


Figure 4-4. Time-dependent (A) frequency shift and (B) energy dissipation at the third overtone upon adsorption of TF-3 onto the CPPs connected quartz crystal surface at different concentrations of TF-3: (a) 0.1 mg/mL; (b) 0.3 mg/mL; (c) 0.5 mg/mL; (d) 0.7 mg/mL; (e) 0.9 mg/mL. TF-3 solution was injected at t_1 and the TF-3 adsorbed surface was rinsed with 0.15 M NaCl at t_2 . (C) Ratios of frequency shift to the corresponding overtone number ($\Delta F_n/n$) at different overtones ($n = 3, 5, 7$) upon 0.9 mg/mL TF-3 adsorbing on CPPs surface.

The Freundlich model assumes that the mass of adsorbed adsorbate increases with the concentration of adsorbate. According to the Freundlich model, the amount of adsorbate on the adsorbent can be calculated by

$$M = K_f C^{\frac{1}{n}} \quad \text{eq. 4-17}$$

where K_f and n are constants; C is the concentration of adsorbate. It can be expressed in logarithmic form

$$\log M = \log K_n + \frac{1}{n} \log C \quad \text{eq. 4-18}$$

As shown in Figure 4-5C and D, Langmuir model and Freundlich model have the correlation coefficients of 0.993 and 0.9722, respectively. Studies revealed that well fits of Langmuir model and Freundlich model represent that the interactions on the solid-liquid interface are governed by hydrogen bond and hydrophobic interactions, respectively^{211, 219}. Although both models had high correlation coefficients, the fact that increasing the TF-3 concentration from 0.7 mg/mL to 0.9 mg/mL did not increase the mass and thickness of TF-3 adsorbed on the CPPs surface let us believe that the Langmuir model may be a better model for explaining the interactions between TF-3 and CPPs. Therefore, it is concluded that hydrogen bond was the predominant attractive force between CPPs and TF-3 on the solid-liquid interface, which was similar as their association in the aqueous environment.

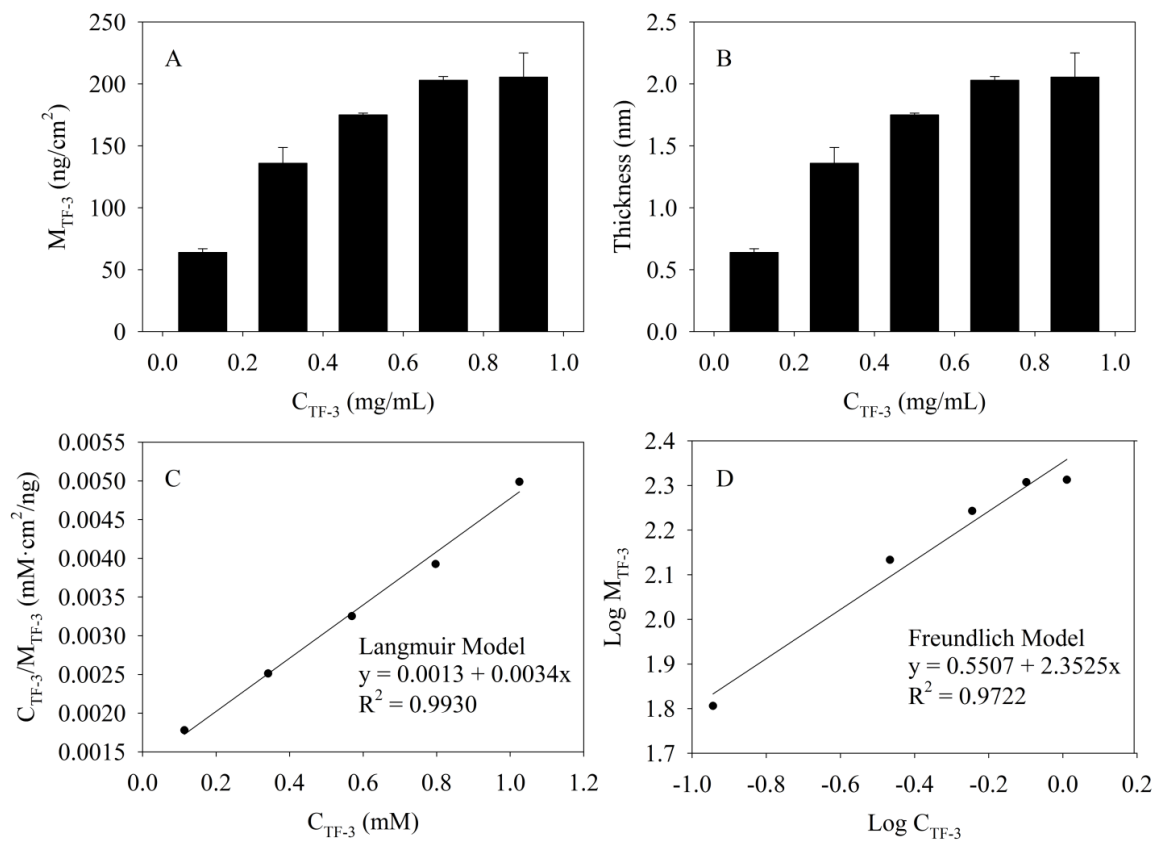


Figure 4-5. (A) Mass per unit area and (B) thickness of adsorbed TF-3 on CPPs surface at different TF-3 concentration. Adsorption isotherm of TF-3 onto CPPs surface fitted by (C) Langmuir model and (D) Frundlich model.

4.5. Conclusions

In summary, the interactions between CPPs and TF-3 in the aqueous environment and on the solid-liquid interface, and the conformational changes of CPPs accompanied with these interactions were investigated. Fluorescence quenching study revealed that TF-3 associated with CPPs through hydrogen bond in the aqueous phase, and the binding process was enthalpy driven. These interactions did not change the secondary structures of CPPs. SAXS results revealed that addition of TF-3 did not change the R_g of CPPs, but it induced aggregation of CPPs. The size of the

aggregates increased with the concentration of TF-3. At the solid-liquid interface, hydrogen bond was also involved in their interactions.

CHAPTER V. ENCAPSULATION OF THEAFLAVIN-3,3'- DIGALLATE IN THE CHITOSAN- CASEINOPHOSPHOPEPTIDES NANOCOMPLEX

As of submission of this dissertation, the work in this chapter has been written as two research papers in the titles of “Assembly of Chitosan-Caseinophosphopeptides Nanocomplexes to Encapsulate and Enhance Intestinal Permeation of Theaflavin-3,3'-digallate” and “Microstructures of Chitosan-Caseinophosphopeptides Nanocomplexes Encapsulated with Theaflavin-3,3'-digallate: A Small Angle X-Ray Scattering and Ultra-Small Angle X-Ray Scattering Study” which are ready for submission.

5.1. Abstract

The CS-CPPs nanocomplex was applied to encapsulate TF-3, which showed almost 100% encapsulation efficiency. These nanocomplexes were positively charged. As the concentration of TF-3 increased, the particle size increased from 214 nm to 295 nm. However, the radius of gyration of these nanocomplexes decreased as the concentration of TF-3 increased. The increased hydrodynamic radius was resulted from large aggregates. These nanocomplexes had low cytotoxicity. The intestinal permeability of TF-3 encapsulated in the CS-CPPs nanocomplex was significantly increased.

5.2. Introduction

Polyphenols are ubiquitous in fruits and vegetables. They have a wide spectrum of bioactivities, such as antioxidation¹⁴⁴, antiinflammation¹⁴⁵, anticancer¹⁴⁶, and cardiovascular protective effect¹⁴⁸. However, the discrepancies between *in vitro* and *in vivo* effects were reported. An example is the TFs. Although TFs displayed inhibitory effect on cancer cells through diverse mechanisms^{220, 221}, the *in vitro* results are not always supported by *in vivo* and epidemiological studies^{185, 186}. This inconsistency is very likely related to their low bioavailabilities as reviewed in section 1.5.3.

Besides fast metabolism, which is essentially hard to modulate, the bioavailability of polyphenols is usually restricted by low water solubility and/or intestinal permeability. TFs are polyhydroxylated polyphenols. The hydroxyl groups can bind with surrounding water molecules to form a large hydration shell, which makes it hard for them to penetrate through the lipophilic cell membrane (transcellular route)²²². Therefore, the low bioavailability of TFs is very likely resulted from their low intestinal permeability. The emulsion-based delivery systems were used to improve the bioavailability of polyphenols with low solubility²²³, meanwhile using the permeation enhancers such as polysaccharide-based delivery systems is an promising approach to increase the bioavailability of polyphenols with low intestinal permeability²²⁴.

CS is a permeation enhancer as described in section 1.3. In this chapter, TF-3 was encapsulated in the CS-CPPs nanocomplex, in order to improve its intestinal permeability.

5.3. Materials and Methods

5.3.1. Materials

CS was purchased from Kunpoong Bio. Co., Ltd. (South Korea) and used as received without further treatment. CPPs was purchased from Greencream Biotechnology Co., Ltd. (Guangzhou, China). TF-1 and TF-3 were purified from black tea as described in section 2.2.8. Ultracentrifuge tubes were purchased from EMD Millipore Co. (MA, USA). Caco-2 cell line was purchased from American Type Culture Collection (ATCC). Dulbecco's modified Eagle's medium (DMEM), non-essential amino acid, phosphate buffered saline (PBS), and fetal bovine serum (FBS) were purchased from Life Technologies (Gibco[®], NY, USA). 3-[4,5-dimethylthiazol-2-yl]-2,5-diphenyltetrazolium bromide (MTT), dimethyl sulfoxide (DMSO), and Hanks' balanced salt solution (HBSS) were purchased from Sigma-Aldrich (MO, USA). Milli-Q water was used in all experiments.

5.3.2. Encapsulate TF-3 in the CS-CPPs Nanocomplex

CS was dissolved in 1% acetic acid (0.01 M NaCl) with moderate stirring, and adjusted to pH 6 after fully dissolved. CPPs and TF-3 were dissolved in 0.01 M NaCl and their pH was adjusted to pH 6. To encapsulate TF-3 in the CS-CPPs nanocomplex, TF-3 solution was added drop-wise into equal volume of CPPs solution with constant stirring at ambient temperature to ensure CPPs interact with TF-3 thoroughly. Then equal volumes of the TF-3/CPPs mixture and CS solution were then mixed at room temperature.

Particle size, PDI, and ζ – potential of the CS-CPPs nanocomplexes encapsulated with different concentrations of TF-3 were measured by a Zetasizer Nano ZS90 (Malvern Instruments Ltd, Westborough, MA). The measurements were conducted in triplicate at 25°C.

The morphology of the CS-CPPs nanocomplexes encapsulated with TF-3 was monitored by a Nanoscope IIIa Multi-Mode AFM (Veeco Instruments Inc., Santa Barbara, CA) with tapping mode. Fresh made nanocomplexes encapsulated with TF-3 were dripped on the surface of pre-cleaned mica slides for 1 h. The surface of the mica slides was rinsed with Milli-Q water and dried with nitrogen.

The microstructural information of the CS-CPPs nanocomplexes encapsulated with TF-3 was obtained from the USAXS and SAXS experiments using the same method described in section 3.3.4.

The fresh made TF-3 loaded nanocomplexes were subjected to ultracentrifugation (MWCO of 10 kDa) to determine the encapsulation efficiency. After centrifugation at 6,000 g for 40 min, the amount of TF-3 in the filtrate was determined by HPLC. The HPLC method was same as described in section 2.2.9. The amount of TF-3 encapsulated in the nanocomplexes was obtained by subtracting the amount of TF-3 in the filtrate from the total amount of TF-3 that was used in

generating the nanocomplexes. The encapsulation efficiency was calculated by the following equation

$$\text{Encapsulation Efficiency (\%)} = \frac{\text{Amount of TF-3 Loaded in Nanocomplexes}}{\text{Total Amount of TF-3}} \times 100 \quad \text{eq. 5-1}$$

5.3.3. Evaluation of Cytotoxicity

The cytotoxicity was determined by the MTT assay using the Caco-2 cell line. Caco-2 cells were seeded in 96-well plate with the density of 5,000 cells/well, and cultured in 100 μ L DMEM at 37°C and 5% CO₂ for 24 h. The culture medium was then replaced with 200 μ L DMEM containing different samples and cultured at 37°C and 5% CO₂. After the designed treatment time (24h, 48h, and 72h), the sample solutions were decanted and all wells were rinsed with PBS. PBS was then replaced with 100 μ L MTT solution (0.5 mg/mL) and incubated at 37°C for 4 h. The MTT solution was then decanted and 100 μ L DMSO was added in each well to dissolve the insoluble formazan. The absorbance of the solution in each well was measured by a microplate reader (BioTek Instruments Inc., VT, USA) at 570 nm. All experiments were performed in triplicate.

5.3.4. Caco-2 Transport Experiment

0.5 mL Caco-2 cells (6×10^5 cell/mL) was seeded in each apical compartment (diameter 12 mm, pore size 0.4 μ m permeable membrane) of 12 well plate (Costar®, Corning Inc., NY, USA), and 1.5 mL culture medium was added in each basolateral chamber. Cells were cultivated at 37°C and 5% CO₂ for 25 days before the transport experiment. Culture media in both apical and basolateral chambers were replaced every two days and the media were finally replaced 24 h before the experiment. TF-3 in the pure form and encapsulated in the CS-CPPs nanocomplex (CS:CPPs=2) were diluted with HBSS (containing 0.01% ascorbic acid, pH 6) as the donor solutions. The final concentration of TF-3 in all the donor solutions was 20 μ M. To start the experiment, medium in the apical side was decanted and the filters were transferred to a new 12 well plate containing 1.5 mL pre-warmed HBSS (containing 0.01% ascorbic acid, pH 7.4, 37°C) in each well. 0.5 mL of pre-

warmed HBSS (containing 0.01% ascorbic acid, pH 6, 37°C) was added to each apical compartment to rinse the Caco-2 monolayer under gentle shaking (100 rpm) for 20 min at 37°C. The pH of HBSS in the apical chambers was adjusted to pH 6 to simulate the “microclimate” of small intestine^{121, 122}. Transepithelial resistance (TER) of each filter was measured at the end of the rinsing step. The buffer was then decanted from the filters and the filters were transferred to a new 12-well plate containing 1.2 mL of pre-warmed HBSS (containing 0.01% ascorbic acid, pH 7.4, 37°C) in each well. 0.45 mL donor solutions were added to the filters, and 0.05 mL sample was withdrawn from each filter immediately. The plate was incubated at 37°C under gentle shaking. 0.6 mL samples were withdrawn from the basolateral chambers at 20, 40, 60, 80, 100, 120 min, and replaced with 0.6 mL pre-warmed HBSS (containing 0.01% ascorbic acid, pH 7.4, 37°C). 0.05 mL sample was withdrawn from each apical compartment at the end of the experiment. TER of each filter was measured before sampling at each time interval. After 2 h experiment, HBSS in both apical and basolateral chambers were replaced with culture medium and incubated at 37°C for another 22 h, and TER was measured after incubation.

To analyze the concentration of TF-3 in the samples, 100 µL TF-1 dissolved in 0.1 M HCl solution was added into each sample as the internal standard. The samples were extracted with 600 µL ethyl acetate twice. The upper phases were collected and dried completely with N₂. The residues were dissolved in 100 µL 0.1 M HCl, and the concentrations of TF-1 and TF-3 were determined by the simplified HPLC as described in section 2.2.9.

The apparent permeability coefficient (P_{app}) was calculated by the following equation²²⁵

$$P_{app} = \frac{dQ}{dt} \frac{1}{AC_0} \quad \text{eq. 5-2}$$

where dQ/dt is the steady-state flux (µmol/s), A is the surface area of the filter (1.131 cm²), C_0 is the initial concentration of TF-3 in the donor solutions (µM).

5.4. Results and Discussion

5.4.1. Characterization of the CS-CPPs Nanocomplexes Encapsulated with TF-3

The CS-CPPs nanocomplex composed of CS:CPPs = 2 was used to encapsulate TF-3. The encapsulation process can be described as: TF-3 was first bonded to CPPs molecules through hydrogen bond (CHAPTER IV), then the TF-3/CPPs mixture interacted with CS via predominantly electrostatic interaction (CHAPTER III).

When increasing amount of TF-3 was incorporated into the nanocomplex, the particle size increased from 186 nm (TF-3:CPPs=0, Table 3-1) to 295 nm (TF-3:CPPs=1) accordingly (Table 5-1). The PDI values were all in the range of 0.2 – 0.3, indicating that the size distribution of the CS-CPPs nanocomplexes encapsulated with TF-3 was narrow. The ζ – potential values were almost consistent at + 22 mV when TF-3:CPPs increased from 0.1 to 1. The high positive ζ – potential indicates that the CS-CPPs nanocomplex was a promising delivery system for TF-3 since the positive charges could facilitate the electrostatic interaction between the TF-3 loaded nanocomplexes and the negatively charged biological barriers, such as mucus layer and cell membrane. The encapsulation efficiencies of all tested groups were all higher than 98%, indicating that the TF-3 molecules were strongly associated with the CS-CPPs nanocomplexes.

AFM was utilized with tapping mode to study the morphology of the CS-CPPs nanocomplexes encapsulated with TF-3 (Figure 5-1). When small amount of TF-3 (TF-3:CPPs = 0.1, Figure 5-1B) was encapsulated, the nanocomplexes still remained sphere, and the surface was smooth, which was similar as the nanocomplex (CS:CPPs=2) without encapsulation of TF-3 (Figure 5-1A). When high concentration of TF-3 (TF-3:CPPs = 1, Figure 5-1C) was incorporated, the shape of the nanocomplex became irregular, which is due to formation of aggregates.

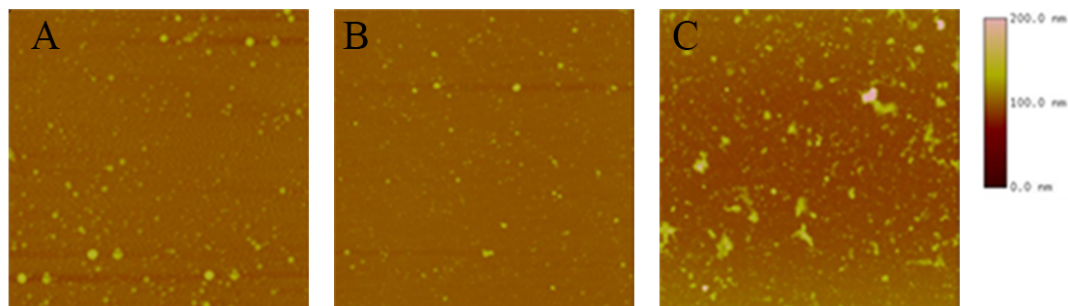


Figure 5-1. Morphologies of the CS-CPPs nanocomplexes encapsulated with TF-3 at TF-3:CPPs ratios of (A) 0, (B) 0.1 and (C) 1.

Table 5-1. Particle size, PDI, ζ – potential and encapsulation efficiency of the CS-CPPs nanocomplexes encapsulated with different concentrations of TF-3

TF-3 : CPPs	Particle Size (nm)	PDI	ζ - Potential (mV)	Encapsulation Efficiency (%)
0.1 : 1	214.5±7.6	0.274±0.046	+ 22.4±0.3	100±0.1
0.2 : 1	218.0±5.9	0.236±0.026	+ 22.2±0.6	100±0.2
0.4 : 1	240.3±2.8	0.274±0.055	+ 22.5±0.3	99.8±0.2
0.6 : 1	246.1±4.8	0.202±0.026	+ 21.6±0.1	99.7±0.4
0.8 : 1	281.8±4.3	0.226±0.019	+ 21.6±0.4	99.7±0.1
1 : 1	295.4±3.3	0.211±0.011	+ 21.6±0.6	98.3±0.5

The microstructures of the CS-CPPs nanocomplexes encapsulated with TF-3 were characterized by USAXS and SAXS. The scattering profiles of the nanocomplexes after encapsulation showed similar pattern as the non-encapsulated curve in $q > 0.01 \text{ \AA}^{-1}$, where these scattering curves displayed the decay of $I(q) \sim q^{-4}$ (Figure 5-2A), suggesting presence of globular structures with smooth surface. However, in the ultra-small q range ($q < 0.001 \text{ \AA}^{-1}$), notable difference is observed. All the scattering curves of the encapsulated groups upturn. This feature

represents that incorporation of TF-3 lead to aggregation of the nanocomplexes in fractal ways ($I(q) \sim q^{-1.3}$ to $\sim q^{-2.0}$). The Kratky plot also show peaks (Figure 5-2B), suggesting the nanocomplexes encapsulated with TF-3 remained in folded structures. The position of the peak gradually shifts to larger q as TF-3 concentration increases, which corresponds to a reduction of R_g of the nanocomplexes.

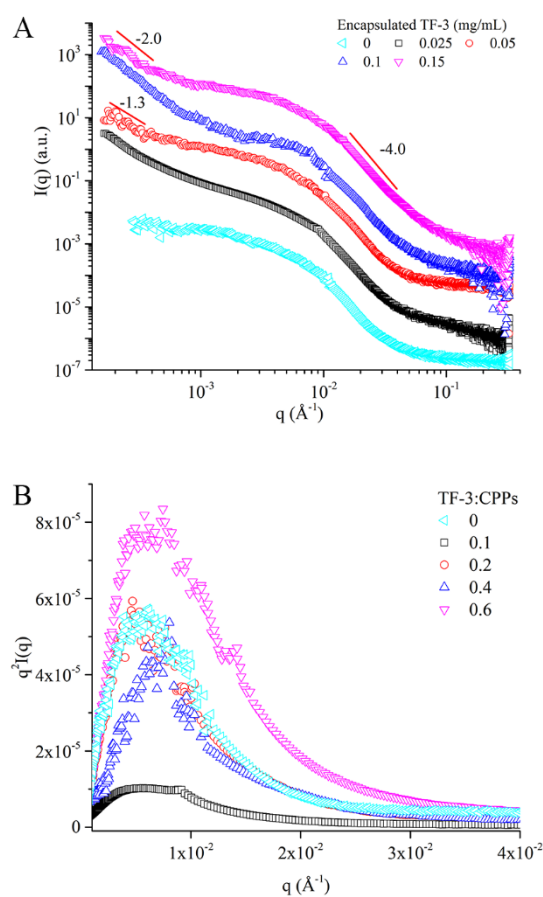


Figure 5-2. (A) Scattering profiles of the nanocomplexes encapsulated with different concentrations of TF-3. The scattering curves were vertically shifted for clear visualization. (B) Kratky plot of the nanocomplexes encapsulated with different concentrations of TF-3.

Table 5-2 lists the R_g of the nanocomplexes encapsulated with different concentrations of TF-3. The R_g decreased as the concentration of encapsulated TF-3 increased. When TF-3 was incorporated, it can bind with both CS and CPPs, which condensed the nanocomplexes into a more compact structure. Nevertheless, increasing TF-3 concentration could expose more TF-3 at the surface of a basic structure of the nanocomplex, which could associate with other neighboring nanocomplex particle and form aggregates. As a result, the hydrodynamic size increased (Table 5-1).

Table 5-2. Radius of gyration of the CS-CPPs nanocomplexes (CS:CPPs=2:1) encapsulated with different amount of TF-3

TF-3:CPPs	R_g (Å)
0.1:1	376±7.14
0.2:1	353±6.71
0.4:1	271±6.71
0.6:1	236±5.05

5.4.2. Evaluation of Cytotoxicity

The cytotoxicity of the nanocomplexes composed of different CS:CPPs weight ratios, pure TF-3 at different concentrations, and the nanocomplex (CS:CPPs=2) encapsulated with different amount of TF-3 were evaluated by the MTT assay against the Caco-2 cell line.

As shown in Figure 5-3A, the Caco-2 cells treated with the complexes composed of different CS:CPPs weight ratios for 24h remained more than 80% viability, which means that these complexes had low cytotoxicity.

The cytotoxicity of TF-3 (0-50 μ M) was investigated for 24h to 72h (Figure 5-3B). After 24h treatment, TF-3 at these concentrations did not lead to reduction of cell viability. However, treating Caco-2 cells with TF-3 for 48h and longer resulted in the cell viability lower than 80% at TF-3 concentration ≥ 30 μ M. Su *et al.* reported that almost all TF-3 degraded in about 6h at the pH of

cell culture medium¹⁵⁴. The pH induced degradation of theaflavins yields thearubigins through auto-oxidation¹⁵⁶. The reduced cell viability after 48h treatment is therefore more likely resulted from thearubigins.

Although treating the cells with the nanocomplexes encapsulated with TF-3 for 24h resulted in relatively lower cell viability than pure TF-3 at corresponding concentrations, there were still more than 75% of viable cells (Figure 5-3C). For longer treatments (48h-72h), the cells treated with the nanocomplexes encapsulated with TF-3 had almost identical viabilities as the cells treated with pure TF-3 at same concentration, which means the reduced cell viability would be resulted from TF-3 (or thearubigins). These results demonstrate that the CS-CPPs nanocomplexes as the encapsulation systems are low cytotoxic.

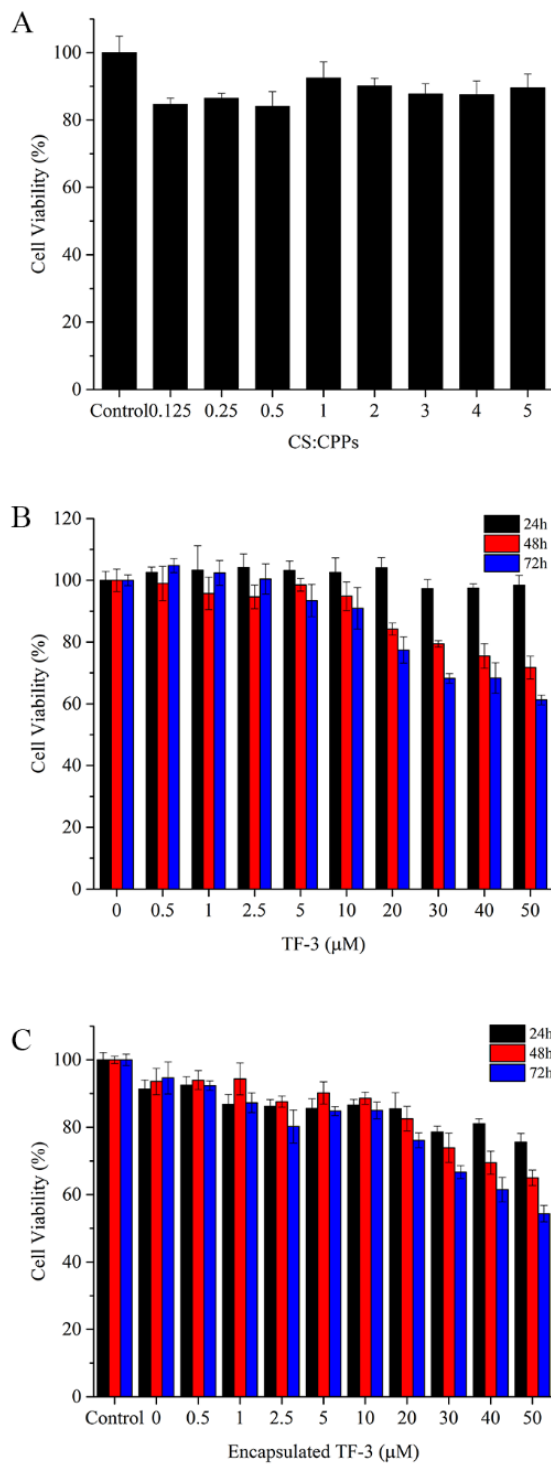


Figure 5-3. Caco-2 cell viability after treating with (A) the CS-CPPs nanocomplexes composed of different CS:CPPs weight ratios; (B) 0–50 μM TF-3; and (C) the CS-CPPs nanocomplex encapsulated with 0–50 μM TF-3.

5.4.3. Caco-2 Transport Experiment

The bioavailability of TF-3 is very likely restricted by its low intestinal permeability. The CS-CPPs nanocomplexes were designed to encapsulate TF-3, aiming to improve its permeability. The Caco-2 monolayer transport experiment was performed to investigate the effectiveness of encapsulation on the intestinal permeability of TF-3.

During 2h experiment, the total amount of transported TF-3 increased 9 times when TF-3 was encapsulated in the CS-CPPs nanocomplex. The P_{app} of pure TF-3 was 3.0×10^{-6} cm/s, while the P_{app} of TF-3 encapsulated in the nanocomplex increased to 2.7×10^{-5} cm/s, which means TF-3 became highly permeable through the Caco-2 monolayer after being encapsulated in the CS-CPPs nanocomplex. This result demonstrates that the CS-CPPs nanocomplex can effectively increase the intestinal permeability of TF-3, which would potentially increase its bioavailability.

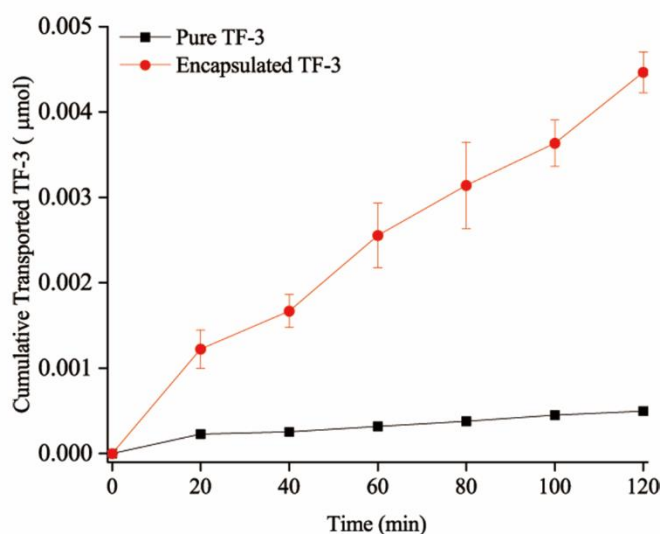


Figure 5-4. Cumulative amount of transported TF-3 in pure form and encapsulated by the CS-CPPs nanocomplex

The enhanced permeability is attributed to CS, which can reversibly and transiently open the tight junctions between small intestinal epithelial cells¹¹⁴. This process can facilitate paracellular

transport of hydrophilic molecules, such as TF-3. The integrity of the monolayer and status of the tight junctions were monitored during the experiment by measuring the TER. Before the experiment, the TER of all monolayers was above $1000 \Omega \cdot \text{cm}^{-2}$, which means the monolayers were intact and the tight junctions were closed. By adding the CS-containing samples to the monolayers, the TER decreased dramatically to $400\text{-}500 \Omega \cdot \text{cm}^{-2}$, indicating opening of the tight junctions. After removal of the CS-containing samples and re-culture of the monolayers with cell culture medium for another 22h, the TER recovered to the initial values, indicating closure of the tight junctions. This result indicates the enhanced permeation of TF-3 could be attribute to CS in the nanocomplex

5.5. Conclusions

In this chapter, TF-3 was encapsulated in the CS-CPPs nanocomplex with very high encapsulation efficiency. These nanocomplexes remained positively charged. Incorporation of TF-3 made the nanocomplex more compact as reflected by decrease of R_g . However, the hydrodynamic size of these nanocomplexes increased with the concentration of TF-3 due to formation of aggregates. The cytotoxicity of these nanocomplexes was low. In addition, the CS-CPPs nanocomplex can effectively improve the intestinal permeability of TF-3.

CHAPTER VI. ENHANCING INTESTINAL PERMEABILITY OF THEAFLAVIN-3,3'-DIGALLATE BY GENIPIN CROSSLINKED CHITOSAN-CASEINOPHOSHOPEPTIDES NANOCOMPLEXES

As of submission of this dissertation, the work in this chapter has been written as a research paper in the title of "Enhancing Intestinal Permeability of Theaflavin-3,3'-digallate by Genipin Crosslinked Chitosan-Caseinophosphopeptides Nanocomplexes" which is ready for submission.

6.1. Abstract

The CS-CPPs nanocomplex encapsulated with TF-3 was chemically crosslinked by genipin, in order to prevent the acid-induced burst release of TF-3. The crosslinking reaction was conducted in the presence of different concentrations of genipin for different crosslinking durations. The resulting genipin crosslinked CS-CPPs nanocomplexes (GCNs) showed much better resistance to the acid-induced size increase. The GCNs encapsulated with TF-3 can effectively improve the intestinal permeability of TF-3 as demonstrated in the Caco-2 monolayer transport experiment.

6.2. Introduction

The CS-CPPs nanocomplex was designed to encapsulate TF-3, aiming to improve its intestinal permeability, which would potentially increase its bioavailability. However, as mentioned in section 1.1.2, the polysaccharide-protein/polypeptide complexes are assembled predominantly through electrostatic attraction, which is susceptible to change of environmental factors, such as pH, ionic strength, and temperature. Therefore, using the polysaccharide-protein/polypeptide complexes as oral delivery systems may have some problems when the complexes go through the human GIT where the pH changes dramatically from very acidic pH in the stomach to weak acidic to neutral pH in the small intestine²²⁶. Using crosslinkers to covalently crosslink the polysaccharide-

protein/polypeptide complexes is a feasible approach to solve this problem. Genipin is a natural crosslinker that is usually obtained by hydrolyzing geniposide, which is isolated from the fruit of *Gardenia jasminoides* Ellis. Genipin is thousand times less toxic than the traditionally used synthetic crosslinker glutaraldehyde²²⁷. It is used as a precursor of edible blue pigments in food industry²²⁸.

In this chapter, the CS-CPPs nanocomplex was crosslinked by genipin. The crosslinking process at different conditions was monitored by the UV-Vis spectra. The genipin crosslinked CS-CPPs nanocomplexes (GCNs) were applied to encapsulate TF-3. The particle size, ζ -potential, morphology, microstructure, and pH stability of these GCNs in the absence and presence of TF-3 were characterized. Caco-2 transport experiment was performed to evaluate the effectiveness of encapsulation on the intestinal permeability of TF-3.

6.3. Materials and Methods

6.3.1. Materials

CS was purchased from Kunpoong Bio. Co., Ltd. (South Korea) and used as received without further treatment. CPPs was purchased from Greencream Biotechnology Co., Ltd. (Guangzhou, China). Genipin (purity > 98%) was purchased from Wako Pure Chemical Industries, Ltd. (VA, USA). TF-1 and TF-3 were purified from black tea extract as described in section 2.2.8. Caco-2 cell line was purchased from ATCC. DMEM, FBS, non-essential amino acid, and PBS were purchased from Life Technologies (Gibco®, NY, USA). MTT, DMSO, and HBSS were purchased from Sigma-Aldrich (MO, USA). Milli-Q water was used in all the experiments.

6.3.2. Preparation and Characterization of the GCNs Encapsulated with TF-3

CS was dissolved in 1% acetic acid containing 10 mM NaCl. CPPs was dissolved in Milli-Q water containing 10 mM NaCl. The pH of CS and CPPs solutions was adjusted to 6. To prepare the GCNs, genipin was mixed with 1 mg/mL CS solution for 5 min followed by addition of same

volume of 0.5 mg/mL CPPs solution dropwise during stirring. To prepare the GCNs encapsulated with TF-3, equal volumes of TF-3 and 1 mg/mL CPPs were mixed and added into the CS/genipin mixture during stirring (the final concentration of genipin was kept at 0.5 mg/mL). The crosslinking reaction was carried at 25°C.

The UV-Vis spectra of the CS-CPPs nanocomplexes crosslinked with different concentrations of genipin and different crosslinking durations were measured on a Cary 60 UV-Vis Spectrophotometer (Agilent Technologies, CA, USA). The GCNs were diluted with Milli-Q water (10 mM NaCl, pH 6) and the UV-Vis spectra were collected from 800 nm to 200 nm with the scan rate of 300 nm/min.

The particle sizes of the GCNs and GCNs encapsulated with TF-3 were measured on a 90Plus Particle Size Analyzer equipped with a Brookhaven BI-9000AT digital correlator (Brookhaven Instruments Corporation, NY, USA). All measurements were conducted at the fixed scattering angle of 90°. The particle size was obtained through a series of calculations from the intensity-intensity autocorrelation function $G(q,t)$ ²²⁹.

Measurements of the ζ -potentials were conducted on a Nano ZS Zetasizer (Malvern Instruments Ltd., MA, USA). The GCNs and GCNs encapsulated with TF-3 were diluted 1:2 with Milli-Q water (10 mM NaCl, pH 6) before measurements. The electrophoretic mobility of these particles was measured and converted to their ζ -potentials by the Helmholtz-Smoluchowski equation. The measurements were triplicated at 25°C.

The morphologies were monitored by a Nanoscope IIIa Multi-Mode AFM (Veeco Instruments Inc., CA, USA) with tapping mode. Freshly made samples were diluted with Milli-Q water (10 mM NaCl, pH 6) and dripped on the surface of pre-cleaned mica slides. The surface of the mica slides was then rinsed with Milli-Q water and dried with N₂ for analysis.

The USAXS and SAXS experiments were conducted at beamline 9 ID-C at the APS of Argonne National Laboratory (Chicago, USA). Samples were filled in the 1 mm-thick silicone isolators (Grace Bio-Labs, Inc., OR, USA) and sealed with glass slides. The USAXS and SAXS data were processed and analyzed by the software packages of Indra 2, Irena 2, and Nika 1^{197, 230}.

The pH Stability of the GCNs was investigated by adjusting the pH to 2 and stirring for 2h to simulate retention at the human gastric pH. The particle size was monitored afterwards.

6.3.3. Evaluation of Cytotoxicity

The cytotoxicity of GCNs was evaluated by the MTT assay using Caco-2 cell line. The Caco-2 cells were cultured according to ATCC recommended method. To start the experiments, 10,000 cell/well Caco-2 cells were seeded in 96 well plate and cultured in 100 μ L DMEM (containing 20% FBS and 1% non-essential amino acid) at 37°C and 5% CO₂ for 24h. The culture medium was decanted and the cells were treated with 100 μ L GCNs samples (diluted by cell culture medium) and cultured at 37°C and 5% CO₂ for another 24h. The samples were then removed and the cells were rinsed with 100 μ L PBS. PBS was then replaced with 100 μ L MTT (0.5 mg/mL) and incubated at 37°C and 5% CO₂ for 4h. The MTT solution was then decanted and 100 μ L DMSO was added in each well. The absorbance of the solution in each well was measured by a microplate reader (BioTek Instruments Inc., VT, USA) at 570 nm. All experiments were performed in triplicate.

6.3.4. Caco-2 Transport Experiment

The Caco-2 transport experiments were performed according to Hubatsch *et al.* method²²⁵. 0.5 mL Caco-2 cell (6×10^5 cell/mL) was seeded in each apical compartment (diameter 12 mm, pore size 0.4 μ m permeable membrane) of 12 well plate (Costar®, Corning Inc., NY, USA), and 1.5 mL culture medium was added in each basolateral chamber. Cells were cultivated at 37°C and 5% CO₂ for 25 days before the transport experiment. Culture media in both apical and basolateral chambers were replaced every two days and the media were finally replaced 24 h before the experiment. Pure

TF-3 and the GCNs encapsulated with TF-3 (crosslinked by 0.1 mg/mL, 0.5 mg/mL, and 1 mg/mL genipin for 4h) were diluted with HBSS (containing 0.01% ascorbic acid, pH 6) as the donor solutions. The final concentration of TF-3 in all the donor solutions was 20 μ M. To start the experiment, medium in the apical side was decanted and the filters were transferred to a new 12 well plate containing 1.5 mL pre-warmed HBSS (containing 0.01% ascorbic acid, pH 7.4, 37°C) in each well. 0.5 mL of pre-warmed HBSS (containing 0.01% ascorbic acid, pH 6, 37°C) was added to each apical compartment to rinse the Caco-2 monolayer under gentle shaking (100 rpm) for 20 min at 37°C. The pH of HBSS in the apical chambers was adjusted to pH 6 to simulate the “microclimate” of small intestine^{121, 122}. TER of each filter was measured at the end of the rinsing step. The buffer was then decanted from the filters and the filters were transferred to a new 12-well plate containing 1.2 mL of pre-warmed HBSS (containing 0.01% ascorbic acid, pH 7.4, 37°C) in each well. 0.45 mL donor solutions were added to the filters, and 0.05 mL sample was withdrawn from each filter immediately. The plate was incubated at 37°C under gentle shaking. 0.6 mL samples were withdrawn from the basolateral chambers at 20, 40, 60, 80, 100, 120 min, and replaced with 0.6 mL pre-warmed HBSS (containing 0.01% ascorbic acid, pH 7.4, 37°C). 0.05 mL sample was withdrawn from each apical compartment at the end of the experiment. TER of each filter was measured before sampling at each time interval. After 2 h experiment, HBSS in both apical and basolateral chambers were replaced with culture medium and incubated at 37°C for another 22 h, and TER was measured after incubation.

To analyze the concentration of TF-3 in the samples, 100 μ L TF-1 dissolved in 0.1 M HCl solution was added into each sample as the internal standard. The samples were extracted with 600 μ L ethyl acetate twice. The upper phases were collected and dried completely with N₂. The residues were dissolved in 100 μ L 0.1 M HCl, and the concentrations of TF-1 and TF-3 were determined by HPLC as described in section 2.2.9. The P_{app} was calculated by eq. 5-2²²⁵.

6.4. Results and Discussion

Genipin is a natural crosslinker. It can react with the primary amine groups. The crosslinking reactions of genipin with primary amine groups are pH dependent. In the acidic to neutral conditions, the primary amine group nucleophilically reacts with the carbon atom on C3 position of genipin molecule, followed by opening of the dihydropyran ring and formation of an aldehyde group. This intermediate aldehyde group further reacts with the secondary amine group, forming a heterocyclic molecule. Another crosslinking route that happens in acidic to neutral conditions involves the conversion of the ester group on genipin molecule into the secondary amide bond²³¹. These molecules can further undergo dimerization, trimerization, and tetramerization^{232, 233}. In the basic condition, genipin molecules can undergo self-polymerization through aldol condensation^{232, 234}. The polymerized genipin then reacts with molecules that contain primary amine groups.

6.4.1. UV-Vis Spectrum

The UV-Vis spectrum was firstly used to monitor the crosslinking process. The CS-CPPs nanocomplex without genipin crosslinking exhibited identical UV-Vis spectra during 16h stirring (Figure 6-1A). However, after addition of genipin, the absorption peak at 240 nm appeared at the beginning (0h) of the crosslinking reaction. This peak gradually decreased as the reaction extended (Figure 6-1B and C). The peak at 240 nm was attributed to absorption of genipin molecules²³⁵. Decreasing of this peak therefore owes to decreased amount of free genipin molecules during the crosslinking reaction. Another peak at 290 nm appeared after 2h reaction and the intensity of this peak gradually increased as the reaction extended. This characteristic peak at 290 nm was attributed to absorption of the heterocyclic molecule formed in acidic to neutral conditions²³⁵. These results demonstrate that the crosslinking process was initiated after 2h reaction.

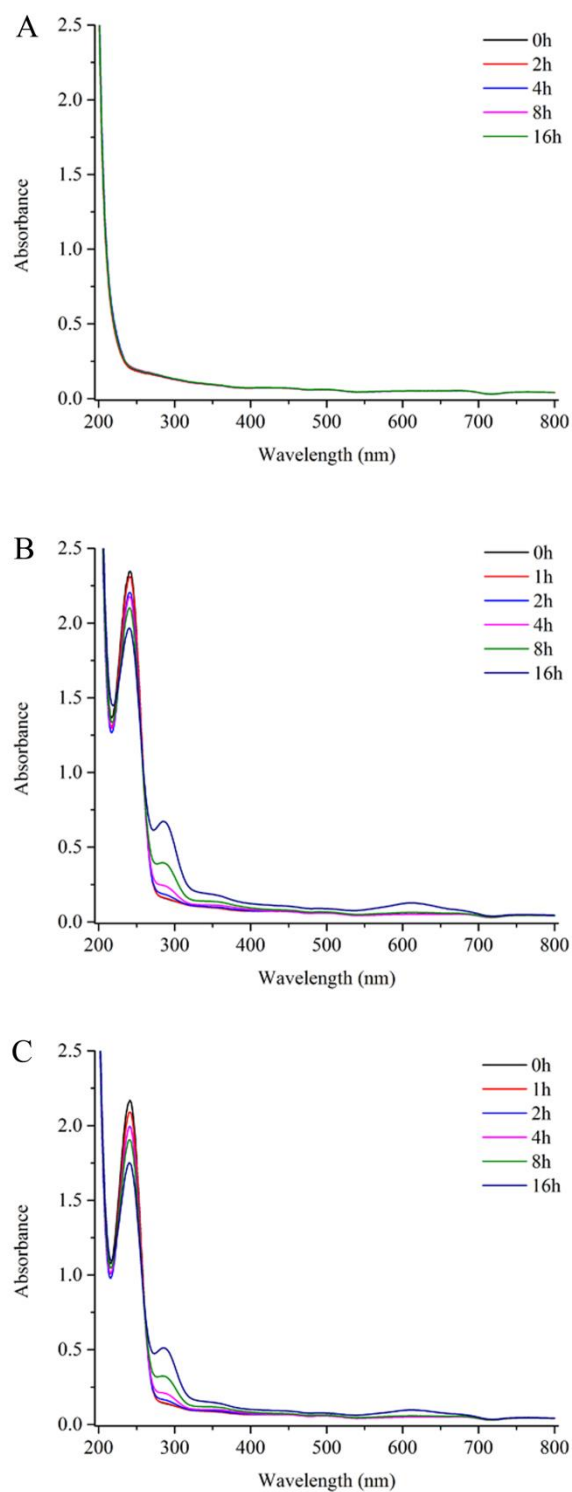


Figure 6-1. UV-Vis spectra of the CS-CPPs nanocomplexes crosslinked by (A) 0 mg/mL, (B) 0.5 mg/mL, and (C) 1mg/mL genipin for different crosslinking durations

6.4.2. Characterization of the GCNs Encapsulated with TF-3

The particle sizes of the CS-CPPs nanocomplexes crosslinked by different concentrations of genipin with different crosslinking durations are shown in Figure 6-2A. When the nanocomplexes were crosslinked by 0.1-0.3 mg/mL genipin, the particle size kept decreasing over 48h crosslinking reaction, suggesting that these nanocomplexes became more compact upon crosslinking. The particle size of the nanocomplex crosslinked by 0.5 mg/mL genipin first decreased and then leveled off. When the concentration of genipin increased to 0.7 mg/mL, the particle size decreased until 16h and then increased. Visible large aggregates were observed after even longer crosslinking. The sizes of these aggregates were unable to be measured. Rise of particle size after 16h crosslinking was due to the dimerization, trimerization, tetramerization process. Further increasing the genipin concentration to 1 mg/mL led to faster decrease of the particle size until 16h followed by formation of large aggregates.

Different concentrations of TF-3 (TF-3:CPPs = 0.1, 0.4, 0.8) were then encapsulated in the GCNs (concentration of genipin was 0.5 mg/mL). As shown in Figure 6-2B, after encapsulation, the particle size increased with the concentration of encapsulated TF-3. The size of these GCNs encapsulated TF-3 also decreased as the crosslinking reaction extended until 16h and then leveled off, which was similar to the nanocomplex crosslinked by 0.5 mg/mL genipin without encapsulation of TF-3.

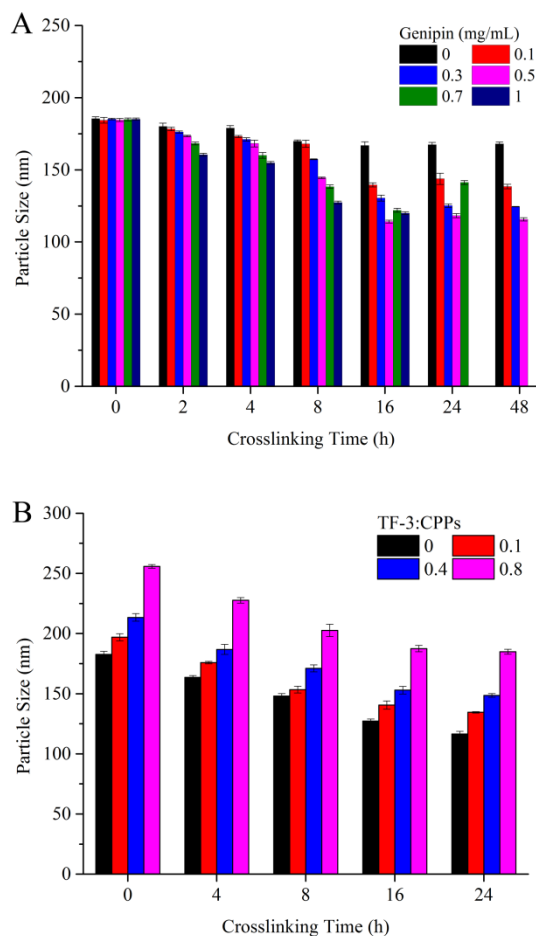


Figure 6-2. Particle sizes of (A) the CS-CPPs nanocomplexes crosslinked by different concentrations of genipin (0-1 mg/mL) and different crosslinking durations (0-48h), and (B) GCNs encapsulated with different concentrations of TF-3 (TF-3:CPPs = 0-0.8, concentration of genipin was 0.5 mg/mL).

The ζ -potentials of the nanocomplexes without crosslinking remained almost constant while the ζ -potentials of the GCNs decreased as the crosslinking reaction extended (Figure 6-3A). Higher concentration of genipin led to faster decrease of the ζ -potential. The decrease of ζ -potential was due to loss of the primary amine groups which carried positive charges at pH 6. After incorporation of TF-3 into the GCNs, the ζ -potentials did not change significantly compared to the non-encapsulated group (Figure 6-3B). The positive charges can facilitate binding of GCNs with the

negatively charged mucus layer¹¹³, which could prolong the retention time of the GCNs loaded with TF-3 on small intestinal epithelial cells.

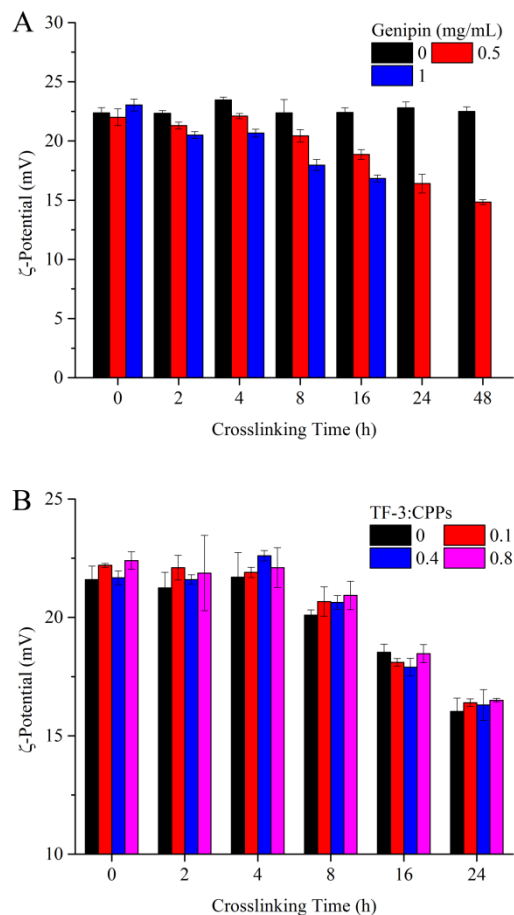


Figure 6-3. ζ -potentials of (A) CS-CPPs nanocomplexes crosslinked by different concentrations of genipin (0, 0.5, 1 mg/mL) for different crosslinking durations (0-48h), and (B) GCNs encapsulated with different concentrations of TF-3 (TF-3:CPPs=0-0.8, concentration of genipin was 0.5 mg/mL).

Figure 6-4 shows the morphologies of the nanocomplexes crosslinked by 0.5 mg/mL genipin for different crosslinking durations (Figure 6-4A-C) and encapsulated with different amount of TF-3 (Figure 6-4D-F). Generally, these GCNs remained as spherical particles. The relative sizes of

these GCNs observed from the AFM images were same as the dynamic light scattering results (Figure 6-2).

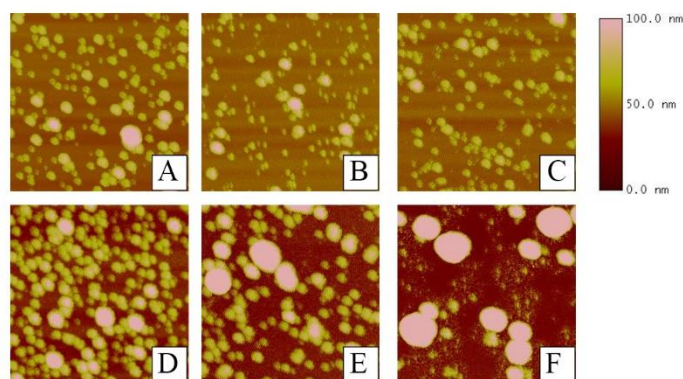


Figure 6-4. AFM images of the CS-CPPs nanocomplexes crosslinked by 0.5 mg/mL genipin for (A) 0h, (B) 8h, and (C) 24h, and crosslinked by 0.5 mg/mL genipin for 4 h and encapsulated with TF-3 with the TF-3:CPPs weight ratio of (D) 0.1, (E) 0.4, and (F) 0.8.

The microstructures of the GCNs in the absence and presence of TF-3 were characterized by the USAXS coupled with SAXS, which provide the structural information at the length scale from nanometer to micrometer. The scattering profiles of the CS-CPPs nanocomplexes crosslinked by different concentrations of genipin with different crosslinking durations are displayed in Figure 6-5. The conformation of an object in solution is usually described by its fractal dimension α . The scattering intensity $I(q)$ of the object with fractal dimension α follows the power law $I(q) \sim q^{-\alpha}$. The overall structure of a single GCN particle is reflected in the small to intermediate q range ($0.004 \text{ \AA}^{-1} < q < 0.03 \text{ \AA}^{-1}$). As shown in Figure 6-5, after 4h crosslinking reaction, the scattering decay changed from $I(q) \sim q^{-2.3}$ to $I(q) \sim q^{-1.6}$ as the concentration of genipin increased from 0 mg/mL to 1 mg/mL, which means the crosslinking reaction changed the shape of the GCNs. It was also noticed that at the ultra-small q range, the nanocomplexes without crosslinking (0 mg/mL genipin) showed upturned intensity at $q < 0.001 \text{ \AA}^{-1}$, suggesting large aggregates formed and the aggregates existed in globular shape ($I(q) \sim q^{-3}$). The nanocomplexes crosslinked with 0.1 mg/mL genipin for

4h still aggregated, but the aggregates existed in a different fractal way ($I(q) \sim q^{-2.5}$). However, the nanocomplexes crosslinked by higher concentrations of genipin (0.5-1 mg/mL) showed plateau at $q < 0.001 \text{ \AA}^{-1}$, indicating these particles became more homogeneous.

However, when the crosslinking reaction extended to 8h and longer, all the scattering curves upturned at $q < 0.001 \text{ \AA}^{-1}$ (Figure 6-5B-D), which means longer crosslinking resulted in aggregation (dimerization, trimerization, and tetramerization). The fractal dimension of these aggregates was around 1. It was also observed that as the crosslinking reaction continued, the scattering curves in the intermedium q range tend to decay in $I(q) \sim q^{-1.7}$. This result demonstrated that the shape of GCNs crosslinked by different concentrations of genipin may eventually become identical upon 24h reaction.

It is interesting to observe that there was a peak appearing at 0.43 \AA^{-1} , which correspond to the length scale of 14.6 \AA in the real space. This is probably related to the internal structure within the GCNs.

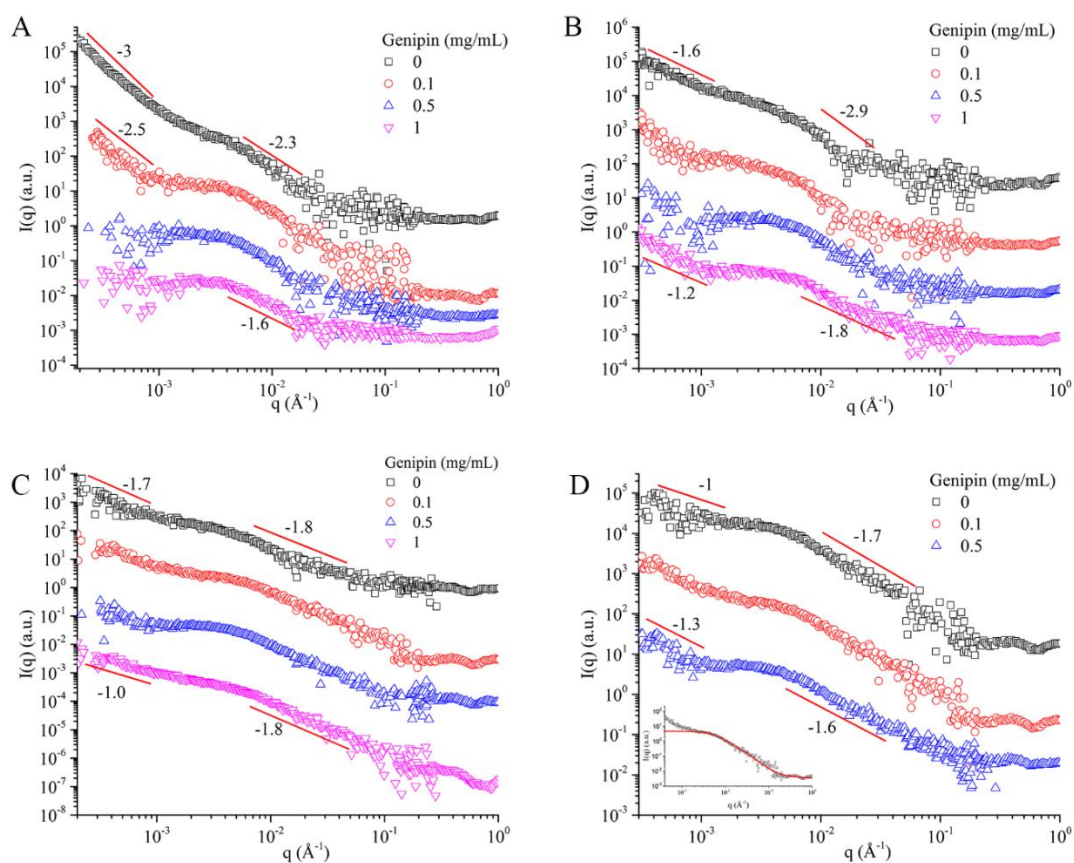


Figure 6-5. USAXS and SAXS of the CS-CPPs nanocomplexes crosslinked by different concentrations of genipin for (A) 4h, (B) 8h, (C) 16h, and (D) 24h (inset is the fitting of nanocomplex crosslinked by 0.1 mg/mL genipin for 24h). The scattering curves were vertically shifted for better visualization.

The R_g of the GCNs was calculated by the Irena software by fitting the scattering curves (Figure 6-5D inset). As listed in Table 6-1, the R_g of the GCNs changed in the same way as the hydrodynamic size (Figure 6-2A) when the crosslinking reaction extended.

Table 6-1. Radius of gyration of the CS-CPPs nanocomplexes crosslinked by different concentrations of genipin for different crosslinking durations

Crosslinking Duration (h)	R_g (Å)			
	0 mg/mL genipin	0.1 mg/mL genipin	0.5 mg/mL genipin	1 mg/mL genipin
4	351.1	282.0	271.3	264.8
8	332.6	275.6	229.6	207.3
16	297.3	240.0	227.5	211.6
24	245.6	235.0	227.4	N/A

N/A: not applicable

The microstructures of the GCNs (crosslinked by 0.5 mg/mL genipin) encapsulated with different concentrations of TF-3 were further characterized. Generally, the encapsulated groups displayed similar scattering pattern as the non-encapsulated groups (Figure 6-6), which indicates incorporation of TF-3 did not significantly change the shape of the GCNs.

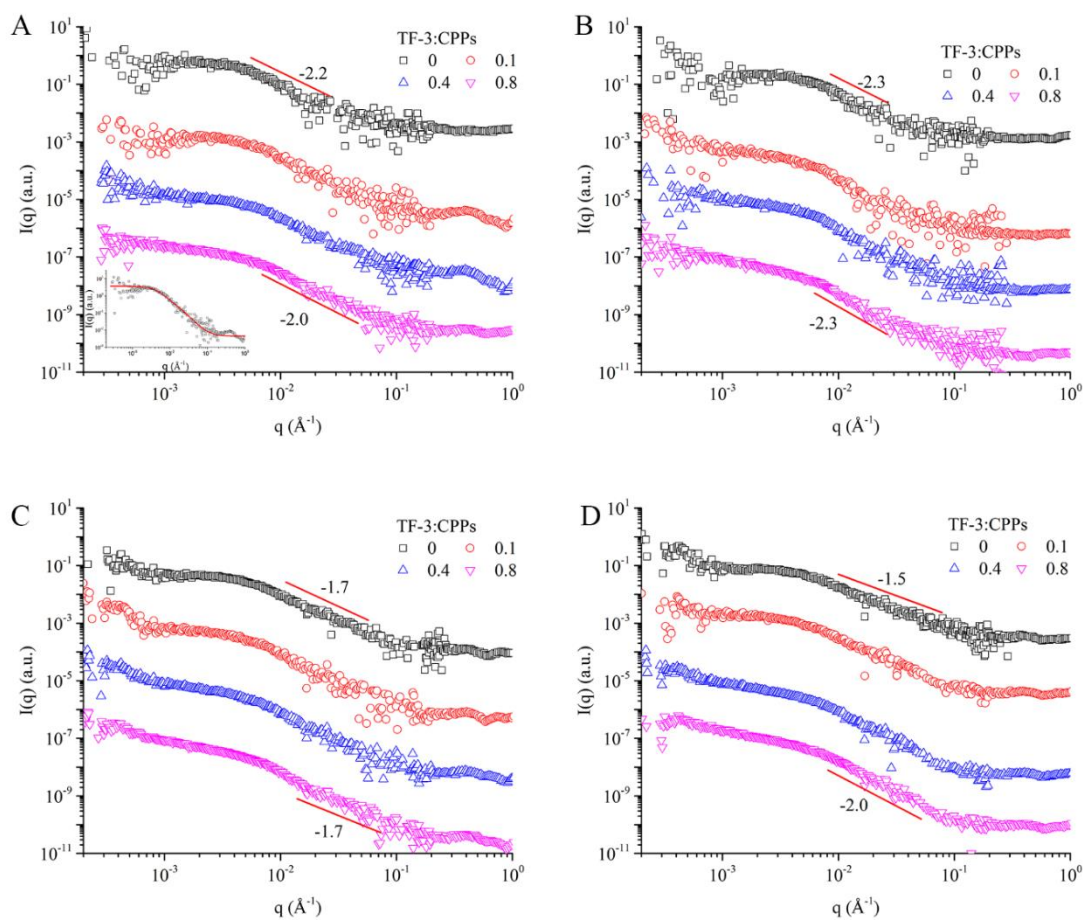


Figure 6-6. USAXS and SAXS of the nanocomplexes encapsulated with different amount of TF-3 and crosslinked by 0.5 mg/mL genipin for (A) 4h (inset is the fitting of TF-3:CPPs=0.1), (B) 8h, (C) 16h, and (D) 24h. The scattering curves are vertically shifted for better visualization.

Table 6-2 list the R_g of the GCNs encapsulated with different concentrations of TF-3. It was noticed that incorporation of TF-3 increased the R_g of GCNs, which is also similar as the trend of hydrodynamic size change (Figure 6-2B). Higher concentration of TF-3 lead to larger R_g .

Table 6-2. Radius of gyration of the GCNs encapsulated with different concentrations of TF-3

Crosslinking Duration (h)	R_g (Å)			
	TF-3:CPPs =	TF-3:CPPs =	TF-3:CPPs =	TF-3:CPPs =
	0	0.1	0.4	0.8
4	271.3	273.2	278.1	284.4
8	229.6	244.9	253.4	265.5
16	227.5	241.4	248.4	262.2
24	227.4	235.8	240.5	248.6

The polysaccharide-protein/polypeptide complexes are predominantly associated by electrostatic interaction, which is susceptible to pH change. Exposing these complexes in acidic environment *e.g.* gastric environment may cause burst release of the loaded molecules. One way to solve this problem is using crosslinker to covalently crosslink the polysaccharide-protein/polypeptide complexes. The pH of the GCNs after crosslinking was adjusted to pH 2 and stayed for 2h to mimic retention at gastric environment. The particle sizes after exposure to pH 2 were compared with their initial sizes (at pH 6). As shown in Figure 6-7, the particle size of the nanocomplexes without crosslinking increased dramatically. Nanocomplexes crosslinked by genipin were more resistant to acid-induced size increase. Higher concentration of genipin and longer crosslinking duration lead to smaller increase of the particle size because these two parameters can give rise to higher degree of crosslinking. This result demonstrates that using genipin to crosslink the CS-CPPs nanocomplexes can effectively inhibit dissociation of the nanocomplexes, and therefore prevent burst release of the encapsulated TF-3.

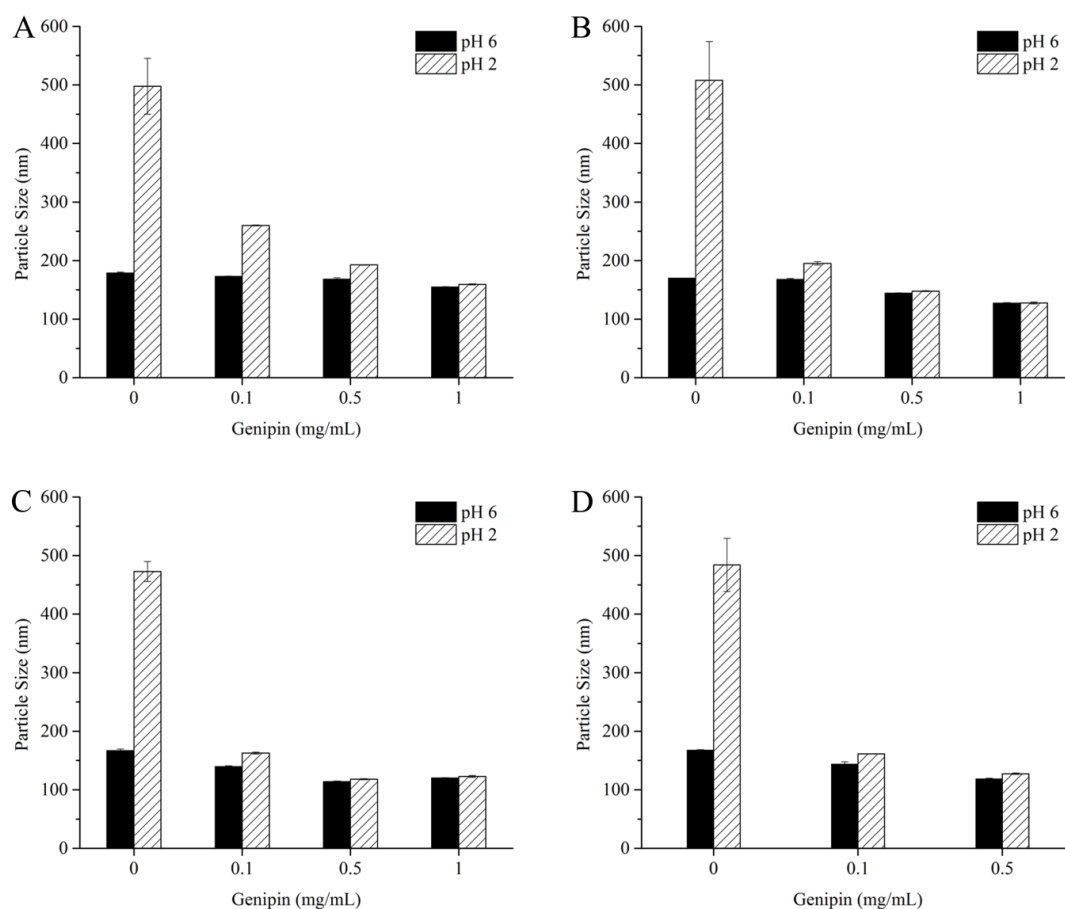


Figure 6-7. Comparison of the particle sizes of the nanocomplexes crosslinked with 0 - 1 mg/mL genipin for (A) 4h, (B) 8h, (C) 16h, and (D) 24h at pH 6 and after exposing at pH 2 for 2h.

6.4.3. Evaluation of the Cytotoxicity

The cytotoxicity of the GCNs on Caco-2 cell line was screened using MTT assay before the transport experiment. Generally, these GCNs were low-cytotoxic as reflected by cell viability higher than 80% viability in most conditions except for the groups treated with high level of GCNs which were crosslinked by high concentration of genipin and/or for long crosslinking duration (*i.e.* 75 μ g/mL GCNs crosslinked by 1 mg/ml genipin for 4h and 8h, 37.5-75 μ g/mL GCNs crosslinked by 1 mg/ml genipin for 16h, and 75 μ g/mL GCNs crosslinked by 0.5 mg/ml genipin for 24h) (Figure 6-8).

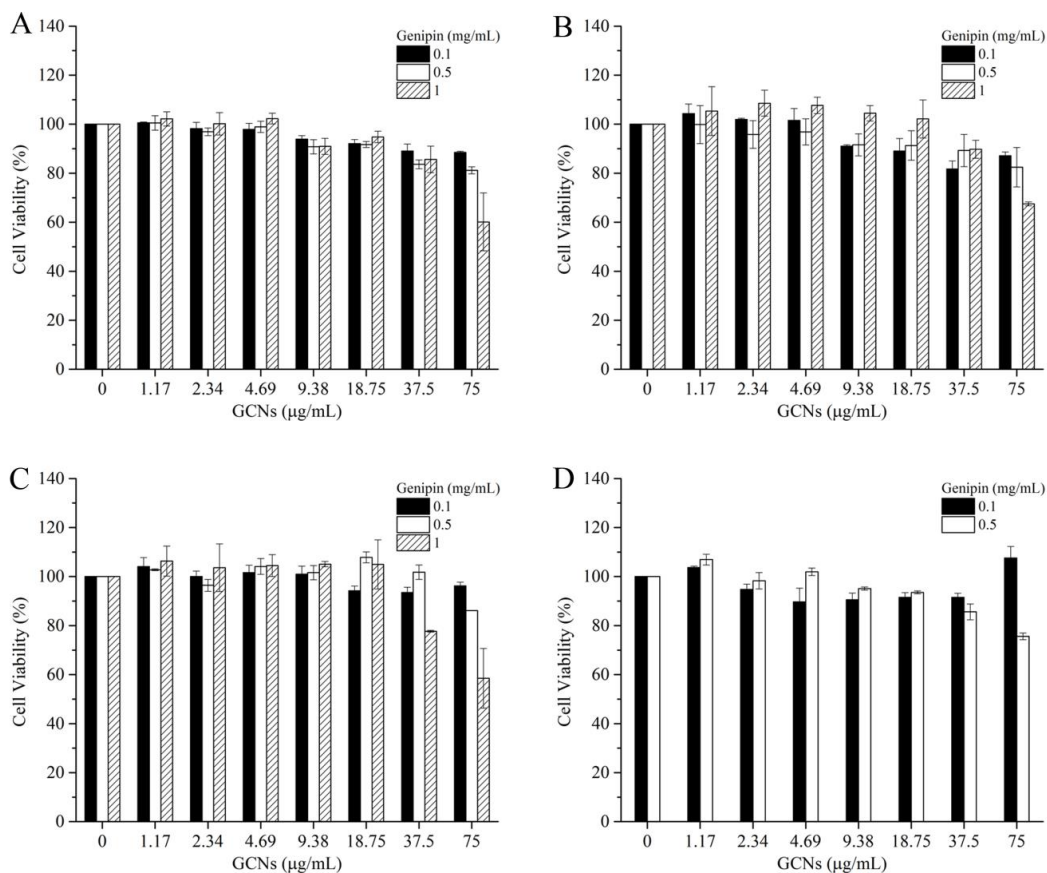


Figure 6-8. Viabilities of Caco-2 cell treated with GCNs crosslinked with 0.1-1 mg/mL genipin for (A) 4h, (B) 8h, (C) 16h, and (D) 24h at 25°C

6.4.4. Evaluation of the Intestinal Permeability

The bioavailability of TFs is extremely low¹⁸⁷. According to the Lipinski's "rule of 5", any molecule meets 2 of the following 4 conditions would be expected to have poor absorption or permeation: (i) Mw over 500, (ii) logP over 5 or MlogP over 4.15, (iii) has more than 5 hydrogen bond donors, (iv) has more than 10 hydrogen bond acceptors¹⁹³. TF-3 is a polyhydroxylated polyphenol with 13 hydroxyl groups and molecular weight of 868 g/mol. Therefore, it is very likely that the low bioavailability of TF-3 stems from its low permeability through small intestinal epithelium.

The human colon carcinoma Caco-2 cells grown on a permeable filter for at least 21 days can differentiate into a monolayer which has similar functionality of human small intestinal villus epithelium. Therefore, the Caco-2 monolayer model is a golden standard to predict the *in vitro* permeability and absorption of drugs²²⁵. The intestinal permeability of TF-3 in pure form and in encapsulated form was investigated by the Caco-2 monolayer transport model for 2h. As shown in Figure 6-9, the total amount of transported TF-3 encapsulated in the GCNs was 7.8 to 9.5 folds of pure TF-3. GCNs crosslinked by higher concentration of genipin slightly lowered the cumulative amount of transported TF-3, which is probably due to slower release of TF-3 from the GCNs crosslinked by higher concentration of genipin.

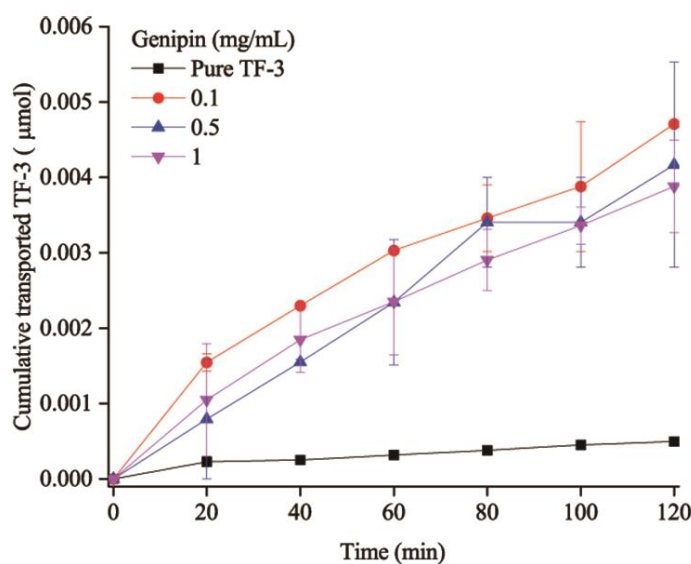


Figure 6-9. Cumulative fraction of transported TF-3

The P_{app} of pure TF-3 was 3.05×10^{-6} cm/s, while the P_{app} increased significantly to 2.89×10^{-5} cm/s, 2.56×10^{-5} cm/s, and 2.38×10^{-5} cm/s when TF-3 was encapsulated in the GCNs which were crosslinked for 4h with 0.1 mg/mL, 0.5 mg/mL, and 1 mg/mL genipin, respectively. This result demonstrated that TF-3 encapsulated in the GCNs became highly intestinal permeable.

The increased intestinal permeability was resulted from CS, which is a permeability enhancer. It was proved both *in vitro* and *in vivo* that CS can reversibly and transiently open the tight junctions between small intestinal epithelial cells^{114, 116, 118}. This process can facilitate paracellular transport of hydrophilic drugs and nutraceuticals¹²¹. Before treating the Caco-2 monolayers with the samples, the TER of every monolayer was measured which showed higher than 800 $\Omega\cdot\text{cm}^2$ in all the monolayers, indicating the integrity of the monolayer. During 2h transport experiment, decrease of TER of the monolayers treated with GCNs encapsulated with TF-3 was observed, which indicates opening of the tight junctions. Nevertheless, the TER of the monolayer treated with pure TF-3 did not decrease. After removal of the CS-containing samples and re-culture of the monolayer with cell culture medium, the TER recovered to initial values, which represents closure of the tight junctions.

6.5. Conclusions

In this chapter, the CS-CPPs nanocomplexes were crosslinked by genipin, a natural crosslinker. The crosslinking reaction was conducted in the presence of different concentrations of genipin for different crosslinking durations. The GCNs were used to encapsulate TF-3. It was found that after crosslinking, the nanocomplexes became more resistant to the acid-induced size increase, which may be helpful to prevent the burst release of encapsulated TF-3 in human gastric environment. The Caco-2 transport experiment proved that GCNs can effectively enhance the intestinal permeability of TF-3, which may improve the bioavailability of TF-3.

CHAPTER VII. FABRICATION AND CHARACTERIZATION OF PIKCERING EMULSIONS STABILIZED BY THE CHITOSAN- CASEINOPHOSHOPEPTIDES NANOCOMPLEXES

As of submission of this dissertation, the work in this chapter has been written as a research paper in the title of "Fabrication and Characterization of Emulsions Stabilized by Chitosan-Caseinophosphopeptides Nanocomplexes" which is ready for submission.

7.1. Abstract

The nanocomplexes assembled from CS and CPPs were utilized to stabilize Pickering emulsions with medium chain triglyceride (MCT) as the oil phase. Three kinds of CS-CPPs nanocomplexes composed of different CS:CPPs weight ratios [1:1 (C1P1), 2:1 (C2P1), 4:1 (C4P1)] were prepared and characterized in terms of their particle sizes, contact angles and surface tensions. Their abilities to stabilize Pickering emulsions were compared. The concentration ranges of these nanocomplexes that can stabilize Pickering emulsion decreased in the following way, C1P1 > C2P1 > C4P1. The oil fraction (Φ) that can be stabilized by these three kinds of nanocomplexes at 0.15 wt% concentration was similar ($\Phi \sim 0.5$, w/w). Increasing complex concentration can stabilize even higher fraction of MCT. The fluorescence microscopic image indicates that the Pickering emulsions were O/W type Pickering emulsions. These emulsions were stable against ionic strength (0-0.3 M NaCl) changes after 24h storage but low pH could affect their sizes. The CS-CPPs nanocomplexes stabilized Pickering emulsions showed gel-like behavior as proved by the rheological characterization.

7.2. Introduction

As introduced in section 1.2, Pickering emulsions are stabilized by solid particles. They received extensive attention due to their excellent stability against coalescence and Ostwald ripening⁹⁵. Moreover, the feature of surfactants-free during preparation makes them possible to

avoid the adverse effects that are associated with these surfactants, such as irritancy, hemolytic behavior, colitis, and metabolic syndromes^{97, 98}. Extensive work has been done on Pickering emulsions stabilized by inorganic and non-food grade organic particles^{97, 99-101}. Although people now start to pay attention to the food-grade particles such as proteins¹⁰²⁻¹⁰⁴ or polysaccharides^{105, 106}, using the polysaccharide-protein/polypeptide complexes as the Pickering stabilizers were relatively less reported.

In this chapter, the CS-CPPs nanocomplexes were used to stabilize Pickering emulsion with MCT as the oil phase. Three kinds of nanocomplexes were compared in terms of their ability to stabilize the Pickering emulsions. The stabilities of the Pickering emulsions against pH and ionic strength changes were characterized. The rheological properties of these Pickering emulsions were also investigated.

7.3. Materials and Methods

7.3.1. Materials

CS was purchased from Kunpoong Bio. Co., Ltd. (South Korea) and used as received without further treatment. CPPs was purchased from Greencream Biotechnology Co., Ltd. (Guangzhou, China). Neobee® 1053 MCT was provided by Stepan Company (IL, USA). Nile red was purchased from Chem-Impex International, Inc. (IL, USA). Fluorescein isothiocyanate (FITC) was purchased from Sigma-Aldrich (MO, USA). Milli-Q water was used in all the experiments.

7.3.2. Preparation and Characterization of the CS-CPPs Nanocomplexes

CS was dissolved in 1% acetic acid containing 10 mM NaCl. CPPs were dissolved in Milli-Q water containing 10 mM NaCl. The pH of CS and CPPs solutions was adjusted to pH 6 followed by addition of the CPPs solution dropwise into same volume of CS solution during magnetic stirring to generate the nanocomplexes.

The FITC labeled CS-CPPs nanocomplexes were prepared in the same way described above using CPPs and FITC-labeled CS. The FITC-labeled CS was synthesized as described elsewhere²³⁶ with little modification. Briefly, 50 mL dehydrated methanol and 25 mL 1 mg/mL FITC (dissolved in methanol) were added into 50 mL 1% CS solution (dissolved in 1% acetic acid) and stirred in the dark for 3h at ambient temperature. The FITC-labeled CS was then precipitated in 0.25 M NaOH. The unreacted FITC was removed by centrifugation at 4,000 g for 10 min and washing the precipitate with methanol:water (70:30, v/v) repeatedly until no fluorescence was detected at $\lambda_{\text{ex}}=492$ nm and $\lambda_{\text{em}}=520$ nm in the supernatant. The precipitate was re-dissolved in 1% acetic acid and dialyzed in distilled water for 2 days in the dark. The distilled water was replaced every 6h. The FITC-labeled CS was then freeze dried for further use.

The particle size of the CS-CPPs nanocomplexes was measured by a 90Plus Particle Size Analyzer equipped with a Brookhaven BI-9000AT digital correlator (Brookhaven Instruments Corporation, NY, USA). All measurements were conducted at the fixed scattering angle of 90°. The particle size of the CS-CPPs nanocomplexes was obtained from the intensity-intensity autocorrelation function

$$G(q, t) = a + b \times \left(\exp\left(-\left(\frac{t}{c}\right)^d\right) \right)^2 \quad \text{eq. 7-1}$$

The normalized autocorrelation function $g(q,t)$ was obtained using Sigert relation

$$g(q, t) = [G(q, t) - 1]^{1/2} \quad \text{eq. 7-2}$$

The William-Watts (WW) stretched exponential function was used to fit $g(q,t)$

$$g(q, t) = \exp\left[-\left(\frac{t}{\tau}\right)^\beta\right] \quad \text{eq. 7-3}$$

where β is the distribution parameter ranging from 0 to 1. The mean relaxation times were obtained from

$$\langle \tau \rangle = \tau \frac{\Gamma(1/\beta)}{\beta} \quad \text{eq. 7-4}$$

The diffusion coefficient D was calculated from

$$D = \langle \tau \rangle^{-1} q^{-2} \quad \text{eq. 7-5}$$

where q is the amplitude of scattering vector obtained from

$$q = \frac{4\pi n}{\lambda} \sin\left(\frac{\theta}{2}\right) \quad \text{eq. 7-6}$$

where n is the solution refractive index; λ is the laser wavelength; θ is the scattering angle. The hydrodynamics diameter was then calculated by the Stokes-Einstein equation

$$d = \frac{kT}{3\pi\eta D} \quad \text{eq. 7-7}$$

where k is the Boltzmann constant; T is the absolute temperature; η is the solvent viscosity.

The morphology of the CS-CPPs nanocomplexes was monitored by a Nanoscope IIIa Multi-Mode AFM (Veeco Instruments Inc., CA, USA) with tapping mode. Fresh made CS-CPPs nanocomplexes were dripped on the surface of pre-cleaned mica slides and kept for 1h. The surface of the mica slides was then rinsed with Milli-Q water and dried for analysis.

7.3.3. Contact Angle Measurement

The contact angle was measured on a VCA-Optima XE Dynamic Contact Angle Analyzer (AST Products, Inc., MA, USA). The CS-CPPs nanocomplexes (8 mg/mL) were dripped onto the pre-cleaned glass slides and dried before measuring. The images were captured by a CCD camera immediately after a drop of Milli-Q water (2 μ L) was deposited onto the nanocomplexes film surface. The contact angle was determined by the software associated with the analyzer. At least ten measurements were repeated and averaged for each sample.

7.3.4. Surface Tension Measurement

The surface tension of the CS-CPPs nanocomplexes was studied using a contact angle goniometer (Rame-Hart Instrument Co., NJ, USA). The pendant drop method was applied to measure the surface tension. Briefly, the CS-CPPs nanocomplexes droplets (5mg/mL) were hanging to the end of a needle that was immersed in MCT. The shape of the droplets was captured by a super-speed digital camera and analyzed by the KSV CAM101 software. The surface tension was calculated by

$$\sigma = \Delta\rho g R^2 / \beta \quad \text{eq. 7-8}$$

where $\Delta\rho$ is the difference of density between nanocomplexes and MCT; g is the gravity constant; R is the radius of the curvature of the droplet; β is the shape factor determined by Young-Laplace equation. At least ten measurements were repeated and averaged for each sample.

7.3.5. Preparation and Characterization of the Pickering Emulsions

The CS-CPPs nanocomplexes stabilized Pickering emulsions were generated by mixing MCT with the CS-CPPs nanocomplexes on a vortex mixer. A typical emulsion (oil fraction $\Phi = 0.5$ w/w) stabilized by 0.5 wt% C1P1 nanocomplexes, for example, was fabricated as follows: 2 g MCT and 2 g 1 wt% C1P1 were slowly added into a glass vial. This mixture was vigorously mixed on a vortex mixer for 1 min at room temperature. The fluorescence labeled Pickering emulsions ($\Phi = 0.5$ w/w) were prepared in the same way using Nile red (1 μM)-stained MCT and FITC-labeled CS-CPPs nanocomplexes.

The stability of the Pickering emulsions against pH change was determined by 1:5 diluting the cream layer of the Pickering emulsions with Milli-Q water at pH 2, 4, 6, and 8. Similarly, the stability against ionic strength change was determined by 1:5 diluting the cream layer of the Pickering emulsions with Milli-Q water containing 0 M, 0.05 M, 0.1 M, 0.15 M, and 0.3 M NaCl. The microscopic images were then observed by microscope after 24h storage.

7.3.6. Visualization of the Pickering Emulsions

The microscopic images of Pickering emulsions were monitored by a Nikon TE-2000-U inverted fluorescence microscope equipped with a CCD camera (Retiga Exi, Q-imaging). For visualizing the fluorescence of the Pickering emulsions prepared with Nile red-stained MCT and FITC-labeled nanocomplexes, the light was filtered through the bandpass filters, which yielded the excitation wavelengths of 488 ± 10 nm for FITC and 550 ± 10 nm for Nile red. The fluorescence images were processed by the SimplePCI C-Imaging software (Compix, Inc., PA, USA).

7.3.7. Rheological Measurement

The rheological properties of the Pickering emulsions ($\Phi = 0.5$ w/w) were measured on a Discovery HR-2 Hybrid Rheometer (TA Instruments, DE, USA) with 25 mm stainless-steel parallel plate geometry and a temperature-controlled stainless-steel Peltier plate. Dynamic strain sweep tests (0.1%-100% strain at 0.1 Hz frequency) were carried out to determine the linear viscoelastic region before each dynamic frequency sweep test, which adopted the strain value of 5% and the angular frequency ω from 0.1 to 100 rad/s with 20 data points per decade. All the measurements were carried out at 25°C.

7.4. Results and Discussion

7.4.1. Preparation and Characterization of the CS-CPPs Nanocomplexes

Three kinds of CS-CPPs nanocomplexes were assembled with CS:CPPs weight ratio of 1:1 (C1P1), 2:1 (C2P1), and 4:1 (C4P1). The CS molecules were cationic and CPPs were anionic at pH 6. They strongly associated with each other via predominantly electrostatic attraction. Different concentrations of the CS-CPPs nanocomplexes were prepared and their representative AFM height images are shown in Figure 7-1A-C. 0.3 wt% C1P1 (Figure 7-1A) and C2P1 (Figure 7-1B) were almost single particles with spherical shape, while C4P1 (Figure 7-1C) at the same concentration had irregular shape, which could be resulted from the aggregation of single particles. The particle

sizes were obtained by fitting the correlation functions (Figure 7-1D-F) and calculated by eq. 7-1 to eq. 7-7. Generally, the particle size of the nanocomplex increased with the content of CS. The particle sizes of 0.3 wt% C1P1, C2P1 and C4P1 were 295 nm, 340 nm, and 386 nm, respectively.

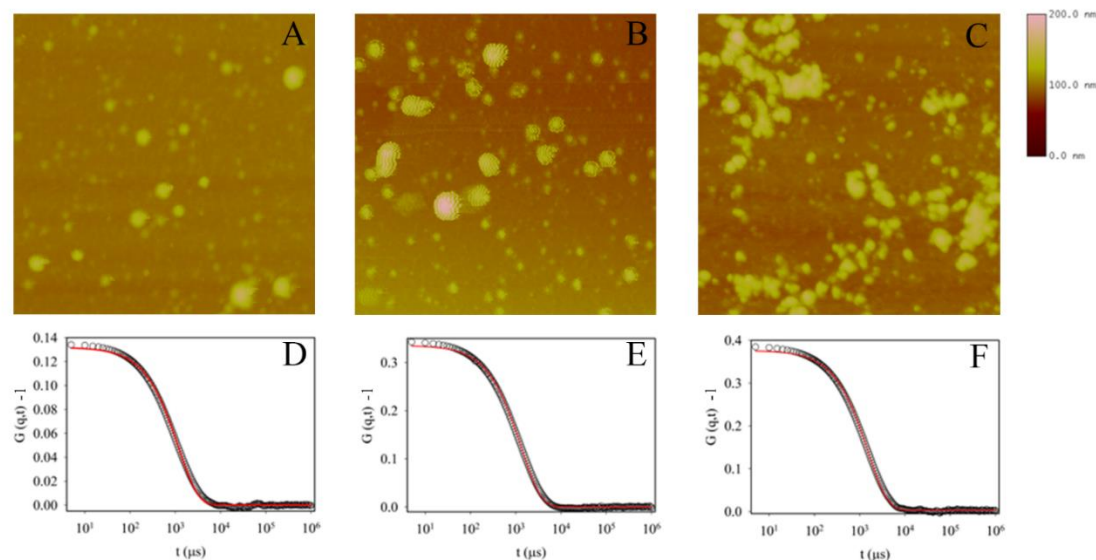


Figure 7-1. AFM height images of 0.3 wt% (A) C1P1, (B) C2P1, and (C) C4P1. Correlation function fitting for mean size of 0.3 wt% (D) C1P1, (E) C2P1, and (F) C4P1.

The contact angles of C1P1, C2P1, and C4P1 at the air-water interface were measured at constant concentration (8 mg/mL). The representative data of the contact angles are shown in Figure 7-2. Their contact angles at the air-water interface were $37.5 \pm 5.3^\circ$, $26.9 \pm 2.5^\circ$, and $17.0 \pm 1.9^\circ$, respectively. This decreased contact angle indicates that the surface hydrophilicity of the nanocomplexes increased. This phenomenon may be attributed to increasing proportion of CS in the nanocomplexes. CS is the *N*-deacetylated derivative of chitin (β -(1 \rightarrow 4)-*N*-acetyl-D-glucosamine). The CS molecule itself is hydrophilic due to presence of the amine groups when environmental pH is below its pK_a value (6.3~6.4)¹¹². Therefore, the nanocomplexes became more hydrophilic when the surface was more saturated with CS molecules.

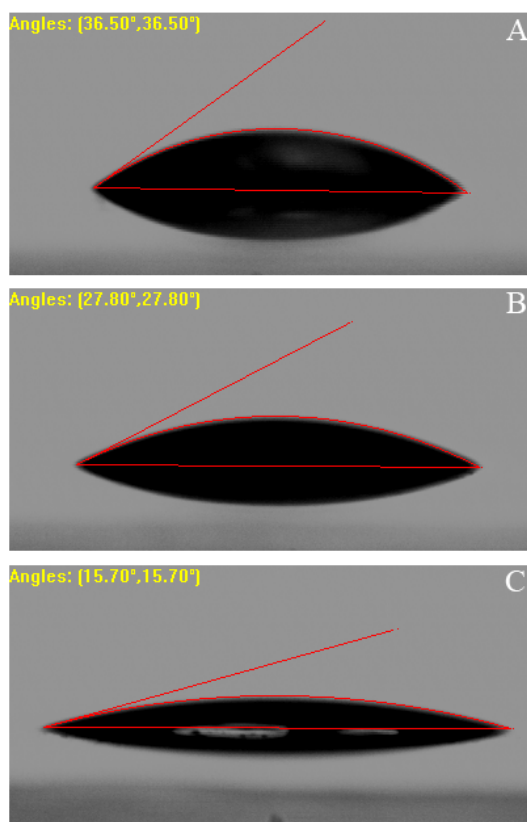


Figure 7-2. Representative contact angles of 8 mg/mL (A) C1P1, (B) C2P1, and (C) C4P1 at the air-water interface.

The interfacial properties of the CS-CPPs nanocomplexes were also characterized by measuring their surface tensions at the oil-water interface. The surface tensions of 5 mg/mL C1P1, C2P1, and C4P1 were 18.49 ± 0.58 mN/m, 19.28 ± 0.76 mN/m, and 20.01 ± 0.13 mN/m, respectively. It was reported that the peptides hydrolyzed from caseins were surface active²³⁷⁻²³⁹, which could reduce the surface tension. Thus, higher CS:CPPs weight ratio which reduced the opportunity of exposing CPPs at the nanocomplex surface could increase the surface tension between the nanocomplexes and MCT.

7.4.2. Characterization of the Pickering Emulsions

To study the impacts of nanocomplex composition on their ability as the Pickering stabilizer, C1P1, C2P1, and C4P1 were mixed with equal weight of MCT (oil fraction $\Phi = 0.5$ w/w), yielding

the final nanocomplex concentrations ranged from 0.05 wt% to 0.5 wt%. As shown in Figure 7-3, C1P1 can stabilize the Pickering emulsions at the concentration ranging from 0.05 wt% to 0.5 wt%, while for the other two kinds of CS-CPPs nanocomplexes, only 0.05-0.25 wt% C2P1 and 0.05-0.15 wt% C4P1 can form stable Pickering emulsions. The reason for the narrower concentration ranges of C2P1 and C4P1 that can stabilize Pickering emulsion could be attributed to their higher surface hydrophilicity. The droplet size of Pickering emulsion stabilized by C1P1 decreased gradually from 400-500 μm (0.05 wt% C1P1) to 150-200 μm (0.25 wt% C1P1). Further increasing C1P1 concentration did not significantly change the emulsion droplet size. This result is similar to the general observations that the droplet size of Pickering emulsion decreases with increasing concentrations of the colloidal particles to a certain value, after which the droplet size becomes almost constant^{102, 106}. The reduction of emulsion droplet size was related to higher amount of nanocomplexes that can cover larger interfacial area. It was also found that the sizes of emulsion stabilized by C2P1 and C4P1 were larger than those stabilized by C1P1 at corresponding concentrations. In all the Pickering emulsions, creaming was observed. As the concentration of the nanocomplexes increased, the serum layer became more turbid, indicating that excess amount of nanocomplexes that were not adsorbed to the oil-water interface was appearing in the serum layer.

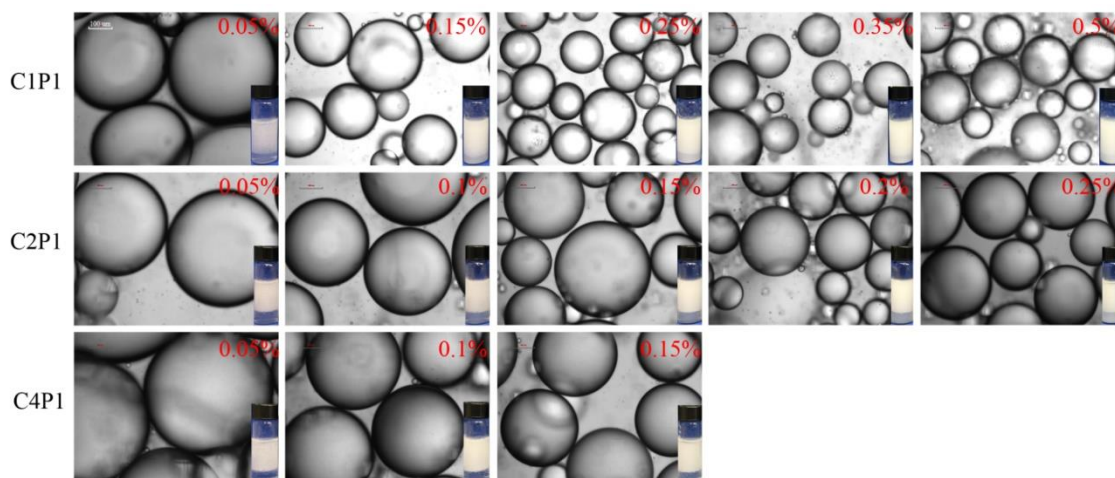


Figure 7-3. Pickering emulsions stabilized by different concentrations of the CS-CPPs nanocomplexes, $\Phi = 0.5$ w/w. The scale bar is 100 μm .

Fluorescence labeling was used to determine the type of the CS-CPPs nanocomplexes stabilized Pickering emulsions. MCT was pre-stained with Nile red, which released red fluorescence. CS molecules were labeled with FITC, which emitted green fluorescence. As shown in Figure 7-4, the red oil droplets were surrounded by the green nanocomplexes, indicating that the CS-CPPs nanocomplexes were adsorbed on the surface of the oil droplets. This result demonstrates that the CS-CPPs nanocomplex stabilized Pickering emulsions were O/W emulsions.

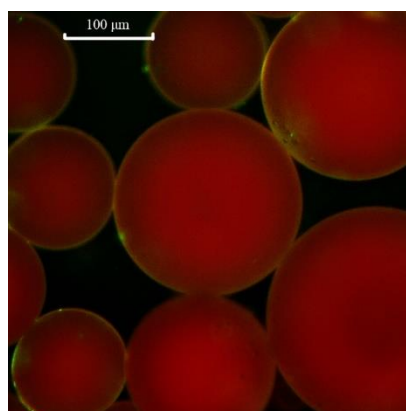


Figure 7-4. Fluorescence microscopy (overlay) images of Pickering emulsion formed by Nile red (1 μM)-stained MCT and FITC-labeled 0.25 wt% C1P1. The scale bar is 100 μm .

The fraction of oil that can be stabilized by the CS-CPPs nanocomplexes were investigated at $\Phi = 20\%$ -80% (w/w). As shown in Figure 7-5, the Pickering emulsions containing 20%-40% MCT can be stabilized by 0.15 wt% C1P1, C2P1, and C4P1, while higher oil fraction (60%-80%) cannot be stabilized. Therefore, it is concluded that these three kinds of nanocomplexes at 0.15 wt% concentration can stabilize at least 50% MCT (Figure 7-3). When the concentration of C1P1 increased to 0.25 wt%, 60% MCT was stabilized, indicating that more oil can be stabilized with higher concentration of nanocomplexes. It was observed that the emulsion droplet sizes increased with the oil fraction, because the amount of available nanocomplexes for covering the oil-water interface became relatively less when the oil fraction increased. The thickness of the cream layer also increased with the oil fraction.

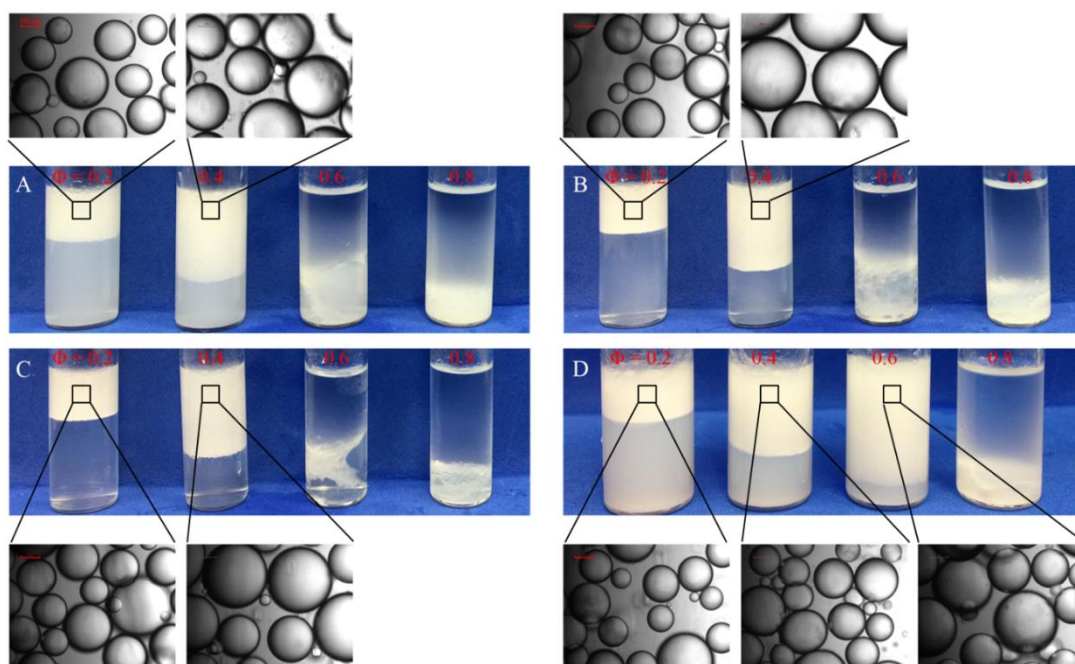


Figure 7-5. Pickering emulsions of different oil fractions ($\Phi = 0.2$ -0.8 w/w) stabilized by (A) 0.15 wt% C1P1, (B) 0.15 wt% C2P1, (C) 0.15 wt% C4P1, and (D) 0.25 wt% C1P1. The scale bar is 100 μm .

Complexation between polysaccharides and proteins/polypeptides depends on environmental pH because pH determines the charge density of these polyelectrolytes (section 3.4.1). The pH stability of the CS-CPPs nanocomplexes stabilized Pickering emulsions was characterized by diluting the cream layers of the Pickering emulsions with Milli-Q water at pH 2-8. This pH range covered 3 states of the CS-CPPs binary components system. At pH 2, CS and CPPs repelled with each other and they cannot assemble into complex because they all carried positive charges. At pH 4 and 6, CS and CPPs carried opposite net charges and they self-assembled into complexes through electrostatic attraction. At pH 8, no electrostatic attraction occurred between CS and CPPs because of neutralization of CS (section 3.4.1). This pH range also covered the pH of human stomach, small intestine, and most foods. After 24h storage, no macroscopic phase separation was observed (Figure 7-6). Microscopic images show that at pH 2 the droplet sizes of the tested Pickering emulsions became smaller. These emulsions were also easier to spread on the glass slides upon microscopical observation. This phenomenon could be resulted from disassembly of the nanocomplexes at pH 2. The droplet size at pH 4-8 did not change much. Jourdain *et al.* reported that the pH stability of Pickering emulsions stabilized by dextran sulfate-sodium caseinate complex depended on the concentration of dextran sulfate²⁴⁰. In their study, higher concentration of dextran sulfate provided better resistance to acidification. In the present system, the pH stability was relatively independent on the concentration of CS. Higher concentration of C1P1 did not improve the stability at pH 2.

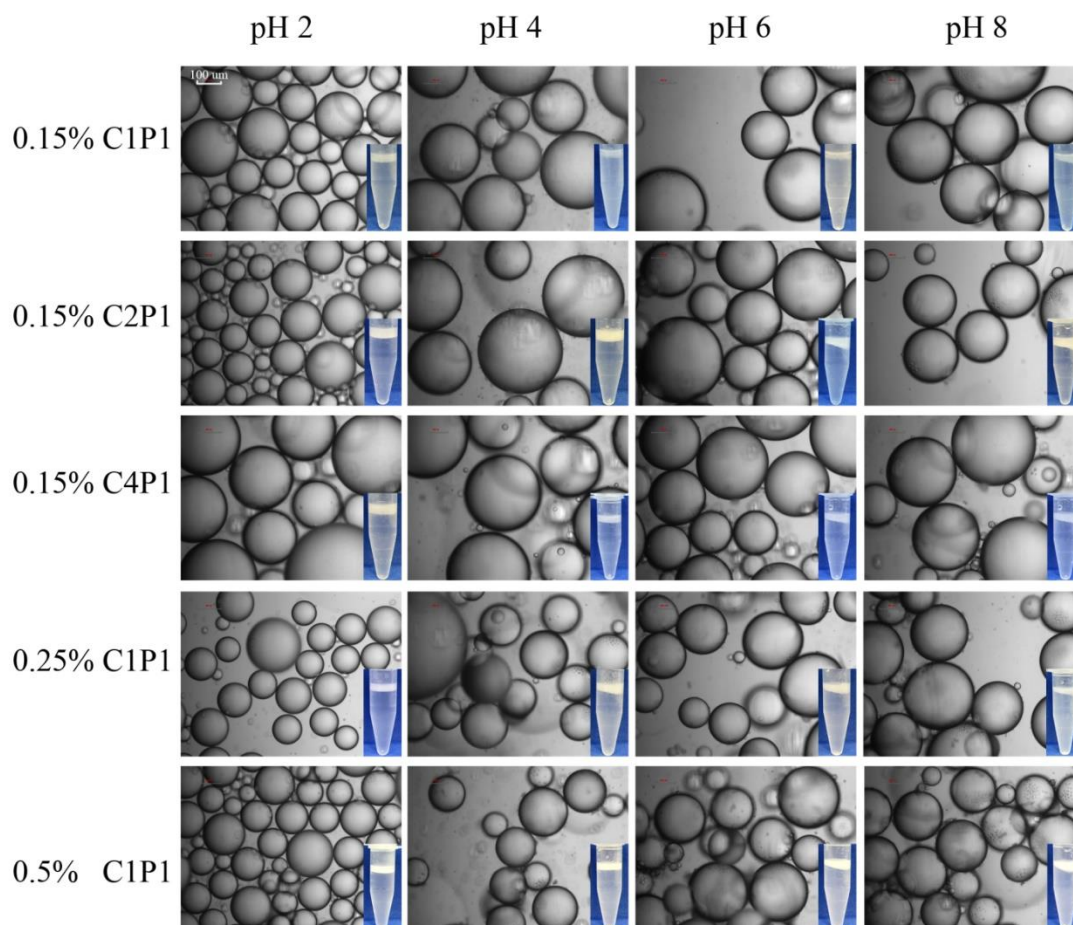


Figure 7-6. pH stability of Pickering emulsions stabilized by the CS-CPPs nanocomplexes, $\Phi = 0.5$ w/w. The scale bar is 100 μm .

It is well documented that NaCl at high concentrations can inhibit the electrostatic interaction between proteins/polypeptides and polysaccharides since NaCl can screen the charge density. This phenomenon was also observed in complexation between CS and CPPs (CHAPTER III). Herein the stability of Pickering emulsions against ionic strength change was studied. As shown in Figure 7-7, when subjected to 0-0.3 M NaCl, the emulsion droplet size remained almost unchanged after 24h storage, which means that these Pickering emulsions were stable at this ionic strength range. This result also implies that the CS-CPPs nanocomplexes stabilized Pickering emulsions could be stable at physiological ionic strength (0.15 M NaCl).

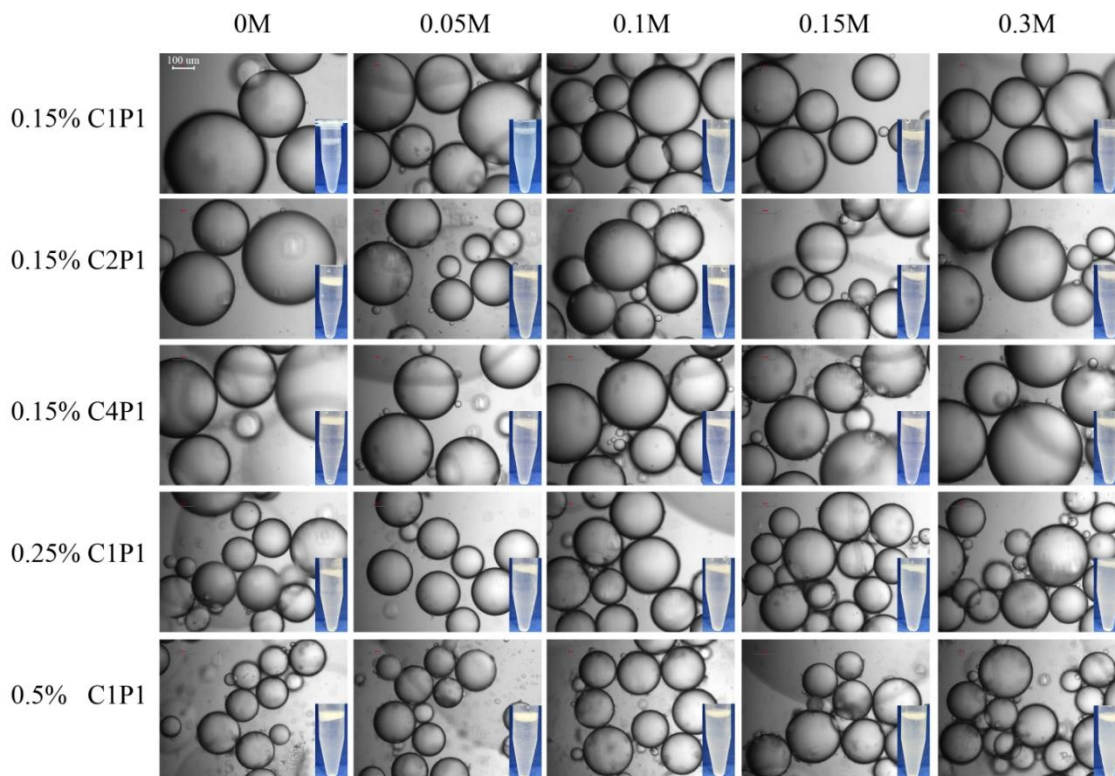


Figure 7-7. Stability of CS-CPPs nanocomplexes stabilized Pickering emulsions against ionic strength change, $\Phi = 0.5$ w/w. The scale bar is 100 μm .

7.4.3. Rheological Properties

Before each oscillating frequency sweep, the dynamic strain sweep tests were carried out from 0.1% to 100% strain at fixed 0.1 Hz frequency to obtain the linear viscoelastic regions. The strain value of 5% was adopted as it was within the linear viscoelastic regions of all the tested Pickering emulsions.

In a rheological study of the Pickering emulsion stabilized by CS-sodium caseinate complex, the storage modulus G' was consistently lower than the loss modulus G'' over the frequency range of 0.1-100 Hz²⁴¹. The CS-CPPs nanocomplexes stabilized Pickering emulsions did not show same rheological manners. These Pickering emulsions were highly viscous. They did not flow even when the vials were inverted, which means they may behave like gel. The rheological behaviors of the

Pickering emulsions stabilized by different nanocomplexes at 0.15 wt% concentration were firstly compared. They exhibited similar manner with G' greater than G'' over the tested angular frequency range (Figure 7-8A, B, C). Both G' and G'' were independent of frequency at low angular frequency. These results confirm that the Pickering emulsions stabilized by the CS-CPPs nanocomplexes had gel-like property. This gel-like behavior could be attributed to formation of three-dimensional particle network. When comparing emulsions stabilized by different concentrations of C1P1, it was found that G' and G'' were almost identical in these Pickering emulsions (Figure 7-8A, D, E). The decreasing complex viscosity (η^*) in all the tested Pickering emulsions upon increasing angular frequency reflects breakdown of the network within the emulsions²⁴².

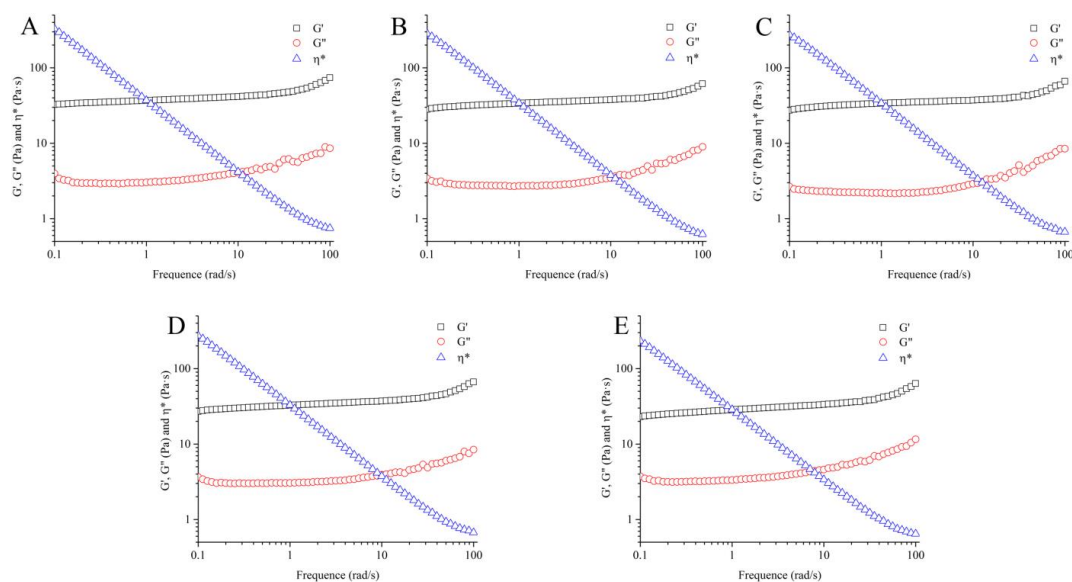


Figure 7-8. Frequency sweep of Pickering emulsions stabilized by (A) 0.15 wt% C1P1, (B) 0.15 wt% C2P1, (C) 0.15 wt% C4P1, (D) 0.25 wt% C1P1, and (E) 0.5 wt% C1P1.

7.5. Conclusions

The CS-CPPs nanocomplexes can stabilize Pickering emulsion with MCT as the oil phase. The surface hydrophilicity and oil-water surface tension of these nanocomplexes increased with the content of CS in the nanocomplexes. The nanocomplex containing higher CPPs content could

stabilize the Pickering emulsion in a wider concentration range. These emulsions had gel-like behavior and they were stable against ionic strength changes after 24h storage. Low pH could affect their stability.

CHAPTER VIII. STABILIZATION OF PICKERING EMULSIONS BY THE GENIPIN CROSSLINKED CHITOSAN- CASEINOPHOSPHOPEPTIDES NANOCOMPLEXES: IMPACTS OF CROSSLINKING DURATION

As of submission of this dissertation, the work in this chapter has been written as a research paper in the title of “Stabilization of Pickering Emulsions by the Genipin Crosslinked Chitosan-Caseinophosphopeptides Nanocomplexes” which is ready for submission.

8.1. Abstract

In this chapter, genipin was used to covalently crosslink the CS-CPPs nanocomplexes. The crosslinking reaction initiated after 0.5h. The GCNs were characterized by dynamic light scattering, ζ -potential, contact angle, surface tension measurements, AFM, USAXS and SAXS at different reaction time intervals. The GCNs with different crosslinking durations were further applied to stabilize Pickering emulsions with MCT as the oil phase. The effects of GCNs concentration (0.05 - 0.25 wt%) and oil fraction ($\Phi = 0.2 - 0.6$, w/w) on emulsion droplet size and creaming stability were investigated. Generally higher concentration of GCNs led to smaller emulsion droplet size and higher stability against creaming. The Pickering emulsion stabilized by GCNs with longer crosslinking duration had larger droplet size. Higher oil fraction also enhanced the creaming stability but increased emulsion droplet size. These emulsions were O/W type Pickering emulsions. They were stable against both pH and ionic strength changes. Rheological study revealed that these Pickering emulsions were gel-like and GCNs with shorter crosslinking duration stabilized stronger gel-like emulsion.

8.2. Introduction

In CHAPTER VII, the CS-CPPs nanocomplexes were utilized to stabilize Pickering emulsions with MCT as the oil phase. These emulsions were O/W type and they had gel-like rheological behavior due to formation of three-dimensional particle network. Complexation between polysaccharides and proteins/polypeptides in aqueous solution is pH-dependent, which means that altering the environmental pH can affect their associations (CHAPTER I and CHAPTER III). The insoluble complexes only form at a certain pH range where proteins/polypeptides and polysaccharides carry opposite net charges. Beyond this pH range, these biomolecules either form soluble complexes or cosolubilize in solution.

Although no conclusion was reached whether pH can influence the magnitude of association within the polysaccharide-protein/polypeptide complexes anchored at the oil-water interface, there are literatures reporting that changing pH can change the droplet size of the Pickering emulsions stabilized by the complexes^{240, 243}. In CHAPTER VII, it was observed that the droplet sizes of the CS-CPPs nanocomplexes stabilized Pickering emulsions decreased at pH 2, and the emulsions were less viscous at this pH. These phenomena could be due to disassembly of the CS-CPPs nanocomplexes at this very acidic condition. Similarly, the polysaccharide-protein/polypeptide complexes are usually susceptible to ionic strength change. High concentration of NaCl can suppress their interactions (section 3.4.1). Therefore, ionic strength change may potentially affect the stability of the complex stabilized Pickering emulsions. Besides, the major interactions involved in formation of the polysaccharide-protein/polypeptide complexes are electrostatic interaction, hydrogen bond, and hydrophobic interactions, which are all weak interactions (section 1.1.1). Subjecting to high shear, *e.g.* high-speed homogenization during preparing the Pickering emulsions may disrupt the structures of the complexes. Using crosslinker to covalently crosslink the proteins/polypeptides and polysaccharides is a strategy to solve the aforementioned problems. Littoz *et al.* reported that the pectin- β -lactoglobulin stabilized emulsion crosslinked by laccase had

better stability against high concentration of NaCl than non-crosslinked emulsion²⁴⁴. In another study, the pH stability of pectin-gelatin stabilized emulsion was improved after being crosslinked by laccase²⁴⁵.

Genipin is a natural crosslinker that is usually enzymatically hydrolyzed from its parent compound geniposide, which is isolated from the fruit of *Gardenia jasminoides Ellis*. The fruit of *Gardenia jasminoides Ellis* has been used in traditional Chinese medicine for long time²⁴⁶. Genipin is the major compound that is responsible for the pharmacological properties of gardenia including anti-carcinogenic, anti-inflammatory, neuroprotective, and choleric effects^{246, 247}. In food industry, genipin is applied as a precursor of blue pigments²²⁸. The toxicity of genipin is thousand times lower than the traditionally used crosslinker glutaraldehyde²⁴⁸. Besides, genipin is biodegradable. It is biotransformed through demethylation, ring-opening, cysteine-conjugation, hydroformylation, glucuronidation, and sulfation²⁴⁷.

In this chapter, genipin was used to crosslink the CS-CPPs nanocomplexes for different crosslinking durations and these GCNs were characterized and applied to stabilize Pickering emulsions. Their capacities as the Pickering stabilizers were compared. The Pickering emulsions stabilized by GCNs with different crosslinking durations were also investigated.

8.3. Materials and Methods

8.3.1. Materials

CS was purchased from Kunpoong Bio. Co., Ltd. (South Korea) and used as received without further treatment. CPPs was purchased from Greencream Biotechnology Co., Ltd. (Guangzhou, China). Neobee[®] 1053 MCT was provided by Stepan Company (IL, USA). Genipin (purity > 98%) was purchased from Wako Pure Chemical Industries, Ltd. (VA, USA). Coumarin 6 was purchased from Sigma-Aldrich (MO, USA). Milli-Q water was used in all the experiments.

8.3.2. Preparation and Characterization of the GCNs

CS was dissolved in 1% acetic acid containing 10 mM NaCl. CPPs was dissolved in Milli-Q water containing 10 mM NaCl. Before generating the GCNs, the pH of CS and CPPs solutions was adjusted to 6. To start preparing the GCNs, genipin was mixed with CS solution at room temperature for 5 min, and then equal volume of CPPs solution was added dropwise into the CS-genipin solution during magnetic stirring. The final concentrations of CS, CPPs, and genipin were 2.5 mg/mL, 2.5 mg/mL, and 0.5 mg/mL, respectively. The crosslinking reaction was carried out at 40°C.

The UV-Vis measurements were conducted on a Cary 60 UV-Vis Spectrophotometer (Agilent Technologies, CA, USA). The GCNs were diluted with Milli-Q water (10 mM NaCl, pH 6) for 50 times. The UV-Vis spectra were recorded from 800 nm to 200 nm with the scan rate of 300 nm/min.

The particle size of GCNs was measured by the 90Plus Particle Size Analyzer equipped with a Brookhaven BI-9000AT digital correlator (Brookhaven Instruments Corporation, NY, USA). All measurements were conducted at the fixed scattering angle of 90°. The particle size of the GCNs was obtained through a series of calculation. The normalized autocorrelation function $g(q,t)$ was calculated from the intensity-intensity autocorrelation function $G(q,t)$ same as eq. 7-1 to eq. 7-7.

The ζ -potentials of the GCNs were measured using a Nano ZS Zetasizer (Malvern Instruments Ltd., MA, USA). The GCNs with different reaction time were 1:5 diluted with 10 mM NaCl solution (pH 6) before measuring. The measurements were triplicated at 25°C.

The contact angles were measured using a VCA-Optima XE Dynamic Contact Angle Analyzer (AST Products, Inc., MA, USA). The GCNs (0.5 wt%) with different crosslinking durations were dripped onto pre-cleaned glass slides and dried in a vacuum oven before measuring. The images were captured by a CCD camera immediately after a drop of Milli-Q water (2 μ L) was deposited

onto the GCNs film surface. The contact angle was determined by the software associated with the analyzer. At least twenty measurements were conducted and averaged for each sample.

The surface tension of the GCNs with different reaction durations was investigated on a contact angle goniometer (Rame-Hart Instrument Co., NJ, USA) with pendant drop method. Briefly, the GCNs were hanging to the end of a needle that was immersed in MCT. The shape of the droplets was captured by a super-speed digital camera and analyzed by the KSV CAM101 software. The surface tension was calculated by eq. 7-8. At least ten measurements were repeated and averaged for each sample.

The morphology of the GCNs was monitored by a Nanoscope IIIa Multi-Mode AFM (Veeco Instruments Inc., CA, USA) with tapping mode. Fresh made GCNs were diluted with Milli-Q water (10 mM NaCl, pH 6) and dripped on the surface of pre-cleaned mica slides. The surface of the mica slides was then rinsed with Milli-Q water and dried with N₂ for analysis.

The fluorescence emission spectrum of the GCNs was recorded on a FluoroMax-3 spectrofluorometer (Horiba Jobin Yvon, Inc., NJ, USA). GCNs solution was excited at 550 nm (λ_{ex}) and the emission spectrum was recorded from 610 to 800 nm (λ_{em}).

The USAXS and SAXS experiments were performed at beamline 9 ID-C at the APS of Argonne National Laboratory (Chicago, USA). Samples were filled in the 1 mm-thick silicone isolators (Grace Bio-Labs, Inc., OR, USA) and sealed with glass slides. The USAXS and SAXS data were processed and analyzed by the software packages of Indra 2, Irena 2, and Nika 1^{197, 230}.

8.3.3. Preparation and Characterization of the GCNs Stabilized Pickering Emulsions

The GCNs stabilized Pickering emulsions were prepared by mixing different amount of MCT (oil fraction Φ , w/w) with GCNs. The mixtures were subjected to high-speed homogenization (T25 digital ULTRA-TURRAX®, IKA Works Inc., USA) at 12,000 rpm for 1 min. A typical emulsion ($\Phi=0.5$, w/w) stabilized by 0.25 wt% GCNs for example was prepared by mixing 2 g MCT with 2

g 0.5 wt% GCNs in a glass vial which was then subjected to high speed homogenization. The fluorescence labeled Pickering emulsion was prepared in the same way using coumarin 6 - prestained MCT as the oil phase.

The heights of total emulsion (H_t) and bottom serum layer (H_s) were measured after 24h storage. The creaming index (CI) was calculated by

$$CI(\%) = \frac{H_s}{H_t} \times 100\% \quad \text{eq. 8-1}$$

The microscopic images of Pickering emulsions were monitored by a Nikon TE-2000-U inverted fluorescence microscope equipped with a CCD camera (Retiga Exi, Q-imaging). For visualizing the fluorescence of the Pickering emulsions, the light was filtered through the bandpass filters, which yielded the excitation wavelengths of 488 ± 10 nm for coumarin 6 and 550 ± 10 nm for GCNs. The fluorescence images were processed by the SimplePCI C-Imaging software (Compix, Inc., PA, USA) and the images were overlaid by the ImageJ software.

The diameters of the Pickering emulsion droplets were measured by the ImageJ software. At least 500 droplets were measured and averaged for each sample (except for 0.05 wt% GCNs stabilized emulsions). The size distribution fittings were performed on the @Risk software version 7 (Palisade Corporation, NY, USA).

The pH stability of the GCNs stabilized Pickering emulsions ($\Phi = 0.5, 0.25$ wt% GCNs) was evaluated by diluting the cream layer of the emulsions 1:5 with Milli-Q water at pH 2, 4, 6, 8, 10. Similarly, the stability of the GCNs stabilized Pickering emulsions ($\Phi = 0.5, 0.25$ wt% GCNs) against ionic strength change was evaluated by diluting the cream layer of the emulsions 1:5 with Milli-Q water containing 0 M, 0.05 M, 0.1 M, 0.15 M, and 0.3 M NaCl. The droplet sizes of the diluted Pickering emulsions at these conditions were measured after 24h storage at room temperature.

The rheological properties of the Pickering emulsions ($\Phi = 0.5, 0.25$ wt% GCNs) were measured on a Discovery HR-2 Hybrid Rheometer (TA Instruments, DE, USA) with 25 mm stainless-steel parallel plate geometry and a temperature-controlled stainless-steel Peltier plate. First dynamic strain sweep tests (0.1%-100% strain at 0.1 Hz frequency) were carried out to determine the linear viscoelastic region before each dynamic frequency sweep test, which adopted the strain value of 1% and the angular frequency ω from 0.1 to 100 rad/s with 20 data points per decade. All the measurements were carried out at 25°C.

8.4. Results and Discussion

8.4.1. UV-Vis Measurements

The reason genipin can serve as a crosslinker is that it can react with the primary amine groups. This reaction is pH dependent. At acidic to neutral conditions, the olefinic carbon atom at the C3 position on genipin is firstly nucleophilically attacked by the primary amine groups which opens the dihydropyran ring of genipin, forming an intermediate aldehyde group. This aldehyde group then reacts with the secondary amine group formed in the first step, forming a heterocyclic structure, which is covalently connected to the molecules containing primary amine groups, such as CS and CPPs^{231, 246}. At basic conditions, the crosslinking reaction is initiated by nucleophilic attack from the hydroxyl ions in aqueous solution, resulting in ring-opening and formation of intermediate aldehyde groups on genipin. The aldehyde groups then undergo aldol condensation followed by Schiff reaction with the amine groups to form crosslinked compounds²⁴⁶.

UV-Vis was firstly utilized to monitor the crosslinking reaction process. As shown in Figure 8-1, although not very significantly, the peak at 240 nm decreased as the crosslinking reaction went on. The absorption peak at 240 nm was attributed to genipin molecule per se²⁴⁹. The decreased absorption at 240 nm was due to the reduced amount of free genipin molecules in solution during the crosslinking reaction. The peak at about 290 nm gradually appeared after 0.5 h reaction. Park

et al. reported that a colorless compound that had maximum UV absorption at 292 nm was the intermediate of the blue pigments in the reaction of genipin with methylamine²³⁵. This intermediate is same as the heterocyclic structure formed in the reaction between genipin and primary amine group at acidic to neutral conditions^{231, 235}. Therefore, the increased absorption peak at about 290 nm should be attributed to formation of the heterocyclic compound and it indicates that the crosslinking process had already been initiated after 0.5h reaction. The peak at around 610 nm became obvious after 2h reaction. This peak was resulted from the blue pigments. It can be visually observed that the blue color of the solution became darker as the crosslinking process went on.

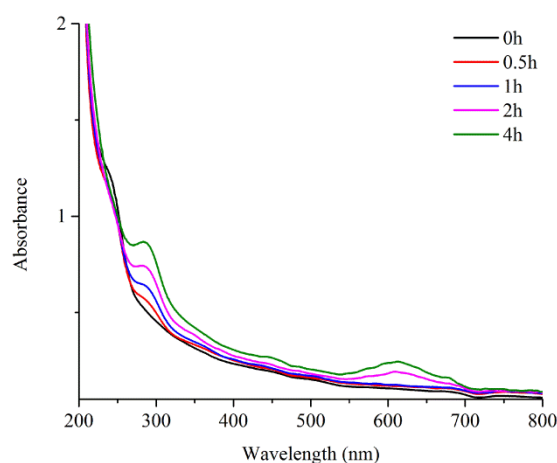


Figure 8-1. UV-Vis spectra of GCNs with different crosslinking durations

8.4.2. Characterization of the GCNs

The CS-CPPs nanocomplexes were used as the Pickering stabilizers in CHAPTER VII. Based on that, herein genipin was used to covalently crosslink the CS-CPPs nanocomplexes and the GCNs were further applied as the Pickering stabilizer.

The stability of Pickering emulsions is determined by eq. 1-4 expressed as:

$$E = \gamma\pi R^2(1 - |\cos \theta|)^2$$

where E is the free energy of detachment of a spherical particle from the interface; γ is the oil-water interfacial tension; R is the radius of particle; θ is the oil-water-particle three phase contact angle. Higher free energy of detachment E indicates stronger affinity of the particles that are anchored at the oil-water interface. From this equation, multiple parameters contribute together to the stability of Pickering emulsions.

The particle sizes of the GCNs with different crosslinking durations were firstly investigated, which was obtained by fitting the autocorrelation function (Figure 8-2A inset) followed by calculation with eq. 7-2 to eq. 7-7. As shown in Figure 8-2A, at the first 8h, the particle size of GCNs gradually decreased from 328 nm (0h) to 218 nm (8h). Extending the crosslinking reaction led to increase of the particle size. The increase of particle size after 8h reaction was due to dimerization, oligomerization, and esterization between the heterocyclic structures of GCNs^{233, 249, 250}. These dimer, oligomer, and ester structures were detected in the blue pigments during the reaction between genipin with methylamine²⁵¹, which explains why the blue color of the system became darker when the crosslinking reaction continued.

One of the important factors that maintain the stability of Pickering emulsions is electrostatic repulsion, which is correlated with the surface charges of the Pickering stabilizers. The surface charges of the GCNs with different crosslinking durations were investigated by measuring their ζ -potentials (Figure 8-2B). At the first 8h of the crosslinking reaction, ζ -potential slightly decreased from +21.8 mV (0h) to +20 mV (8h). Then the ζ -potential of GCNs experienced a dramatic decrease to +14.1 mV (16h) and further decreased to +13.6 mV (24h). Since genipin reacted with the primary amine groups which carried positive charges at the tested pH (pH 6), it is not surprising that the amount of positive charges on GCNs surface decreased as the reaction continued.

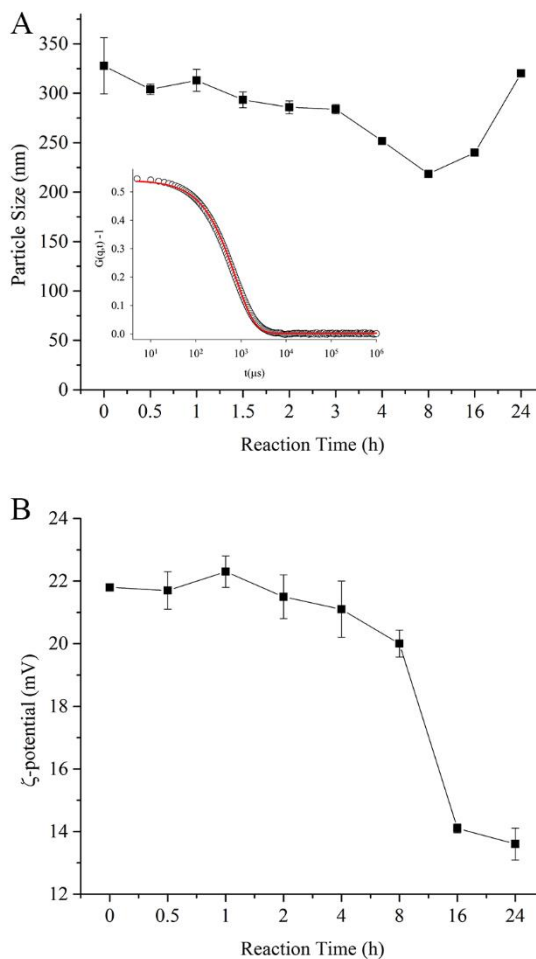


Figure 8-2. (A) Particle sizes (inset is an example of auto correlation function fitting of GCN crosslinked for 8h) and (B) ζ -potentials of GCNs with different crosslinking durations.

The surface hydrophilicity/hydrophobicity is critical in determining the type and stability of Pickering emulsions. Hydrophilic particles which are preferentially wetted by water phase stabilize O/W type Pickering emulsions while hydrophobic particles which are preferentially wetted by oil phase stabilize W/O type Pickering emulsions¹⁰⁴. The surface hydrophilicity/hydrophobicity of the GCNs were investigated by measuring their contact angles at the particle-air-water interface. As shown in Figure 8-3A, the contact angle did not change much at the first 8h, and then it became smaller as the crosslinking reaction extended, indicating that the GCNs became more hydrophilic

after 8h reaction. In another study, a similar phenomenon that the surface hydrophilicity increased with genipin crosslinking duration was also reported²⁵².

The oil-water (GCNs suspension) interfacial tensions were measured by the pendant drop method and the results are shown in Figure 8-3B. The surface tension between MCT and GCNs suspension almost remained consistent within first 8h reaction. The surface tension then increased dramatically when crosslinking reaction reached 16h and longer.

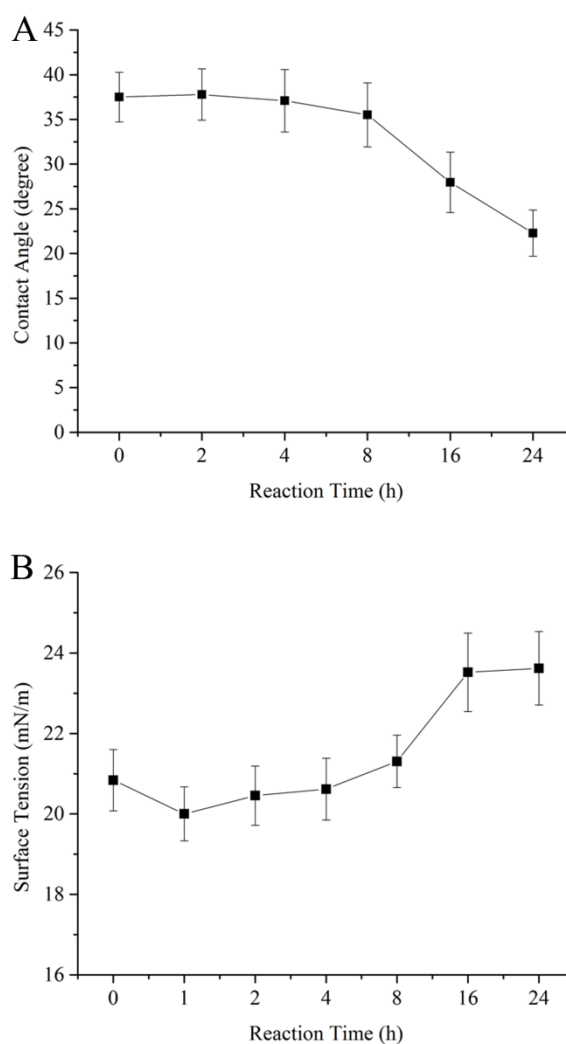


Figure 8-3. (A) Contact angles and (B) surface tensions of GCNs with different crosslinking durations

The morphologies of the GCNs with different crosslinking durations were monitored by the AFM. As shown in Figure 8-4, at the early crosslinking stage (0-8h), the GCNs were almost single spherical particles, and the particle size gradually decreased (Figure 8-4A-D), which is consistent with the particle size measurement results (Figure 8-2A). When the crosslinking reaction extended to 16h, paired particles were observed, which could be the dimers of the GCNs as described above. Large aggregates also appeared (Figure 8-4E). When the crosslinking reaction further extended to 24h, even larger aggregates were observed (Figure 8-4F).

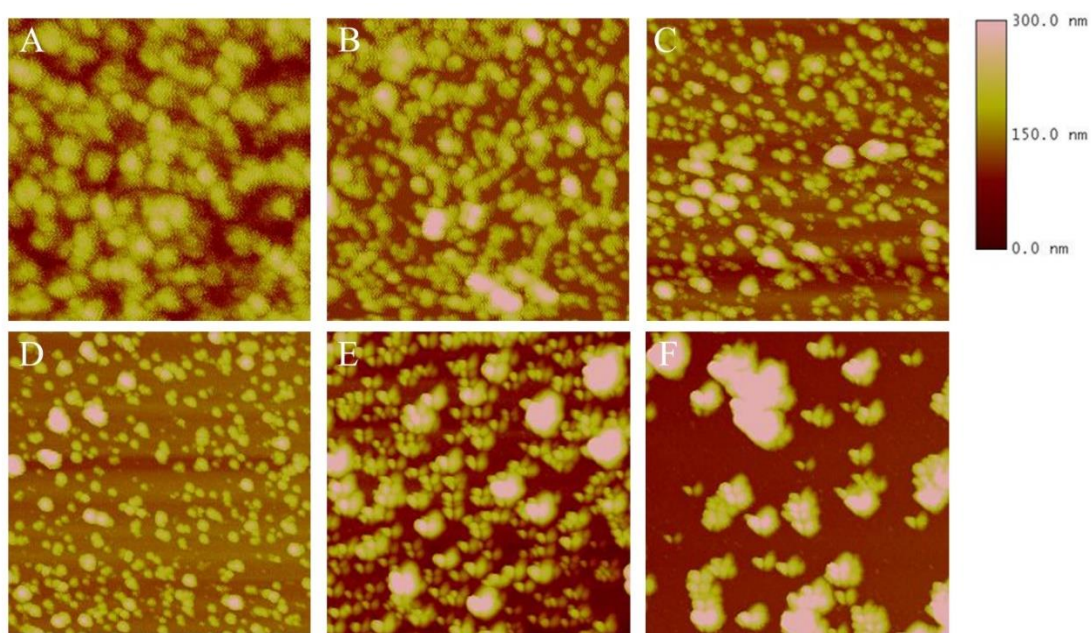


Figure 8-4. AFM height images of GCNs with (A) 0h, (B) 2h, (C) 4h, (D) 8h, (E) 16h, and (F) 24h reaction.

The microstructures of the GCNs were investigated by the USAXS and SAXS. The scattering curves of the GCNs with different crosslinking durations are shown in Figure 8-5A. The conformation of molecules in solution is usually described by the term fractal dimension α . The scattering intensity $I(q)$ of the molecule with fractal dimension α follows the power law $I(q) \sim q^{-\alpha}$. The USAXS and SAXS results show that the GCNs have hierarchical structures. The overall shape

of the GCNs which is reflected in the small q range ($q < 0.01 \text{ \AA}^{-1}$) was sphere and the surface of the GCNs became relatively rougher [$I(q) \sim q^{-3.88}$ to $I(q) \sim q^{-3.14}$] as the crosslinking reaction extended. The internal structures of the GCNs are reflected from the fractal dimensions at higher q range. A small shoulder presented in all the scattering curves at $q \approx 0.01 \text{ \AA}^{-1}$, corresponding to the length scale of 628 \AA in real space. At larger q , the scattering curves decayed in two distinct fractal ways. As the crosslinking duration increased, the transition position shifted from $q \sim 0.02 \text{ \AA}^{-1}$ to $q \sim 0.03 \text{ \AA}^{-1}$, corresponding to a distance decreased from 314 \AA to 209 \AA in real space, which could be related to the structural change of inner subunits. A small correlation peak at approximately 0.4 \AA^{-1} which corresponded to a distance about 16 \AA in real space was also observed when the crosslinking duration was longer than 16h.

The scattering curves were fitted by the Irena software package (Figure 8-5B solid lines) and the R_g of the GCNs were quantitatively calculated, which are listed in Table 8-1. Generally, the change of R_g follows the trend of change of the particle size of the GCNs (Figure 8-2A). The R_g initially decreased until 8h and longer crosslinking led to increase of R_g .

Table 8-1. Radius of gyration of the GCNs with different crosslinking durations

Crosslinking Duration (h)	R_g (\AA)
4	681 ± 11
8	641 ± 9
16	665 ± 9
24	692 ± 8

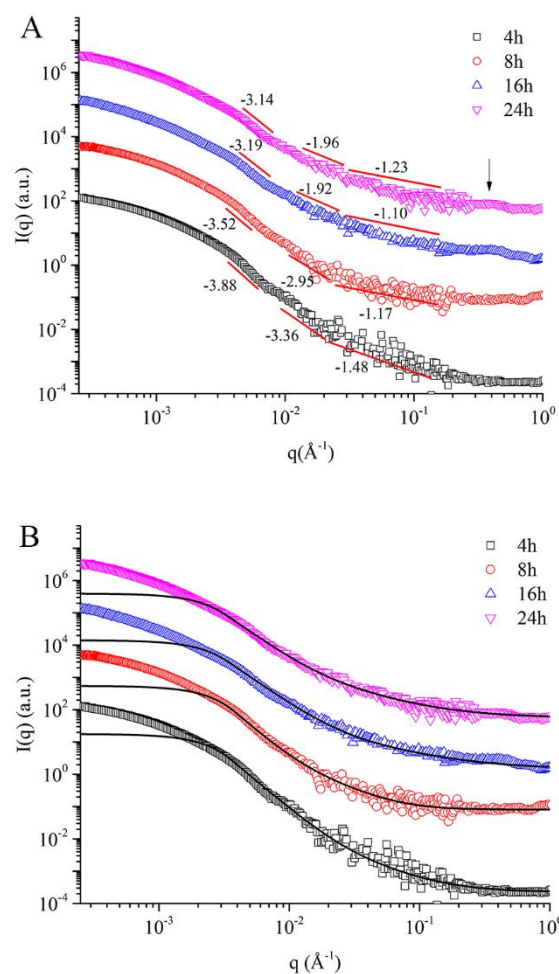


Figure 8-5. (A) Scattering profiles and (B) fitting (black solid line) of the GCNs with different crosslinking durations. The scattering intensities were vertically shifted for clear visualization.

8.4.3. Characterization of the GCNs Stabilized Pickering Emulsions

The effect of GCNs concentration on stabilization of Pickering emulsions was first investigated (oil fraction $\Phi=0.5$ w/w). Figure 8-6 shows the Pickering emulsions stabilized by GCNs with 4h crosslinking reaction. Pickering emulsions were formed at all the tested concentrations (0.05-0.25 wt%) and creaming was observed in all the emulsions. A thicker creaming layer was observed with increasing concentration of GCNs (Table 8-2). Similar phenomenon was observed in the emulsions stabilized by GCNs with longer crosslinking durations (8h, 16h, and 24h). However, after 16h and

24h reactions, 0.05 wt% GCNs cannot stabilize the Pickering emulsions (Figure 8-7), and the emulsion stabilized by 0.1 wt% GCNs with 24h reaction was very unstable after 24h storage. These results indicate that longer crosslinking reaction could reduce the capacity of GCNs as the Pickering stabilizer at low concentrations.

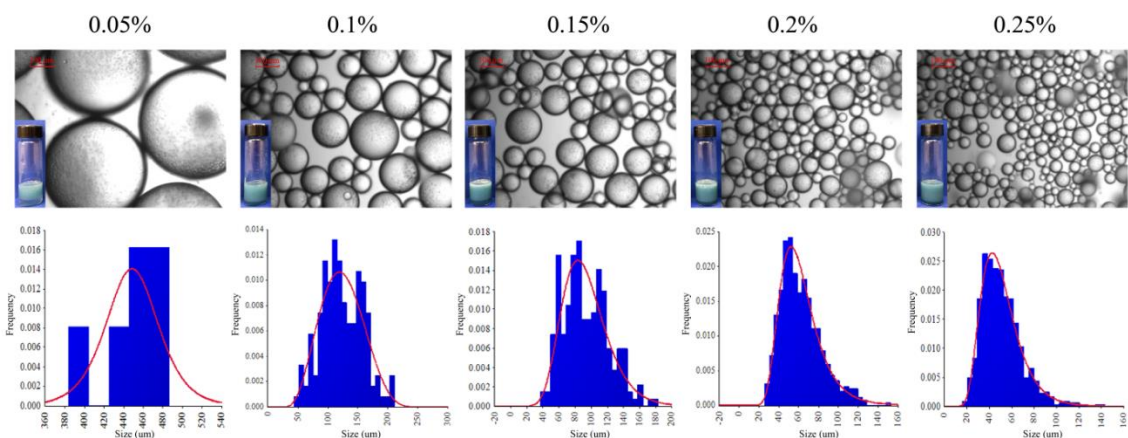


Figure 8-6. Macroscopic and microscopic images of Pickering emulsions ($\Phi=0.5$ w/w) stabilized by GCNs (4h reaction) and emulsion droplet size distribution fitting

The emulsion droplet sizes were measured by the ImageJ software for at least 500 measurements (except for the 0.05 wt% GCNs groups). The droplet sizes of Pickering emulsions ($\Phi=0.5$ w/w) stabilized by different concentrations of GCNs with different crosslinking durations are summarized in Figure 8-7. Generally, the droplet size of Pickering emulsions stabilized by GCNs with 4h and 8h reactions initially decreased dramatically as the concentration of GCNs increased from 0.05 wt% to 0.1 wt%. The emulsion droplet size further decreased as the GCNs concentration increased from 0.1 wt% to 0.2 wt% while the droplet size did not change much when the concentration of GCNs increased from 0.2 wt% to 0.25 wt%. Similar trend that increasing concentration of Pickering stabilizer reduced the emulsion droplet size until a specific concentration beyond which the emulsion droplet size remained almost consistent was observed in the Pickering emulsions stabilized by the CS-CPPs nanocomplexes. This phenomenon was also

reported in other literatures^{102, 106}. The decreased emulsion droplet size was attributed to increasing amount of available GCNs to cover the newly created oil-water interface. The emulsion droplet size also became more normally distributed and the distribution became narrower as GCNs concentration increased, indicating that the emulsion droplet size became more homogenous (Figure 8-6). When the GCNs with 16h and 24h reactions were investigated, the emulsion droplet sizes kept decreasing in the studied concentrations. It was also noticed that as the crosslinking duration increased, the size of Pickering emulsion stabilized by same concentration of GCNs increased accordingly (Figure 8-7). The reason could be that GCNs with longer crosslinking duration were more hydrophilic and they could cover smaller interfacial area.

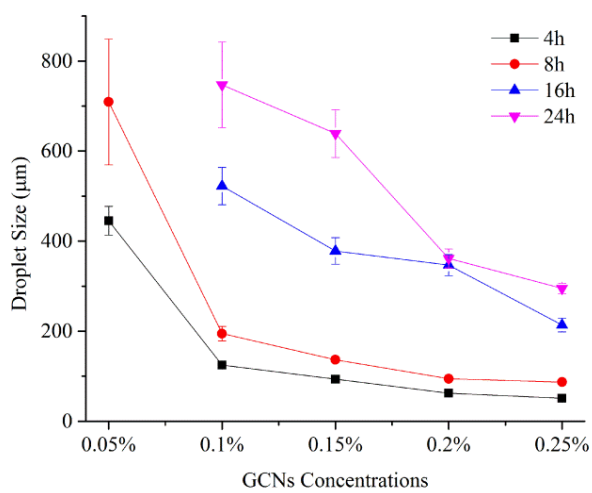


Figure 8-7. Droplet sizes of Pickering emulsions ($\Phi=0.5$ w/w) stabilized by GCNs with different crosslinking durations at different concentrations

The CI were calculated by eq. 8-1 and the values of CI of the Pickering emulsions ($\Phi=0.5$ w/w) stabilized by different concentrations of GCNs with different crosslinking durations are listed in Table 8-2. As the concentration of GCNs increased, the proportion of the serum layer decreased, indicating that the stability of these emulsions against creaming increased with the concentration of GCNs.

Table 8-2. Creaming indexes of Pickering emulsions ($\Phi=0.5$) stabilized by different concentrations of GCNs with different crosslinking durations

GCNs Concentration (wt%)	Creaming Index (%)			
	4h	8h	16h	24h
0.05	33.3	38.9	-	-
0.1	27.8	22.2	31.6	31.6
0.15	22.2	22.2	26.3	26.3
0.2	15.8	15.8	26.3	21.0
0.25	15.8	15.8	21.0	21.0

The fraction of oil that can be stabilized by GCNs was also characterized. The microscopic images of the Pickering emulsions ($\Phi=0.2-0.6$, w/w) stabilized by 0.2 wt% GCNs are shown in Figure 8-8. All these GCNs at 0.2 wt% concentration can stabilize at least $\Phi=0.6$ MCT. The emulsion droplet size increased with the oil fraction, which was due to fewer amounts of GCNs that were available to cover the oil-water interface. The CI of these emulsions are listed in Table 8-3. The thickness of the creaming layer increased with the fraction of oil. Creaming was almost inhibited in the emulsions stabilized by 0.2 wt% GCNs with 4h and 8h crosslinking reactions.

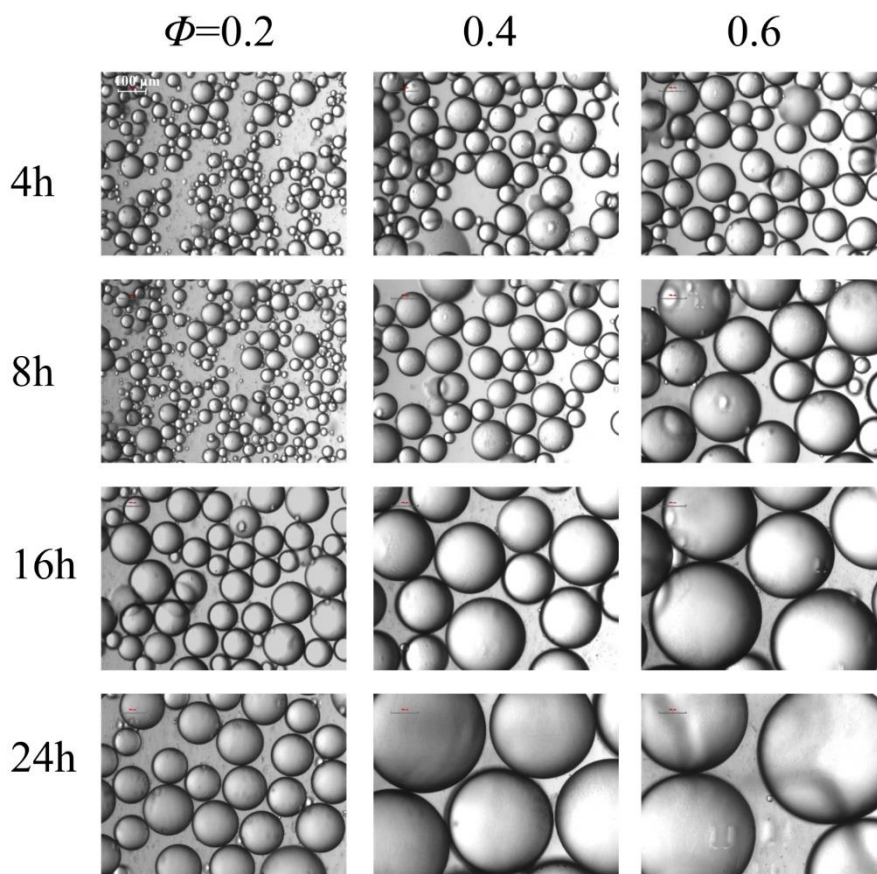


Figure 8-8. Microscopic images of Pickering emulsions containing different fractions of oil ($\Phi=0.2-0.6$ w/w) stabilized by 0.2 wt% GCNs with different crosslinking durations

Table 8-3. Creaming indexes of Pickering emulsions containing different fractions of oil (Φ) stabilized by 0.2 wt% GCNs with different crosslinking durations

Oil Fraction (Φ)	Creaming Index (%)			
	4h	8h	16h	24h
0.2	61.1	61.1	61.1	61.1
0.4	31.6	36.8	36.8	36.8
0.6	5.3	5.3	10.5	15.8

It was reported that the genipin crosslinked product was fluorescent²²⁷. The fluorescence emission spectrum of GCNs excited at 550 nm showed a peak at 650 nm (Figure 8-9 inset), which was red fluorescence. The fluorescence microscope was used to monitor the fluorescence of GCNs stabilized Pickering emulsion. The fluorescence images were taken by exciting either coumarin 6 (green fluorescence) or GCNs (red fluorescence) and fluorescence images were overlaid to identify the position of each phase. As shown in Figure 8-9, the red fluorescence was located at the edge of the emulsion droplets, indicating the GCNs were anchored at the oil-water interface. The green fluorescence was located inside the red fluorescence shell. These results demonstrate that the GCNs stabilized Pickering emulsion was the O/W type emulsion.

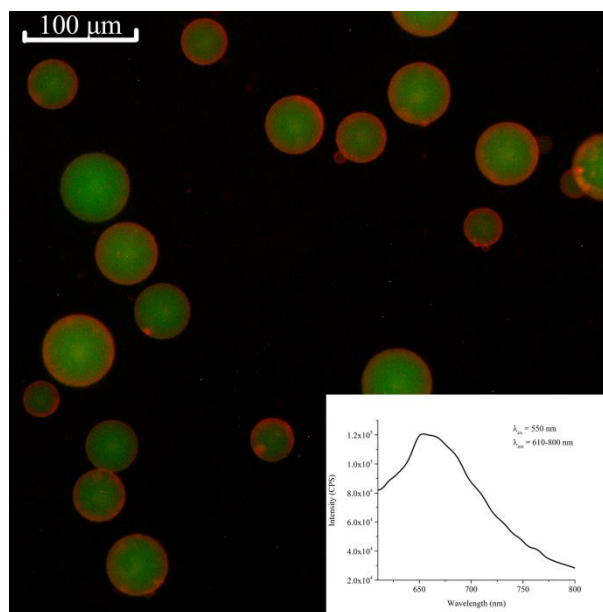


Figure 8-9. Fluorescence image of GCNs stabilized Pickering emulsion. Inset is the fluorescence emission spectrum of GCNs excited at 550 nm. Emission wavelength was recorded from 610-800 nm

The polysaccharide-protein/polypeptide complexes are susceptible to pH change in solution (section 1.1.2). The insoluble complexes only form at the pH range where polysaccharides and proteins/polypeptides carry opposite net charges. The droplet sizes of the CS-CPPs nanocomplexes

stabilized Pickering emulsions were smaller at pH 2 compared to those at higher pH after 24h storage (CHAPTER VII). This result could be resulted from disassembly of the nanocomplexes at pH 2. In the present study, the pH stability of the GCNs stabilized Pickering emulsions was investigated from pH 2 to pH 10, which covers the gastric pH, intestinal pH, and pH of most foods. As shown in Figure 8-10A, the droplet sizes of the emulsions ($\Phi=0.5$ w/w) stabilized by 0.25 wt% GCNs with different crosslinking durations were relatively consistent in the tested pH range, which means that the GCNs stabilized Pickering emulsions were stable against pH change.

Ionic strength is also an important factor that affects the associations between polysaccharides and proteins/polypeptides. It is well known that high concentration of NaCl can screen the charges on charged polysaccharides, proteins and polypeptides, and therefore dissociate the polysaccharide-protein/polypeptides complexes (section 1.1.2). The stability of the Pickering emulsions against ionic strength change was tested from 0 to 0.3 M NaCl. Their droplet sizes at these ionic strengths are shown in Figure 8-10B. Similar to the pH stability test, the tested ionic strengths did not change the droplet size of the Pickering emulsions ($\Phi=0.5$ w/w) stabilized by 0.25 wt% GCNs with different crosslinking durations. Altogether, both pH and ionic strength did not affect the stability of the GCNs stabilized Pickering emulsions. It is reasonable since the GCNs were crosslinked by covalent bonds, which are stable against pH and ionic strength changes.

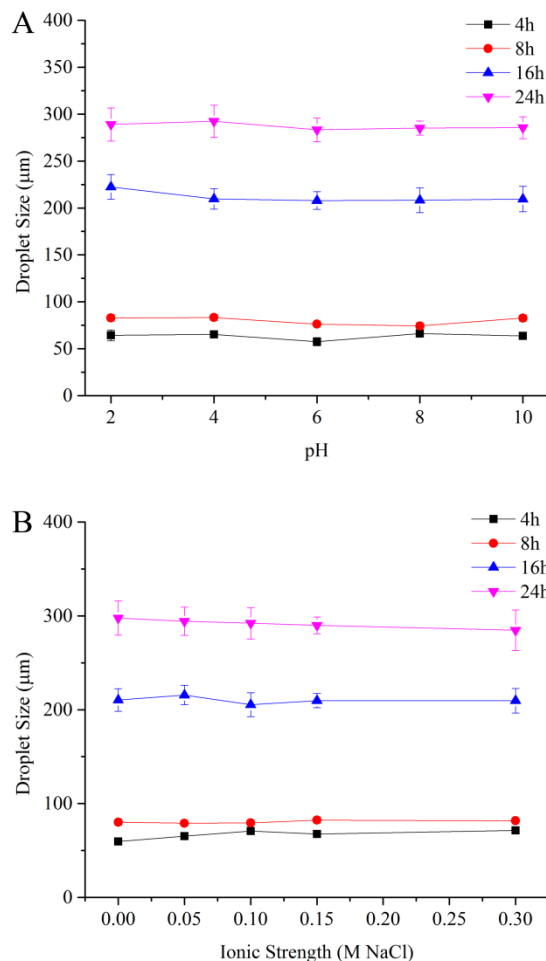


Figure 8-10. Droplet sizes of Pickering emulsions ($\Phi=0.5$ w/w) stabilized by 0.25 wt% GCNs with different crosslinking durations (4, 8, 16, 24h) after 24h storage at different (A) pH and (B) ionic strength

The oscillating frequency sweep tests of the Pickering emulsions stabilized by GCNs with different crosslinking durations were conducted at 1% strain, which was within the linear viscoelastic region of dynamic strain sweep test. The Pickering emulsions ($\Phi=0.5$ w/w) stabilized by 0.25 wt% GCNs with different crosslinking durations were compared. It was found that all these emulsions showed gel-like property as G' was consistently one order of magnitude higher than G'' (Figure 8-11A). The gel-like behavior could be resulted from formation of three-dimensional particle network. The emulsion stabilized by GCNs with longer crosslinking duration had lower G'

and G'' , indicating that GCNs with longer crosslinking duration may form weaker gel-like emulsion. The three-dimensional network broke down upon increasing the angular frequency as reflected by decreasing of complex viscosity (η^* , Figure 8-11B).

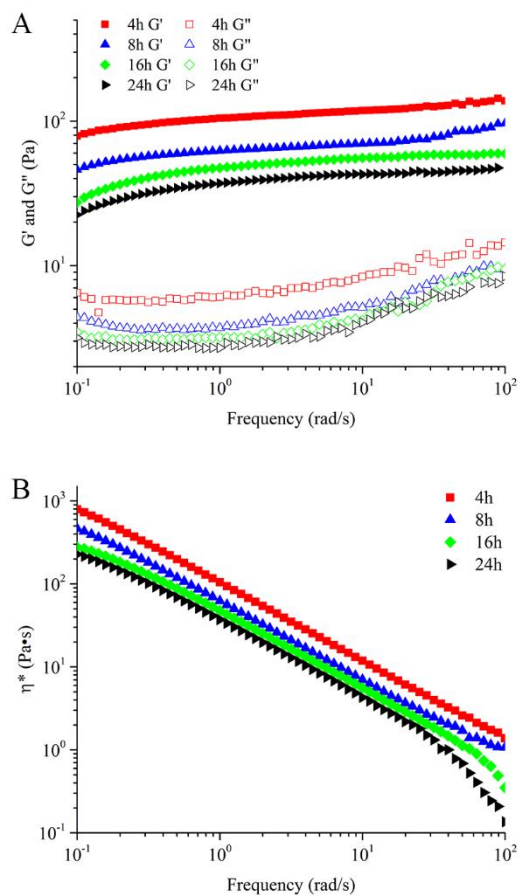


Figure 8-11. (A) Storage modulus G' , loss modulus G'' and (B) complex viscosity η^* of Pickering emulsions ($\Phi=0.5$ w/w) stabilized by 0.25 wt% GCNs with different crosslinking durations

8.5. Conclusions

In this chapter, the CS-CPPs nanocomplexes were crosslinked with genipin. The particle size of the GCNs initially decreased until 8h reaction, after which the particle size increased. ζ -potential of the GCNs decreased as the crosslinking duration increased, which could be attributed to loss of

the primary amine groups. It was also observed that as the crosslinking reaction went on, the GCNs became more hydrophilic and the surface tension between GCNs and MCT increased. After being anchored at the oil-water interface, the GCNs can stabilize O/W type Pickering emulsions and higher concentration of GNCs led to smaller emulsion droplet size and higher creaming stability. Higher fraction of MCT can also increase the creaming stability but it increased the emulsion droplet size. The droplet size of the Pickering emulsions was also affected by crosslinking duration. GCNs with longer crosslinking duration stabilized larger emulsion droplets. The GCNs stabilized Pickering emulsions were stable against pH and ionic strength changes. They showed gel-like behavior, and GCNs with shorter crosslinking duration can form stronger gel-like emulsions.

**CHAPTER IX. STABILIZATION OF PICKERING EMULSIONS
BY THE GENIPIN CROSSLINKED CHITOSAN-
CASEINOPHOSPHOPEPTIDES NANOCOMPLEXES: IMPACTS
OF CROSSLINKER CONCENTRATION AND CROSSLINKING
TEMPERATURE**

As of submission of this dissertation, the work in this chapter has been written as a research paper in the title of “Impacts of Crosslinking Temperature and Crosslinker Concentration on Stabilization of Gel-Like Pickering Emulsions by Crosslinked Polysaccharide-Polypeptides Nanocomplexes” which is ready for submission.

9.1. Abstract

The CS-CPPs nanocomplexes were covalently crosslinked by genipin at different conditions (0.1 mg/mL, 0.5 mg/mL, and 1 mg/mL genipin at 30°C, 40°C, and 50°C for 4h). These GCNs were spherical particles varied in size, ζ -potential, and surface hydrophilicity. The GCNs were applied to stabilize Pickering emulsions with MCT as the oil phase. Most of the GCNs can stabilize Pickering emulsions at the concentration as low as 0.05 wt%. There was a size reduction of the Pickering emulsions as the GCNs concentration increased. The sizes of the Pickering emulsions were almost correlated to the size of GCNs. These emulsions were O/W type in a wide oil weight fraction range ($\Phi = 0.3-0.7$, w/w). They showed gel-like behavior. The GCNs crosslinked with higher concentration of genipin could stabilize Pickering emulsions with higher storage modulus, loss modulus, and complex viscosity, while those crosslinked at higher temperature stabilized Pickering emulsions with lower storage modulus, loss modulus, and complex viscosity.

9.2. Introduction

In CHAPTER VII, the CS-CPPs nanocomplexes have been applied to stabilize Pickering emulsions. However, these Pickering emulsions showed relatively low stabilities at low pH because the interactions involved in formation of the CS-CPPs nanocomplexes were weak interactions, such as electrostatic interaction and hydrogen bond. They were susceptible to pH and ionic strength changes. The CS-CPPs nanocomplexes were crosslinked by a natural crosslinker genipin. Genipin can react with the primary amine groups in pH-dependent ways²³². Genipin is less toxic than other commonly used synthetic crosslinkers such as glutaraldehyde, formaldehyde, and epoxy compounds²⁵³. The Pickering emulsions stabilized by the GCNs showed outstanding stabilities against pH and ionic strength changes.

To further understand how is the characters of Pickering emulsions affected by the crosslinking reaction, in this chapter, the impacts of crosslinking parameters, *i.e.* genipin concentration and crosslinking temperature on the ability of the GCNs as the Pickering stabilizer, as well as the physical properties of the resulting Pickering emulsions were systematically investigated

9.3. Materials and Methods

9.3.1. Materials

CS was purchased from Kunpoong Bio. Co., Ltd. (South Korea) and used without further treatments. CPPs was purchased from Greencream Biotechnology Co., Ltd. (Guangzhou, China). Neobee® 1053 MCT was provided by Stepan Company (IL, USA). Genipin (purity > 98%) was purchased from Wako Pure Chemical Industries, Ltd. (VA, USA). Coumarin 6 was purchased from Sigma-Aldrich (MO, USA). Milli-Q water was used in all the experiments.

9.3.2. Preparation and Characterization of the GCNs

CS was dissolved in 1% acetic acid (containing 10 mM NaCl) at 5 mg/mL and the pH was adjusted to pH 6 after CS was fully dissolved. CPPs was dissolved in Milli-Q water (containing 10

mM NaCl) at 5 mg/mL and its pH was also adjusted to pH 6. To crosslink the CS-CPPs nanocomplexes, genipin was premixed with CS solution for 10 min. Equal volume of CPPs solution was then added dropwise into the CS/genipin solution during magnetic stirring. The concentrations of genipin were 0.1 mg/mL (GCNs1), 0.5 mg/mL (GCNs5), and 1 mg/mL (GCNs10) in the system. The crosslinking reactions were carried out at 30°C, 40°C, and 50°C for 4h. The GCNs were subjected to analysis immediately after preparation.

The particle size of the GCNs was calculated from the intensity-intensity auto-correlation function $G(q,t)^{229}$ obtained from a 90Plus Particle Size Analyzer equipped with a Brookhaven BI-9000AT digital correlator (Brookhaven Instruments Corporation, NY, USA). The measurements were performed at a fixed scattering angle of 90°.

The electrophoretic mobility of the GCNs was measured by a Nano ZS Zetasizer (Malvern Instruments Ltd., MA, USA). The ζ -potential was calculated by the Smoluchowski equation. The GCNs were diluted 1:5 with 10 mM NaCl solution (pH 6) for measurements, which were triplicated at 25°C.

The contact angles were measured by a VCA-Optima XE Dynamic Contact Angle Analyzer (AST Products, Inc., MA, USA). GCNs were dripped onto pre-cleaned glass slides and dried in a vacuum oven before measuring. The images were captured by a CCD camera immediately after a drop of Milli-Q water (2 μ L) was deposited onto the GCNs film surface. The contact angle was determined by the software associated with the analyzer. At least 50 measurements were conducted and averaged for each sample.

A Nanoscope IIIa Multi-Mode AFM (Veeco Instruments Inc., CA, USA) was used to monitor the morphology of the GCNs with tapping mode. The GCNs were diluted 1:50 with 10 mM NaCl (pH 6) and added onto the surface of pre-cleaned mica slides. After 1h, the mica slides were rinsed with Milli-Q water and dried with N₂ for analyzing.

9.3.3. Preparation and Characterization of the GCNs Stabilized Pickering Emulsions

The Pickering emulsions were prepared by mixing MCT with GCNs at different weight ratios by high-speed homogenizer (T25 digital ULTRA-TURRAX®, IKA Works Inc., USA) at 12,000 rpm for 1 min. The Pickering emulsions were kept at ambient condition for 24h before analysis. The fluorescence labeled Pickering emulsions were prepared by homogenizing GCNs with coumarin 6 pre-stained MCT at same condition.

The CI of the Pickering emulsions was calculated by eq. 8-1 described as

$$CI(\%) = \frac{H_s}{H_t} \times 100\%$$

where H_t and H_s are the heights of total emulsion and bottom serum layer, respectively.

The microscopic images of the Pickering emulsions were observed by a Nikon TE-2000-U inverted fluorescence microscope equipped with a CCD camera (Retiga Exi, Q-imaging). To observe the fluorescence labeled Pickering emulsions, the light was filtered through the bandpass filters, which yielded the excitation wavelengths of 488 ± 10 nm for coumarin 6 and 550 ± 10 nm for GCNs. The fluorescence images were processed by the SimplePCI C-Imaging software (Compix, Inc., PA, USA) and the images were overlaid by the ImageJ software. The sizes of the Pickering emulsions were measured by the ImageJ software. At least 500 measurements were conducted for each emulsion sample. The size distribution fittings were performed on the @Risk software (version 7, Palisade Corporation, NY, USA).

The rheological properties of the Pickering emulsions ($\Phi=0.7$, w/w) stabilized by 0.15 wt% GCNs were studied with a Discovery HR-2 Hybrid Rheometer (TA Instruments, DE, USA) with 25 mm stainless-steel parallel plate geometry and a temperature-controlled stainless-steel Peltier plate. Dynamic strain sweep tests from 0.1% to 100% strain at 0.1 Hz frequency were carried out to determine the linear viscoelastic region before each dynamic frequency sweep test, which

adopted the strain value of 1% and the angular frequency ω from 0.1 to 100 rad/s with 10 data points per decade. All the measurements were carried out at 25°C.

9.4. Results and Discussion

9.4.1. Characterization of the GCNs

The colloidal solid particles can irreversibly adsorb at the oil-water interface because the attachment energy of a particle to the interface is usually thousand times higher than the kinetic energy of Brownian motion²⁵⁴. The energy required for a particle to detach from the oil-water interface is described by eq. 1-4 as

$$E = \gamma\pi R^2(1 - |\cos \theta|)^2$$

where γ is the oil-water interfacial tension; R is the radius of the particle; θ is the oil-water-particle three phase contact angle. Hence, multiple factors are involved in regulating the ability of a particle as the Pickering stabilizer.

The size of Pickering stabilizer can affect the size of resulting Pickering emulsion¹⁰¹. The particle sizes of the GCNs were calculated by fitting the auto-correlation functions (Figure 9-1 inset) obtained from dynamic light scattering. The results are given in Figure 9-1. At 30°C the size of the GCNs decreased slightly from 306.8 nm to 271.4 nm as the genipin concentration increased from 0.1 mg/mL to 1 mg/mL. Genipin can covalently crosslink the CS-CPPs nanocomplexes by reacting with the primary amine groups on both CS and CPPs. Therefore, higher concentration of genipin resulted in higher degree of crosslinking, which yielded more compact structures. At 40°C the sizes of the nanocomplexes crosslinked by 0.1-0.5 mg/mL genipin were smaller than the nanocomplexes crosslinked by corresponding concentration of genipin at 30°C because higher temperature promoted the crosslinking reaction. However, when crosslinked by 1 mg/mL genipin, the size of GCNs increased dramatically since strong crosslinking condition (high concentration of genipin

and high temperature) could accelerate the crosslinking reaction to the stage where GCNs undergo oligomerization^{232, 249}. At 50°C only 0.5 mg/mL genipin was required to significantly increase the size of GCNs. Further increasing the genipin concentration to 1 mg/mL resulted in visible large aggregates which was beyond the measurable size range of the dynamic light scattering.

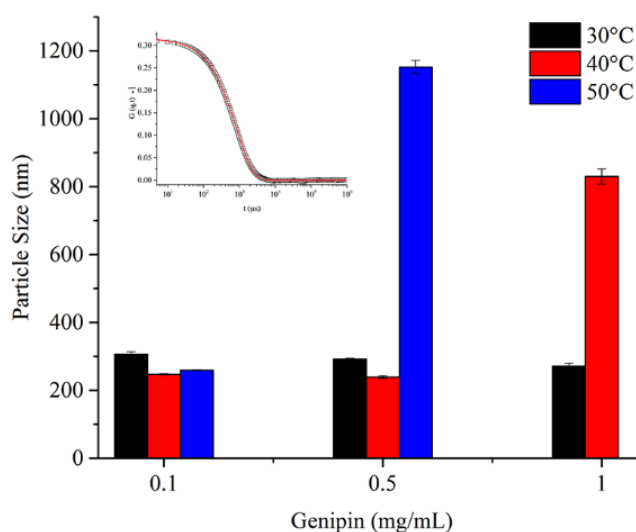


Figure 9-1. Particle sizes of the CS-CPPs nanocomplexes crosslinked by 0.1 mg/mL, 0.5 mg/mL, and 1 mg/mL genipin at 30°C, 40°C, and 50°C for 4h. Inset is the fitting (red line) of the auto-correlation function of the CS-CPPs nanocomplexes crosslinked by 0.1 mg/mL genipin at 40°C.

Surface charge of the Pickering stabilizer is an important factor for the stability of Pickering emulsions. The charged particles at the oil-water interface can provide electrostatic repulsion against coalescence of the emulsion droplets. The ζ -potentials of the GCNs are presented in Figure 9-2. Generally, high temperature and high concentration of genipin facilitated decrease of ζ -potential. Genipin can react with the primary amine groups on both CS and CPPs, which carried positive charges at the tested condition (pH 6, 10 mM NaCl). Therefore, strong reaction conditions favored loss of the positive charges.

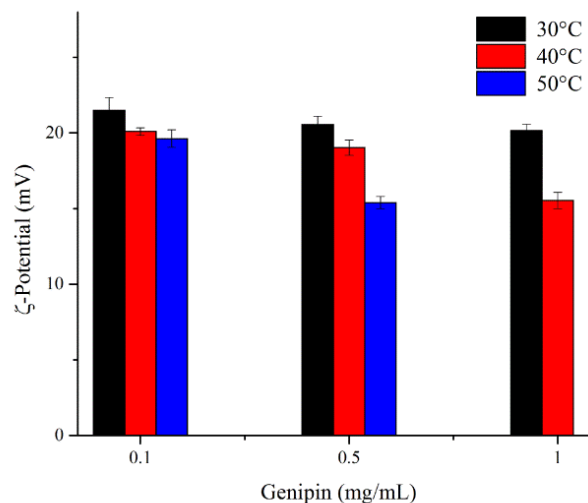


Figure 9-2. ζ -potentials of the CS-CPPs nanocomplexes crosslinked by 0.1 mg/mL, 0.5 mg/mL, and 1 mg/mL genipin at 30°C, 40°C, and 50°C for 4h.

The type of Pickering emulsions can be predicted by the wettability of the Pickering stabilizer. The Particles at the oil-water interface lead to bending of the interface in the direction of the phase where the particles have less wettability²⁵⁴. If the particles are preferentially wetted by the water phase, they stabilize the O/W Pickering emulsion. On the contrary, if the particles are preferentially wetted by the oil phase, they stabilize the W/O Pickering emulsion. The contact angles of the GCNs were measured which can reflect their wettability. As shown in Figure 9-3, the contact angles were smaller than 90°, which means they were more preferentially wetted by water. Theoretically these GCNs should stabilize O/W type Pickering emulsions, as it shall be confirmed later by fluorescence labeling. Crosslinking at 50°C notably lowered the contact angles, rendering them more hydrophilic. As reported in CHAPTER VIII, GCNs with longer crosslinking duration had lower contact angle. Therefore, it was speculated that higher extent of crosslinking resulted in more hydrophilic GCNs. Similar result was reported in reference²⁵³.

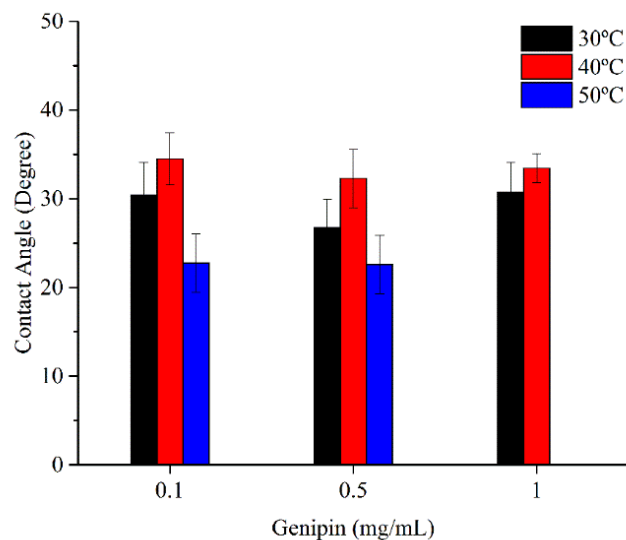


Figure 9-3. Contact angles of Milli-Q water on GCNs film.

The shape of the Pickering stabilizer can significantly affect its interfacial characteristics²⁵⁴ and the properties of the Pickering emulsions²⁵⁵. The morphologies of the GCNs monitored by AFM are given in Figure 9-4. Basically, these GCNs existed as globular particles. Large aggregates were observed when the genipin concentration was high (Figure 9-4C) and temperature was high (Figure 9-4F), which is consistent with the size measurements (Figure 9-1).

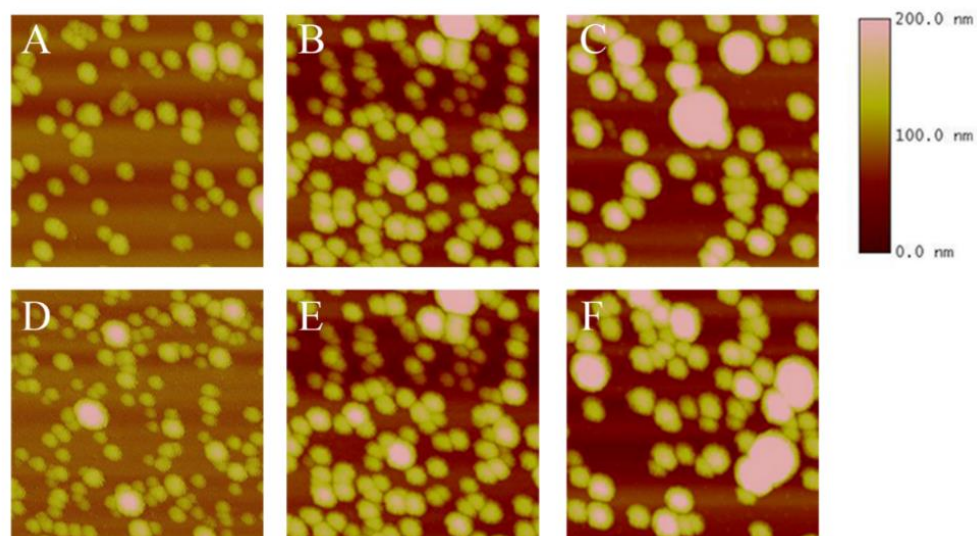


Figure 9-4. AFM images of (A) GCNs1, (B) GCNs5, and (C) GCNs10 crosslinked at 40°C for 4h, and GCNs5 crosslinked at (D) 30°C, (E) 40°C, and (F) 50°C for 4h.

9.4.2. Characterization of the Pickering Emulsions

The stability of Pickering emulsions could be controlled by the oil-water interfacial coverage, which is associated with the concentration of the Pickering stabilizers⁹⁶. Different concentrations of GCNs (0.05 wt%-0.25 wt%) were firstly applied to stabilize Pickering emulsions at a fixed oil weight fraction ($\Phi=0.5$, w/w). Most of the GCNs can stabilize Pickering emulsions at the concentration as low as 0.05 wt% except for those crosslinked at weak conditions (low genipin concentration and low temperature, *i.e.* GCNs1 and GCNs5 crosslinked at 30°C) and strong conditions (high genipin concentration and high temperature, *i.e.* GCNs10 crosslinked at 40°C, and GCNs5 crosslinked at 50°C) (Figure 9-5). Although creaming occurred in all the Pickering emulsions, the creaming index decreased as the GCNs concentration increased (Table 9-1).

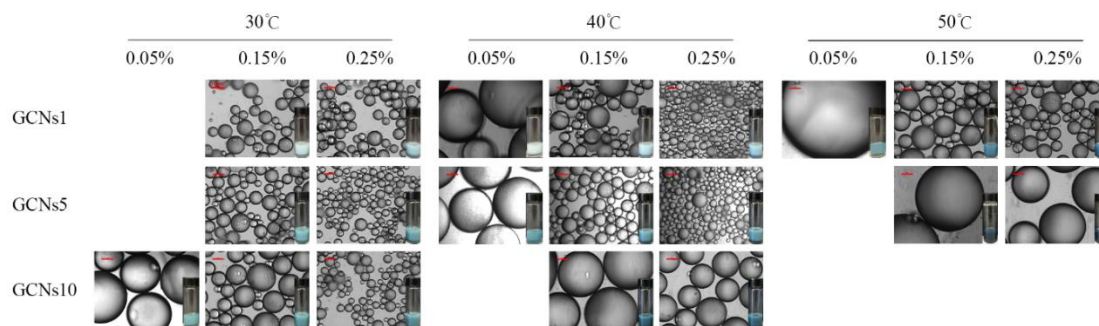


Figure 9-5. Macro- and micro-scopic images of Pickering emulsions ($\Phi=0.5$, w/w) stabilized by 0.05 wt%- 0.25 wt% of GCNs. The scale is 100 μm .

Table 9-1. Creaming indexes (%) of the Pickering emulsions ($\Phi=0.5$, w/w) stabilized by 0.05 wt%-0.25 wt% of GCNs

	30°C					40°C					50°C				
	0.05%	0.1%	0.15%	0.2%	0.25%	0.05%	0.1%	0.15%	0.2%	0.25%	0.05%	0.1%	0.15%	0.2%	0.25%
GCNs1	N/A	27.8	27.8	27.8	22.2	27.8	22.2	21.0	21.0	16.7	38.9	33.3	26.3	26.3	26.3
GCNs5	N/A	27.8	22.2	22.2	16.7	27.8	21.6	18.4	16.7	16.7	N/A	31.6	27.8	26.3	22.2
GCNs10	33.3	27.8	26.3	17.6	17.6	N/A	27.0	26.3	21.0	16.2	NA	N/A	N/A	N/A	N/A

N/A: not applicable, Pickering emulsion did not form

The sizes of these Pickering emulsions were quantitatively measured. Generally, as the concentration of GCNs increased, the emulsion droplet size initially decreased dramatically and then the size slightly decreased (Table 9-2). The size reduction is because more GCNs were available to cover the oil-water interface. These emulsions show narrower Size distribution as the GCNs concentration increased (Figure 9-6A-C). The effect of genipin concentration on the size of Pickering emulsions was firstly compared. When crosslinked at 30°C and 40°C, GCNs5 could stabilize slightly smaller Pickering emulsions than GCNs1 at same concentrations. These emulsions exhibited similar size distribution width (Figure 9-6D-E). Nevertheless, GCNs10 crosslinked at these temperatures stabilized larger emulsions which had wider size distribution (Figure 9-6F). Dissimilarly, the emulsions stabilized by GCNs5 crosslinked at 50°C had much larger sizes and wider size distribution than those stabilized by GCNs1. When considering the effect of crosslinking temperature, the Pickering emulsions stabilized by GCNs1 and GCNs5 crosslinked at 40°C were slightly smaller than those crosslinked at 30°C, whereas they had similar size distribution width (Figure 9-6G-H). The droplet size and size distribution (Figure 9-6I) width increased dramatically when stabilized by these GCNs crosslinked at 50°C. GCNs10 crosslinked at 40°C could stabilize much larger Pickering emulsions which had wider distribution than those crosslinked at 30°C. The sizes of the Pickering emulsions were basically positively related to the sizes of GCNs. The only exception *i.e.* emulsion stabilized by GCNs1 crosslinked at 50°C could be resulted from the high surface hydrophilicity²⁵⁶.

Table 9-2. Droplet sizes (μm) of the Pickering emulsions ($\Phi=0.5$, w/w) stabilized by 0.05 wt%-0.25 wt% of GCNs

	30°C					40°C				
	0.05%	0.1%	0.15%	0.2%	0.25%	0.05%	0.1%	0.15%	0.2%	0.25%
GCNs1	N/A	159.1±27.0	106.8±2.9	96.2±3.1	87.5±3.3	443.2±167.4	152.7±19.8	101.6±5.7	67.7±2.9	56.8±2.9
GCNs5	N/A	158.2±9.6	103.7±7.9	76.2±5.2	63.0±2.5	445.3±32.0	124.7±7.8	93.6±5.7	62.5±2.9	51.1±3.8
GCNs10	377.1±43.4	299.2±32.0	166.7±38.6	83.1±3.3	71.1±5.5	N/A	848.6±115.1	389.1±16.2	292.4±26.6	216.9±10.9

Table 9-2. Droplet sizes (μm) of the Pickering emulsions ($\Phi=0.5$, w/w) stabilized by 0.05%-0.25% of GCNs (continue)

	50°C				
	0.05%	0.1%	0.15%	0.2%	0.25%
GCNs1	>1000	225.4±31.7	150.9±9.9	109.1±6.9	97.9±6.5
GCNs5	N/A	909.2±50.6	682.2±79.3	494.5±62.8	335.1±16.2
GCNs10	N/A	N/A	N/A	N/A	N/A

N/A: not applicable, Pickering emulsion did not form

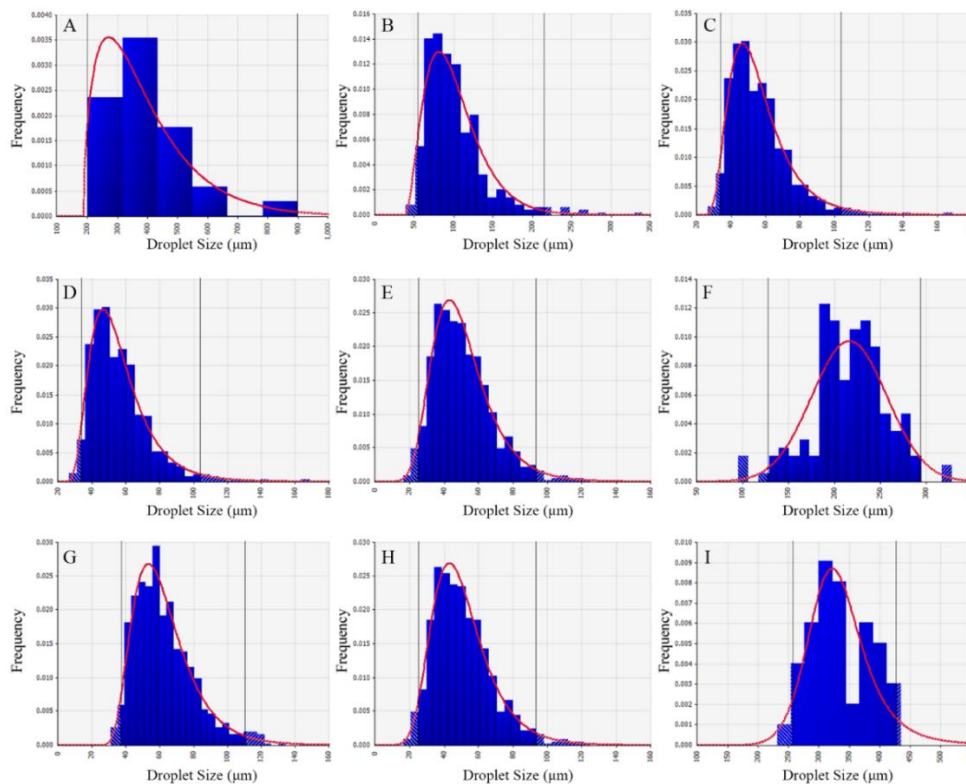


Figure 9-6. Size distribution fitting of the Pickering emulsions stabilized by (A) 0.05 wt%, (B) 0.15 wt%, and (C) 0.25 wt% of GCNs1 crosslinked at 40°C; 0.25 wt% (D) GCNs 1, (E) GCNs5, and (F) GCNs10 crosslinked at 40°C; and 0.25 wt% GCNs5 crosslinked at (G) 30°C, (H) 40°C, and (I) 50°C.

We recall the results that were reported in CHAPTER VIII and present the size of the Pickering emulsions ($\Phi = 0.5$, w/w) stabilized by 0.25 wt% GCNs crosslinked at different genipin concentrations, temperatures, and crosslinking durations in Figure 9-7. It can be concluded that generally GCNs crosslinked at stronger crosslinking conditions (higher temperature, higher concentration of genipin, longer crosslinking duration) could stabilize larger size and more heterogeneous Pickering emulsions.

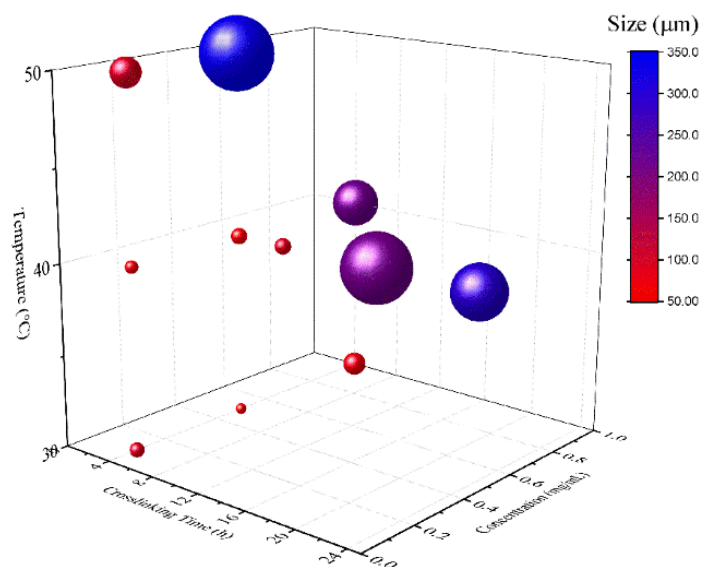


Figure 9-7. Droplet sizes of Pickering emulsions ($\Phi = 0.5$, w/w) stabilized by 0.25 wt% GCNs crosslinked at different conditions. The diameter of the balls represents their relative size distribution.

The macro- and micro-scopic images of the Pickering emulsions containing different oil fractions ($\Phi = 0.3-0.7$, w/w) stabilized by a fixed concentration (0.15 wt%) of GCNs are displayed in Figure 9-8. These GCNs exhibited good ability to stabilize high volume of oil. Except for GCNs5 crosslinked at 50°C which was relatively larger and more hydrophilic than other GCNs, all the nanocomplexes crosslinked at different conditions can stabilize at least $\Phi=0.7$ MCT at 0.15 wt% concentration. The Pickering emulsions containing $\Phi=0.7$ MCT can almost be regarded as the high

internal phase emulsion, which is defined as the emulsion whose volume fraction of internal phase is larger than 0.74.

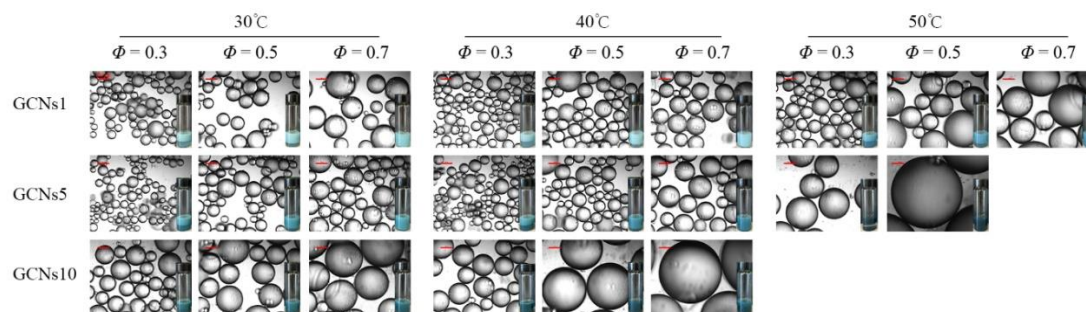


Figure 9-8. Macro- and micro-scopic images of Pickering emulsions ($\Phi = 0.3-0.7$ w/w) stabilized by 0.15 wt% GCNs. The scale is 100 μm .

Although creaming was observed at $\Phi=0.3$ and 0.5, the creaming index decreased as the oil fraction increased. Creaming was completely inhibited at $\Phi=0.7$ (Table 9-3). The sizes of these Pickering emulsions increased with the oil fraction (Table 9-4) since there were relatively less amount of GCNs that could cover the oil-water interface. The Pickering emulsions containing higher oil fraction also display wider size distribution (Figure 9-9).

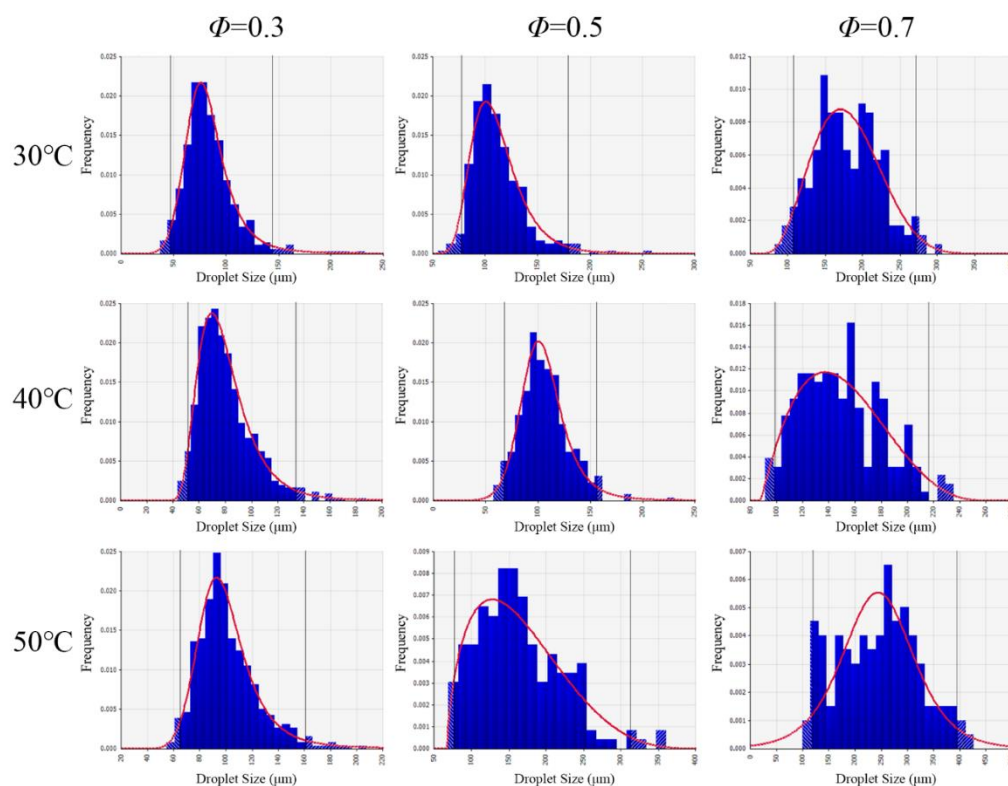


Figure 9-9. Size distribution fitting of the Pickering emulsions containing different oil fractions ($\Phi = 0.3$ - 0.7 w/w) stabilized by 0.15 wt% GCNs1.

Table 9-3. Creaming indexes (%) of the Pickering emulsions containing different oil fractions

	30°C			40°C			50°C		
	$\Phi=0.3$	$\Phi=0.5$	$\Phi=0.7$	$\Phi=0.3$	$\Phi=0.5$	$\Phi=0.7$	$\Phi=0.3$	$\Phi=0.5$	$\Phi=0.7$
GCNs1	47.4	27.8	0	39.5	21.0	0	47.4	26.3	0
GCNs5	42.1	22.2	0	42.1	18.4	0	52.6	27.8	N/A
GCNs10	42.1	26.3	0	52.8	26.3	0	N/A	N/A	N/A

N/A: not applicable, Pickering emulsion did not form

Table 9-4. Droplet size (μm) of the Pickering emulsions containing different oil fractions

	30°C			40°C			50°C		
	$\Phi=0.3$	$\Phi=0.5$	$\Phi=0.7$	$\Phi=0.3$	$\Phi=0.5$	$\Phi=0.7$	$\Phi=0.3$	$\Phi=0.5$	$\Phi=0.7$
GCNs1	84.8±5.4	111.5±4.4	182.7±16.4	80.6±3.4	106.7±5.5	149.7±6.0	101.7±4.4	156.4±18.0	246.9±22.1
GCNs5	67.3±5.3	101.0±5.6	133.5±7.5	68.7±2.4	97.6±8.2	169.3±19.0	256.8±17.8	694.0±33.4	N/A
GCNs10	130.2±6.7	173.9±16.2	291.0±88.8	150.6±41.9	393.8±46.6	598.2±173.9	N/A	N/A	N/A

N/A: not applicable, Pickering emulsion did not form

In some Pickering emulsions, phase inversion occurred when the oil to water ratio changed²⁵⁷. To test the type of the GCNs stabilized Pickering emulsions at different oil fractions, MCT was stained with coumarin 6, which emits green fluorescence. GCNs was intrinsically fluorescent. The GCNs stabilized Pickering emulsions were excited at 488 nm and 550 nm to excite coumarin 6-labeled MCT and GCNs, respectively. The fluorescence images were overlaid and shown in Figure 9-10. The green fluorescence was located inside the red fluorescence (GCNs) edge, which means the GCNs stabilized Pickering emulsions were O/W type emulsions. Phase inversion did not occur at higher oil fractions ($\Phi=0.5$ and 0.7 , data not show). These Pickering emulsions remained as the O/W type in all the tested oil to water ratios.

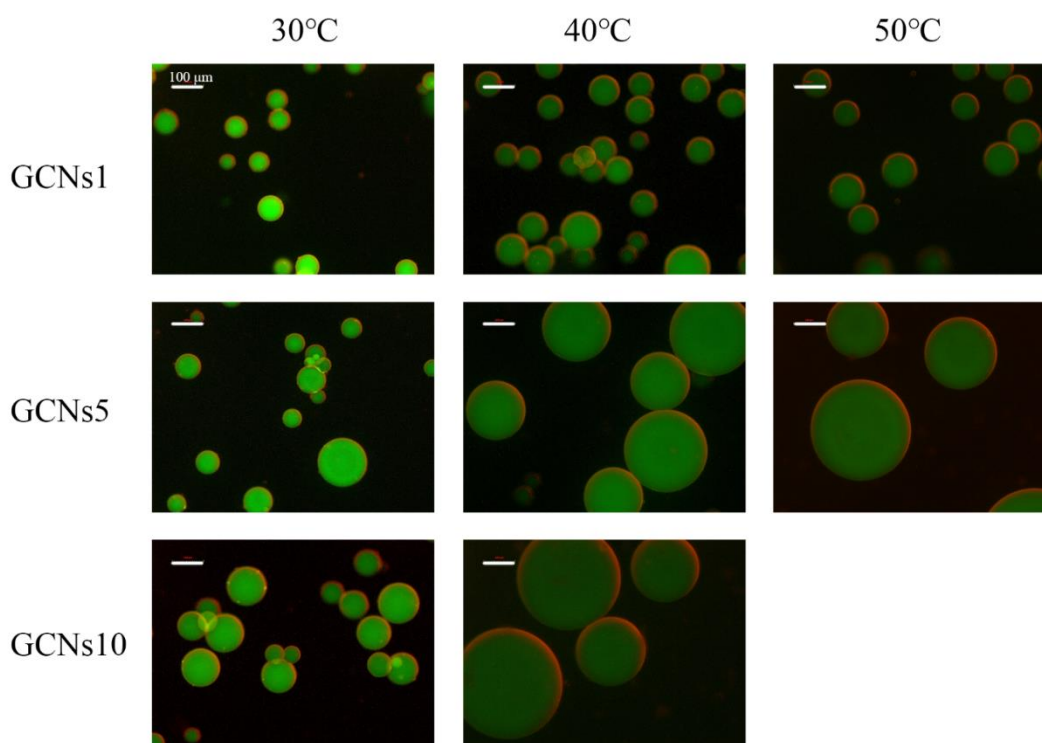


Figure 9-10. Microscopic images of the fluorescence labeled Pickering emulsions ($\Phi=0.3$, w/w) stabilized by 0.15 wt% GCNs. The green fluorescence is the coumarin 6 labeled MCT. The red fluorescence is the GCNs. The scale is 100 μm .

The Pickering emulsions containing $\Phi=0.7$ MCT were subjected to dynamic frequency sweep rheological measurement. The storage modulus G' was almost one order of magnitude higher than the loss modulus G'' over the whole frequency range and both G' and G'' were nearly frequency-independent in all the emulsions (Figure 9-11A-C), indicating these Pickering emulsions behaved like gel. This gel-like property was originated from existence of three-dimensional network in the Pickering emulsions. Possible explanations of this three-dimensional network could be partially bridging between emulsion droplets²⁵⁸ or depletion flocculation¹⁰⁶. When considering the impacts of genipin concentration and crosslinking temperature, they affect G' and G'' in opposite way. When considering the effect of genipin concentration, GCNs crosslinked by higher concentration of genipin slightly increased the magnitudes of both G' and G'' . When considering the effect of crosslinking temperatures, GCNs crosslinked at higher temperatures reduced the magnitudes of both G' and G'' .

Similar as the behaviors of G' and G'' , the complex viscosity was also higher for the Pickering emulsions which were stabilized by GCNs crosslinked by higher concentration of genipin. Higher crosslinking temperature could also decrease the viscosity of the emulsions (Figure 9-11D-F).

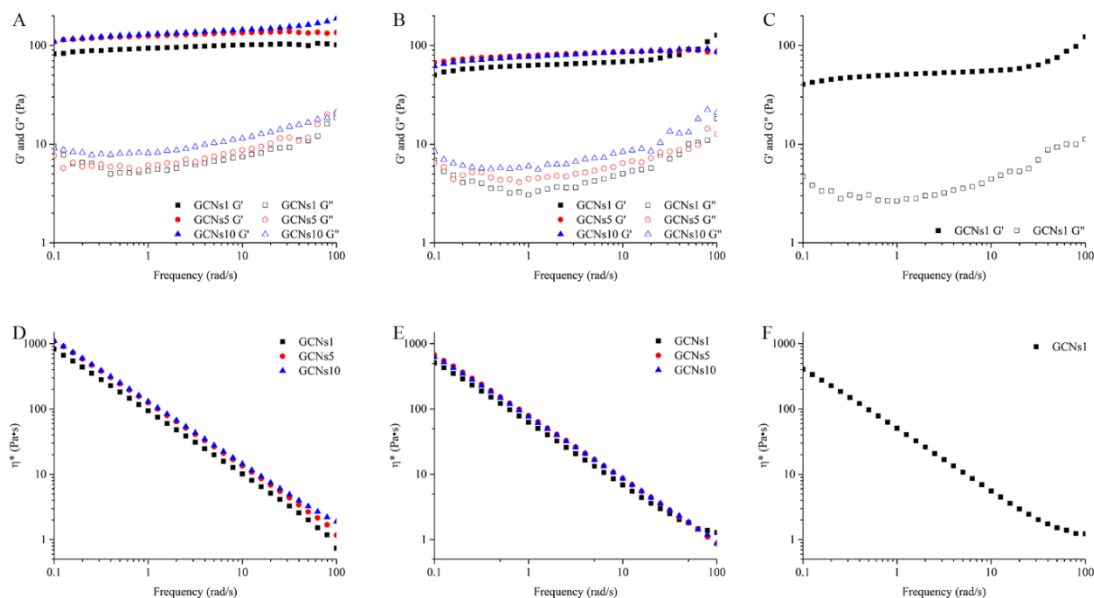


Figure 9-11. Storage modulus G' and loss modulus G'' of the Pickering emulsions ($\Phi = 0.7$, w/w) stabilized by 0.15 wt% GCNs crosslinked at (A) 30°C, (B) 40°C, and (C) 50°C. Complex viscosity η^* of the Pickering emulsions ($\Phi = 0.7$, w/w) stabilized by 0.15 wt% GCNs crosslinked at (D) 30°C, (E) 40°C, and (F) 50°C.

9.5. Conclusions

The crosslinking parameters greatly affect the properties of GCNs and the resulting Pickering emulsions. In this chapter, impacts of crosslinking temperature and crosslinker concentration on the features of GCNs and the resulting Pickering emulsions were further investigated. It was found that these two factors had huge impacts on the major characters of GCNs as Pickering stabilizers, *i.e.* size, surface charge, wettability, and morphology. Most of GCNs except for those crosslinked at weak (low genipin concentration and low temperature) and strong (high genipin concentration and high temperature) conditions can stabilize Pickering emulsions at the concentration as low as 0.05 wt%. These GCNs exhibited outstanding ability to stabilize O/W Pickering emulsions in a wide oil-to-water ratio range. These emulsions showed gel-like properties which were also governed by the crosslinking conditions. GCNs crosslinked by higher concentration of genipin and

at lower temperature could increase the storage modulus, loss modulus, and complex viscosity of the emulsions.

CHAPTER X. ENHANCING ANTIOXIDANT CAPACITY OF PICKERING EMULSIONS BY INCORPORATING THEAFLAVIN-3,3'-DIGALLATE

As of submission of this dissertation, the work in this chapter has been written as a research paper in the title of “Enhancing Antioxidant Capacity of Pickering Emulsions by Incorporating Theaflavin-3,3'-digallate” which is ready for submission.

10.1. Abstract

Emulsions are common colloidal systems in food, pharmaceutical, and cosmetic products. The quality of emulsion-based products is often deteriorated by lipid oxidation. Therefore, it is important to prevent oxidation in emulsions. In this chapter, TF-3 was introduced to improve the stability of Pickering emulsion stabilized by GCNs against lipid oxidation. Various amount of TF-3 was encapsulated in the GCNs and it was found that incorporation of TF-3 did not change the surface charge of GCNs but increased the size due to aggregation. The GCNs encapsulated with TF-3 (GTs) were further applied to stabilize Pickering emulsions with sunflower oil as the oil phase. These Pickering emulsions were O/W type emulsions with gel-like property. They exhibited better stability against lipid oxidation than the oil-water physical mixture and conventional emulsion emulsified by tween 80 as reflected by lower amount of oxidation products during storage at 40°C for 20 days. The level of oxidation products decreased as the concentration of TF-3 increased. It was also observed that TF-3 had better protection against lipid oxidation when located at the oil-water interface compared to located in either oil phase or water phase.

10.2. Introduction

Emulsions are common systems in food, pharmaceutical, and cosmetic products. Conventional emulsions are emulsified by amphiphilic small molecules, phospholipids, or proteins. Unlike conventional emulsions, Pickering emulsions are stabilized by solid particles, which are not

necessary amphiphilic. Pickering emulsions have attracted a great attention recently because they are more stable against coalescence than the conventional emulsions⁹⁶. In addition, the feature of surfactant-free could avoid the potential adverse effects that are associated with the conventional emulsifiers^{97, 98}. A variety of inorganic and organic particles have been investigated as the Pickering stabilizers^{91, 99, 100, 102, 103, 105, 255, 259}.

Although emulsions are versatile in different areas, their qualities are often deteriorated by lipid oxidation, especially in conventional emulsions, which usually have larger oil-water interfacial areas than bulk oil. The larger oil-water interfacial area provides more opportunities for the prooxidants *e.g.* metal ions in the aqueous phase to interact with lipids²⁶⁰. Lipid oxidation leads to rancidity, off-flavor, and consequently reduces the nutritional value and shorten the shelf life of foods. Lipid oxidation can also occur in human GIT after food consumption²⁶¹⁻²⁶³. The oxidation products are potential cytotoxic and genotoxic^{264, 265}. Consuming oxidized foods may give rise to oxidative stress in human body, which is closely related to the pathogenesis of inflammation, atherosclerosis, aging, and cancer, *etc*^{168, 261, 266, 267}. Lipid oxidation can also cause co-oxidation of proteins, DNA, and other molecules *in vitro* and *in vivo*, causing loss of the functionality and mutation²⁶⁸.

It is therefore very important to inhibit lipid oxidation both *in vitro* and *in vivo*. Our human body is protected by inherent enzymes (such as superoxide dismutase, catalase, glutathione peroxidase, glutathione reductase, and glutathione transferase) and exogenous antioxidants (such as ascorbic acid). A tremendous amount of work has been done to avoid lipid oxidation in the food products, especially emulsion-based food products. One important strategy is to add antioxidants, including synthetic antioxidants *e.g.* butylated hydroxyanisole (BHA), butylated hydroxytoluene (BHT), propyl gallate (PG), and tertiary butylhydroquinone (TBHQ) and natural antioxidants *e.g.* tocopherol, ascorbic acid, and carotenoids. The natural antioxidants become more popular because they can avoid the negative health issues that are associated with synthetic antioxidants²⁶⁰. Phenolic

compounds are ubiquitous in fruits and vegetables. Several phenolic compounds have strong antioxidative activity resulted from multiple mechanisms including donating hydrogen atoms to the lipid radicals and/or chelating metal ions. As a polyhydroxylated polyphenol, TF-3 has potent antioxidative ability (section 1.5.2).

In the chapter, TF-3 was encapsulated in the GCNs. The GTs were applied to stabilize Pickering emulsion with sunflower oil as the oil phase, aiming to protect the resulting Pickering emulsions from oxidation.

10.3. Materials and Methods

10.3.1. Materials

CS was purchased from Kunpoong Bio. Co., Ltd. (South Korea) and used as received without further treatment. CPPs was purchased from Greencream Biotechnology Co., Ltd. (Guangzhou, China). Genipin (purity > 98%) was purchased from Wako Pure Chemical Industries, Ltd. (VA, USA). TF-3 was purified from black tea extract as described in section 2.2.8. Sunflower oil was purchased from local supermarket and purified through column liquid chromatography to remove the inherent antioxidants and oxidation products. Silica gel (Sorbent Technologies, Inc., GA, USA) was used as the stationary phase and hexane (Pharmco-AAPER, CT, USA) was used as the mobile phase. Ferrous sulfate, barium chloride dihydrate, coumarin-6, isopropanol, and 1-butanol were purchased from Sigma-Aldrich (MO, USA). Ammonium thiocyanate was purchased from Alfa Aesar (MA, USA). Isooctane was purchased from EMD Millipore (MA, USA). Methanol was purchased from Pharmco-AAPER (CT, USA). Milli-Q water was used in all the experiments.

10.3.2. Preparation and Characterization of the GTs

CS was dissolved in 1% acetic acid (containing 10 mM NaCl) and the pH was adjusted to pH 6 after CS was fully dissolved and hydrated. CPPs and TF-3 were dissolved in Milli-Q water (containing 10 mM NaCl) and their pH were adjusted to pH 6. To prepare GCNs without

encapsulation of TF-3 (GT0), genipin was premixed with 5 mg/mL CS solution followed by addition of same volume of 5 mg/mL CPPs solution. To prepare the GCNs loaded with TF-3 (GTs), TF-3 solution was added dropwise into same volume of 10 mg/mL CPPs solution during magnetic stirring. This TF-3/CPPs mixture was then added into same volume of 5 mg/mL CS, which was premixed with genipin. The final concentration of genipin in all the systems was 0.5 mg/mL. All the crosslinking reactions were conducted at 30°C for 4h. Hereinafter, the GT consisted of TF-3:CPPs=0, 0.1, 0.2, and 0.4 were abbreviated as GT0, GT1, GT2, and GT4, respectively.

The sizes of GT0, GT1, and GT2 were calculated from the intensity-intensity auto-correlation function $G(q,t)^{229}$, obtained from a 90Plus Particle Size Analyzer equipped with a Brookhaven BI-9000AT digital correlator (Brookhaven Instruments Corporation, NY, USA). The samples were diluted 1:5 with 10 mM NaCl solution (pH 6). All measurements were conducted at a fixed scattering angle of 90° and wavelength of 660 nm. The size of GT4 was measured and averaged from its microscopic images by the ImageJ software since its size was larger than the measurable size range of the particle size analyzer.

The ζ -potentials of the GTs were calculated by the Smoluchowski equation from measuring their electrophoretic mobilities on a Nano ZS Zetasizer (Malvern Instruments Ltd., MA, USA). The samples were diluted 1:5 with 10 mM NaCl solution (pH 6) for measurements, which were triplicated at 25°C.

The shapes of the GTs were visualized by a Nanoscope IIIa Multi-Mode AFM (Veeco Instruments Inc., CA, USA) with tapping mode. The samples were diluted 1:50 with 10 mM NaCl (pH 6) and dripped onto the surface of pre-cleaned mica slides. After 1h, the mica slides were rinsed with Milli-Q water and dried with N₂ for analyzing.

10.3.3. Preparation and Characterization of the Pickering Emulsions

The Pickering emulsions were prepared by mixing sunflower oil and GTs at the weight ratio of 7:3 (oil fraction $\Phi=0.7$, w/w) by a high-speed homogenizer (T25 digital ULTRA-TURRAX®, IKA Works Inc., USA) at 12,000 rpm for 1 min. The fluorescence labeled Pickering emulsions were prepared by homogenizing GTs and sunflower oil pre-stained with coumarin-6 at the same homogenization condition. The concentration of GTs in the Pickering emulsions was 0.15 wt%.

The microscopic images of the Pickering emulsions were obtained by a Nikon TE-2000-U inverted fluorescence microscope equipped with a CCD camera (Retiga Exi, Q-imaging). To observe the fluorescence labeled Pickering emulsions, the light was filtered through the bandpass filters, which yielded the excitation wavelengths of 488 ± 10 nm for coumarin 6 and 550 ± 10 nm for GTs. The fluorescence images were processed by the SimplePCI C-Imaging software (Compix, Inc., PA, USA) and the images were overlaid by the ImageJ software. The sizes of the Pickering emulsions were measured by the ImageJ software. At least 500 measurements were conducted for each emulsion sample. The size distribution fittings were performed on the @Risk software (version 7, Palisade Corporation, NY, USA).

The Pickering emulsions standing at room temperature for 24h after preparation was subjected to rheological studies on a Discovery HR-2 Hybrid Rheometer (TA Instruments, DE, USA) with 25 mm stainless-steel parallel plate geometry and a temperature-controlled stainless-steel Peltier plate. All the studies were conducted at 25°C. Dynamic strain sweep tests from 0.1% to 100% strain at 0.1 Hz frequency were carried out to determine the linear viscoelastic region before each dynamic frequency sweep test, which adopted the 1% strain and the angular frequency ω from 0.1 to 100 rad/s with 10 data points per decade.

10.3.4. Determination of the Oxidation Products

To study the relationship between emulsion type and antioxidant capacity, sunflower oil and water (oil:water=7:3, w/w) were physically mixed by high speed homogenizer (12,000 rpm for 1 min) as a control. A conventional emulsion (sunflower oil:water=7:3, w/w) stabilized by tween 80 was also prepared. To investigate the effect of antioxidant concentration, Pickering emulsions stabilized by GT0, GT1, GT2, and GT4 were prepared ($\Phi=0.7$, 0.15 wt% GTs). To compare the impact of location of antioxidant, TF-3 was first dissolved in ethanol at 50 mg/mL. Small volume of this TF-3 solution was then mixed with either sunflower oil or GT0. As the volume of TF-3 was very small, it did not change concentration of GT0. The Pickering emulsion with TF-3 located in the oil phase was prepared by homogenizing GT0 and sunflower oil premixed with TF-3. The Pickering emulsion with TF-3 located in the water phase was prepared by homogenizing pure sunflower oil and GT0 premixed with TF-3. The Pickering emulsion with TF-3 located at the interface was prepared by homogenizing pure sunflower oil and GT1. The amount of TF-3 located in the oil phase or water phase was same as the amount of TF-3 in the Pickering emulsion stabilized by GT1. The oil-water physical mixture, conventional emulsion, and Pickering emulsions were placed in the sealed screw cap glass vials and stored in an oven at 40°C for 20 days.

The content of primary oxidation products was characterized by measuring the peroxide value (PV) using the ferric thiocyanate method²⁶⁹. Briefly, 0.2 g sample was mixed with 1.5 mL isooctane/isopropanol mixture (3:1, v/v) on a vortex mixer for 20 s followed by centrifugation at 10,000 rpm for 5 min. Then 0.2 mL supernatant was added into 2.8 mL methanol/1-butanol (2:1, v/v) followed by addition of 15 μ L 3.94 M ammonium thiocyanate and 15 μ L ferrous solution. The ferrous solution was freshly prepared each time from the supernatant of the mixture of 0.132 M BaCl_2 in 0.4 M HCl and 0.144 M FeSO_4 . After 20 min the absorbance was measured at 510 nm on a microplate reader (BioTek Instruments Inc., VT, USA).

10.4. Results and Discussion

10.4.1. Characterization of the GTs

As studied in CHAPTER III and CHAPTER IV, TF-3 can bind with CPPs through hydrogen bond. This TF-3/CPPs mixture further associated with CS via predominantly electrostatic attraction. Consequently, TF-3 can be encapsulated in the CS-CPPs nanocomplexes. The CS-CPPs nanocomplexes encapsulated with various amount of TF-3 were chemically crosslinked by genipin. Their sizes are presented in Figure 10-1. Generally, incorporation of TF-3 increased the particle size. This increase was dramatically when TF-3:CPPs increased from 0.2 (GT2) to 0.4 (GT4). The increase of the particle size stems from TF-3 that were exposed at the surface of the nanocomplexes bridged neighboring nanocomplexes and formed large size aggregates.

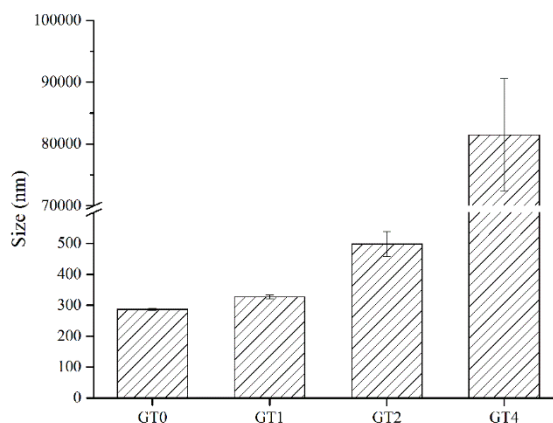


Figure 10-1. Particle sizes of GT0, GT1, GT2, and GT4

The surface charge on the Pickering stabilizers is important for the stability of Pickering emulsions because the surface charge provides electrostatic hindrance against coalescence. As reported in previous chapters, the CS-CPPs nanocomplexes and GCNs were positively charged due to the protonated primary amine groups on CS. As shown in Figure 10-2, incorporation of TF-3 in the GCNs did not change the ζ -potential, which maintained at around +20 mV.

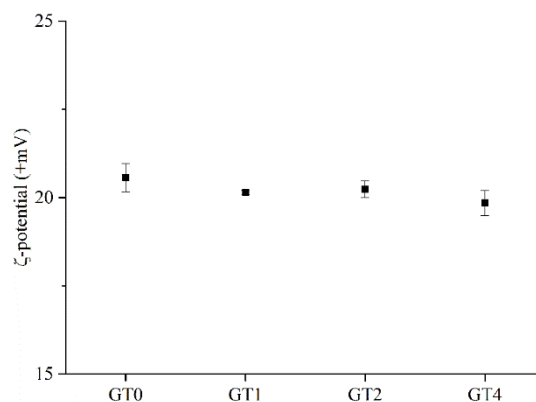


Figure 10-2. ζ -potentials of GT0, GT1, GT2, and GT4

The morphology of particles could significantly affect their abilities for stabilizing emulsions²⁷⁰. The morphologies of GTs were characterized by AFM, which are displayed in Figure 10-3. When TF-3 was not encapsulated (GT0), the nanocomplexes existed as small single particles (Figure 10-3A). When TF-3 was encapsulated, the nanocomplexes started to aggregate, and the size of aggregates increased with the concentration of TF-3 (Figure 10-3B and C). When the concentration of TF-3 further increased, although small particles still existed, exceptionally large aggregates were observed (Figure 10-3D). The observation from the AFM images accords with the particle size measurement (Figure 10-1).

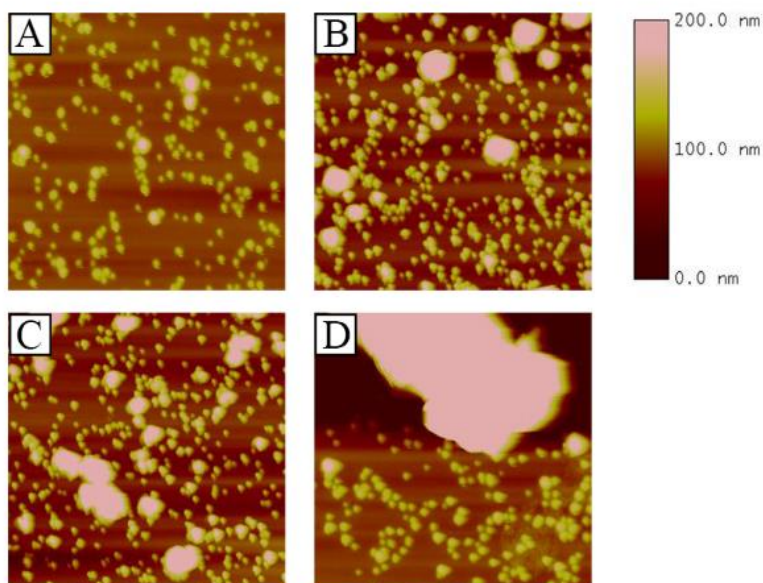


Figure 10-3. AFM height images of (A) GT0, (B) GT1, (C) GT2, and (D) GT4

10.4.2. Characterization of the Pickering Emulsions

The solid particles can irreversibly anchor at the oil-water interface because the energy ($E = \gamma\pi R^2(1 - |\cos \theta|)^2$, where γ is the oil-water interfacial tension; R is the radius of particle; θ is the oil-water-particle three phase contact angle) required to remove a single particle from the interface is thousands of times higher than the kinetic energy of Brownian motion¹⁰⁴. These solid particles anchored at the oil-water interface can stabilize Pickering emulsions.

The GTs were used to stabilize Pickering emulsions with sunflower oil as the oil phase. The oil fraction (Φ) of all Pickering emulsions was 0.7 (w/w) and the concentration of GTs in the Pickering emulsions was fixed at 0.15 wt%. No creaming was observed in all the Pickering emulsions stored at 40°C for at least 20 days. When stored at room temperature, these Pickering emulsions were stable against creaming for at least three months. The droplet size of the Pickering emulsions stabilized by GT0, GT1, and GT2 were $178.8 \pm 37.9 \mu\text{m}$, $189.2 \pm 22.7 \mu\text{m}$, and $179.3 \pm 19.2 \mu\text{m}$, respectively. The droplet size of the Pickering emulsion stabilized by GT4 increased

dramatically to $237.6 \pm 44.0 \mu\text{m}$. Although the Pickering emulsions stabilized by GT0, GT1, and GT2 had similar size, their size distribution was different. The Pickering emulsions stabilized by GT1 and GT2 displayed a more normally distributed manner compared to the Pickering emulsion stabilized by GT0. The peaks of their size distribution fitting curves also shifted to larger size. The droplet size of the Pickering emulsion stabilized by GT4 was more broadly distributed, which means the Pickering emulsion stabilized by GT4 was the most heterogenous among these four Pickering emulsions (Figure 10-4).

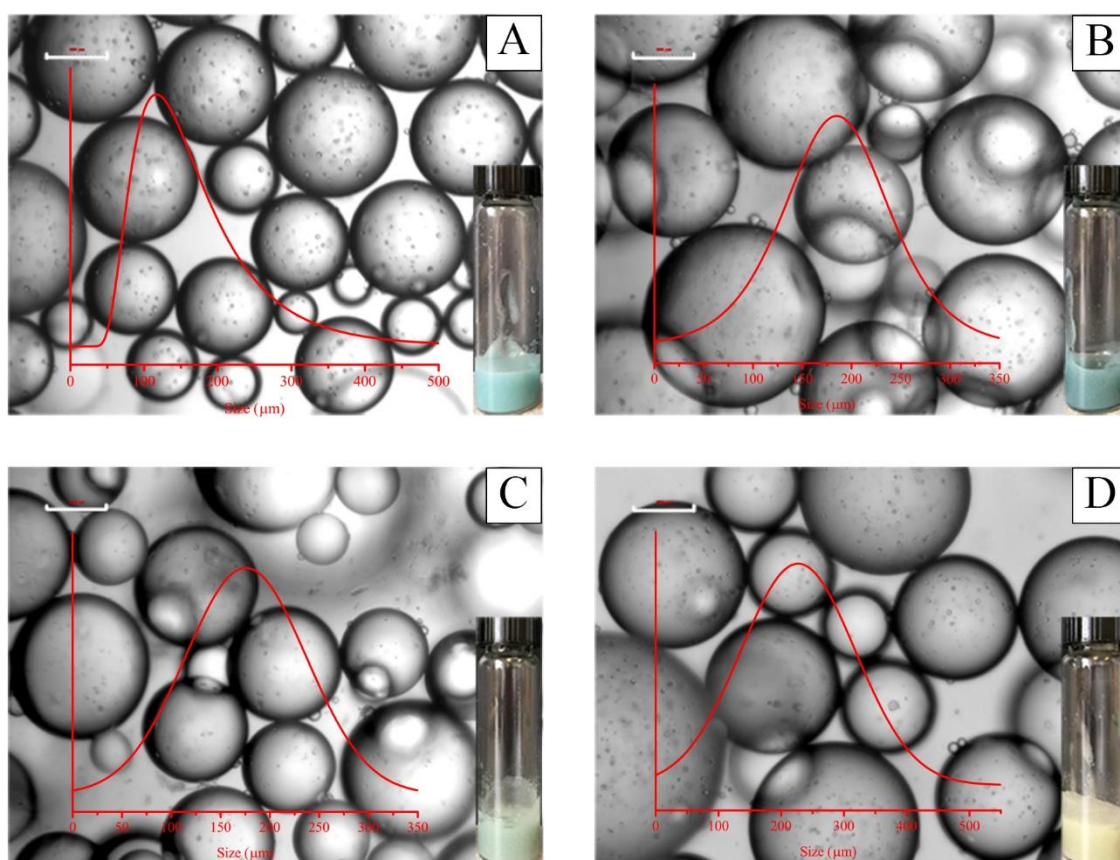


Figure 10-4. Macroscopic and microscopic images and size distribution of the Pickering emulsions ($\Phi=0.7$, w/w) stabilized by 0.15 wt% (A) GT0, (B) GT1, (C) GT2, and (D) GT4. The scale bar is $100 \mu\text{m}$.

The type of emulsions *i.e.* O/W type and W/O type affects their applications and oxidation rate^{271, 272}. The type of Pickering emulsion is determined by the surface hydrophilicity of the Pickering stabilizer. Hydrophilic particles can stabilize O/W Pickering emulsions and hydrophobic particles can stabilize W/O Pickering emulsions¹⁰⁴. To determine the type of the Pickering emulsions stabilized by the GTs, sunflower oil was pre-stained with coumarin-6, which emitted green fluorescence. The GTs had intrinsic fluorescence. As presented in Figure 10-5, the oil droplets (green fluorescence) were surrounded by the GTs (red fluorescence), which means the Pickering emulsions stabilized by GTs were O/W type Pickering emulsions.

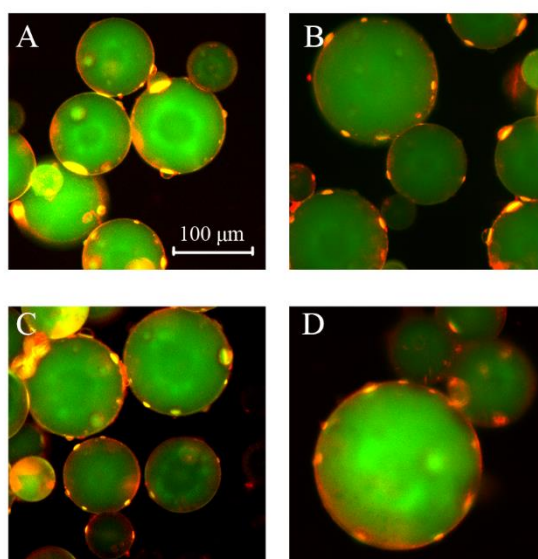


Figure 10-5. Microscopic images of fluorescence labeled Pickering emulsions ($\Phi=0.7$, w/w) stabilized by 0.15 wt% (A) GT0, (B) GT1, (C) GT2, and (D) GT4. The scale bar is 100 μm .

These Pickering emulsions behaved like stick gel. They did not flow when the vials were inverted. The rheological studies revealed that the storage moduli (G') of all Pickering emulsions were higher than the loss moduli (G'') in the whole frequency range (Figure 10-6A), which means three-dimensional gel-like networks were formed in these Pickering emulsions. It was also noticed that both G' , G'' , and the complex viscosity (η^*) were increased with the concentration of TF-3

(Figure 10-6). This indicates that incorporating TF-3 in the GCNs strengthened the network within the Pickering emulsions.

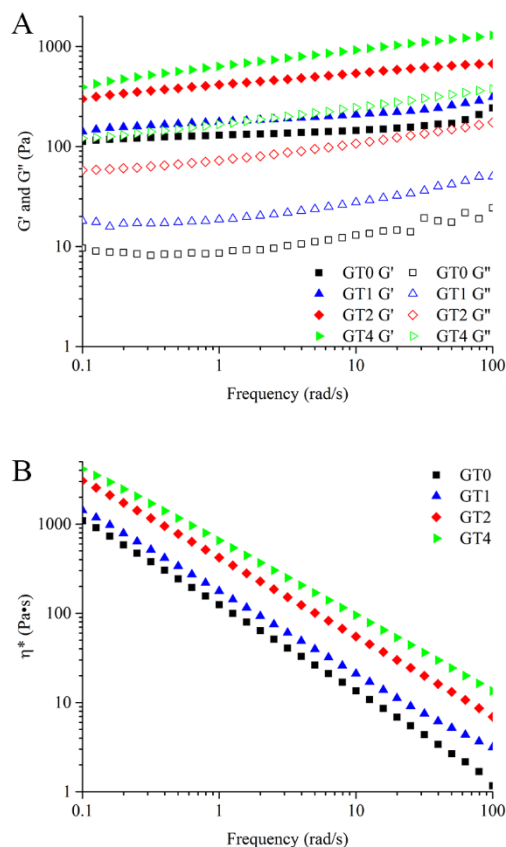


Figure 10-6. (A) Storage moduli G' and loss moduli G'' and (B) complex viscosities η^* of the Pickering emulsions ($\Phi=0.7$, w/w) stabilized by 0.15 wt% GT0, GT1, GT2, and GT4.

10.4.3. Determination of the Oxidation Products

Sunflower oil is considered as a healthy oil because it is rich in polyunsaturated fatty acid (PUFA), for example linoleic acid, which is an essential fatty acid for humans. Sunflower oil also contains oleic acid, which is a monounsaturated fatty acid. These unsaturated fatty acids, however, are highly susceptible to oxidation. Lipid oxidation is a series of free radical chain reactions which can be generally divided into three stages including initiation, propagation, and termination. In the initiation stage, the initiators such as light and heat generate the alkyl radicals ($L\cdot$). In the

propagation stage, the oxygen adds to the alkyl radicals to form the peroxy radicals (LOO \cdot). The peroxy radicals could further abstract hydrogen from neighboring lipid molecules to extend the free radical chain reaction. The termination stage involves recombination of the free radicals to form non-radicals. The real lipid oxidation process could be more complicated than this classic theory²⁷³.

Lipid oxidation in conventional emulsions has been extensively investigated^{274, 275}. As an emerging type of emulsion, study on oxidation in Pickering emulsions is scarce. It was reported that lipid oxidation in Pickering emulsion was weaker than in conventional emulsion²⁶⁹. The degree of oxidation in the Pickering emulsions is affected by concentration of Pickering stabilizer and environmental pH²⁷⁶.

To investigate whether oxidation of sunflower oil can be inhibited in the Pickering emulsion, the levels of primary oxidation products in oil-water physical mixture, conventional emulsion emulsified by tween 80, and Pickering emulsion stabilized by GT0 were compared by measuring their PV.

It is known that the speed of lipid oxidation is related to the oil-water interfacial area. Larger interfacial area usually leads to faster oxidation because larger interfacial area provides more opportunity for the prooxidants to contact with oil²⁷⁴. Therefore, emulsions usually oxidize faster than bulk oil because emulsions usually have smaller droplet sizes than bulk oil, which means emulsions have larger interfacial area than bulk oil. In this study, the oil-water mixture was used as a control. A conventional O/W emulsion emulsified by tween 80 was also formulated. The size of this conventional emulsion was $67.8 \pm 4.5 \mu\text{m}$, which was much smaller than the droplet size of the Pickering emulsions stabilized by GT0. It is therefore not surprising to observe that lipid oxidized fastest and strongest in the conventional emulsion. Pickering emulsion stabilized GT0

displayed much lower PV than the oil-water mixture and conventional emulsions, which means lipid oxidation was effectively inhibited in the Pickering emulsion (Figure 10-7A).

After incorporating TF-3 in the GCNs, PV of the Pickering emulsions behaved in a TF-3 concentration-dependent decrease manner, which demonstrates that higher concentration of TF-3 in the GCNs provided stronger protection for the Pickering emulsion against lipid oxidation (Figure 10-7B).

The effect of location of TF-3 was also investigated by dispersing TF-3 in the oil- or water-phase or located at the oil-water interface. TF-3 encapsulated in the GCNs which were located at the oil-water interface displayed the lowest PV. While TF-3 distributed in the water phase had higher PV and located in the oil phase had the highest PV (Figure 10-7C). This result indicates that TF-3 distributed at the oil-water interface had the most potent capacity against lipid oxidation in the Pickering emulsion, followed by being distributed in the water phase and then in the oil phase. Similar result was reported in another study where lipophilic antioxidant curcumin was used to prevent oxidation in Pickering emulsion stabilized by CS-zein complex particles. Curcumin was encapsulated either in the particles or in the oil phase. It was found that curcumin encapsulated in the CS-zein complex particles which were anchored at the oil-water interface had the strongest antioxidant ability followed by present in the oil and then absence of curcumin⁹³. It is known that the oil-water interface is a crucial site in lipid oxidation because the interfacial area is where the prooxidants and oxygen in the water phase contact with the oil. TF-3 encapsulated in the GCNs was distributed at the interface and it can therefore effectively inhibit lipid oxidation from where oxidation is prevalent. TF-3 located in the water phase may either distributed in the water or stick to the surface of GT0. It can prevent any free radical or metal ions presented in the water phase from contacting the oil. Thus, inhibit the lipid oxidation. Essentially TF-3 has low solubility in oil. When located in the oil phase, although TF-3 was pre-dissolved in ethanol, it may not be evenly distributed in the sunflower oil, which resulted in the lowest antioxidant ability.

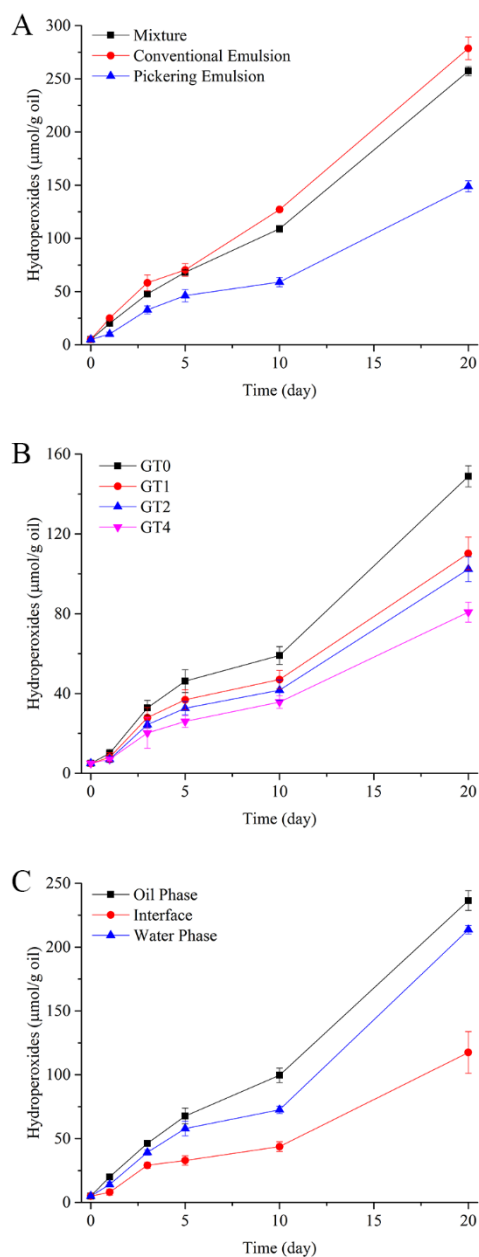


Figure 10-7. Hydroperoxide production in (A) oil-water mixture, conventional emulsion emulsified by tween 80, and Pickering emulsions stabilized by GT0; (B) Pickering emulsions stabilized by 0.15 wt% GT0, GT1, GT2, and GT4; (C) Pickering emulsions with TF-3 located in the oil phase, oil-water interface, and water phase. The oil to water weight ratio of all samples was 7:3.

The lowered amount of oxidation products in the Pickering emulsions compared to the conventional emulsion and oil-water mixture indicates that the Pickering emulsions stabilized by GTs had better protective effect for oil containing unsaturated fatty acids against oxidation, which could be attributed to several mechanisms. Firstly, the GTs were positive charged. They can electrostatically repel any metal ions presented in the systems, which are catalysts for lipid oxidation. Secondly, it was reported that CPPs are antioxidant. As a result, the nanocomplexes consisted of CPPs may be antioxidant. Thirdly, the Pickering emulsions had higher viscosities than the oil-water mixture and conventional emulsions, which can inhibit migration of the metal ions to the oil-water interface, and therefore further retard the process of lipid oxidation. These three mechanisms can explain why Pickering emulsion stabilized by GT0 had significantly lower amount of oxidation products than the oil-water mixture and conventional emulsion. The most important mechanism is due to presence of TF-3, which is a potent antioxidant. It was reported that TF-3 can prevent oxidation via chelating metal ions and scavenging free radicals^{160, 161, 163, 165}. TF-3 can also relieve the oxidative stress in the cell¹⁶². As a result, the Pickering emulsions displayed a dose-dependent decrease of the oxidation products as the concentration of TF-3 increased.

10.5. Conclusions

Using natural antioxidants such as polyphenols is an effective approach to retard lipid oxidation in emulsions. Herein, the potent natural antioxidant TF-3 was encapsulated in the GCNs and the GTs were applied to stabilize O/W Pickering emulsions, which displayed gel-like properties. Incorporation of TF-3 not only increased the size but also strengthened the network of the yielding Pickering emulsions. These Pickering emulsions were stable against creaming and more importantly they can inhibit oxidation of sunflower oil in the Pickering emulsion as reflected by less production of the oxidation products compared to the oil-water mixture and conventional emulsion. The level of the oxidation products was inversely related to the concentration of

incorporated TF-3. It was also found that TF-3 distributed at the oil-water interface had better antioxidant ability than being distributed in either oil phase or water phase.

SUMMARY AND FUTURE WORK

To summarize the work in this dissertation, the novel polysaccharide-polypeptides nanocomplex assembled from CS and CPPs provides multiple platforms as the encapsulation systems for hydrophilic polyphenols such as TF-3. The CS-CPPs nanocomplexes can not only improve the intestinal permeation of TF-3, which may potentially increase its bioavailability, but also improve the stability of lipid in the form of Pickering emulsion against oxidation, which can protect the healthy unsaturated fatty acids especially PUFA from oxidation.

There is definitely a lot of work that can be done to extend the current work. It has been proved in this dissertation that the CS-CPPs nanocomplexes (with and without being crosslinked by genipin) can enhance the intestinal permeability of TF-3, which would be beneficial for improving its bioavailability. It is necessary to know whether the enhanced intestinal permeability can lead to higher bioavailability of TF-3. Therefore, *in vivo* animal study is required in the future to compare the pharmacokinetics of TF-3 encapsulated in the CS-CPPs nanocomplexes (with and without being crosslinked by genipin) with pure TF-3, which will demonstrate the effectiveness of encapsulation on the bioavailability of TF-3. It is also interesting to know whether the enhanced intestinal permeability could bring any improvement of *in vivo* bioefficacies, for example anticancer effect.

TF-3 is only a model hydrophilic polyphenol. The rest components of TFs and other hydrophilic bioactive molecules (nutraceuticals) that have low intestinal permeability can be encapsulated in the CS-CPPs nanocomplexes (with and without being crosslinked by genipin) to overcome the limitation. The ultimate goal is to fortify the nanocomplexes encapsulated with diverse nutraceuticals in the food products, for example beverages, to exert their bioefficacies in human body. Safety evaluation is obviously the prerequisite before achieving this goal.

Another area that is worth exploring is application of the CS-CPPs nanocomplexes- and GCNs-stabilized Pickering emulsions, for example, using these Pickering emulsions as oral delivery system for nutraceuticals.

The biopharmaceutics classification system generally divides drugs into four classes based on their water solubility and intestinal permeability. Molecules in class 1 have good solubility and permeability. Molecules in class 2 have good permeability but the water solubility is low. Molecules in class 3 have good solubility but low permeability. The solubility and permeability of molecules in class 4 are poor²²⁴. This system can also be used to categorize nutraceuticals. Nutraceuticals in class 1 usually have no problems in terms of bioavailability. The bioavailability of nutraceuticals in class 2 is generally limited by low solubility, which can be solved by the emulsion-based delivery systems²²³. The bioavailability of class 3 nutraceuticals such as TFs is obviously restricted by their permeability, which can be solved by the CS-based delivery systems. The nutraceuticals in class 4 whose solubility and permeability are low require a combination of the approaches for class 2 and class 3 nutraceuticals to improve their bioavailability, *i.e.* enhancing both solubility and permeability. Pickering emulsions stabilized by the CS-CPPs nanocomplexes or GCNs stand out as the potential oral delivery systems for class 4 nutraceuticals. As Pickering emulsion is also an emulsion-based system, it can solubilize the lipophilic nutraceuticals. Meanwhile, the particles anchored at the oil-water interface are composed of CS, which can open the tight junctions to increase the permeability. In a word, the Pickering emulsions stabilized by the CS-CPPs nanocomplexes or GCNs may increase the solubility and permeability of nutraceuticals simultaneously. This hypothesis definitely requires support from more experiments especially *in vivo* animal studies.

REFERENCES

1. Damodaran, S.; Parkin, K. L.; Fennema, O. R., *Fennema's food chemistry*. CRC press: 2007.
2. Liu, Z.; Jiao, Y.; Wang, Y.; Zhou, C.; Zhang, Z., Polysaccharides-based nanoparticles as drug delivery systems. *Advanced Drug Delivery Reviews* **2008**, 60, (15), 1650-1662.
3. Francis Suh, J. K.; Matthew, H. W. T., Application of chitosan-based polysaccharide biomaterials in cartilage tissue engineering: a review. *Biomaterials* **2000**, 21, (24), 2589-2598.
4. Liu, G.; Gu, Z.; Hong, Y.; Cheng, L.; Li, C., Electrospun starch nanofibers: Recent advances, challenges, and strategies for potential pharmaceutical applications. *Journal of Controlled Release* **2017**, 252, 95-107.
5. Mascal, M.; Nikitin, E. B., Direct, High-Yield Conversion of Cellulose into Biofuel. *Angewandte Chemie* **2008**, 120, (41), 8042-8044.
6. Lairon, D.; Arnault, N.; Bertrais, S.; Planells, R.; Clero, E.; Hercberg, S.; Boutron-Ruault, M.-C., Dietary fiber intake and risk factors for cardiovascular disease in French adults. *The American Journal of Clinical Nutrition* **2005**, 82, (6), 1185-1194.
7. Liu, S.; Buring, J. E.; Sesso, H. D.; Rimm, E. B.; Willett, W. C.; Manson, J. E., A prospective study of dietary fiber intake and risk of cardiovascular disease among women. *Journal of the American College of Cardiology* **2002**, 39, (1), 49-56.
8. Kaczmarczyk, M. M.; Miller, M. J.; Freund, G. G., The health benefits of dietary fiber: Beyond the usual suspects of type 2 diabetes mellitus, cardiovascular disease and colon cancer. *Metabolism* **2012**, 61, (8), 1058-1066.
9. Trompette, A.; Gollwitzer, E. S.; Yadava, K.; Sichelstiel, A. K.; Sprenger, N.; Ngom-Bru, C.; Blanchard, C.; Junt, T.; Nicod, L. P.; Harris, N. L.; Marsland, B. J., Gut microbiota metabolism of dietary fiber influences allergic airway disease and hematopoiesis. *Nat Med* **2014**, 20, (2), 159-166.
10. Hartmann, R.; Meisel, H., Food-derived peptides with biological activity: from research to food applications. *Current Opinion in Biotechnology* **2007**, 18, (2), 163-169.
11. Sarmadi, B. H.; Ismail, A., Antioxidative peptides from food proteins: A review. *Peptides* **2010**, 31, (10), 1949-1956.
12. Kizilay, E.; Kayitmazer, A. B.; Dubin, P. L., Complexation and coacervation of polyelectrolytes with oppositely charged colloids. *Advances in Colloid and Interface Science* **2011**, 167, (1-2), 24-37.
13. Schmitt, C.; Sanchez, C.; Desobry-Banon, S.; Hardy, J., Structure and Technofunctional Properties of Protein-Polysaccharide Complexes: A Review. *Critical Reviews in Food Science and Nutrition* **1998**, 38, (8), 689-753.
14. de Kruif, C. G.; Weinbreck, F.; de Vries, R., Complex coacervation of proteins and anionic polysaccharides. *Current Opinion in Colloid & Interface Science* **2004**, 9, (5), 340-349.
15. Wang, X.; Wang, Y.-W.; Ruengruglikit, C.; Huang, Q., Effects of Salt Concentration on Formation and Dissociation of β -Lactoglobulin/Pectin Complexes. *Journal of Agricultural and Food Chemistry* **2007**, 55, (25), 10432-10436.
16. Weinbreck, F.; Nieuwenhuijse, H.; Robijn, G. W.; de Kruif, C. G., Complexation of Whey Proteins with Carrageenan. *Journal of Agricultural and Food Chemistry* **2004**, 52, (11), 3550-3555.
17. Weinbreck, F.; de Vries, R.; Schrooyen, P.; de Kruif, C. G., Complex Coacervation of Whey Proteins and Gum Arabic. *Biomacromolecules* **2003**, 4, (2), 293-303.
18. Li, X.; Fang, Y.; Al-Assaf, S.; Phillips, G. O.; Yao, X.; Zhang, Y.; Zhao, M.; Zhang, K.; Jiang, F., Complexation of Bovine Serum Albumin and Sugar Beet Pectin: Structural Transitions and Phase Diagram. *Langmuir* **2012**, 28, (27), 10164-10176.

19. Girard, M.; Turgeon, S. L.; Gauthier, S. F., Thermodynamic Parameters of β -Lactoglobulin–Pectin Complexes Assessed by Isothermal Titration Calorimetry. *Journal of Agricultural and Food Chemistry* **2003**, 51, (15), 4450-4455.
20. Aberkane, L.; Jasniewski, J.; Gaiani, C.; Scher, J.; Sanchez, C., Thermodynamic Characterization of Acacia Gum– β -Lactoglobulin Complex Coacervation. *Langmuir* **2010**, 26, (15), 12523-12533.
21. Galazka, V. B.; Smith, D.; Ledward, D. A.; Dickinson, E., Complexes of bovine serum albumin with sulphated polysaccharides: effects of pH, ionic strength and high pressure treatment. *Food Chemistry* **1999**, 64, (3), 303-310.
22. Molina Ortiz, S. E.; Puppo, M. C.; Wagner, J. R., Relationship between structural changes and functional properties of soy protein isolates–carrageenan systems. *Food Hydrocolloids* **2004**, 18, (6), 1045-1053.
23. Gilsenan, P. M.; Richardson, R. K.; Morris, E. R., Associative and segregative interactions between gelatin and low-methoxy pectin: Part 1. Associative interactions in the absence of Ca^{2+} . *Food Hydrocolloids* **2003**, 17, (6), 723-737.
24. Weinbreck, F.; Nieuwenhuijse, H.; Robijn, G. W.; de Kruif, C. G., Complex Formation of Whey Proteins: Exocellular Polysaccharide EPS B40. *Langmuir* **2003**, 19, (22), 9404-9410.
25. Girard, M.; Sanchez, C.; Laneuville, S. I.; Turgeon, S. L.; Gauthier, S. F., Associative phase separation of β -lactoglobulin/pectin solutions: a kinetic study by small angle static light scattering. *Colloids and Surfaces B: Biointerfaces* **2004**, 35, (1), 15-22.
26. Wang, X.; Li, Y.; Wang, Y.-W.; Lal, J.; Huang, Q., Microstructure of β -Lactoglobulin/Pectin Coacervates Studied by Small-Angle Neutron Scattering. *The Journal of Physical Chemistry B* **2007**, 111, (3), 515-520.
27. Wang, Y.; Qiu, D.; Cosgrove, T.; Denbow, M. L., A small-angle neutron scattering and rheology study of the composite of chitosan and gelatin. *Colloids and Surfaces B: Biointerfaces* **2009**, 70, (2), 254-258.
28. Weinbreck, F.; Tromp, R. H.; de Kruif, C. G., Composition and Structure of Whey Protein/Gum Arabic Coacervates. *Biomacromolecules* **2004**, 5, (4), 1437-1445.
29. Morfin, I.; Buhler, E.; Cousin, F.; Grillo, I.; Boué, F., Rodlike Complexes of a Polyelectrolyte (Hyaluronan) and a Protein (Lysozyme) Observed by SANS. *Biomacromolecules* **2011**, 12, (4), 859-870.
30. Schmidt, I.; Cousin, F.; Huchon, C.; Boué, F.; Axelos, M. A. V., Spatial Structure and Composition of Polysaccharide–Protein Complexes from Small Angle Neutron Scattering. *Biomacromolecules* **2009**, 10, (6), 1346-1357.
31. Wang, X.; Lee, J.; Wang, Y.-W.; Huang, Q., Composition and Rheological Properties of β -Lactoglobulin/Pectin Coacervates: Effects of Salt Concentration and Initial Protein/Polysaccharide Ratio. *Biomacromolecules* **2007**, 8, (3), 992-997.
32. Chourpa, I.; Ducel, V.; Richard, J.; Dubois, P.; Boury, F., Conformational Modifications of α Gliadin and Globulin Proteins upon Complex Coacervates Formation with Gum Arabic as Studied by Raman Microspectroscopy. *Biomacromolecules* **2006**, 7, (9), 2616-2623.
33. Zhang, S.; Zhang, Z.; Lin, M.; Vardhanabuthi, B., Raman Spectroscopic Characterization of Structural Changes in Heated Whey Protein Isolate upon Soluble Complex Formation with Pectin at Near Neutral pH. *Journal of Agricultural and Food Chemistry* **2012**, 60, (48), 12029-12035.
34. Lii, C. y.; Liaw, S. C.; Lai, V. M. F.; Tomasik, P., Xanthan gum–gelatin complexes. *European Polymer Journal* **2002**, 38, (7), 1377-1381.
35. Girard, M.; Turgeon, S. L.; Gauthier, S. F., Quantification of the Interactions between β -Lactoglobulin and Pectin through Capillary Electrophoresis Analysis. *Journal of Agricultural and Food Chemistry* **2003**, 51, (20), 6043-6049.

36. Li, Y.; Huang, Q., Influence of Protein Self-Association on Complex Coacervation with Polysaccharide: A Monte Carlo Study. *The Journal of Physical Chemistry B* **2013**, 117, (9), 2615-2624.
37. Li, Y.; Shi, T.; An, L.; Huang, Q., Monte Carlo Simulation on Complex Formation of Proteins and Polysaccharides. *The Journal of Physical Chemistry B* **2012**, 116, (10), 3045-3053.
38. Perry, S. L.; Sing, C. E., PRISM-Based Theory of Complex Coacervation: Excluded Volume versus Chain Correlation. *Macromolecules* **2015**, 48, (14), 5040-5053.
39. Kayitmazer, A. B.; Seeman, D.; Minsky, B. B.; Dubin, P. L.; Xu, Y., Protein-polyelectrolyte interactions. *Soft Matter* **2013**, 9, (9), 2553-2583.
40. Harnsilawat, T.; Pongsawatmanit, R.; McClements, D. J., Characterization of β -lactoglobulin–sodium alginate interactions in aqueous solutions: A calorimetry, light scattering, electrophoretic mobility and solubility study. *Food Hydrocolloids* **2006**, 20, (5), 577-585.
41. Zhao, Y.; Li, F.; Carvajal, M. T.; Harris, M. T., Interactions between bovine serum albumin and alginate: An evaluation of alginate as protein carrier. *Journal of Colloid and Interface Science* **2009**, 332, (2), 345-353.
42. Saravanan, M.; Rao, K. P., Pectin–gelatin and alginate–gelatin complex coacervation for controlled drug delivery: Influence of anionic polysaccharides and drugs being encapsulated on physicochemical properties of microcapsules. *Carbohydrate Polymers* **2010**, 80, (3), 808-816.
43. Croguennoc, P.; Durand, D.; Nicolai, T.; Clark, A., Phase Separation and Association of Globular Protein Aggregates in the Presence of Polysaccharides: 1. Mixtures of Preheated β -Lactoglobulin and κ -Carrageenan at Room Temperature. *Langmuir* **2001**, 17, (14), 4372-4379.
44. Voron'ko, N. G.; Derkach, S. R.; Vovk, M. A.; Tolstoy, P. M., Formation of κ -carrageenan–gelatin polyelectrolyte complexes studied by ^1H NMR, UV spectroscopy and kinematic viscosity measurements. *Carbohydrate Polymers* **2016**, 151, 1152-1161.
45. Girod, S.; Boissière, M.; Longchambon, K.; Begu, S.; Tourne-Pétheil, C.; Devoisselle, J. M., Polyelectrolyte complex formation between iota-carrageenan and poly(l-lysine) in dilute aqueous solutions: a spectroscopic and conformational study. *Carbohydrate Polymers* **2004**, 55, (1), 37-45.
46. Jiang, Y. Micro-and nano-encapsulation and controlled-release of phenolic compounds and other food ingredients. Rutgers University-Graduate School-New Brunswick, 2009.
47. Burova, T. V.; Grinberg, N. V.; Grinberg, V. Y.; Usov, A. I.; Tolstoguzov, V. B.; de Kruif, C. G., Conformational Changes in ι - and κ -Carrageenans Induced by Complex Formation with Bovine β -Casein. *Biomacromolecules* **2007**, 8, (2), 368-375.
48. Hill, R. D.; Zadow, J. G., The precipitation of whey proteins by carboxymethyl cellulose of differing degrees of substitution. *Journal of Dairy Research* **2009**, 41, (3), 373-380.
49. Lee, A.-C.; Hong, Y.-H., Coacervate formation of α -lactalbumin–chitosan and β -lactoglobulin–chitosan complexes. *Food Research International* **2009**, 42, (5–6), 733-738.
50. Bekale, L.; Agudelo, D.; Tajmir-Riahi, H. A., Effect of polymer molecular weight on chitosan–protein interaction. *Colloids and Surfaces B: Biointerfaces* **2015**, 125, 309-317.
51. Huang, G.-Q.; Sun, Y.-T.; Xiao, J.-X.; Yang, J., Complex coacervation of soybean protein isolate and chitosan. *Food Chemistry* **2012**, 135, (2), 534-539.
52. Bastos, D. S.; Barreto, B. N.; Souza, H. K. S.; Bastos, M.; Rocha-Leão, M. H. M.; Andrade, C. T.; Gonçalves, M. P., Characterization of a chitosan sample extracted from Brazilian shrimps and its application to obtain insoluble complexes with a commercial whey protein isolate. *Food Hydrocolloids* **2010**, 24, (8), 709-718.
53. Galazka, V. B.; Ledward, D. A.; Sumner, I. G.; Dickinson, E., Influence of High Pressure on Bovine Serum Albumin and Its Complex with Dextran Sulfate. *Journal of Agricultural and Food Chemistry* **1997**, 45, (9), 3465-3471.
54. Schmitt, C.; Palma da Silva, T.; Bovay, C.; Rami-Shojaei, S.; Frossard, P.; Kolodziejczyk, E.; Leser, M. E., Effect of Time on the Interfacial and Foaming Properties of β -

- Lactoglobulin/Acacia Gum Electrostatic Complexes and Coacervates at pH 4.2. *Langmuir* **2005**, 21, (17), 7786-7795.
55. Schmitt, C.; Sanchez, C.; Lamprecht, A.; Renard, D.; Lehr, C.-M.; de Kruif, C. G.; Hardy, J., Study of β -lactoglobulin/acacia gum complex coacervation by diffusing-wave spectroscopy and confocal scanning laser microscopy. *Colloids and Surfaces B: Biointerfaces* **2001**, 20, (3), 267-280.
56. Mekhloufi, G.; Sanchez, C.; Renard, D.; Guillemin, S.; Hardy, J., pH-Induced Structural Transitions during Complexation and Coacervation of β -Lactoglobulin and Acacia Gum. *Langmuir* **2005**, 21, (1), 386-394.
57. Ye, A.; Flanagan, J.; Singh, H., Formation of stable nanoparticles via electrostatic complexation between sodium caseinate and gum arabic. *Biopolymers* **2006**, 82, (2), 121-133.
58. Bungenberg de Jong, H.; Kruyt, H., Coacervation (partial miscibility in colloid systems). *Proc Koninklijke Nederlandse Akademie Wetenschappen* **1929**, 32, 849-856.
59. Liu, S.; Low, N. H.; Nickerson, M. T., Effect of pH, Salt, and Biopolymer Ratio on the Formation of Pea Protein Isolate–Gum Arabic Complexes. *Journal of Agricultural and Food Chemistry* **2009**, 57, (4), 1521-1526.
60. Liu, S.; Cao, Y.-L.; Ghosh, S.; Rousseau, D.; Low, N. H.; Nickerson, M. T., Intermolecular Interactions during Complex Coacervation of Pea Protein Isolate and Gum Arabic. *Journal of Agricultural and Food Chemistry* **2010**, 58, (1), 552-556.
61. Girard, M.; Turgeon, S. L.; Gauthier, S. F., Interbiopolymer complexing between β -lactoglobulin and low- and high-methylated pectin measured by potentiometric titration and ultrafiltration. *Food Hydrocolloids* **2002**, 16, (6), 585-591.
62. Redigueri, C. F.; de Freitas, O.; Lettinga, M. P.; Tuinier, R., Thermodynamic Incompatibility and Complex Formation in Pectin/Caseinate Mixtures. *Biomacromolecules* **2007**, 8, (11), 3345-3354.
63. Guzey, D.; McClements, D. J., Characterization of β -lactoglobulin–chitosan interactions in aqueous solutions: A calorimetry, light scattering, electrophoretic mobility and solubility study. *Food Hydrocolloids* **2006**, 20, (1), 124-131.
64. Seyrek, E.; Dubin, P. L.; Tribet, C.; Gamble, E. A., Ionic Strength Dependence of Protein-Polyelectrolyte Interactions. *Biomacromolecules* **2003**, 4, (2), 273-282.
65. Jones, O. G.; McClements, D. J., Recent progress in biopolymer nanoparticle and microparticle formation by heat-treating electrostatic protein–polysaccharide complexes. *Advances in Colloid and Interface Science* **2011**, 167, (1–2), 49-62.
66. Doublier, J. L.; Garnier, C.; Renard, D.; Sanchez, C., Protein–polysaccharide interactions. *Current Opinion in Colloid & Interface Science* **2000**, 5, (3), 202-214.
67. Veis, A., A review of the early development of the thermodynamics of the complex coacervation phase separation. *Advances in Colloid and Interface Science* **2011**, 167, (1), 2-11.
68. Aberkane, L.; Jasniewski, J.; Gaiani, C.; Hussain, R.; Scher, J.; Sanchez, C., Structuration mechanism of β -lactoglobulin – acacia gum assemblies in presence of quercetin. *Food Hydrocolloids* **2012**, 29, (1), 9-20.
69. Turgeon, S. L.; Schmitt, C.; Sanchez, C., Protein–polysaccharide complexes and coacervates. *Current Opinion in Colloid & Interface Science* **2007**, 12, (4–5), 166-178.
70. Turgeon, S. L.; Beaulieu, M.; Schmitt, C.; Sanchez, C., Protein–polysaccharide interactions: phase-ordering kinetics, thermodynamic and structural aspects. *Current Opinion in Colloid & Interface Science* **2003**, 8, (4–5), 401-414.
71. Janes, K. A.; Calvo, P.; Alonso, M. J., Polysaccharide colloidal particles as delivery systems for macromolecules. *Advanced Drug Delivery Reviews* **2001**, 47, (1), 83-97.
72. Sonia, T. A.; Sharma, C. P., An overview of natural polymers for oral insulin delivery. *Drug Discovery Today* **2012**, 17, (13), 784-792.
73. Pan, Y.; Li, Y.-j.; Zhao, H.-y.; Zheng, J.-m.; Xu, H.; Wei, G.; Hao, J.-s.; Cui, F.-d., Bioadhesive polysaccharide in protein delivery system: chitosan nanoparticles improve the

- intestinal absorption of insulin in vivo. *International Journal of Pharmaceutics* **2002**, 249, (1), 139-147.
74. Sarmento, B.; Ribeiro, A.; Veiga, F.; Ferreira, D.; Neufeld, R., Oral Bioavailability of Insulin Contained in Polysaccharide Nanoparticles. *Biomacromolecules* **2007**, 8, (10), 3054-3060.
75. Sarmento, B.; Ribeiro, A.; Veiga, F.; Sampaio, P.; Neufeld, R.; Ferreira, D., Alginate/Chitosan Nanoparticles are Effective for Oral Insulin Delivery. *Pharmaceutical Research* **2007**, 24, (12), 2198-2206.
76. Krauland, A. H.; Guggi, D.; Bernkop-Schnürch, A., Oral insulin delivery: the potential of thiolated chitosan-insulin tablets on non-diabetic rats. *Journal of Controlled Release* **2004**, 95, (3), 547-555.
77. Yin, L.; Ding, J.; He, C.; Cui, L.; Tang, C.; Yin, C., Drug permeability and mucoadhesion properties of thiolated trimethyl chitosan nanoparticles in oral insulin delivery. *Biomaterials* **2009**, 30, (29), 5691-5700.
78. Madene, A.; Jacquot, M.; Scher, J.; Desobry, S., Flavour encapsulation and controlled release – a review. *International Journal of Food Science & Technology* **2006**, 41, (1), 1-21.
79. Dumitriu, S.; Chornet, E., Inclusion and release of proteins from polysaccharide-based polyion complexes. *Advanced Drug Delivery Reviews* **1998**, 31, (3), 223-246.
80. Chu, H.; Gao, J.; Chen, C.-W.; Huard, J.; Wang, Y., Injectable fibroblast growth factor-2 coacervate for persistent angiogenesis. *Proceedings of the National Academy of Sciences* **2011**, 108, (33), 13444-13449.
81. Awada, H. K.; Johnson, N. R.; Wang, Y., Sequential delivery of angiogenic growth factors improves revascularization and heart function after myocardial infarction. *Journal of Controlled Release* **2015**, 207, 7-17.
82. Zimet, P.; Livney, Y. D., Beta-lactoglobulin and its nanocomplexes with pectin as vehicles for ω -3 polyunsaturated fatty acids. *Food Hydrocolloids* **2009**, 23, (4), 1120-1126.
83. Eratte, D.; McKnight, S.; Gengenbach, T. R.; Dowling, K.; Barrow, C. J.; Adhikari, B. P., Co-encapsulation and characterisation of omega-3 fatty acids and probiotic bacteria in whey protein isolate–gum Arabic complex coacervates. *Journal of Functional Foods* **2015**.
84. Ron, N.; Zimet, P.; Bargarum, J.; Livney, Y. D., Beta-lactoglobulin–polysaccharide complexes as nanovehicles for hydrophobic nutraceuticals in non-fat foods and clear beverages. *International Dairy Journal* **2010**, 20, (10), 686-693.
85. Luo, Y.; Teng, Z.; Wang, Q., Development of Zein Nanoparticles Coated with Carboxymethyl Chitosan for Encapsulation and Controlled Release of Vitamin D3. *Journal of Agricultural and Food Chemistry* **2012**, 60, (3), 836-843.
86. Teng, Z.; Luo, Y.; Wang, Q., Carboxymethyl chitosan–soy protein complex nanoparticles for the encapsulation and controlled release of vitamin D3. *Food Chemistry* **2013**, 141, (1), 524-532.
87. Luo, Y.; Zhang, B.; Whent, M.; Yu, L.; Wang, Q., Preparation and characterization of zein/chitosan complex for encapsulation of α -tocopherol, and its in vitro controlled release study. *Colloids and Surfaces B: Biointerfaces* **2011**, 85, (2), 145-152.
88. Somchue, W.; Sermsri, W.; Shiowatana, J.; Siripinyanond, A., Encapsulation of α -tocopherol in protein-based delivery particles. *Food Research International* **2009**, 42, (8), 909-914.
89. Xiao, J.; Nian, S.; Huang, Q., Assembly of kafirin/carboxymethyl chitosan nanoparticles to enhance the cellular uptake of curcumin. *Food Hydrocolloids* **2015**, 51, 166-175.
90. Robert, P.; Torres, V.; García, P.; Vergara, C.; Sáenz, C., The encapsulation of purple cactus pear (*Opuntia ficus-indica*) pulp by using polysaccharide-proteins as encapsulating agents. *LWT - Food Science and Technology* **2015**, 60, (2, Part 1), 1039-1045.
91. Tikekar, R. V.; Pan, Y.; Nitin, N., Fate of curcumin encapsulated in silica nanoparticle stabilized Pickering emulsion during storage and simulated digestion. *Food Research International* **2013**, 51, (1), 370-377.

92. Tan, H.; Sun, G.; Lin, W.; Mu, C.; Ngai, T., Gelatin Particle-Stabilized High Internal Phase Emulsions as Nutraceutical Containers. *ACS Applied Materials & Interfaces* **2014**, 6, (16), 13977-13984.
93. Wang, L.-J.; Hu, Y.-Q.; Yin, S.-W.; Yang, X.-Q.; Lai, F.-R.; Wang, S.-Q., Fabrication and Characterization of Antioxidant Pickering Emulsions Stabilized by Zein/Chitosan Complex Particles (ZCPs). *Journal of Agricultural and Food Chemistry* **2015**, 63, (9), 2514-2524.
94. Shah, B. R.; Li, Y.; Jin, W.; An, Y.; He, L.; Li, Z.; Xu, W.; Li, B., Preparation and optimization of Pickering emulsion stabilized by chitosan-tripolyphosphate nanoparticles for curcumin encapsulation. *Food Hydrocolloids* **2016**, 52, 369-377.
95. Rayner, M.; Marku, D.; Eriksson, M.; Sjö, M.; Dejmek, P.; Wahlgren, M., Biomass-based particles for the formulation of Pickering type emulsions in food and topical applications. *Colloids and Surfaces A: Physicochemical and Engineering Aspects* **2014**, 458, (0), 48-62.
96. Pawar, A. B.; Caggioni, M.; Ergun, R.; Hartel, R. W.; Spicer, P. T., Arrested coalescence in Pickering emulsions. *Soft Matter* **2011**, 7, (17), 7710-7716.
97. Chevalier, Y.; Bolzinger, M.-A., Emulsions stabilized with solid nanoparticles: Pickering emulsions. *Colloids and Surfaces A: Physicochemical and Engineering Aspects* **2013**, 439, (0), 23-34.
98. Chassaing, B.; Koren, O.; Goodrich, J. K.; Poole, A. C.; Srinivasan, S.; Ley, R. E.; Gewirtz, A. T., Dietary emulsifiers impact the mouse gut microbiota promoting colitis and metabolic syndrome. *Nature* **2015**, 519, (7541), 92-96.
99. Frelichowska, J.; Bolzinger, M.-A.; Chevalier, Y., Pickering emulsions with bare silica. *Colloids and Surfaces A: Physicochemical and Engineering Aspects* **2009**, 343, (1), 70-74.
100. Ashby, N. P.; Binks, B. P., Pickering emulsions stabilised by Laponite clay particles. *Physical Chemistry Chemical Physics* **2000**, 2, (24), 5640-5646.
101. Binks, B. P.; Lumsdon, S. O., Pickering Emulsions Stabilized by Monodisperse Latex Particles: Effects of Particle Size. *Langmuir* **2001**, 17, (15), 4540-4547.
102. Liu, F.; Tang, C.-H., Soy Protein Nanoparticle Aggregates as Pickering Stabilizers for Oil-in-Water Emulsions. *Journal of Agricultural and Food Chemistry* **2013**, 61, (37), 8888-8898.
103. de Folter, J. W. J.; van Ruijven, M. W. M.; Velikov, K. P., Oil-in-water Pickering emulsions stabilized by colloidal particles from the water-insoluble protein zein. *Soft Matter* **2012**, 8, (25), 6807-6815.
104. Destribats, M.; Rouvet, M.; Gehin-Delval, C.; Schmitt, C.; Binks, B. P., Emulsions stabilised by whey protein microgel particles: towards food-grade Pickering emulsions. *Soft Matter* **2014**, 10, (36), 6941-6954.
105. Liu, H.; Wang, C.; Zou, S.; Wei, Z.; Tong, Z., Simple, Reversible Emulsion System Switched by pH on the Basis of Chitosan without Any Hydrophobic Modification. *Langmuir* **2012**, 28, (30), 11017-11024.
106. Tzoumaki, M. V.; Moschakis, T.; Kiosseoglou, V.; Biliaderis, C. G., Oil-in-water emulsions stabilized by chitin nanocrystal particles. *Food Hydrocolloids* **2011**, 25, (6), 1521-1529.
107. Evans, M.; Ratcliffe, I.; Williams, P. A., Emulsion stabilisation using polysaccharide-protein complexes. *Current Opinion in Colloid & Interface Science* **2013**, 18, (4), 272-282.
108. Guzey, D.; McClements, D. J., Formation, stability and properties of multilayer emulsions for application in the food industry. *Advances in Colloid and Interface Science* **2006**, 128, 227-248.
109. Rinaudo, M., Chitin and chitosan: Properties and applications. *Progress in Polymer Science* **2006**, 31, (7), 603-632.
110. Dodane, V.; Vilivalam, V. D., Pharmaceutical applications of chitosan. *Pharmaceutical Science & Technology Today* **1998**, 1, (6), 246-253.
111. Kean, T.; Thanou, M., Biodegradation, biodistribution and toxicity of chitosan. *Advanced Drug Delivery Reviews* **2010**, 62, (1), 3-11.

112. Kumar, M. N. V. R.; Muzzarelli, R. A. A.; Muzzarelli, C.; Sashiwa, H.; Domb, A. J., Chitosan Chemistry and Pharmaceutical Perspectives. *Chemical Reviews* **2004**, 104, (12), 6017-6084.
113. Sogias, I. A.; Williams, A. C.; Khutoryanskiy, V. V., Why is Chitosan Mucoadhesive? *Biomacromolecules* **2008**, 9, (7), 1837-1842.
114. Sonaje, K.; Chuang, E.-Y.; Lin, K.-J.; Yen, T.-C.; Su, F.-Y.; Tseng, M. T.; Sung, H.-W., Opening of Epithelial Tight Junctions and Enhancement of Paracellular Permeation by Chitosan: Microscopic, Ultrastructural, and Computed-Tomographic Observations. *Molecular Pharmaceutics* **2012**, 9, (5), 1271-1279.
115. Steed, E.; Balda, M. S.; Matter, K., Dynamics and functions of tight junctions. *Trends in Cell Biology* **2010**, 20, (3), 142-149.
116. Yeh, T.-H.; Hsu, L.-W.; Tseng, M. T.; Lee, P.-L.; Sonjae, K.; Ho, Y.-C.; Sung, H.-W., Mechanism and consequence of chitosan-mediated reversible epithelial tight junction opening. *Biomaterials* **2011**, 32, (26), 6164-6173.
117. Vllasaliu, D.; Exposito-Harris, R.; Heras, A.; Casettari, L.; Garnett, M.; Illum, L.; Stolnik, S., Tight junction modulation by chitosan nanoparticles: Comparison with chitosan solution. *International Journal of Pharmaceutics* **2010**, 400, (1), 183-193.
118. Hsu, L.-W.; Lee, P.-L.; Chen, C.-T.; Mi, F.-L.; Juang, J.-H.; Hwang, S.-M.; Ho, Y.-C.; Sung, H.-W., Elucidating the signaling mechanism of an epithelial tight-junction opening induced by chitosan. *Biomaterials* **2012**, 33, (26), 6254-6263.
119. Smith, J. M.; Dornish, M.; Wood, E. J., Involvement of protein kinase C in chitosan glutamate-mediated tight junction disruption. *Biomaterials* **2005**, 26, (16), 3269-3276.
120. Chen, M.-C.; Mi, F.-L.; Liao, Z.-X.; Hsiao, C.-W.; Sonaje, K.; Chung, M.-F.; Hsu, L.-W.; Sung, H.-W., Recent advances in chitosan-based nanoparticles for oral delivery of macromolecules. *Advanced Drug Delivery Reviews* **2013**, 65, (6), 865-879.
121. Schipper, N. M.; Vårum, K.; Artursson, P., Chitosans as Absorption Enhancers for Poorly Absorbable Drugs. 1: Influence of Molecular Weight and Degree of Acetylation on Drug Transport Across Human Intestinal Epithelial (Caco-2) Cells. *Pharmaceutical Research* **1996**, 13, (11), 1686-1692.
122. Schipper, N. G. M.; Vårum, K. M.; Stenberg, P.; Ocklind, G.; Lennernäs, H.; Artursson, P., Chitosans as absorption enhancers of poorly absorbable drugs: 3: Influence of mucus on absorption enhancement. *European Journal of Pharmaceutical Sciences* **1999**, 8, (4), 335-343.
123. Dalgleish, D. G.; Corredig, M., The Structure of the Casein Micelle of Milk and Its Changes During Processing. *Annual Review of Food Science and Technology* **2012**, 3, (1), 449-467.
124. Elzoghby, A. O.; Abo El-Fotoh, W. S.; Elgindy, N. A., Casein-based formulations as promising controlled release drug delivery systems. *Journal of Controlled Release* **2011**, 153, (3), 206-216.
125. Huppertz, T., Chemistry of the Caseins. In *Advanced Dairy Chemistry*, McSweeney, P. L. H.; Fox, P. F., Eds. Springer US: 2013; pp 135-160.
126. Malin, E.; Alaimo, M.; Brown, E.; Aramini, J.; Germann, M.; Farrell, H., Jr.; McSweeney, P. H.; Fox, P., Solution Structures of Casein Peptides: NMR, FTIR, CD, and Molecular Modeling Studies of α 1-Casein, 1-23. *Journal of Protein Chemistry* **2001**, 20, (5), 391-404.
127. Farrell Jr, H. M.; Wickham, E. D.; Unruh, J. J.; Qi, P. X.; Hoagland, P. D., Secondary structural studies of bovine caseins: temperature dependence of β -casein structure as analyzed by circular dichroism and FTIR spectroscopy and correlation with micellization. *Food Hydrocolloids* **2001**, 15, (4-6), 341-354.
128. Hasni, I.; Bourassa, P.; Hamdani, S.; Samson, G.; Carpentier, R.; Tajmir-Riahi, H.-A., Interaction of milk α - and β -caseins with tea polyphenols. *Food Chemistry* **2011**, 126, (2), 630-639.
129. West, D. W., Structure and function of the phosphorylated residues of casein. *Journal of Dairy Research* **1986**, 53, (02), 333-352.

130. Dalgleish, D. G., On the structural models of bovine casein micelles-review and possible improvements. *Soft Matter* **2011**, 7, (6), 2265-2272.
131. Thorn, D. C.; Meehan, S.; Sunde, M.; Rekas, A.; Gras, S. L.; MacPhee, C. E.; Dobson, C. M.; Wilson, M. R.; Carver, J. A., Amyloid Fibril Formation by Bovine Milk κ -Casein and Its Inhibition by the Molecular Chaperones α S- and β -Casein. *Biochemistry* **2005**, 44, (51), 17027-17036.
132. Kim, G.-N.; Jang, H.-D.; Kim, C.-I., Antioxidant capacity of caseinophosphopeptides prepared from sodium caseinate using Alcalase. *Food Chemistry* **2007**, 104, (4), 1359-1365.
133. García-Nebot, M. J.; Cilla, A.; Alegría, A.; Barberá, R., Caseinophosphopeptides exert partial and site-specific cytoprotection against H₂O₂-induced oxidative stress in Caco-2 cells. *Food Chemistry* **2011**, 129, (4), 1495-1503.
134. FitzGerald, R. J., Potential Uses of Caseinophosphopeptides. *International Dairy Journal* **1998**, 8, (5-6), 451-457.
135. FitzGerald, R.; Meisel, H., Caseinophosphopeptides (CPPs) as functional ingredients. *Functional dairy products* **2003**, 187-202.
136. Zidane, F.; Matéos, A.; Cakir-Kiefer, C.; Miclo, L.; Rahuel-Clermont, S.; Girardet, J.-M.; Corbier, C., Binding of divalent metal ions to 1-25 β -caseinophosphopeptide: An isothermal titration calorimetry study. *Food Chemistry* **2012**, 132, (1), 391-398.
137. Ferraretto, A.; Signorile, A.; Gravaghi, C.; Fiorilli, A.; Tettamanti, G., Casein Phosphopeptides Influence Calcium Uptake by Cultured Human Intestinal HT-29 Tumor Cells. *The Journal of Nutrition* **2001**, 131, (6), 1655-1661.
138. Heaney, R.; Saito, Y.; Orimo, H., Effect of caseinophosphopeptide on absorbability of co-ingested calcium in normal postmenopausal women. *Journal of Bone and Mineral Metabolism* **1994**, 12, (1), 77-81.
139. Bouhallab, S.; Cinga, V.; Aít-Oukhatar, N.; Bureau, F.; Neuville, D.; Arhan, P.; Maubois, J.-L.; Bouglé, D., Influence of Various Phosphopeptides of Caseins on Iron Absorption. *Journal of Agricultural and Food Chemistry* **2002**, 50, (24), 7127-7130.
140. Silva, S. V.; Malcata, F. X., Caseins as source of bioactive peptides. *International Dairy Journal* **2005**, 15, (1), 1-15.
141. Chabance, B.; Marteau, P.; Rambaud, J. C.; Migliore-Samour, D.; Boynard, M.; Perrotin, P.; Guillet, R.; Jollès, P.; Fiat, A. M., Casein peptide release and passage to the blood in humans during digestion of milk or yogurt. *Biochimie* **1998**, 80, (2), 155-165.
142. Meisel, H.; Fairweather-Tait, S.; FitzGerald, R. J.; Hartmann, R.; Lane, C. N.; McDonagh, D.; Teucher, B.; Wal, J. M., Detection of caseinophosphopeptides in the distal ileostomy fluid of human subjects. *British Journal of Nutrition* **2003**, 89, (03), 351-358.
143. Sang, S.; Lambert, J. D.; Ho, C.-T.; Yang, C. S., The chemistry and biotransformation of tea constituents. *Pharmacological Research* **2011**, 64, (2), 87-99.
144. Pietta, P.-G., Flavonoids as Antioxidants. *Journal of Natural Products* **2000**, 63, (7), 1035-1042.
145. Pan, M. H.; Lai, C. S.; Ho, C. T., Anti-inflammatory activity of natural dietary flavonoids. *Food & Function* **2010**, 1, (1), 15-31.
146. Surh, Y.-J., Cancer chemoprevention with dietary phytochemicals. *Nature Reviews Cancer* **2003**, 3, (10), 768-780.
147. Pan, M.-H.; Ho, C.-T., Chemopreventive effects of natural dietary compounds on cancer development. *Chemical Society Reviews* **2008**, 37, (11), 2558-2574.
148. Peterson, J. J.; Dwyer, J. T.; Jacques, P. F.; McCullough, M. L., Associations between flavonoids and cardiovascular disease incidence or mortality in European and US populations. *Nutrition Reviews* **2012**, 70, (9), 491-508.
149. Haslam, E., Thoughts on thearubigins. *Phytochemistry* **2003**, 64, (1), 61-73.
150. Balentine, D. A.; Wiseman, S. A.; Bouwens, L. C., The chemistry of tea flavonoids. *Critical Reviews in Food Science & Nutrition* **1997**, 37, (8), 693-704.

151. Wang, H.; Helliwell, K., Determination of flavonols in green and black tea leaves and green tea infusions by high-performance liquid chromatography. *Food Research International* **2001**, *34*, (2–3), 223-227.
152. Drynan, J. W.; Clifford, M. N.; Obuchowicz, J.; Kuhnert, N., The chemistry of low molecular weight black tea polyphenols. *Natural Product Reports* **2010**, *27*, (3), 417-462.
153. Li, S.; Lo, C.-Y.; Pan, M.-H.; Lai, C.-S.; Ho, C.-T., Black tea: chemical analysis and stability. *Food & Function* **2013**.
154. Lun Su, Y.; Leung, L. K.; Huang, Y.; Chen, Z.-Y., Stability of tea theaflavins and catechins. *Food Chemistry* **2003**, *83*, (2), 189-195.
155. Jhoo, J.-W.; Lo, C.-Y.; Li, S.; Sang, S.; Ang, C. Y. W.; Heinze, T. M.; Ho, C.-T., Stability of Black Tea Polyphenol, Theaflavin, and Identification of Theanaphthoquinone as Its Major Radical Reaction Product. *Journal of Agricultural and Food Chemistry* **2005**, *53*, (15), 6146-6150.
156. Tanaka, T.; Inoue, K.; Betsumiya, Y.; Mine, C.; Kouno, I., Two Types of Oxidative Dimerization of the Black Tea Polyphenol Theaflavin. *Journal of Agricultural and Food Chemistry* **2001**, *49*, (12), 5785-5789.
157. Block, G.; Patterson, B.; Subar, A., Fruit, vegetables, and cancer prevention: A review of the epidemiological evidence. *Nutrition and Cancer* **1992**, *18*, (1), 1-29.
158. Liu, S.; Manson, J. E.; Lee, I.-M.; Cole, S. R.; Hennekens, C. H.; Willett, W. C.; Buring, J. E., Fruit and vegetable intake and risk of cardiovascular disease: the Women's Health Study. *The American Journal of Clinical Nutrition* **2000**, *72*, (4), 922-928.
159. Cooper, A. J.; Sharp, S. J.; Lentjes, M. A. H.; Luben, R. N.; Khaw, K.-T.; Wareham, N. J.; Forouhi, N. G., A Prospective Study of the Association Between Quantity and Variety of Fruit and Vegetable Intake and Incident Type 2 Diabetes. *Diabetes Care* **2012**, *35*, (6), 1293-1300.
160. Yang, Z.; Jie, G.; Dong, F.; Xu, Y.; Watanabe, N.; Tu, Y., Radical-scavenging abilities and antioxidant properties of theaflavins and their gallate esters in H₂O₂-mediated oxidative damage system in the HPF-1 cells. *Toxicology In Vitro* **2008**, *22*, (5), 1250-1256.
161. Sang, S.; Tian, S.; Jhoo, J.-w.; Wang, H.; Stark, R. E.; Rosen, R. T.; Yang, C. S.; Ho, C.-T., Chemical studies of the antioxidant mechanism of theaflavins: radical reaction products of theaflavin 3,3'-digallate with hydrogen peroxide. *Tetrahedron Letters* **2003**, *44*, (30), 5583-5587.
162. Lin, J.-K.; Chen, P.-C.; Ho, C.-T.; Lin-Shiau, S.-Y., Inhibition of Xanthine Oxidase and Suppression of Intracellular Reactive Oxygen Species in HL-60 Cells by Theaflavin-3,3'-digallate, (-)-Epigallocatechin-3-gallate, and Propyl Gallate. *Journal of Agricultural and Food Chemistry* **2000**, *48*, (7), 2736-2743.
163. Miller, N. J.; Castelluccio, C.; Tijburg, L.; Rice-Evans, C., The antioxidant properties of theaflavins and their gallate esters — radical scavengers or metal chelators? *FEBS Letters* **1996**, *392*, (1), 40-44.
164. Leung, L. K.; Su, Y.; Chen, R.; Zhang, Z.; Huang, Y.; Chen, Z.-Y., Theaflavins in Black Tea and Catechins in Green Tea Are Equally Effective Antioxidants. *The Journal of Nutrition* **2001**, *131*, (9), 2248-2251.
165. O'Coinceanainn, M.; Bonnely, S.; Baderschneider, B.; Hynes, M. J., Reaction of iron(III) with theaflavin: complexation and oxidative products. *Journal of Inorganic Biochemistry* **2004**, *98*, (4), 657-663.
166. Pan, M.-H.; Lai, C.-S.; Ho, C.-T., Anti-inflammatory activity of natural dietary flavonoids. *Food & Function* **2010**, *1*, (1), 15-31.
167. Dedon, P. C.; Tannenbaum, S. R., Reactive nitrogen species in the chemical biology of inflammation. *Archives of Biochemistry and Biophysics* **2004**, *423*, (1), 12-22.
168. Reuter, S.; Gupta, S. C.; Chaturvedi, M. M.; Aggarwal, B. B., Oxidative stress, inflammation, and cancer: How are they linked? *Free Radical Biology and Medicine* **2010**, *49*, (11), 1603-1616.
169. Huang, M.-T.; Liu, Y.; Ramji, D.; Lo, C.-Y.; Ghai, G.; Dushenkov, S.; Ho, C.-T., Inhibitory effects of black tea theaflavin derivatives on 12-O-tetradecanoylphorbol-13-acetate-

induced inflammation and arachidonic acid metabolism in mouse ears. *Molecular Nutrition & Food Research* **2006**, 50, (2), 115-122.

170. Lin, Y.-L.; Tsai, S.-H.; Lin-Shiau, S.-Y.; Ho, C.-T.; Jen-Kun, L., Theaflavin-3,3'-digallate from black tea blocks the nitric oxide synthase by down-regulating the activation of NF- κ B in macrophages. *European Journal of Pharmacology* **1999**, 367, (2-3), 379-388.

171. Duffy, S. J.; Keaney Jr, J. F.; Holbrook, M.; Gokce, N.; Swerdloff, P. L.; Frei, B.; Vita, J. A., Short- and Long-Term Black Tea Consumption Reverses Endothelial Dysfunction in Patients With Coronary Artery Disease. *Circulation* **2001**, 104, (2), 151-156.

172. Ross, R., Atherosclerosis — An Inflammatory Disease. *New England Journal of Medicine* **1999**, 340, (2), 115-126.

173. Vinson, J. A.; Teufel, K.; Wu, N., Green and Black Teas Inhibit Atherosclerosis by Lipid, Antioxidant, and Fibrinolytic Mechanisms. *Journal of Agricultural and Food Chemistry* **2004**, 52, (11), 3661-3665.

174. Witztum, J. L.; Steinberg, D., Role of oxidized low density lipoprotein in atherogenesis. *The Journal of Clinical Investigation* **1991**, 88, (6), 1785-1792.

175. Yoshida, H.; Ishikawa, T.; Hosoai, H.; Suzukawa, M.; Ayaori, M.; Hisada, T.; Sawada, S.; Yonemura, A.; Higashi, K.; Ito, T., Inhibitory effect of tea flavonoids on the ability of cells to oxidize low density lipoprotein. *Biochemical Pharmacology* **1999**, 58, (11), 1695-1703.

176. Steptoe, A.; Gibson, E. L.; Vuononvirta, R.; Hamer, M.; Wardle, J.; Rycroft, J. A.; Martin, J. F.; Erusalimsky, J. D., The effects of chronic tea intake on platelet activation and inflammation: a double-blind placebo controlled trial. *Atherosclerosis* **2007**, 193, (2), 277-282.

177. Stangl, V.; Dreger, H.; Stangl, K.; Lorenz, M., *Molecular targets of tea polyphenols in the cardiovascular system*. 2007; Vol. 73, p 348-358.

178. Pan, M.-H.; Chiou, Y.-S.; Wang, Y.-J.; Ho, C.-T.; Lin, J.-K., Multistage carcinogenesis process as molecular targets in cancer chemoprevention by epicatechin-3-gallate. *Food & Function* **2011**, 2, (2), 101-110.

179. Feng, Q.; Torii, Y.; Uchida, K.; Nakamura, Y.; Hara, Y.; Osawa, T., Black Tea Polyphenols, Theaflavins, Prevent Cellular DNA Damage by Inhibiting Oxidative Stress and Suppressing Cytochrome P450 1A1 in Cell Cultures. *Journal of Agricultural and Food Chemistry* **2001**, 50, (1), 213-220.

180. Liang, Y.-C.; Chen, Y.-C.; Lin, Y.-L.; Lin-Shiau, S.-Y.; Ho, C.-T.; Lin, J.-K., Suppression of extracellular signals and cell proliferation by the black tea polyphenol, theaflavin-3,3'-digallate. *Carcinogenesis* **1999**, 20, (4), 733-736.

181. Prasad, S.; Kaur, J.; Roy, P.; Kalra, N.; Shukla, Y., Theaflavins induce G2/M arrest by modulating expression of p21 waf1/cip1, cdc25C and cyclin B in human prostate carcinoma PC-3 cells. *Life Sciences* **2007**, 81, (17), 1323-1331.

182. Siddiqui, I. A.; Zaman, N.; Aziz, M. H.; Reagan-Shaw, S. R.; Sarfaraz, S.; Adhami, V. M.; Ahmad, N.; Raisuddin, S.; Mukhtar, H., Inhibition of CWR22Rv1 tumor growth and PSA secretion in athymic nude mice by green and black teas. *Carcinogenesis* **2006**, 27, (4), 833-839.

183. Maeda-Yamamoto, M.; Kawahara, H.; Tahara, N.; Tsuji, K.; Hara, Y.; Isemura, M., Effects of Tea Polyphenols on the Invasion and Matrix Metalloproteinases Activities of Human Fibrosarcoma HT1080 Cells. *Journal of Agricultural and Food Chemistry* **1999**, 47, (6), 2350-2354.

184. Sazuka, M.; Imazawa, H.; Shoji, Y.; Mita, T.; Hara, Y.; Isemura, M., Inhibition of Collagenases from Mouse Lung Carcinoma Cells by Green Tea Catechins and Black Tea Theaflavins. *Bioscience, Biotechnology, and Biochemistry* **1997**, 61, (9), 1504-1506.

185. Goldbohm, R. A.; Hertog, M. G. L.; Brants, H. A. M.; van Poppel, G.; van den Brandt, P. A., Consumption of Black Tea and Cancer Risk: a Prospective Cohort Study. *JNCI: Journal of the National Cancer Institute* **1996**, 88, (2), 93-100.

186. Sun, C.-L.; Yuan, J.-M.; Koh, W.-P.; Yu, M. C., Green tea, black tea and breast cancer risk: a meta-analysis of epidemiological studies. *Carcinogenesis* **2006**, 27, (7), 1310-1315.

187. Mulder, T. P. J.; van Platerink, C. J.; Wijnand Schuyf, P. J.; van Amelsvoort, J. M. M., Analysis of theaflavins in biological fluids using liquid chromatography–electrospray mass spectrometry. *Journal of Chromatography B: Biomedical Sciences and Applications* **2001**, 760, (2), 271-279.
188. Fernández-García, E.; Carvajal-Lérida, I.; Pérez-Gálvez, A., In vitro bioaccessibility assessment as a prediction tool of nutritional efficiency. *Nutrition Research* **2009**, 29, (11), 751-760.
189. Joye, I. J.; Davidov-Pardo, G.; McClements, D. J., Nanotechnology for increased micronutrient bioavailability. *Trends in Food Science & Technology* **2014**, 40, (2), 168-182.
190. Jöbstl, E.; O'Connell, J.; Fairclough, J. P. A.; Williamson, M. P., Molecular Model for Astringency Produced by Polyphenol/Protein Interactions. *Biomacromolecules* **2004**, 5, (3), 942-949.
191. Hong, J.; Lambert, J. D.; Lee, S.-H.; Sinko, P. J.; Yang, C. S., Involvement of multidrug resistance-associated proteins in regulating cellular levels of (–)-epigallocatechin-3-gallate and its methyl metabolites. *Biochemical and Biophysical Research Communications* **2003**, 310, (1), 222-227.
192. Hong, J.; Lu, H.; Meng, X.; Ryu, J.-H.; Hara, Y.; Yang, C. S., Stability, Cellular Uptake, Biotransformation, and Efflux of Tea Polyphenol (–)-Epigallocatechin-3-Gallate in HT-29 Human Colon Adenocarcinoma Cells. *Cancer Research* **2002**, 62, (24), 7241-7246.
193. Lipinski, C. A.; Lombardo, F.; Dominy, B. W.; Feeney, P. J., Experimental and computational approaches to estimate solubility and permeability in drug discovery and development settings. *Advanced Drug Delivery Reviews* **2001**, 46, (1–3), 3-26.
194. Lavertu, M.; Xia, Z.; Serreqi, A. N.; Berrada, M.; Rodrigues, A.; Wang, D.; Buschmann, M. D.; Gupta, A., A validated ¹H NMR method for the determination of the degree of deacetylation of chitosan. *Journal of Pharmaceutical and Biomedical Analysis* **2003**, 32, (6), 1149-1158.
195. Li, Y.; Xia, Q.; Shi, K.; Huang, Q., Scaling Behaviors of α -Zein in Acetic Acid Solutions. *The Journal of Physical Chemistry B* **2011**, 115, (32), 9695-9702.
196. Neves, S.; Polo Fonseca, C., Determination of fractal dimension of polyaniline composites by SAXS and electrochemical techniques. *Electrochemistry Communications* **2001**, 3, (1), 36-43.
197. Ilavsky, J.; Jemian, P. R., Irena: tool suite for modeling and analysis of small-angle scattering. *Journal of Applied Crystallography* **2009**, 42, (2), 347-353.
198. Philippova, O. E.; Volkov, E. V.; Sitnikova, N. L.; Khokhlov, A. R.; Desbrieres, J.; Rinaudo, M., Two Types of Hydrophobic Aggregates in Aqueous Solutions of Chitosan and Its Hydrophobic Derivative. *Biomacromolecules* **2001**, 2, (2), 483-490.
199. Dressman, J.; Berardi, R.; Dermentzoglou, L.; Russell, T.; Schmaltz, S.; Barnett, J.; Jarvenpaa, K., Upper Gastrointestinal (GI) pH in Young, Healthy Men and Women. *Pharmaceutical Research* **1990**, 7, (7), 756-761.
200. Fallingborg, J., Intraluminal pH of the human gastrointestinal tract. *Danish Medical Bulletin* **1999**, 46, (3), 183-196.
201. Kataoka, M.; Tokunaga, F.; Kuwajima, K.; Goto, Y., Structural characterization of the molten globule of α -lactalbumin by solution X-ray scattering. *Protein Science* **1997**, 6, (2), 422-430.
202. Arts, M. J. T. J.; Haenen, G. R. M. M.; Wilms, L. C.; Beetstra, S. A. J. N.; Heijnen, C. G. M.; Voss, H. P.; Bast, A., Interactions between flavonoids and proteins: Effect on the total antioxidant capacity. *Journal of Agricultural and Food Chemistry* **2002**, 50, (5), 1184-1187.
203. Xiao, J.; Mao, F.; Yang, F.; Zhao, Y.; Zhang, C.; Yamamoto, K., Interaction of dietary polyphenols with bovine milk proteins: Molecular structure–affinity relationship and influencing bioactivity aspects. *Molecular Nutrition & Food Research* **2011**, 55, (11), 1637-1645.
204. Serafini, M.; Ghiselli, A.; Ferro-Luzzi, A., In vivo antioxidant effect of green and black tea in man. *Eur J Clin Nutr* **1996**, 50, (1), 28-32.

205. Langley-Evans, S. C., Consumption of black tea elicits an increase in plasma antioxidant potential in humans. *International Journal of Food Sciences and Nutrition* **2000**, 51, (5), 309-315.
206. Leenen, R.; Roodenburg, A.; Tijburg, L.; Wiseman, S., A single dose of tea with or without milk increases plasma antioxidant activity in humans. *Eur J Clin Nutr* **2000**, 54, (1), 87.
207. Kyle, J. A. M.; Morrice, P. C.; McNeill, G.; Duthie, G. G., Effects of Infusion Time and Addition of Milk on Content and Absorption of Polyphenols from Black Tea. *Journal of Agricultural and Food Chemistry* **2007**, 55, (12), 4889-4894.
208. Record, I. R.; Dreosti, I. E., Protection by tea against UV-A + B-induced skin cancers in hairless mice. *Nutrition and Cancer* **1998**, 32, (2), 71-75.
209. Weisburger, J. H.; Rivenson, A.; Garr, K.; Aliaga, C., Tea, or tea and milk, inhibit mammary gland and colon carcinogenesis in rats. *Cancer Letters* **1997**, 114, (1-2), 323-327.
210. Huang, Q. R.; Frank, C. W.; Mecerreyes, D.; Volksen, W.; Miller, R. D., Phase Separation Behavior of Poly(methyl methacrylate-co-dimethylaminoethyl methacrylate)/Methyl Silsesquioxane Hybrid Nanocomposites Studied by Dansyl Fluorescence. *Chemistry of Materials* **2005**, 17, (6), 1521-1528.
211. Wang, X.; Ho, C.-T.; Huang, Q., Investigation of Adsorption Behavior of (-)-Epigallocatechin Gallate on Bovine Serum Albumin Surface Using Quartz Crystal Microbalance with Dissipation Monitoring. *Journal of Agricultural and Food Chemistry* **2007**, 55, (13), 4987-4992.
212. Lakowicz, J. R., *Principles of fluorescence spectroscopy*. Springer: 2009.
213. Hu, B.; Wang, S. S.; Li, J.; Zeng, X. X.; Huang, Q. R., Assembly of Bioactive Peptide-Chitosan Nanocomplexes. *The Journal of Physical Chemistry B* **2011**, 115, (23), 7515-7523.
214. Ross, P. D.; Subramanian, S., Thermodynamics of protein association reactions: forces contributing to stability. *Biochemistry* **1981**, 20, (11), 3096-3102.
215. Farrell, H. M., Jr.; Qi, P. X.; Wickham, E. D.; Unruh, J. J., Secondary Structural Studies of Bovine Caseins: Structure and Temperature Dependence of β -Casein Phosphopeptide (1-25) as Analyzed by Circular Dichroism, FTIR Spectroscopy, and Analytical Ultracentrifugation. *Journal of Protein Chemistry* **2002**, 21, (5), 307-321.
216. Kelly, S. M.; Price, N. C., The Use of Circular Dichroism in the Investigation of Protein Structure and Function. *Current Protein and Peptide Science* **2000**, 1, (4), 349-384.
217. Georgiades, P.; di Cola, E.; Heenan, R. K.; Pudney, P. D. A.; Thornton, D. J.; Waigh, T. A., A combined small-angle X-ray and neutron scattering study of the structure of purified soluble gastrointestinal mucins. *Biopolymers* **2014**, 101, (12), 1154-1164.
218. Reviakine, I.; Johannsmann, D.; Richter, R. P., Hearing What You Cannot See and Visualizing What You Hear: Interpreting Quartz Crystal Microbalance Data from Solvated Interfaces. *Analytical Chemistry* **2011**, 83, (23), 8838-8848.
219. Chitpan, M.; Wang, X.; Ho, C.-T.; Huang, Q., Monitoring the Binding Processes of Black Tea Thearubigin to the Bovine Serum Albumin Surface Using Quartz Crystal Microbalance with Dissipation Monitoring. *Journal of Agricultural and Food Chemistry* **2007**, 55, (25), 10110-10116.
220. Yang, G. Y.; Liao, J.; Kim, K.; Yurkow, E. J.; Yang, C. S., Inhibition of growth and induction of apoptosis in human cancer cell lines by tea polyphenols. *Carcinogenesis* **1998**, 19, (4), 611-616.
221. Lahiry, L.; Saha, B.; Chakraborty, J.; Adhikary, A.; Mohanty, S.; Hossain, D. M. S.; Banerjee, S.; Das, K.; Sa, G.; Das, T., Theaflavins target Fas/caspase-8 and Akt/pBad pathways to induce apoptosis in p53-mutated human breast cancer cells. *Carcinogenesis* **2010**, 31, (2), 259-268.
222. Lambert, J. D.; Yang, C. S., Cancer chemopreventive activity and bioavailability of tea and tea polyphenols. *Mutation Research/Fundamental and Molecular Mechanisms of Mutagenesis* **2003**, 523-524, (0), 201-208.
223. Ting, Y.; Jiang, Y.; Lan, Y.; Xia, C.; Lin, Z.; Rogers, M. A.; Huang, Q., Viscoelastic Emulsion Improved the Bioaccessibility and Oral Bioavailability of Crystalline Compound: A

Mechanistic Study Using in Vitro and in Vivo Models. *Molecular Pharmaceutics* **2015**, 12, (7), 2229-2236.

224. Kawabata, Y.; Wada, K.; Nakatani, M.; Yamada, S.; Onoue, S., Formulation design for poorly water-soluble drugs based on biopharmaceutics classification system: Basic approaches and practical applications. *International Journal of Pharmaceutics* **2011**, 420, (1), 1-10.

225. Hubatsch, I.; Ragnarsson, E. G. E.; Artursson, P., Determination of drug permeability and prediction of drug absorption in Caco-2 monolayers. *Nat. Protocols* **2007**, 2, (9), 2111-2119.

226. Evans, D. F.; Pye, G.; Bramley, R.; Clark, A. G.; Dyson, T. J.; Hardcastle, J. D., Measurement of gastrointestinal pH profiles in normal ambulant human subjects. *Gut* **1988**, 29, (8), 1035-1041.

227. Chen, H.; Ouyang, W.; Lawuyi, B.; Prakash, S., Genipin Cross-Linked Alginate-Chitosan Microcapsules: Membrane Characterization and Optimization of Cross-Linking Reaction. *Biomacromolecules* **2006**, 7, (7), 2091-2098.

228. Di Tommaso, S.; David, P.; Picolet, K.; Gabant, M.; David, H.; Morancais, J.-L.; Gomar, J.; Leroy, F.; Adamo, C., Structure of genipin in solution: a combined experimental and theoretical study. *RSC Advances* **2013**, 3, (33), 13764-13771.

229. Huang, Y.; Yu, H.; Guo, L.; Huang, Q., Structure and Self-Assembly Properties of a New Chitosan-Based Amphiphile. *The Journal of Physical Chemistry B* **2010**, 114, (23), 7719-7726.

230. Ilavsky, J., Nika: software for two-dimensional data reduction. *Journal of Applied Crystallography* **2012**, 45, (2), 324-328.

231. Butler, M. F.; Ng, Y.-F.; Pudney, P. D. A., Mechanism and kinetics of the crosslinking reaction between biopolymers containing primary amine groups and genipin. *Journal of Polymer Science Part A: Polymer Chemistry* **2003**, 41, (24), 3941-3953.

232. Mi, F.-L.; Shyu, S.-S.; Peng, C.-K., Characterization of ring-opening polymerization of genipin and pH-dependent cross-linking reactions between chitosan and genipin. *Journal of Polymer Science Part A: Polymer Chemistry* **2005**, 43, (10), 1985-2000.

233. Mi, F.-L.; Sung, H.-W.; Shyu, S.-S., Synthesis and characterization of a novel chitosan-based network prepared using naturally occurring crosslinker. *Journal of Polymer Science Part A: Polymer Chemistry* **2000**, 38, (15), 2804-2814.

234. Mu, C.; Zhang, K.; Lin, W.; Li, D., Ring-opening polymerization of genipin and its long-range crosslinking effect on collagen hydrogel. *Journal of Biomedical Materials Research Part A* **2013**, 101A, (2), 385-393.

235. Park, J.-E.; Lee, J.-Y.; Kim, H.-G.; Hahn, T.-R.; Paik, Y.-S., Isolation and Characterization of Water-Soluble Intermediates of Blue Pigments Transformed from Geniposide of *Gardenia jasminoides*. *Journal of Agricultural and Food Chemistry* **2002**, 50, (22), 6511-6514.

236. Hu, B.; Ting, Y.; Zeng, X.; Huang, Q., Cellular uptake and cytotoxicity of chitosan-caseinophosphopeptides nanocomplexes loaded with epigallocatechin gallate. *Carbohydrate Polymers* **2012**, 89, (2), 362-370.

237. Caessens, P. W. J. R.; Gruppen, H.; Visser, S.; van Aken, G. A.; Voragen, A. G. J., Plasmin Hydrolysis of β -Casein: Foaming and Emulsifying Properties of the Fractionated Hydrolysate. *Journal of Agricultural and Food Chemistry* **1997**, 45, (8), 2935-2941.

238. Shimizu, M.; Lee, S. W.; Kaminogawa, S.; Yamauchi, K., Emulsifying Properties of an N-Terminal Peptide Obtained from the Peptic Hydrolyzate of α 1-Casein. *Journal of Food Science* **1984**, 49, (4), 1117-1120.

239. Lee, S. W.; Shimizu, M.; Kaminogawa, S.; Yamauchi, K., Emulsifying Properties of Peptides Obtained from the Hydrolyzates of β -Casein. *Agricultural and Biological Chemistry* **1987**, 51, (1), 161-166.

240. Jourdain, L.; Leser, M. E.; Schmitt, C.; Michel, M.; Dickinson, E., Stability of emulsions containing sodium caseinate and dextran sulfate: Relationship to complexation in solution. *Food Hydrocolloids* **2008**, 22, (4), 647-659.

241. Zinoviadou, K. G.; Scholten, E.; Moschakis, T.; Biliaderis, C. G., Properties of emulsions stabilised by sodium caseinate–chitosan complexes. *International Dairy Journal* **2012**, 26, (1), 94-101.
242. Diftis, N. G.; Biliaderis, C. G.; Kiosseoglou, V. D., Rheological properties and stability of model salad dressing emulsions prepared with a dry-heated soybean protein isolate–dextran mixture. *Food Hydrocolloids* **2005**, 19, (6), 1025-1031.
243. Yin, B.; Deng, W.; Xu, K.; Huang, L.; Yao, P., Stable nano-sized emulsions produced from soy protein and soy polysaccharide complexes. *Journal of Colloid and Interface Science* **2012**, 380, (1), 51-59.
244. Littoz, F.; McClements, D. J., Bio-mimetic approach to improving emulsion stability: Cross-linking adsorbed beet pectin layers using laccase. *Food Hydrocolloids* **2008**, 22, (7), 1203-1211.
245. Zeeb, B.; Gibis, M.; Fischer, L.; Weiss, J., Crosslinking of interfacial layers in multilayered oil-in-water emulsions using laccase: Characterization and pH-stability. *Food Hydrocolloids* **2012**, 27, (1), 126-136.
246. Muzzarelli, R. A. A., Genipin-crosslinked chitosan hydrogels as biomedical and pharmaceutical aids. *Carbohydrate Polymers* **2009**, 77, (1), 1-9.
247. Ding, Y.; Hou, J.-W.; Zhang, Y.; Zhang, L.-Y.; Zhang, T.; Chen, Y.; Cai, Z.-Z.; Yang, L., Metabolism of Genipin in Rat and Identification of Metabolites by Using Ultraperformance Liquid Chromatography/Quadrupole Time-of-Flight Tandem Mass Spectrometry. *Evidence-Based Complementary and Alternative Medicine* **2013**, 2013, 13.
248. Tsai, C. C.; Huang, R. N.; Sung, H. W.; Liang, H. C., In vitro evaluation of the genotoxicity of a naturally occurring crosslinking agent (genipin) for biologic tissue fixation. *Journal of biomedical materials research* **2000**, 52, (1), 58-65.
249. Mi, F.-L., Synthesis and Characterization of a Novel Chitosan–Gelatin Bioconjugate with Fluorescence Emission. *Biomacromolecules* **2005**, 6, (2), 975-987.
250. Chen, H.; Ouyang, W.; Lawuyi, B.; Martoni, C.; Prakash, S., Reaction of chitosan with genipin and its fluorogenic attributes for potential microcapsule membrane characterization. *Journal of Biomedical Materials Research Part A* **2005**, 75A, (4), 917-927.
251. Touyama, R.; Takeda, Y.; Inoue, K.; Kawamura, I.; Yatsuzuka, M.; Ikumoto, T.; Shingu, T.; Yokoi, T.; Inouye, H., Studies on the Blue Pigments Produced from Genipin and Methylamine. I. Structures of the Brownish-Red Pigments, Intermediates Leading to the Blue Pigments. *Chemical & Pharmaceutical Bulletin* **1994**, 42, (3), 668-673.
252. Hillberg, A. L.; Kathirgamanathan, K.; Lam, J. B. B.; Law, L. Y.; Garkavenko, O.; Elliott, R. B., Improving alginate-poly-L-ornithine-alginate capsule biocompatibility through genipin crosslinking. *Journal of Biomedical Materials Research Part B: Applied Biomaterials* **2013**, 101B, (2), 258-268.
253. Hillberg, A. L.; Holmes, C. A.; Tabrizian, M., Effect of genipin cross-linking on the cellular adhesion properties of layer-by-layer assembled polyelectrolyte films. *Biomaterials* **2009**, 30, (27), 4463-4470.
254. Ngai, T.; Bon, S. A., *Particle-stabilized emulsions and colloids*. Royal Society of Chemistry: 2014.
255. Madivala, B.; Vandebriel, S.; Fransaer, J.; Vermant, J., Exploiting particle shape in solid stabilized emulsions. *Soft Matter* **2009**, 5, (8), 1717-1727.
256. Binks, B. P.; Lumsdon, S. O., Influence of Particle Wettability on the Type and Stability of Surfactant-Free Emulsions. *Langmuir* **2000**, 16, (23), 8622-8631.
257. Binks, B. P.; Lumsdon, S. O., Catastrophic Phase Inversion of Water-in-Oil Emulsions Stabilized by Hydrophobic Silica. *Langmuir* **2000**, 16, (6), 2539-2547.
258. Lee, M. N.; Chan, H. K.; Mohraz, A., Characteristics of Pickering Emulsion Gels Formed by Droplet Bridging. *Langmuir* **2012**, 28, (6), 3085-3091.

259. Kalashnikova, I.; Bizot, H.; Bertoncini, P.; Cathala, B.; Capron, I., Cellulosic nanorods of various aspect ratios for oil in water Pickering emulsions. *Soft Matter* **2013**, 9, (3), 952-959.
260. Chen, B.; McClements, D. J.; Decker, E. A., Minor Components in Food Oils: A Critical Review of their Roles on Lipid Oxidation Chemistry in Bulk Oils and Emulsions. *Critical Reviews in Food Science and Nutrition* **2011**, 51, (10), 901-916.
261. Kanner, J., Dietary advanced lipid oxidation endproducts are risk factors to human health. *Molecular Nutrition & Food Research* **2007**, 51, (9), 1094-1101.
262. Larsson, K.; Cavonius, L.; Alminger, M.; Undeland, I., Oxidation of Cod Liver Oil during Gastrointestinal in Vitro Digestion. *Journal of Agricultural and Food Chemistry* **2012**, 60, (30), 7556-7564.
263. Del Rio, D.; Stewart, A. J.; Pellegrini, N., A review of recent studies on malondialdehyde as toxic molecule and biological marker of oxidative stress. *Nutrition, Metabolism and Cardiovascular Diseases* **2005**, 15, (4), 316-328.
264. Esterbauer, H., Cytotoxicity and genotoxicity of lipid-oxidation products. *The American Journal of Clinical Nutrition* **1993**, 57, (5), 779S-785S.
265. Hu, W.; Feng, Z.; Eveleigh, J.; Iyer, G.; Pan, J.; Amin, S.; Chung, F.-L.; Tang, M.-s., The major lipid peroxidation product, trans-4-hydroxy-2-nonenal, preferentially forms DNA adducts at codon 249 of human p53 gene, a unique mutational hotspot in hepatocellular carcinoma. *Carcinogenesis* **2002**, 23, (11), 1781-1789.
266. Cohn, J. S., Oxidized fat in the diet, postprandial lipaemia and cardiovascular disease. *Current opinion in lipidology* **2002**, 13, (1), 19-24.
267. BECKMAN, K. B.; AMES, B. N., The Free Radical Theory of Aging Matures. *Physiological Reviews* **1998**, 78, (2), 547-581.
268. Schaich, K. M., Co-oxidation of Proteins by Oxidizing Lipids. In *Lipid Oxidation Pathways*, AOCS Press: Urbana, IL, 2008; Vol. 2, pp 181-272.
269. Kargar, M.; Spyropoulos, F.; Norton, I. T., The effect of interfacial microstructure on the lipid oxidation stability of oil-in-water emulsions. *Journal of Colloid and Interface Science* **2011**, 357, (2), 527-533.
270. Gonzalez-Jordan, A.; Nicolai, T.; Benyahia, L., Influence of the Protein Particle Morphology and Partitioning on the Behavior of Particle-Stabilized Water-in-Water Emulsions. *Langmuir* **2016**, 32, (28), 7189-7197.
271. McClements, D. J., *Food emulsions: principles, practices, and techniques*. CRC press: 2015.
272. Schwarz, K.; Huang, S.-W.; German, J. B.; Tiersch, B.; Hartmann, J.; Frankel, E. N., Activities of Antioxidants Are Affected by Colloidal Properties of Oil-in-Water and Water-in-Oil Emulsions and Bulk Oils. *Journal of Agricultural and Food Chemistry* **2000**, 48, (10), 4874-4882.
273. Shahidi, F., *Bailey's Industrial Oil and Fat Products*. 6 ed.; John Wiley & Sons, Inc.: New Jersey, 2005.
274. Sun, Y.-E.; Wang, W.-D.; Chen, H.-W.; Li, C., Autoxidation of Unsaturated Lipids in Food Emulsion. *Critical Reviews in Food Science and Nutrition* **2011**, 51, (5), 453-466.
275. McClements, D. J.; Decker, E. A., Lipid Oxidation in Oil-in-Water Emulsions: Impact of Molecular Environment on Chemical Reactions in Heterogeneous Food Systems. *Journal of Food Science* **2000**, 65, (8), 1270-1282.
276. Kargar, M.; Fayazmanesh, K.; Alavi, M.; Spyropoulos, F.; Norton, I. T., Investigation into the potential ability of Pickering emulsions (food-grade particles) to enhance the oxidative stability of oil-in-water emulsions. *Journal of Colloid and Interface Science* **2012**, 366, (1), 209-215.

APPENDIX: LIST OF ABBREVIATIONS

Abbreviations	Full Names
11-MUA	11-Mercaptoundecanoic Acid
AA	Arachidonic Acid
AFM	Atomic Force Microscope
APS	Advanced Photon Source
ATCC	American Type Culture Collection
BHA	Butylated Hydroxyanisole
BHT	Butylated Hydroxytoluene
C*	Overlap Concentration
C1P1	CS-CPPs Nanocomplex Composed of CS:CPPs=1:1
C2P1	CS-CPPs Nanocomplex Composed of CS:CPPs=2:1
C4P1	CS-CPPs Nanocomplex Composed of CS:CPPs=4:1
CD	Circular Dichroism
CI	Creaming Index
COX	Cyclooxygenase
CPPs	Caseinophosphopeptides
CS	Chitosan
CYP450	Cytochrome P450
D ₂ O	Deuterium Oxide
DCI	Deuterium Chloride
DD	Degree of Deacetylation
DMEM	Dulbecco's Modified Eagle's Medium
DMSO	Dimethyl Sulfoxide
DPPH	2,2-diphenyl-1-picrylhydrazyl

DSC	Differential Scanning Calorimetry
EC	(-)-epicatechin
ECG	(-)-epicatechin gallate
EDC	1-Ethyl-3-(3-Dimethylaminopropyl)Carbodiimide Hydrochloride
EGC	(-)-epigallocatechin
EGCG	(-)-Epigallocatechin Gallate
FAO	Food and Agriculture Organization
FBS	Fetal Bovine Serum
FDA	Food and Drug Administration
FITC	Fluorescein Isothiocyanate
FTIR	Fourier Transform Infrared Spectroscopy
GCNs	Genipin Crosslinked Chitosan-Caseinophosphopeptides Nanocomplexes
GCNs1	GCNs Crosslinked By 0.1 mg/mL Genipin
GCNs5	GCNs Crosslinked By 0.5 mg/mL Genipin
GCNs10	GCNs Crosslinked By 1 mg/mL Genipin
GIT	Gastrointestinal Tract
GPC-MALLS	Gel Permeation Chromatography Multi-Angle Laser Light Scattering
GRAS	Generally Recognized as Safe
GT	GCNs Encapsulated with TF-3
GT0	GCNs Encapsulated with TF-3 with TF-3:CPPs=0
GT1	GCNs Encapsulated with TF-3 with TF-3:CPPs=0.1
GT2	GCNs Encapsulated with TF-3 with TF-3:CPPs=0.2
GT4	GCNs Encapsulated with TF-3 with TF-3:CPPs=0.4
HBSS	Hanks' Balanced Salt Solution
HPLC	High Performance Liquid Chromatography

IL-1	Interleukin-1
IL-6	Interleukin-6
ITC	Isothermal Titration Calorimetry
JAMs	Junctional Adhesion Molecules
LC-MS/MS	Liquid chromatography-tandem mass spectrometry
LDL	Low-density lipoprotein
LOX	Lipoxygenase
LTs	Leukotrienes
MCT	Medium Chain Triglyceride
MMPs	Matrix Metalloproteinases
MRPs	Multidrug Resistance Proteins
MTT	3-[4,5-Dimethylthiazol-2-yl]-2,5-Diphenyltetrazolium Bromide
M _w	Molecular Weight
NF-κB	Nuclear factor-κB
NHS	N-Hydroxysuccinimide
NMR	Nuclear Magnetic Resonance
ORAC	Oxygen Radical Absorbance Capacity
O/W	Oil-in-Water
P _{app}	Apparent Permeability Coefficient
PBS	Phosphate Buffered Saline
PDI	Polydispersity Index
PG	Propyl Gallate
PGs	Prostaglandins
pI	Isoelectric Point
POD	Peroxidase

PPO	Polyphenol Oxidase
PUFA	Polyunsaturated Fatty Acid
PV	Peroxide Value
QCM-D	Quartz Crystal Microbalance with Dissipation Monitoring
R _g	Radius of Gyration
RNS	Reactive nitrogen species
ROS	Reactive oxygen species
SANS	Small Angle Neutron Scattering
SAXS	Small Angle X-Ray Scattering
SOD	Superoxide Dismutase
TBARS	Thiobarbituric Acid Reactive Substances
TBHQ	Tertiary Butylhydroquinone
TEAC	Trolox Equivalent Antioxidant Capacity
TER	Transepithelial Resistance
TF-1	Theaflavin
TF-2a	Theaflavin-3-gallate
TF-2b	Theaflavin-3'-gallate
TF-3	Theaflavin-3,3'-digallate
TFs	Theaflavins
TNF- α	tumor necrosis factor α
TPA	12- <i>O</i> -tetradecanoylphorbol-13-acetate
USAXS	Ultra-Small Angle X-Ray Scattering
UV	Ultraviolet
UV-Vis	Ultraviolet-Visible
VEGF	Vascular Endothelial Growth Factor

W/O

Water-in-Oil
